

# Advances

## in Clinical and Experimental Medicine

MONTHLY ISSN 1899-5276 (PRINT) ISSN 2451-2680 (ONLINE)

[www.advances.umed.wroc.pl](http://www.advances.umed.wroc.pl)

2020, Vol. 29, No. 8 (August)

Impact Factor (IF) – 1.514  
Ministry of Science and Higher Education – 40 pts.  
Index Copernicus (ICV) – 155.19 pts.



WROCLAW  
MEDICAL UNIVERSITY

Advances  
in Clinical and Experimental  
Medicine



# Advances in Clinical and Experimental Medicine

ISSN 1899-5276 (PRINT)

ISSN 2451-2680 (ONLINE)

www.advances.umed.wroc.pl

**MONTHLY 2020**  
**Vol. 29, No. 8**  
**(August)**

Advances in Clinical and Experimental Medicine is a peer-reviewed open access journal published by Wrocław Medical University. Its abbreviated title is Adv Clin Exp Med. Journal publishes original papers and reviews encompassing all aspects of medicine, including molecular biology, biochemistry, genetics, biotechnology, and other areas. It is published monthly, one volume per year.

---

## Editorial Office

ul. Marcinkowskiego 2–6  
50-368 Wrocław, Poland  
Tel.: +48 71 784 11 36  
E-mail: redakcja@umed.wroc.pl

## Publisher

Wrocław Medical University  
Wybrzeże L. Pasteura 1  
50-367 Wrocław, Poland

© Copyright by Wrocław Medical University,  
Wrocław 2020

Online edition is the original version of the journal

---

## Editor-in-Chief

Maciej Bagłaż

## Vice-Editor-in-Chief

Dorota Frydecka

---

## Editorial Board

Piotr Dziągłiel  
Marian Klinger  
Halina Milnerowicz  
Jerzy Mozrzyński

---

## Thematic Editors

Marzena Bartoszewicz (microbiology)  
Marzena Dominiak (dentistry)  
Paweł Domosławski (surgery)  
Maria Ejma (neurology)  
Jacek Gajek (cardiology)  
Mariusz Kuształ  
(nephrology and transplantology)  
Rafał Matkowski (oncology)  
Ewa Milnerowicz-Nabzdzyk (gynecology)  
Katarzyna Neubauer (gastroenterology)  
Marcin Ruciński (basic sciences)  
Robert Śmigiel (pediatrics)  
Paweł Tabakow (experimental medicine)  
Anna Wiela-Hojeńska  
(pharmaceutical sciences)  
Dariusz Wołowicz (internal medicine)

---

## International Advisory Board

Reinhard Berner (Germany)  
Vladimir Bobek (Czech Republic)  
Marcin Czyż (UK)  
Buddhadeb Dawn (USA)  
Kishore Kumar Jella (USA)

---

## Secretary

Katarzyna Neubauer

---

Piotr Ponikowski  
Marek Sąsiadek  
Leszek Szenborn  
Jacek Szepietowski

---

## Statistical Editors

Dorota Diakowska  
Leszek Noga  
Lesław Rusiecki

## Technical Editorship

Paulina Kunicka  
Marek Misiak

## English Language Copy Editors

Eric Hilton  
Sherill Howard Pociecha  
Jason Schock  
Marcin Tereszewski

---

Pavel Kopel (Czech Republic)  
Tomasz B. Owczarek (USA)  
Ivan Rychlík (Czech Republic)  
Anton Sculean (Switzerland)  
Andriy B. Zimenkovsky (Ukraine)

## Editorial Policy

Advances in Clinical and Experimental Medicine (Adv Clin Exp Med) is an independent multidisciplinary forum for exchange of scientific and clinical information, publishing original research and news encompassing all aspects of medicine, including molecular biology, biochemistry, genetics, biotechnology and other areas. During the review process, the Editorial Board conforms to the "Uniform Requirements for Manuscripts Submitted to Biomedical Journals: Writing and Editing for Biomedical Publication" approved by the International Committee of Medical Journal Editors ([www.ICMJE.org/](http://www.ICMJE.org/)). The journal publishes (in English only) original papers and reviews. Short works considered original, novel and significant are given priority. Experimental studies must include a statement that the experimental protocol and informed consent procedure were in compliance with the Helsinki Convention and were approved by an ethics committee.

For all subscription-related queries please contact our Editorial Office:  
[redakcja@umed.wroc.pl](mailto:redakcja@umed.wroc.pl)

For more information visit the journal's website:  
[www.advances.umed.wroc.pl](http://www.advances.umed.wroc.pl)

Pursuant to the ordinance No. 134/XV R/2017 of the Rector of Wrocław Medical University (as of December 28, 2017) from January 1, 2018 authors are required to pay a fee amounting to 700 euros for each manuscript accepted for publication in the journal Advances in Clinical and Experimental Medicine.

„Podniesienie poziomu naukowego i poziomu umiędzynarodowienia wydawanych czasopism naukowych oraz upowszechniania informacji o wynikach badań naukowych lub prac rozwojowych – zadanie finansowane w ramach umowy 784/p-DUN/2017 ze środków Ministra Nauki i Szkolnictwa Wyższego przeznaczonych na działalność upowszechniającą naukę”.



Indexed in: MEDLINE, Science Citation Index Expanded, Journal Citation Reports/Science Edition, Scopus, EMBASE/Excerpta Medica, Ulrich's™ International Periodicals Directory, Index Copernicus

Typographic design: Monika Kołęda, Piotr Gil  
DTP: Wydawnictwo UMW  
Cover: Monika Kołęda  
Printing and binding: EXDRUK



## Contents

### Original papers

- 903 Yan Zhang, Liping Qu, Huijie Ni, Yuping Wang, Lei Li, Xiaowei Yang, Xiao Wang, Yuanyuan Hou  
**Expression and function of lncRNA MALAT1 in gestational diabetes mellitus**
- 911 Hui Hu, Zongding Wang, Chunlu Tan, Xubao Liu, Hao Zhang, Kezhou Li  
**Dihydroartemisinin/miR-29b combination therapy increases the pro-apoptotic effect of dihydroartemisinin on cholangiocarcinoma cell lines by regulating Mcl-1 expression**
- 921 Maciej Bryl, Jowita Woźniak, Krzysztof Dudek, Bogdan Czapiga, Paweł Tabakow  
**The quality of life after transnasal microsurgical and endoscopic resection of nonfunctioning pituitary adenoma**
- 929 Shuyan Wang, Shishan Guo, Xiaoyan Hou  
**MicroRNA-24 inhibits CDX1 expression in decidual tissues of recurrent spontaneous abortion mice to reduce the abortion risk**
- 937 Anna Modrzyk, Michał Jerzy Pasierbek, Wojciech Korlacki, Andrzej Grabowski  
**Introducing enhanced recovery after surgery protocol in pediatric surgery**
- 943 Bożena Adamczyk, Robert Partyka, Monika Adamczyk-Sowa, Krzysztof Wierzbicki, Paweł Sowa, Danuta Kokocińska  
**Evaluation of serum human epididymis protein 4 in patients with relapsing-remitting multiple sclerosis**
- 949 Izabela Szczuka, Jerzy Wiśniewski, Irena Kustrzeba-Wójcicka, Grzegorz Terlecki  
**The effect of 3-bromopyruvate on the properties of cathepsin B in the aspect of metastatic potential of colon cancer cells**
- 959 Jixing Chen, Cuiqin Huang, Lichao Ye, Boxin Yao, Meili Yang, Qiankun Cai  
**Effect of matrine on JAK2/STAT3 signaling pathway and brain protection in rats with cerebral ischemia-reperfusion**
- 967 Bartosz Bogusz, Adam Mol, Oskar Zgraj, Wojciech Górecki  
**The application of the percutaneous suturing technique in thoracoscopic repair of congenital diaphragmatic hernia**
- 971 Ling Jin, En-Mei Liu, Xiao-Hong Xie, Ying Hu, Wei Liao  
**Comparative analysis of clinical features and risk factors of severe pneumonia development in pediatric patients hospitalized with seasonal influenza or swine-origin influenza infection**
- 979 Andrzej Żyłuk, Paweł Dec, Piotr Puchalski  
**The effect of unilateral carpal tunnel release on the non-operated contralateral hand**
- 983 Bartłomiej Kędzierski, Paweł Gać, Martyna Głośna, Rafał Poręba, Krystyna Pawlas  
**Radiation dose and repeatability of aortic valve measurement by multidetector row computed tomography to assess eligibility for transcatheter aortic valve implantation**

### Reviews

- 993 Peng Chen, Fuchao Chen, Jiexin Lei, Benhong Zhou  
**Clinical outcomes of continuous vs intermittent meropenem infusion for the treatment of sepsis: A systematic review and meta-analysis**
- 1001 Huifeng Li, Xiawei Fei, Yanting Shen, Zhenqi Wu  
**Association of gene polymorphisms of *KLK3* and prostate cancer: A meta-analysis**
- 1011 Wojciech Walas, Maria Wilińska, Monika Bekiesińska-Figatowska, Zenon Halaba, Robert Śmigiel  
**Methods for assessing the severity of perinatal asphyxia and early prognostic tools in neonates with hypoxic-ischemic encephalopathy treated with therapeutic hypothermia**



# Expression and function of lncRNA MALAT1 in gestational diabetes mellitus

\*Yan Zhang<sup>B</sup>, \*Liping Qu<sup>F</sup>, Huijie Ni<sup>F</sup>, Yuping Wang<sup>C</sup>, Lei Li<sup>D</sup>, Xiaowei Yang<sup>E</sup>, Xiao Wang<sup>A</sup>, Yuanyuan Hou<sup>A</sup>

Department of Obstetrics, Yantai Yuhuangding Hospital, China

A – research concept and design; B – collection and/or assembly of data; C – data analysis and interpretation; D – writing the article; E – critical revision of the article; F – final approval of the article

Advances in Clinical and Experimental Medicine, ISSN 1899–5276 (print), ISSN 2451–2680 (online)

*Adv Clin Exp Med.* 2020;29(8):903–910

## Address for correspondence

Yuanyuan Hou  
E-mail: vslkpqbifefkl@sina.com

## Funding sources

None declared

## Conflict of interest

None declared

\*Yan Zhang and Liping Qu contributed equally to this work.

Received on October 22, 2018  
Reviewed on January 24, 2019  
Accepted on April 30, 2020

Published online on August 12, 2020

## Abstract

**Background.** Gestational diabetes mellitus (GDM) severely threatens maternal and fetal health. Long non-coding RNA (lncRNA) participates in the regulation of various cellular processes.

**Objectives.** Previous studies have identified the role of lncRNA MALAT1 in diabetic retinopathy-related inflammation. However, the role of lncRNA MALAT1 in GDM has not been reported yet.

**Material and methods.** Real-time polymerase chain reaction (RT-PCR) was used to measure the lncRNA MALAT1 expression level in placental tissues from GDM patients and from a normal pregnant group. Placental trophoblastic-derived cell line HTR8 cells were divided into a control group, an siRNA negative control group and a MALAT1 siRNA group. The cells underwent RT-PCR analysis of lncRNA MALAT1 expression, an MTT assay of cell proliferation, and a transwell assay of cell invasion and migration. In addition, enzyme-linked immunosorbent assay (ELISA) was used to analyze the level of tumor necrosis factor  $\alpha$  (TNF- $\alpha$ ) and interleukin 6 (IL-6). Western blotting was used to measure the changes of the tumor growth factor  $\beta$  (TGF- $\beta$ )/nuclear factor-kappa B (NF- $\kappa$ B) signaling pathway.

**Results.** Gestational diabetes mellitus placental tissues showed higher lncRNA MALAT1 expression compared to a normal control group ( $p < 0.05$ ). After siRNA intervention, lncRNA MALAT1 showed decreased expression in the trophoblastic layer; inhibited trophoblastic cell proliferation, migration, or invasion; decreased the secretion of inflammatory factors TNF- $\alpha$  and IL-6; and suppressed the expression of TGF- $\beta$  and NF- $\kappa$ B compared to that of the control and siRNA-NC groups ( $p < 0.05$ ).

**Conclusions.** Gestational diabetes mellitus appears to upregulate lncRNA MALAT1. Downregulation of lncRNA MALAT1 inhibits inflammation and suppresses the proliferation, invasion and migration of GDM placental trophoblastic cells, possibly by modulating the TGF- $\beta$ /NF- $\kappa$ B signaling pathway.

**Key words:** gestational diabetes mellitus, lncRNA MALAT1, TGF- $\beta$ /NF- $\kappa$ B signal pathway, cell proliferation, cell migration

## Cite as

Zhang Y, Qu L, Ni H, et al. Expression and function of lncRNA MALAT1 in gestational diabetes mellitus. *Adv Clin Exp Med.* 2020;29(8):903–910. doi:10.17219/acem/121524

## DOI

10.17219/acem/121524

## Copyright

© 2020 by Wrocław Medical University  
This is an article distributed under the terms of the Creative Commons Attribution 3.0 Unported (CC BY 3.0) (<https://creativecommons.org/licenses/by/3.0/>)

## Introduction

Gestational diabetes mellitus (GDM) is frequently caused by abnormal glucose resistance or impairment during the gestational period, and mainly presents as elevated fasting blood glucose and insulin resistance, accompanied with inflammation, increased secretion of inflammatory factors and abnormal body immunity.<sup>1,2</sup> Gestational diabetes mellitus is a unique subtype of diabetes which occurs in pregnant women worldwide.<sup>3</sup> With differential incidence, European countries usually have a GDM prevalence of about 4% and China now has a GDM incidence of about 3%. With lifestyle change and more focus on gestational nutrition, GDM incidence has been continuously increasing over the years.<sup>4,5</sup> Gestational diabetes mellitus patients have elevated glucose levels and glucose catabolic disorder, caused by insulin resistance and leading to cellular glucose metabolic disorder. On the other hand, GDM can cause increased production of reactive oxygen species (ROS) and oxygen free radicals, further leading to oxidative stress and maternal/fetal injury. Elevated blood glucose during pregnancy can cause vascular disease, impair vascular endothelial proliferation and inhibit placental angiogenesis, leading to abnormal placenta blood circulation and placental abnormality caused by ischemia/hypoxia as the result of pathological changes in the placental cells.<sup>6–8</sup> In short, GDM can cause placental abruption, gestational hypertension, premature delivery, or congenital abnormality, leading to severe and long-lasting threats to maternal/fetal health.<sup>9,10</sup> Recent studies have found that long noncoding RNA (lncRNA) participates in the regulation of various cellular processes. For example, lncRNA MALAT1 has been shown to play roles in diabetic retinopathy and related inflammation.<sup>11</sup> However, whether lncRNA MALAT1 plays a role in the development and pathogenesis of GDM remains poorly understood. In the present study, we aimed to uncover the role of lncRNA MALAT1 in GDM and to provide a theory for a novel therapeutic target in the treatment of GDM.

## Material and methods

### Research subject recruitment

A total of 78 women with a confirmed diagnosis of GDM in Yantai Yuhuangding Hospital (China) between June 2016 and December 2017 were selected for the study. All GDM patients were diagnosed with an oral glucose tolerance test (OGTT) from gestation weeks 24 to 28. All patients matched the diagnosis criteria of GDM as stipulated by the World Health Organization (WHO) in 2013.<sup>9</sup>

The exclusive criteria included<sup>10</sup> multiple pregnancy; incompatibility of maternal and fetal blood types; history of surgical operations (including laparoscopic surgery, open surgery and keyhole surgery); complications such as inflammation, malignant tumor, severe diabetes, organ failure, systemic immune disorder, or malignant tumor complications. Furthermore, women who were receiving chemotherapy or radiotherapy or had other gestational complications – such as hypertension, exposure to toxic substances during pregnancy, or an abnormal placental or umbilical cord – were also excluded from the study. A cohort of 38 normal pregnant women was recruited as the normal control group. Informed consent was obtained from all participants prior to the study. This study has been approved by the ethical committee of Yantai Yuhuangding Hospital (China). All placental samples were collected from the maternal side of the placenta after delivery. Small tissue cubes were collected and kept in cryopreserved tubes in liquid nitrogen.

### Major equipment and reagents

Placental trophoblastic derived cell line HTR8 was purchased from ATCC (CRL-3271; Manassas, USA). An RNA extraction kit and reverse transcription kit were purchased from R&D Systems, Inc. (Minneapolis, USA). Other common reagents were purchased from Sangon Biotech (Shanghai, China). Real-time polymerase chain reaction (RT-PCR) reagent was purchased from Thermo Fisher (Waltham, USA). Dulbecco's modified Eagle's medium (DMEM), fetal bovine serum (FBS) and penicillin-streptomycin were purchased from Hyclone (Chicago, USA). Dimethyl sulfoxide (DMSO) and MTT powder were purchased from Gibco (Waltham, USA). Trypsin-EDTA digestion buffer was purchased from Hyclone. Western blot reagents were purchased from Beyotime (Haimen, China). Enhanced chemiluminescence (ECL) reagent was purchased from Amersham Biosciences (Little Chalfont, UK). Rabbit anti-human nuclear factor-kappa B (NF- $\kappa$ B) monoclonal antibody, rabbit anti-human tumor growth factor  $\beta$  (TGF- $\beta$ ) monoclonal antibody, and mouse anti-rabbit horseradish peroxidase (HRP)-conjugated IgG secondary antibody were purchased from Cell Signaling Technology (Leiden, the Netherlands). Enzyme-linked immunosorbent assay (ELISA) kits for measuring the level of tumor necrosis factor  $\alpha$  (TNF- $\alpha$ ) and interleukin 6 (IL-6) were purchased from Cell Signaling Technology. siRNA was synthesized by Gimma Gene (Shanghai, China). A transwell chamber was purchased from Corning (New York, USA). A RT-PCR cyclor was purchased from Applied Biosystems (Waltham, USA). A Gene Amp PCR System 2400 DNA amplification cyclor was purchased from Perkin Elmer (Waltham, USA). A 371 CO<sub>2</sub> cell incubator was purchased from Thermo Fisher.

## HTR8 cell culture and grouping

An HTR8 cell line kept in liquid nitrogen was resuscitated and cultured for passage. Cells in log-growth phase at generations 3–8 were used for assays. The HTR8 cells were kept in 90% high-glucose (25 mmol/L) complete medium plus 10% FBS for attached growth. The cells were then randomly assigned into 3 groups: a control group, which was cultured under normal conditions; an siRNA-NC group that was transfected with lncRNA MALAT1 negative control (NC) plasmid; and an siRNA group which received lncRNA MALAT1 siRNA transfection.

## Liposome transfection of lncRNA MALAT1 siRNA into HTR8 cells

HTR8 cells were transfected with lncRNA MALAT1 siRNA or siRNA-NC. The sequence for lncRNA MALAT1 siRNA was 5'-GAGGA GUGCA GUUCU UCA-3', and the sequence for siRNA-NC was 5'-GACAG UGUGA UUCUA-3'. The cells were seeded into 6-well plates and cultured until 70–80% confluence was reached. Plasmid for lncRNA MALAT1 siRNA or NC control was added into 200  $\mu$ L of serum-free DMEM for 15 min at room temperature for incubation, which was added into a dilution buffer along with Lipo2000 reagent and incubated for 30 min at room temperature. Serum was removed from the culture medium, and the cells were rinsed gently in PBS. Another 1.6 mL of serum-free DMEM was added into the system, and the cells were incubated in a chamber at 37°C with 5% CO<sub>2</sub> for 6 h. Serum-containing DMEM medium was then used for 48-hour continuous incubation for the assays.

## RT-PCR for lncRNA MALAT1 in GDM placental tissues and HTR8 cells

Trizol reagent was used to extract total RNA from the placental tissues of GDM patients or normal placental tissues, or from HTR8 cells in all groups. The RNA was then reverse transcribed into cDNA according to the instructions of the test kit. The primers were designed using PrimerPremier v. 6.0 (Premier Biosoft, San Francisco, USA) based on the target gene sequence, and they were synthesized by Invitrogen (Carlsbad, USA), as shown in Table 1. Real-time PCR was performed on the target genes under the following conditions: 55°C for 1 min, followed by 35 cycles consisting of 92°C for 30 s, 58–60°C for 45 s, and 72°C for 45 s. Data was collected to calculate the threshold

cycle (Ct) values of all samples and standard samples using fluorescent quantification. Based on the CT values of the standard samples, the standard curve was plotted and semi-quantitative analysis was performed using the 2<sup>-ΔCt</sup> method.

## MTT assay for cell proliferation of all groups

HTR8 cells in the log-growth phase were inoculated into 96-well plates using DMEM medium with 10% FBS at a density of 5 × 10<sup>3</sup>/well. After 24 h of incubation, the supernatant was discarded and all wells were filled with 20  $\mu$ L of sterile MTT. Three replicated wells were performed at each time point. After 4 h of continuous incubation, the supernatant was discarded and 150  $\mu$ L of DMSO was added into each well for 10 min of vortex mixing. After complete resolution of violet crystals, absorbance (A) values were measured at a wavelength of 570 nm under a microplate reader in order to calculate the proliferation rate of all groups.

## Transwell chamber assay for measuring invasion from all groups of cells

A transwell invasion assay was performed according to the instruction manual. Serum-free medium was used. After 24 h, the transwell chamber was pre-coated with 1:5 50 mg/L Matrigel dilution buffer on the chamber bottom and the upper phase of the membrane, and the chamber was air-dried at 4°C. The interior of the chamber was filled with 500  $\mu$ L of DMEM containing 10% FBS, and the exterior was filled with 100  $\mu$ L of serum-free medium with the prepared cell suspensions. Three replicated wells were used for each group. Transwell chambers were placed into a 24-well plate. A Matrigel-free chamber was employed for incubation of the control group. After 48 h, the transwell chamber was rinsed in PBS, and the cells on the membrane were removed. The chamber was fixed with iced ethanol and stained with crystal violet. Cells at the lower phase of the membrane were enumerated and the experiment was repeated 3 times.

## Transwell chamber for cell migration

The cell migration of all groups of cells was measured in serum-free medium using the transwell chamber according to the instructions of the test kit.

Table 1. Primer sequence

Gene	Forward primer 5'-3'	Reverse primer 5'-3'
GAPDH	AGTAGTCACCTGTTGCTGG	TAATACGGAGACCTGTCTGGT
lncRNA MALAT1	A CTTACATGTCTGCC TTGG	TCAAAGCTGGTACAGCCA

## Western blot for TGF- $\beta$ /NF- $\kappa$ B signal pathway activity

Total proteins were extracted from all groups of HTR8 cells. In brief, lysis buffer was added and proteins were quantified using the Bradford method at  $-20^{\circ}\text{C}$  storage for western blot. The proteins were separated using 10% SDS-PAGE and transferred to the NC membrane at 100 mA for 1.5 h. Primary antibody (TGF- $\beta$  diluted to 1:2000 and NF- $\kappa$ B monoclonal antibody diluted to 1:2000) was added for overnight incubation at  $4^{\circ}\text{C}$ . The following day, the membrane was rinsed in phosphate-buffered saline with Tween (PBST) and was incubated in goat anti-rabbit secondary antibody diluted to 1:2000 for 30 min at room temperature in the dark. After PBST rinsing, ECL substrate was added for development for 1 min, followed by X-ray exposure. Protein imaging software and Quantity One software (Bio-Rad, Hercules, USA) were used to scan the X-ray film and measure the band density. All experiments were repeated 4 times ( $n = 4$ ) for statistical analysis.

## ELISA for inflammatory cytokine expression in cell culture supernatant

All samples were measured by the expression of inflammatory cytokines TNF- $\alpha$  and IL-6 in the supernatant from the cell cultures using ELISA kits and following the test kit manuals. In brief, a 96-well plate was filled with 50- $\mu\text{L}$  serially diluted standard samples to prepare the standard curve. Fifty-microliter test samples were added to the wells in triplicate. The plate was then washed and dried. Each well was filled with dilution buffer for washing in a vortex for 30 s. Each well then had 50  $\mu\text{L}$  of enzyme-labelled reagent added to it, except for the blank control well. After gentle mixing and incubation at  $37^{\circ}\text{C}$  for 30 min, the plate was rinsed 5 times. Chromogenic substrate A and B (50  $\mu\text{L}$  each) were subsequently added into each well for gentle mixing and  $37^{\circ}\text{C}$  incubation for 10 min. Fifty microliters of quenching buffer was added into each well in order to stop the reaction. The optical density (OD) values of each well were measured at a wavelength of 450 nm using a microplate reader.

## Statistical processing

SPSS v. 16.0 (SPSS Inc., Chicago, USA) software was used for statistical analysis. The measurements are presented as means  $\pm$  standard deviation (SD). One-way analysis of variance (ANOVA) was used for comparisons of the means among multiple groups. Statistically significant values were recognized when  $p < 0.05$ .

## Results

### Characteristics of patients and controls

All patients were aged between 22 and 41 years (average age:  $27 \pm 5.2$  years) with a body mass index (BMI) of  $24.5 \pm 3.2$ . The controls – 38 normal pregnant women – were aged between 21 and 42 years (average age:  $26 \pm 5.1$  years) and had a BMI of  $25.1 \pm 4.6$ . No significant differences were observed regarding age or BMI between the control and GDM groups.

### Expression of lncRNA MALAT1 in GDM

Real-time PCR was used to measure the expression of lncRNA MALAT1 in GDM, which showed that it was significantly higher in placental tissues than in normal pregnant placentas ( $p < 0.05$ ; Fig. 1).

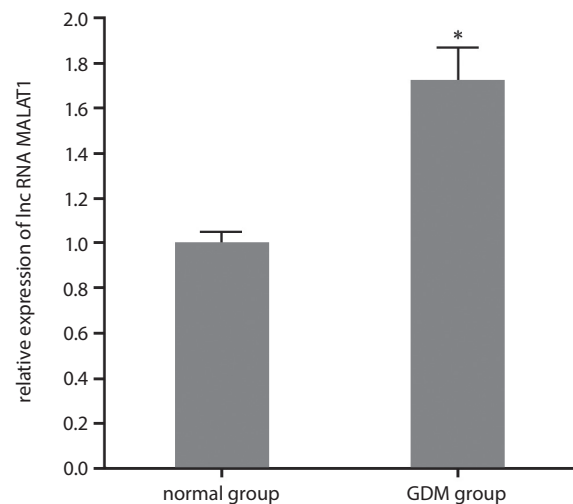


Fig. 1. Expression of lncRNA MALAT1 in GDM

\* $p < 0.05$  compared to the control group.

### Effects of siRNA transfection on the expression of lncRNA MALAT1 in trophoblastic cell HTR8

Compared to the control group and the siRNA-NC group, the HTR8 cells had significantly decreased expression of lncRNA MALAT1 thanks to transfection of lncRNA MALAT1 siRNA ( $p < 0.05$ ; Fig. 2).

### Effects of lncRNA MALAT1 knockdown on HTR8 cell proliferation

To investigate the effect of lncRNA MALAT1 on the proliferation of trophoblastic HTR8 cells, we performed an MTT assay and found that the transfection of lncRNA MALAT1 siRNA for 48 h significantly suppressed the proliferation of HTR8 cells in comparison to the control group ( $p < 0.05$ ; Fig. 3), indicating that downregulation of lncRNA MALAT1 could inhibit HTR8 cell proliferation.



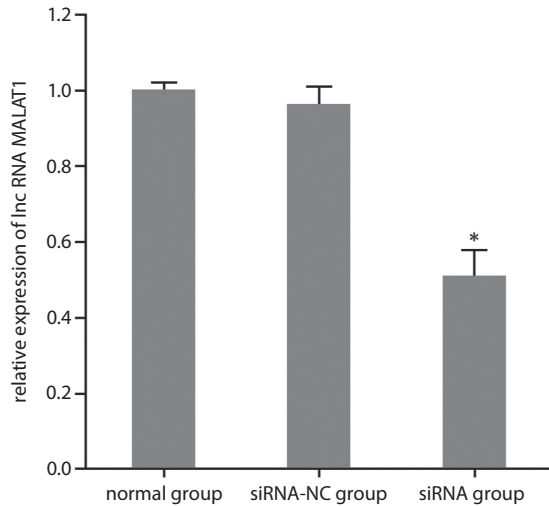


Fig. 2. Expression of lncRNA MALAT1 in trophoblastic cell line HTR8  
\*p < 0.05 compared to the control group.

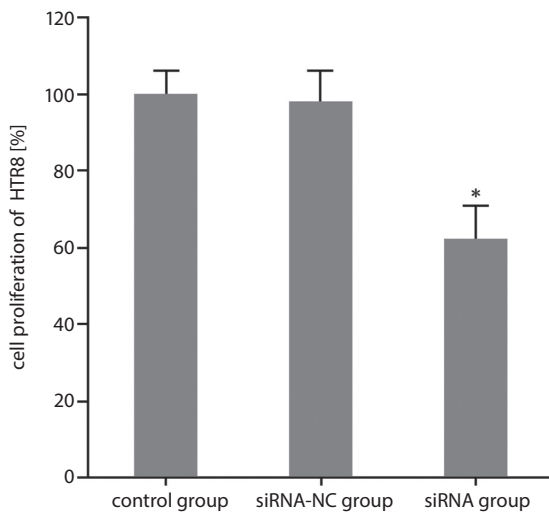


Fig. 3. Effects of lncRNA MALAT1 knockdown on the proliferation of trophoblast cell line HTR8  
\*p < 0.05 compared to the control group.

### Effect of lncRNA MALAT1 knockdown on migration of trophoblast HTR8 cells

We next investigated the effect of lncRNA MALAT1 on the migration of trophoblastic HTR8 cell using a transwell assay and found that transfection of lncRNA MALAT1 siRNA for 48 h significantly inhibited the migration of HTR8 cells when compared to the control group (p < 0.05; Fig. 4).

### Effects of lncRNA MALAT1 knockdown on invasion of trophoblast HTR8 cell

We also used the transwell approach to analyze the effect of lncRNA MALAT1 knockdown on the invasion of trophoblastic cell line HTR8 and found that the transfection of lncRNA MALAT1 siRNA significantly inhibited invasion of HTR8 cells after 48 h compared to the control group (p < 0.05; Fig. 5).

### Effects of lncRNA MALAT1 knockdown on inflammatory cytokine expression in the supernatant of trophoblastic cell line HTR8

The ELISA approach was used to measure the expression of inflammatory cytokines in the supernatant of trophoblastic cell line HTR8 and demonstrated that transfection of lncRNA MALAT1 siRNA for 48 h significantly inhibited TNF-α and IL-6 secretion from HTR8 cells in comparison with the control group (p < 0.05; Fig. 6).

### Effects of lncRNA MALAT1 knockdown on the TGF-β/NF-κB signaling pathway

Western blot was performed to observe the effect of lncRNA MALAT1 knockdown on the TGF-β/NF-κB signaling pathway in trophoblastic cell line HTR8. It revealed that the transfection of lncRNA MALAT1 siRNA significantly reduced the expression of TGF-β and NF-κB when compared to the control group (p < 0.05; Fig. 7).

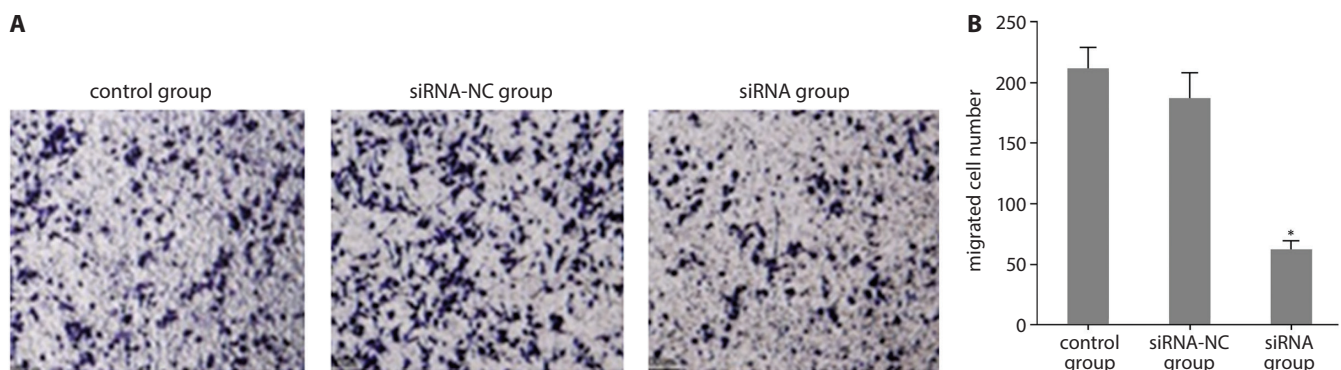
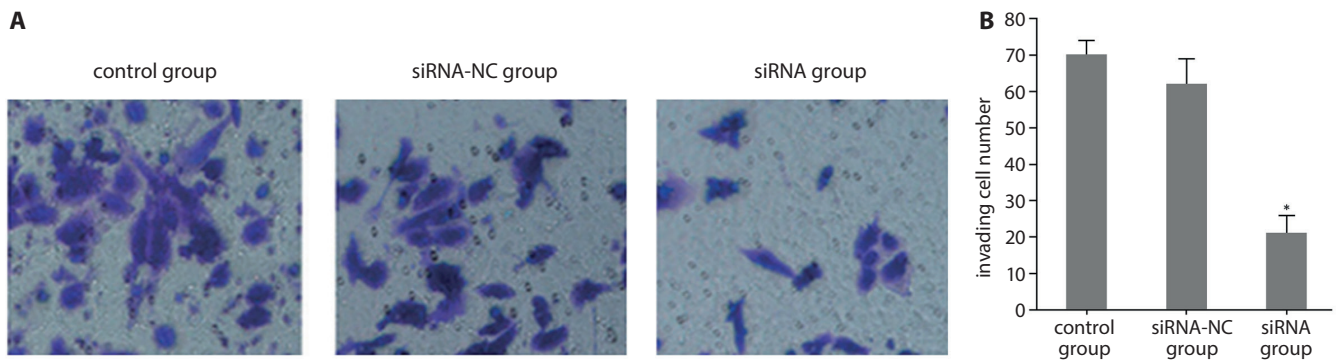


Fig. 4. Effects of lncRNA MALAT1 knockdown on trophoblastic cell HTR8 migration. A. Transwell assay for analyzing the effect of lncRNA MALAT1 knockdown on HTR8 cell migration. B. Analysis for HTR8 cell migration

\*p < 0.05 compared to the control group.



**Fig. 5.** Effects of lncRNA MALAT1 knockdown on invasion of trophoblast cell HTR8. **A.** Transwell chamber assay for analyzing the effect of lncRNA MALAT1 knockdown on HTR8 cell invasion. **B.** Statistical analysis for HTR8 cell invasion

\* $p < 0.05$  compared to the control group.

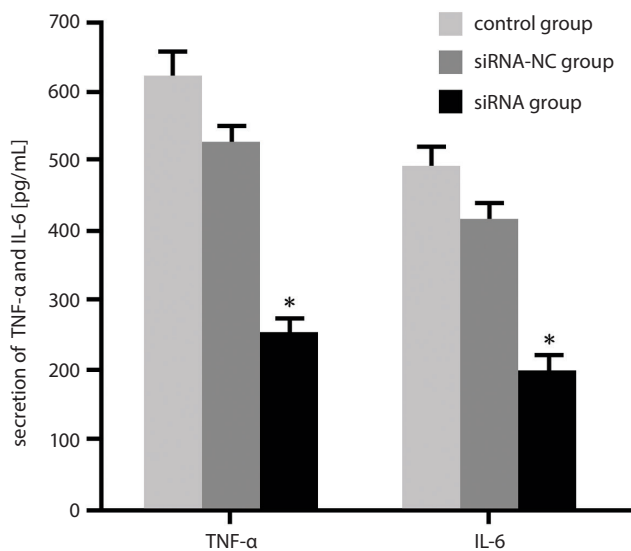


**Fig. 6.** Effect of lncRNA MALAT1 knockdown on inflammatory cytokine factor of trophoblastic cell line HTR8

\* $p < 0.05$  compared to the control group.

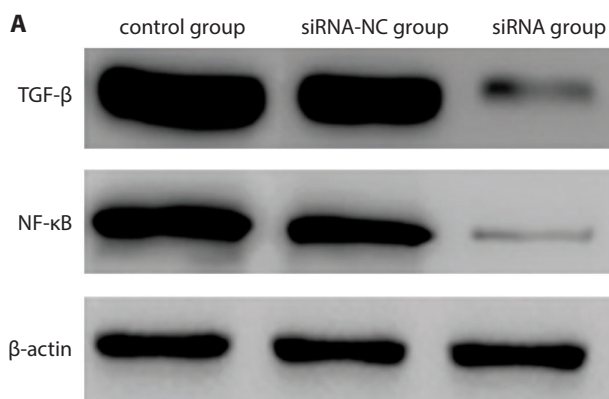
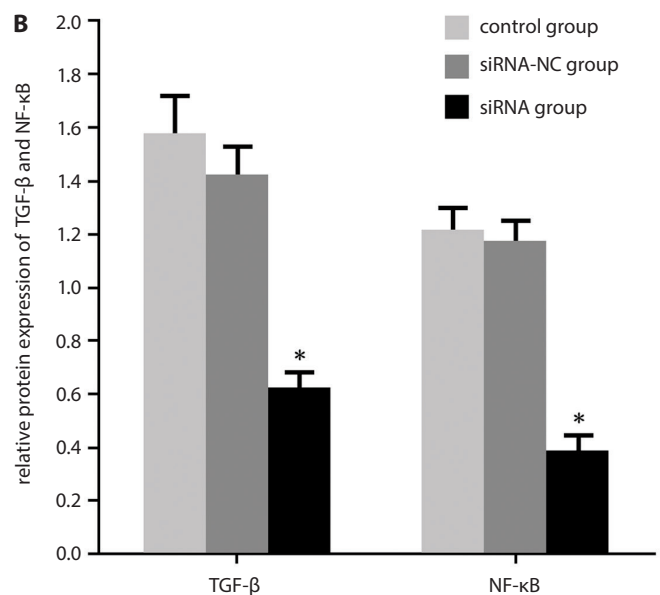


**Fig. 7.** Effect of lncRNA MALAT1 knockdown on the TGF-β/NF-κB signaling pathway in trophoblastic HTR8 cells. **A.** Western blot for the effect of lncRNA MALAT1 knockdown on the TGF-β/NF-κB signaling pathway in trophoblastic cell line HTR. **B.** Statistical analysis for the TGF-β/NF-κB signaling pathway

\* $p < 0.05$  compared to the control group.

## Discussion

Long non-coding RNA was discovered several years ago.<sup>12</sup> Large amounts of non-coding RNA transcripts have been found in eukaryotes and they occupy the majority of the human genome.<sup>13,14</sup> Long non-coding RNA refers to those transcripts longer than 200 nt. Due to the irrelevance to protein coding, lncRNA was initially recognized as “background noise” of gene transcription without any biological function. However, through deeper studies, lncRNA has been found to regulate and participate in gene expression regulation at the epigenetic, transcriptional and post-transcriptional levels.<sup>15</sup> Long non-coding RNA can regulate various physiological events at the genetic level, including chromatin modification, genomic imprinting, nuclear trafficking, chromosomal gene silencing, and transcriptional activation.<sup>16</sup> In addition, lncRNA can regulate both physiological and pathological conditions of cells, including growth, proliferation, cell cycle, and cell apoptosis, making it a critical regulatory factor





for human disease onset and progression.<sup>17</sup> However, few studies have been performed regarding its role in GDM. In diabetes, lncRNA MALAT1 has been found to be abnormally expressed,<sup>11</sup> though the exact role and function of lncRNA MALAT1 in GDM remains poorly understood. This study aimed to investigate the expression of lncRNA MALAT1 in GDM placental tissues. Its expression was found to be upregulated in GDM, indicating that it might be involved in GDM pathogenesis and may affect maternal/fetal health.

We further analyzed the role of lncRNA MALAT1 in GDM and its functional mechanism. As the only maternal–fetal interface and the site for exchange of substances, the placenta is critical for maintaining and protecting normal fetal development.<sup>18</sup> The placenta can provide a route for the transportation of nutrients between maternal and fetal bodies, and it is an important organ for gas exchange, blood circulation and endocrine function. The placenta is also important for investigating glucose metabolism and endocrine disease.<sup>19,20</sup> This study thus selected placental trophoblastic cell line HTR8, which was cultured under a high-glucose environment to mimic the conditions of the GDM placental trophoblastic layer. To investigate the role and function of lncRNA MALAT1 in GDM, we transfected lncRNA MALAT1 siRNA into placental trophoblastic cell HTR8 under high-glucose conditions and found that lncRNA MALAT1 downregulation in placental trophoblastic HTR8 cells under high-glucose conditions inhibited the proliferation, migration and invasion potency of HTR8 cells. These results indicate that lncRNA MALAT1 might affect placental functions in GDM by regulating the biological behaviors of placental trophoblastic cells. On the other hand, pro-inflammation in GDM frequently leads to disease progression and body immune disorder.<sup>21</sup> This study also demonstrated that lncRNA MALAT1 downregulation can inhibit inflammation, possibly by suppressing the secretion of inflammatory factors. The TGF- $\beta$ /NF- $\kappa$ B signaling pathway has been demonstrated to play a role in transcriptional regulation, it is closely related with cell ontogenesis, invasion and metastasis, it can regulate the cytokine network, and it is closely correlated with GDM pathogenesis.<sup>22</sup> The findings of this study are consistent with this, showing that the downregulation of lncRNA MALAT1 inhibited the TGF- $\beta$ /NF- $\kappa$ B signaling pathway, suggesting that lncRNA MALAT1 affects the biological behaviors of HTR8 cells, possibly through regulating the TGF- $\beta$ /NF- $\kappa$ B signaling pathway. However, the exact mechanism by which lncRNA MALAT1 regulates the TGF- $\beta$ /NF- $\kappa$ B signaling pathway remains unclear. In addition, the exact molecular mechanism by which lncRNA MALAT1 is involved in the pathogenesis of GDM remains poorly understood. Future studies are required to investigate these issues in order to provide more evidence for GDM pathogenesis and clinical treatment.

## Conclusions

The GDM patients present upregulation of lncRNA MALAT1. Downregulation of lncRNA MALAT1 inhibits the proliferation, invasion and migration of GDM placental trophoblastic cells, possibly by modulating the TGF- $\beta$ /NF- $\kappa$ B signaling pathway.

### ORCID iDs

Yan Zhang  <https://orcid.org/0000-0002-7929-8369>  
 Liping Qu  <https://orcid.org/0000-0002-8413-1838>  
 Huijie Ni  <https://orcid.org/0000-0003-0537-0513>  
 Yuping Wang  <https://orcid.org/0000-0003-4583-4634>  
 Lei Li  <https://orcid.org/0000-0002-4456-2983>  
 Xiaowei Yang  <https://orcid.org/0000-0002-0841-7703>  
 Xiao Wang  <https://orcid.org/0000-0002-5474-3411>  
 Yuanyuan Hou  <https://orcid.org/0000-0002-5925-3702>

### References

- Riaz SH, Khan MS, Jawa A, Hassan M, Akram J. Lack of uniformity in screening, diagnosis and management of gestational diabetes mellitus among health practitioners across major cities of Pakistan. *Pak J Med Sci.* 2018;34(2):300–304.
- Kashyap H, Sharma D, Gala A, Tejo Pratap O, Murki S. Effect of second trimester and third trimester weight gain on immediate outcomes in neonates born to mothers with gestational diabetes: A retrospective observational study from India. *J Matern Fetal Neonatal Med.* 2019;32(24):4133–4138.
- Carroll X, Liang X, Zhang W, et al. Socioeconomic, environmental and lifestyle factors associated with gestational diabetes mellitus: A matched case-control study in Beijing, China. *Sci Rep.* 2018;8(1):8103.
- Beyerlein A, Lack N, von Kries R. No further improvement in pregnancy-related outcomes in the offspring of mothers with pre-gestational diabetes in Bavaria, Germany, between 2001 and 2016. *Diabet Med.* 2018;35(10):1420–1424.
- Zhou JL, Xing J, Liu CH, et al. Effects of abnormal 75 g oral glucose tolerance test at different time points on neonatal complications and neurobehavioral development in the pregnant women with gestational diabetes mellitus (a STROBE-compliant article). *Medicine (Baltimore).* 2018;97(21):e10743.
- Rotem R, Fishman B, Daniel S, Koren G, Lunenfeld E, Levy A. Risk of major congenital malformations following first trimester exposure to vaginal azoles used for treating vulvovaginal candidiasis: A population-based retrospective cohort study. *BJOG.* 2018;125(12):1550–1556.
- Looman M, Schoenaker D, Soedamah-Muthu SS, Geelen A, Feskens EJM, Mishra GD. Pre-pregnancy dietary carbohydrate quantity and quality, and risk of developing gestational diabetes: The Australian Longitudinal Study on Women's Health. *Br J Nutr.* 2018;120(4):435–444.
- Kim M, Park J, Kim SH, et al. The trends and risk factors to predict adverse outcomes in gestational diabetes mellitus: A 10-year experience from 2006 to 2015 in a single tertiary center. *Obstet Gynecol Sci.* 2018;61(3):309–318.
- Garmendia ML, Corvalan C, Casanella P, et al. Effectiveness on maternal and offspring metabolic control of a home-based dietary counseling intervention and DHA supplementation in obese/overweight pregnant women (MIGHT study): A randomized controlled trial – study protocol. *Contemp Clin Trials.* 2018;70:35–40.
- Reece SW, Parihar HS, Martinez M. Retrospective review of maternal and fetal outcomes in patients with gestational diabetes mellitus in an indigent prenatal clinic. *Diabetes Spectr.* 2018;31(2):200–205.
- Biswas S, Thomas AA, Chen S, et al. MALAT1: An epigenetic regulator of inflammation in diabetic retinopathy. *Sci Rep.* 2018;8(1):6526.
- Ye H, Liu K, Qian K. Overexpression of long noncoding RNA HOTTIP promotes tumor invasion and predicts poor prognosis in gastric cancer. *Oncotargets Ther.* 2016;9:2081–2088.
- Wang SH, Wu XC, Zhang MD, Weng MZ, Zhou D, Quan ZW. Upregulation of H19 indicates a poor prognosis in gallbladder carcinoma and promotes epithelial-mesenchymal transition. *Am J Cancer Res.* 2016;6(1):15–26.

14. Zhang SR, Yang JK, Xie JK, Zhao LC. Long noncoding RNA HOTTIP contributes to the progression of prostate cancer by regulating HOXA13. *Cell Mol Biol (Noisy-le-grand)*. 2016;62(3):84–88.
15. Chang L, Qi H, Xiao Y, et al. Integrated analysis of noncoding RNAs and mRNAs reveals their potential roles in the biological activities of the growth hormone receptor. *Growth Horm IGF Res*. 2016;29:11–20.
16. Li P, Zhang G, Li J, et al. Long noncoding RNA RGMB-AS1 indicates a poor prognosis and modulates cell proliferation, migration and invasion in lung adenocarcinoma. *PLoS One*. 2016;11(3):e0150790.
17. Zhang H, Cai Y, Zheng L, Zhang Z, Lin X, Jiang N. Long noncoding RNA NEAT1 regulate papillary thyroid cancer progression by modulating miR-129-5p/KLK7 expression. *J Cell Physiol*. 2018;233(10):6638–6648.
18. Chen H, Zhou X, Han TL, Baker PN, Qi H, Zhang H. Decreased IL-33 production contributes to trophoblast cell dysfunction in pregnancies with preeclampsia. *Mediators Inflamm*. 2018;2018:9787239.
19. Deng Q, Liu X, Yang Z, Xie L. Expression of N-acetylglucosaminyltransferase III promotes trophoblast invasion and migration in early human placenta. *Reprod Sci*. 2018;26(10):1373–1381.
20. Peng HY, Li MQ, Li HP. High glucose suppresses the viability and proliferation of HTR8/SVneo cells through regulation of the miR137/PRKAA1/IL6 axis. *Int J Mol Med*. 2018;42(2):799–810.
21. Chow JY, Ban M, Wu HL, et al. TGF-beta downregulates PTEN via activation of NF-kappaB in pancreatic cancer cells. *Am J Physiol Gastrointest Liver Physiol*. 2010;298(2):G275–G282.
22. Sriramula S, Francis J. Tumor necrosis factor alpha is essential for angiotensin II-induced ventricular remodeling: Role for oxidative stress. *PLoS One*. 2015;10(9):e0138372.

# Dihydroartemisinin/*miR-29b* combination therapy increases the pro-apoptotic effect of dihydroartemisinin on cholangiocarcinoma cell lines by regulating Mcl-1 expression

Hui Hu<sup>1,A,D</sup>, Zongding Wang<sup>2,B</sup>, Chunlu Tan<sup>3,C,E</sup>, Xubao Liu<sup>3,A,D</sup>, Hao Zhang<sup>3,A,E</sup>, Kezhou Li<sup>3,A,F</sup>

<sup>1</sup> Department of Traumatology, Central Hospital of Chongqing University, Chongqing Emergency Medical Center, China

<sup>2</sup> Department of General Surgery, Peoples's Hospital of Fengjie, Chongqing, China

<sup>3</sup> Departments of Pancreatic Surgery, West China Hospital, Sichuan University, Chengdu, China

A – research concept and design; B – collection and/or assembly of data; C – data analysis and interpretation;

D – writing the article; E – critical revision of the article; F – final approval of the article

Advances in Clinical and Experimental Medicine, ISSN 1899–5276 (print), ISSN 2451–2680 (online)

Adv Clin Exp Med. 2020;29(8):911–919

## Address for correspondence

Kezhou Li

E-mail: likezhou11@126.com

## Funding sources

None declared

## Conflict of interest

None declared

Received on July 29, 2018

Reviewed on November 25, 2018

Accepted on May 1, 2020

Published online on August 13, 2020

## Cite as

Li K, Hu H, Wang Z, Tan C, Liu X, Zhang H. Dihydroartemisinin/*miR-29b* combination therapy increases the pro-apoptotic effect of dihydroartemisinin on cholangiocarcinoma cell lines by regulating Mcl-1 expression. *Adv Clin Exp Med.* 2020;29(8):911–919. doi:10.17219/acem/121919

## DOI

10.17219/acem/121919

## Copyright

© 2020 by Wrocław Medical University

This is an article distributed under the terms of the Creative Commons Attribution 3.0 Unported (CC BY 3.0) (<https://creativecommons.org/licenses/by/3.0/>)

## Abstract

**Background.** Cholangiocarcinoma is a malignant tumor that originates from the neoplastic transformation of bile duct epithelial cells.

**Objectives.** To investigate the role of DHA and *miR-29b* on the proliferation and apoptosis of cholangiocarcinoma cells, and to explore whether DHA exerted its role through the *miR-29b*/Mcl-1 signaling pathway.

**Material and methods.** Human cholangiocarcinoma cell lines HUCCT-1 and FRH201 were treated with dihydroartemisinin (DHA) and DHA+*miR-29b*. The inhibitory effects of DHA and *miR-29b* on proliferation were detected using MTT assay. The effects of DHA and *miR-29b* on apoptosis were detected using flow cytometry (FCM). The mRNA and protein expressions of Mcl-1L and Mcl-1S were evaluated with reverse transcriptase polymerase chain reaction (RT-PCR) and western blotting, respectively.

**Results.** The DHA increased *miR-29b* expression in HUCCT-1 and FRH201 cells. The MTT assay showed that DHA+*miR-29b* combination therapy promoted the inhibition effects on the proliferation of HUCCT-1 and FRH201 cells. The FCM results revealed that DHA and *miR-29b* combination therapy increased the apoptosis of HUCCT-1 and FRH201 cells. The RT-PCR and western blotting analysis found that DHA+*miR-29b* combination therapy significantly decreased Mcl-1L expression and increased Mcl-1S expression in both HUCCT-1 and FRH201 cells. The Mcl-1S:Mcl-1L ratio was notably higher in the DHA+*miR-29b* combination therapy group than in the control group and DHA therapy group, in both HUCCT-1 and FRH201 cells.

**Conclusions.** The DHA and *miR-29b* have a pro-apoptotic effect on cholangiocarcinoma cells through the DHA/*miR-29b*/Mcl-1 pathway, possibly by upregulating the expression of the pro-apoptotic protein Mcl-1S and thus increasing the proportion of Mcl-1S protein among the total amount of Mcl-1 protein.

**Key words:** cholangiocarcinoma, *miR-29b*, dihydroartemisinin, Mcl-1

## Introduction

Cholangiocarcinoma is a malignant tumor that originates from the neoplastic transformation of bile duct epithelial cells, with a particularly high prevalence in Eastern Asia.<sup>1</sup> The malignancy is usually diagnosed at an advanced stage and is already inoperable; compared with other gastrointestinal tumors, it has a poorer response to chemotherapy.<sup>2</sup> While no major advance has been made in investigating pathogenesis and establishing therapy of cholangiocarcinoma, the anti-tumor activity of dihydroartemisinin (DHA) has been widely recognized.<sup>3,4</sup> Compared with artemisinin, dihydroartemisinin is more water-soluble, more absorbable and more effective against malaria.<sup>5–7</sup> A recent study has demonstrated that DHA can promote apoptosis of tumor cells by changing cell autophagy.<sup>8,9</sup>

The protein product encoded by *Mcl-1* is a member of the *Bcl-2* anti-apoptosis gene family. After transcription, this gene can produce a variety of transcripts through different splicing approaches. Specifically, the longest transcript-encoded gene product, myeloid cell leukemia *Mcl-1L*, can improve cell survival by inhibiting apoptosis, while the shorter gene product, *Mcl-1S*, has a pro-apoptotic effect and induces cell death.<sup>10,11</sup> The miRNAs are a class of single-strand, noncoding small RNA molecules (19–25 nucleotides) which play a critical role in various processes, including cell growth, tissue differentiation, and the development and progression of malignant tumors.<sup>12,13</sup> By complete or incomplete complementary pairing with the mRNA 3' untranslated region (UTR) of target genes, they can inhibit or block the translation of target genes without affecting mRNA stability. Abnormal *miR-29b* expression is often closely associated with abnormal apoptotic signaling pathways of tumor cells. The overexpression of *miR-29b* in cells results in a decreased *Mcl-1* protein expression. Also, *miR-29b* expression is elevated in normal immortalized bile duct cells and decreased in malignant cholangiocarcinoma cell lines.<sup>14,15</sup> The regulation of endogenous miRNA (e.g., *miR-29*) may provide a new treatment for cholangiocarcinoma.<sup>14,15</sup> In our previous study, we found that DHA affected the expression of the apoptosis-associated protein *Md-1* through multiple mechanisms, and that DHA therapy increased the *Mcl-1S*:*Mcl-1L* protein ratio, thus inducing apoptosis in cholangiocarcinoma cells (QBC939).<sup>16</sup> HUCCT-1 and FRH0201 cell lines are also classic cholangiocarcinoma cell lines. In order to exclude cell specificity, these 2 cell lines were used in this study.

In the current study, we observed the effects of DHA therapy and DHA+*miR-29b* combination therapy on human cholangiocarcinoma cell lines HUCCT-1 and FRH0201, observed their effects on *Mcl-1* expression, explored whether DHA exerted its role through the *miR-29b*/*Mcl-1* signaling pathway, and investigated the potential role of DHA+*miR-29b* combination therapy in cholangiocarcinoma.

## Material and methods

### Cell lines and main reagents

HUCCT-1 and FRH0201 cell lines were obtained as a courtesy of the Cell Center of Hsiang-ya Medical College, Hunan, China. The DHA was purchased from Sciphar Biotechnology Co. Ltd. (Xian, China). Tetrazolium salt MTT (3-[4,5-dimethylthiazol-2-yl]-2,5-diphenyl tetrazolium bromide), dimethyl sulfoxide (DMSO), Triton-100 and TRIzol were purchased from Sigma Chemical Co. (St. Louis, USA). The *miR-29b* and its transfection kit were purchased from Guangzhou RiboBio Co. Ltd. (Guangzhou, China). Fetal bovine serum was purchased from Zhejiang Tianhang Biological Technology Co. Ltd. (Huzhou, China). RPMI-1640 culture medium and trypsin were purchased from Gibco (Grand Island, USA). A BCA protein assay kit was purchased from Beyotime (Haimen, China). *Mcl-1* gene primers and probes were purchased from Sangon Biotech (Shanghai, China), and *Mcl-1* antibody was sourced from Bioss (Beijing, China).

### Cell culture and treatment

The HUCCT-1 and FRH0201 cell lines were cultured at 37°C in an atmosphere of 5% CO<sub>2</sub> in RPMI-1640 medium containing 10% bovine calf serum and 100 U/mL of a penicillin-streptomycin solution, as specified by the American Type Culture Collection (Manassas, USA). The cells grew adherently and were passaged every 2–3 days. During cell passage, the old culture medium was removed and the cells were washed twice with phosphate-buffered saline (PBS). After the cells were digested with 0.25% trypsin, they were centrifuged at 1,000 rpm for 7 min, re-suspended in fresh medium and seeded into tissue culture flasks. After this step, 5 nmol of lyophilized *miR-29b* RNA powder was dissolved in 250 µL of sterilized deionized distilled water to prepare 20 µM of stock solution. After the fibroblasts were at the 2<sup>nd</sup> and 3<sup>rd</sup> passages, they were subcultured and inoculated in six-well plates. After the cells were at 60–70% confluence, *miR-29b* RNA was added; the cells were then further cultured in a constant-temperature incubator (5% CO<sub>2</sub> at 37°C).

### Detection of the inhibitory effect of DHA on proliferation using an MTT assay

We performed the MTT assay in order to choose the best DHA concentration – one that would be effective and low-toxic. We found that 20 µmol/L of DHA met the requirement. The cells were divided into 3 groups: a control group, treated with 0.1% DMSO only (0 µmol/L DHA); a DHA therapy group, treated with 20 µmol/L of DHA; and a DHA+*miR-29b* combination therapy group, treated with 20 µmol/L of DHA and *miR-29b*. Six duplicate wells were set up for each group. HUCCT-1 and FRH0201 cells in the logarithmic growth phase were collected. After cell



counting, the cells were inoculated into 96-well plates and routinely cultured for 24 h (with  $10^5$  cells in 200  $\mu$ L in each well). The DHA was added to a final concentration of 20  $\mu$ mol/L for the DHA group. For the control group, an equal volume of 0.1% DMSO was added; for the 3<sup>rd</sup> group, DHA was added to a final concentration of 20  $\mu$ mol/L, together with *miR-29b* and a transfection agent. The mixture was cultured at 37°C in an environment with saturated humidity and 5% CO<sub>2</sub> for 12 h, 24 h and 48 h. Each well was treated with 20  $\mu$ L of MTT and then cultured for a further 4 h before the culture was terminated. The culture supernatant was discarded and 150  $\mu$ L of DMSO was added to each well, followed by discoloration and oscillation for 10 min, so that the crystalline material was dispersed homogeneously. Absorbance was measured spectrophotometrically at 490 nm, and the growth inhibition rate was calculated.

### Detection of apoptosis using flow cytometry and caspase 3/7 activity apoptosis assay

The harvested cells were inoculated in 25-cm<sup>2</sup> culture flasks (15 mL/well). After routine culturing for 24 h, they were grouped as described for the MTT assay, with 6 duplicate wells in each group. In the experimental group, the cells were treated with 20  $\mu$ mol/L of DHA and then cultured at 37°C in an environment with saturated humidity and 5% CO<sub>2</sub> for 12 h, 24 h and 48 h. The HUCCT-1 and FRH0201 cells were digested with 0.25% trypsin. After the mixture was suspended and centrifuged at 1,000 rpm for 5 min and the supernatant was discarded, the cells were washed twice with 0.01 mol/L of PBS. After the cells were fixed in precooled 70% ethanol at 4°C for 1 h, the mixture was centrifuged at 1,000 rpm for 5 min; then, the supernatant was discarded and the cells were washed twice with 0.01 mol/L of PBS. Add 1 mL of 0.01 mol/L PBS, followed by the addition of RNAase A and propidium iodide to a final concentration of 50  $\mu$ g/mL for the HUCCT-1 cells and 100  $\mu$ g/mL for the FRH0201 cells. Then, the mixture was stored in the dark at 4°C for 30 min. Finally, the cells were examined using flow cytometry (FCM). We also used a Caspase 3/7 Activity Apoptosis Assay Kit (E607103-0200; Sangon Biotech) to detect apoptosis by evaluating the relative fluorescence units.

### Detection of Mcl-1 mRNA expression using reverse transcriptase polymerase chain reaction (RT-PCR)

$\beta$ -actin was used as an internal control. The experimental grouping was the same as in the MTT assay. Total RNA isolation is briefly described below. In a two-milliliter tube with mechanically disrupted tissue sample, 1 mL of TRIzol was added, vortexed well, and incubated for 5 min at room temperature. Chloroform was added (0.2 mL per 1 mL of TRIzol) for homogenization. The sample was vortexed

very well and incubated for 3 min at room temperature. Then, the samples were centrifuged at maximum speed on table microcentrifuge for 5 min at +4°C. The aqueous phase was transferred to a fresh microcentrifuge 2 mL tube with an equal volume of chloroform, vortexed well and then spun at maximum speed on table microcentrifuge for 5 min. The aqueous phase was transferred to a fresh microcentrifuge two-milliliter tube with an equal volume of 2-propanol, vortexed well and then spun at maximum speed on table microcentrifuge at room temperature for 10 min at +4°C. The pellets were washed once with 1.5 mL of 70% ethanol and spun at maximum speed on table microcentrifuge for 5 min. Next, the pellets were dissolved in 400  $\mu$ L of 1  $\times$  TE at 55°C for about 10 min, with vortex. An equal volume of 10 M LiCl was added and the solution was chilled at –20°C for several hours (overnight). Afterwards, the solution was spun at maximum speed on table microcentrifuge for 10 min at +4°C. The supernatants were carefully removed and discarded. The pellets were then washed with 1.5 mL of 70% ethanol, vortexed well and micro-centrifuged, and the ethanol was discarded. Next, the pellets were dissolved in 200  $\mu$ L of fresh milliQ water. Finally, 2  $\mu$ g RNA was used for the RT-qPCR experiments.

With mRNA as the template, cDNA was synthesized using random hexamer primers. Based on the sequences of 2 transcripts of Mcl-1 in GenBank (*MCL1-001*, representing Mcl-1L, and *MCL1-002*, representing Mcl-1S), the primer and probe sequences of Mcl-1-related genes and the  $\beta$ -actin gene were designed as follows: upstream primer sequence of Mcl-1L – 5'-TTTGGCTACGGAGAAGGAGG-3'; downstream primer sequence of Mcl-1L – 5'-TTCCGAA-GCATGCCTTGGAAG-3' (597-bp sequence fragment); upstream primer sequence of Mcl-1S – 5'-CCGCTTGAGG-AGATGGAAG-3'; downstream primer sequence of Mcl-1S – 5'-CACAAACCCATCCTTGGAAG-3' (382-bp sequence fragment); upstream primer sequence of miR-29b – 5'-GT-TTCATATGGTGGTTTAGAT-3'; downstream primer sequence of miR-29b – 5'-GAACACTGATTTCAAATGGT-3' (61-bp sequence fragment); upstream primer sequence of  $\beta$ -actin – 5'-GAAGATCAAGATCATTGCTCCT-3'; downstream primer sequence of  $\beta$ -actin – 5'-TACTCC-TGCTTGCTGATCCA-3'; probe – 5'-FAM-CTGTCCACC-TTCCAGCAGA-TAMRA-3' (111-bp sequence fragment). The amplification conditions were as follows: initial denaturation at 94°C for 2 min, followed by 45 cycles of denaturation at 94°C for 20 s, annealing at 53°C for 30 s and extension at 60°C for 40 s. After the reaction was completed, Sequence Detection software v. 1.2.3 (Applied Biosystems, Foster City, USA) was used to analyze the threshold cycle (Ct) values of each sample. The specificity of PCR was judged according to the agarose gel electrophoresis and melting curves. The  $2^{-\Delta\Delta C_t}$  method is a convenient way to analyze the relative changes in gene expression from reverse transcriptase quantitative polymerase chain reaction (RT-PCR) experiments.<sup>17,18</sup> Relative quantitative analysis was performed based on the  $2^{-\Delta\Delta C_t}$  method.

## Detection of Mcl-1 protein expression with western blotting

The collected cells were uniformly seeded in 75-cm<sup>2</sup> culture plates (10 mL/well) and inoculated for 24 h. The grouping was the same as described in the MTT assay. After the cells were cultured at 37°C in an environment with saturated humidity and 5% CO<sub>2</sub> for 48 h, the old culture medium was discarded, and the cells were washed twice with 0.01 mol/L of PBS. In each well, 0.01 mol/L of PBS was added, and the cells were collected and centrifuged at 1,000 rpm for 5 min. Protein extracts were obtained by homogenizing the samples in lysis buffer (R0278; Sigma-Aldrich, Welwyn Gardens City, UK), followed by centrifugation at 4°C at 13,000 rpm for 15 min. Protein concentration was determined with the BCA protein assay method (23227; Thermo Fisher Scientific, Loughborough, UK). Equal amounts of protein (20 µg) were loaded per lane for electrophoresis. The separated proteins were transferred to polyvinylidene difluoride (PVDF) membranes, then blocked at room temperature for 3 h and inoculated at 4°C overnight. The membranes were washed, and the mixture was treated with rabbit anti-human Mcl-1 primary antibody. After inoculation at 37°C for 2 h, blocking solution and goat anti-rabbit IgG secondary antibody were added. Following inoculation at 37°C for 2 h, the mixture was held in a shaking water bath with 1X PBS 3 times (5 min each). After color development and photography, the expression of Mcl-1L, Mcl-1S, and β-actin was analyzed using Quantity One software v. 4.4.0 (Bio-Rad Laboratories, Inc., Hercules, USA).

## Statistical analysis

The measurement data are presented as means ± standard deviation (SD). Comparison of the means between 2 groups was performed using Student's t-test. A p-value <0.05 was considered to indicate a statistically significant difference.

## Results

### Effects of DHA on *miR-29b* expression level in HUCCT-1 and FRH201 cells

We used DHA to treat the HUCCT-1 and FRH201 cells, and then evaluated *miR-29b* expression. The DHA therapy significantly increased the expression of *miR-29b* at 48 h in the HUCCT-1 cells compared with the level in the control group (Fig. 1A). The expression of *miR-29b* in the FRH201 cells began to increase after 24 h, and the level of *miR-29b* was significantly higher than that of the control group after 48 h (Fig. 1B).

### DHA and *miR-29b* combination therapy promoted the inhibition effects on the proliferation of HUCCT-1 and FRH201 cells

As shown using MTT assay, treatment with DHA (20 µmol/L) or DHA and *miR-29b* for 12 h significantly inhibited the proliferation of HUCCT-1 cells, and such inhibitory effects increased over time. Statistical analysis revealed that the inhibition rate significantly differed between the DHA+*miR-29b* and DHA groups at 12 h, 24 h and 48 h ( $p < 0.01$ , Fig. 2A).

Treatment with DHA for 12 h significantly inhibited the proliferation of FRH201 cells, and DHA+*miR-29b* combination therapy for 24 h significantly inhibited the proliferation of FRH201 cells (Fig. 2B). Such inhibitory effects became more apparent over time, and the inhibition rate reached 87.3% at 48 h. Statistical analysis revealed that cell proliferation was significantly inhibited in the DHA+*miR-29b* group at 24 h, and in both the DHA and DHA+*miR-29b* groups at 48 h ( $p < 0.01$ , Fig. 2B). In addition, the FRH201 cell growth inhibition rates were also significantly higher in the DHA+*miR-29b* group when compared with those in DHA group at 24 h and 48 h ( $p < 0.05$ , Fig. 2B).

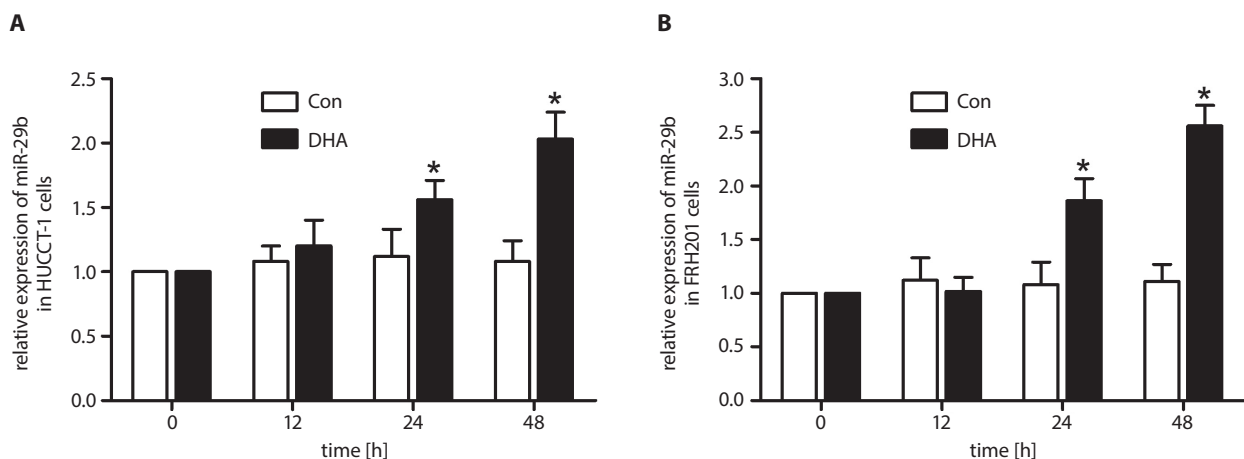


Fig. 1. Effects of DHA on *miR-29b* expression in HUCCT-1 and FRH201 cells. A. Effects on HUCCT-1 cells. B. Effects on FRH201 cells

\*  $p < 0.05$  vs control group.

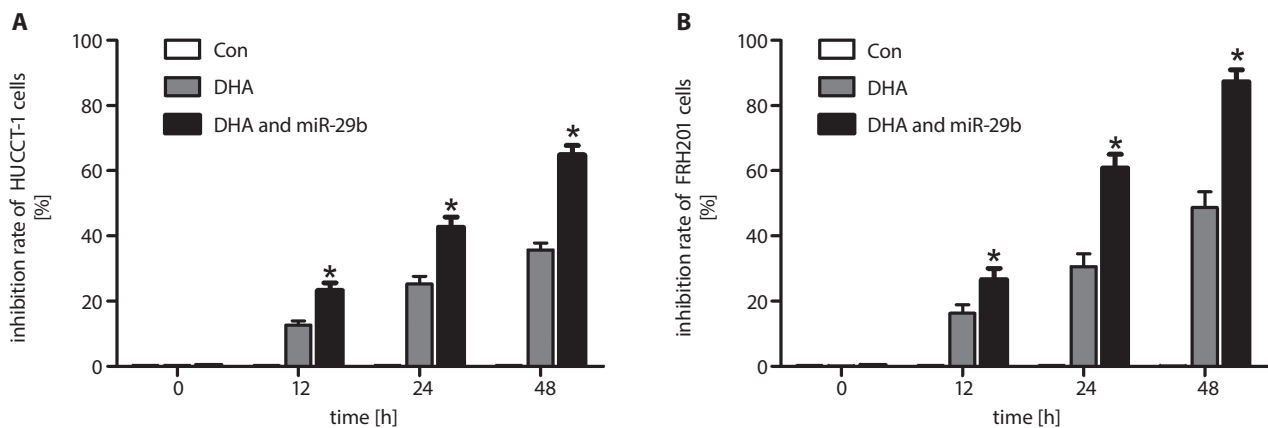


Fig. 2. Inhibitory effects of DHA and *miR-29b* on the growth of HUCCT-1 and FRH201 cells. A. Changes in growth inhibition rate of HUCCT-1 cells after treatment with 20  $\mu\text{mol/L}$  of DHA or DHA and *miR-29b*. B. Changes in growth inhibition rate of FRH201 cells after treatment with 20  $\mu\text{mol/L}$  of DHA or DHA and *miR-29b*

\*  $p < 0.05$  vs DHA group.

### Effects of DHA therapy and DHA+miR-29b combination therapy on apoptosis of HUCCT-1 and FRH201 cells

The detection of apoptosis using FCM and caspase-3 relative fluorescence units (RFU) showed that, in comparison with the control group, treatment with 20  $\mu\text{mol/L}$  of DHA alone or DHA+*miR-29b* combination therapy significantly increased the apoptosis of HUCCT-1 cells at 24 h and 48 h (Fig. 3A,C;  $p < 0.01$ ). The apoptosis rate at 48 h was significantly higher in the combination therapy group than in the DHA group (Fig. 3A). Compared with the control group, treatment with 20  $\mu\text{mol/L}$  of DHA alone or with DHA+*miR-29b* significantly increased the apoptosis rate of FRH201 cells at 24 h and 48 h (Fig. 3B and 3D;  $p < 0.01$ ). The apoptosis rate at 24 h and 48 h was significantly higher in the combination therapy group than in the DHA group (Fig. 3B,D;  $P < 0.01$ ).

### Effects of DHA therapy and DHA+miR-29b combination therapy on Mcl-1 mRNA expression

Reverse transcriptase fluorescence quantitative PCR (qPCR) revealed that Mcl-1L and Mcl-1S genes were expressed in the HUCCT-1 and FRH201 cells. In the HUCCT-1 cell line, Mcl-1L gene expression significantly decreased 24 h after treatment with 20  $\mu\text{mol/L}$  of DHA. Compared with the DHA therapy group, the DHA+*miR-29b* combination therapy group had significantly lower Mcl-1L gene expression (Fig. 4A). The Mcl-1S gene expression level increased; in particular, it significantly increased 48 h after DHA therapy and 24 h and 48 h after DHA+*miR-29b* combination therapy. The Mcl-1S expression levels were significantly higher in the DHA+*miR-29b* combination therapy group than in the DHA therapy group at 24 h and 48 h (Fig. 4B). The Mcl-1S:Mcl-1L ratio increased in the DHA+*miR-29b*

group at all time points. In particular, it was significantly higher at 24 h and 48 h in the DHA+*miR-29b* group than in the control and DHA groups (Fig. 4C).

In the FRH201 cell line, Mcl-1L gene expression also decreased after DHA therapy and DHA+*miR-29b* combination therapy. In particular, it was significantly lower at 24 h, 48 h and 72 h after DHA therapy and 72 h after DHA+*miR-29b* combination therapy (Fig. 4D). Mcl-1S gene expression increased in each treatment group. In particular, it was significantly higher in the DHA therapy group at 48 h and 72 h and in the combination therapy group at 24 h, 48 h and 72 h. Compared with the DHA group, Mcl-1S expression was significantly higher at 24 h, 48 h and 72 h in the DHA+*miR-29b* group (Fig. 4E). Compared with the control group, the Mcl-1S:Mcl-1L ratio increased in the treatment groups at different times. In particular, it was significantly higher in the DHA group at 48 h and 72 h and in the DHA+*miR-29b* group at 24 h and 48 h. Compared with the DHA therapy group, Mcl-1S expression significantly increased at 24 h and 48 h in the combination therapy group (Fig. 4F).

### Effects of DHA therapy and DHA+miR-29b combination therapy on Mcl-1 protein expression profiles in HUCCT-1 and FRH201 cells

Western blotting analysis confirmed the presence of Mcl-1L and Mcl-1S protein expression in HUCCT-1 and FRH201 cells. In the HUCCT-1 cell line, DHA therapy and DHA+*miR-29b* combination therapy significantly decreased Mcl-1L protein expression, whereas Mcl-1S protein expression was increased (Fig. 5A,B). The Mcl-1S:Mcl-1L ratio was significantly higher in the DHA and DHA+*miR-29b* groups (Fig. 5C).

In the FRH201 cell line, Mcl-1L protein expression was also significantly decreased after DHA therapy (Fig. 5D,E).

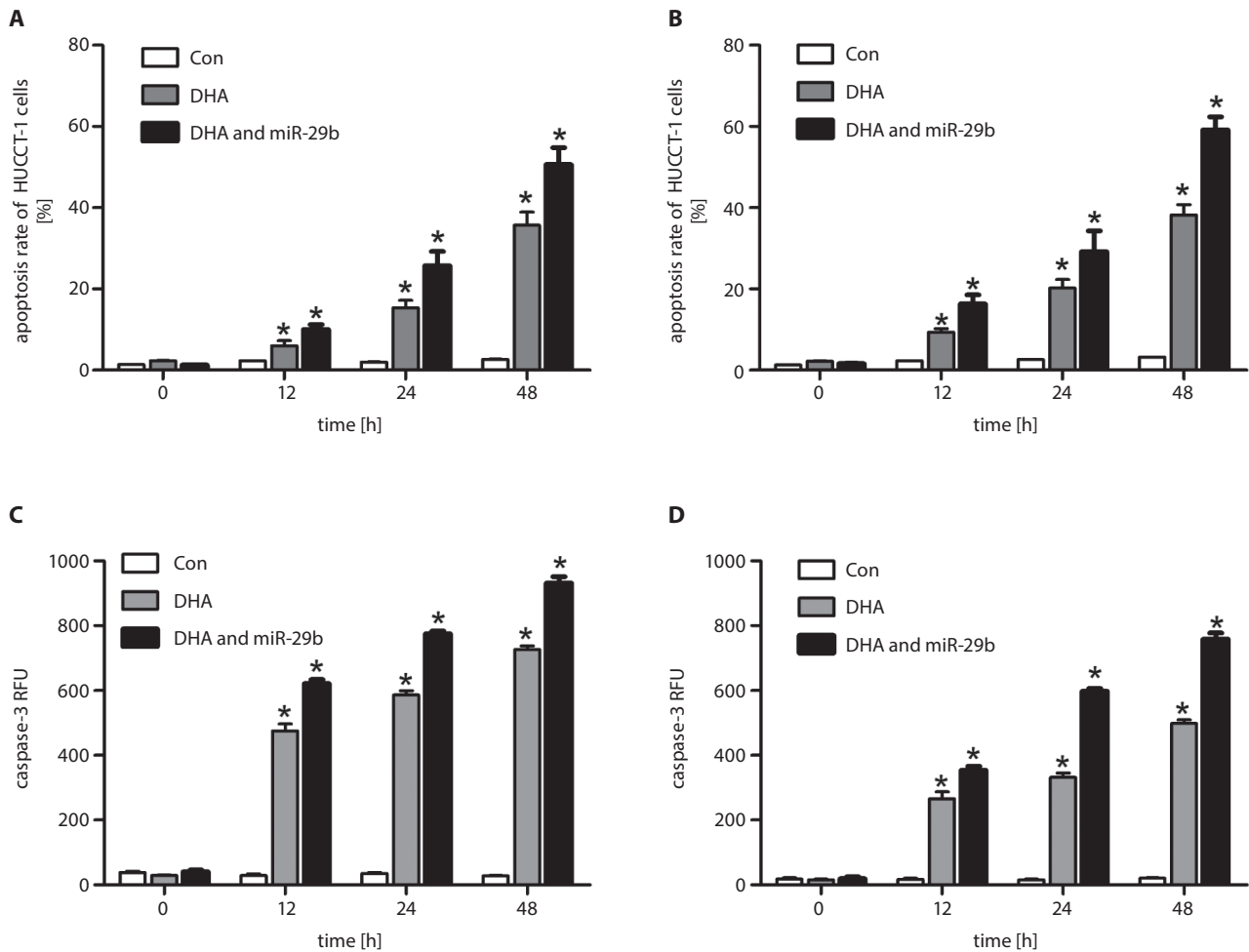


Fig. 3. Effects of DHA therapy and DHA+*miR-29b* combination therapy on the apoptosis of HUCCT-1 and FRH0201 cells. Changes in the apoptosis rate of HUCCT-1 (A) and (C) and on FRH0201 cells (B) and (D) at different time points after 20  $\mu\text{mol/L}$  of DHA therapy or DHA+*miR-29b* combination therapy

\*  $p < 0.05$  vs control group.

After DHA+*miR-29b* combination therapy, Mcl-1L protein expression was significantly higher than that after DHA therapy (Fig. 5D,E). The Mcl-1S protein expression level was significantly higher in each treatment group, and it was significantly higher in the combination therapy group than in the DHA therapy group (Fig. 5D,E). The Mcl-1S:Mcl-1L ratio was significantly higher in the treatment groups compared with the control group, and it was significantly higher in the combination therapy group than in the DHA therapy group (Fig. 5F).

## Discussion

The DHA has a variety of potent anti-tumor effects.<sup>5-7</sup> However, whether DHA can suppress cholangiocarcinoma or induce apoptosis of cholangiocarcinoma cells remains unclear. As a key regulator of Mcl-1 gene expression, we speculated that *miR-29b* may play a synergistic role with DHA in suppressing the growth of cholangiocarcinoma cells, although its underlying mechanism requires further

investigation.<sup>19</sup> In our current experiment, treatment with DHA and *miR-29b* decreased the proliferation of cholangiocarcinoma cells over time, along with an increase in cell growth inhibition rate. The proliferative activity of cholangiocarcinoma cells negatively correlated with the duration of DHA therapy, showing obvious proliferation-suppressing and apoptosis-promoting effects.

Tumorigenesis is associated with uncontrolled cell proliferation and apoptosis. Suppressing tumor-cell proliferation and inducing apoptosis are key methods for controlling and treating tumors, as well as being required indicators in screening for anti-cancer drugs. Many signal regulatory pathways are involved in apoptosis. For instance, p53 may activate apoptosis, and Bcl-2 and Bcl-XL – which belong to the anti-apoptosis family – can suppress apoptosis. These pathways can ultimately increase the release of mitochondrial cytochrome C and enhance activation of downstream caspases, which ultimately induces apoptosis.<sup>20,21</sup> As a member of the Bcl-2 apoptosis regulator gene family, the anti-apoptosis gene Mcl-1 has similar sequence and functions as other Bcl-2 genes and



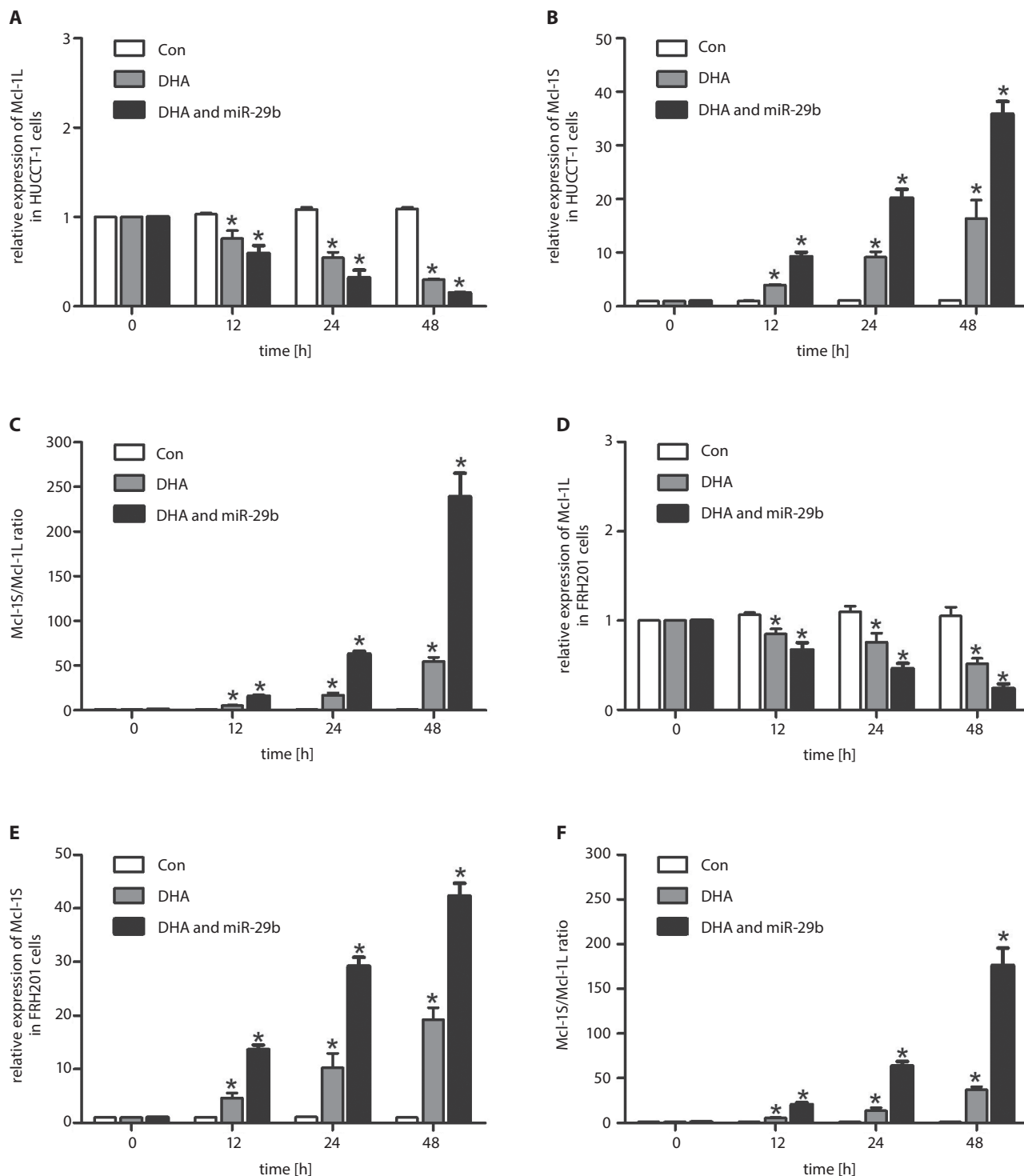


**Fig. 4.** Effects of DHA therapy and DHA+miR-29b combination therapy on mRNA expression of Mcl-1L and Mcl-1S. **A.** Effects of DHA therapy and DHA+miR-29b combination therapy on Mcl-1L mRNA expression at different time points. **B.** Effects of DHA therapy and DHA+miR-29b combination therapy on Mcl-1S mRNA expression at different time points. **C.** Changes in Mcl-1S:Mcl-1L ratio at different time points. **D.** Effects of DHA therapy and DHA+miR-29b combination therapy on Mcl-1L mRNA expression at different time points. **E.** Effects of DHA therapy and DHA+miR-29b combination therapy on Mcl-1S mRNA expression at different time points. **F.** Changes in Mcl-1S:Mcl-1L ratio at different time points

\* p < 0.05 vs control group.

plays a key role in apoptosis. The Mcl-1 gene has 4 transcripts – *Mcl-1-001-003* and *Mcl-1-201*; *Mcl-1-003* does not encode protein products, whereas *Mcl-1-001* is the corresponding mRNA of Mcl-1L and *Mcl-1-002* is the corresponding mRNA of Mcl-1S. Although Mcl-1L and Mcl-1S

are encoded by the same gene, they have opposite functions: the former is pro-apoptotic and the latter is anti-apoptotic. Mcl-1 pre-mRNA undergoes alternative splicing events to produce 2 proteins – the splicing variant Mcl-1S and the non-spliced Mcl-1L. Thus, in normally growing

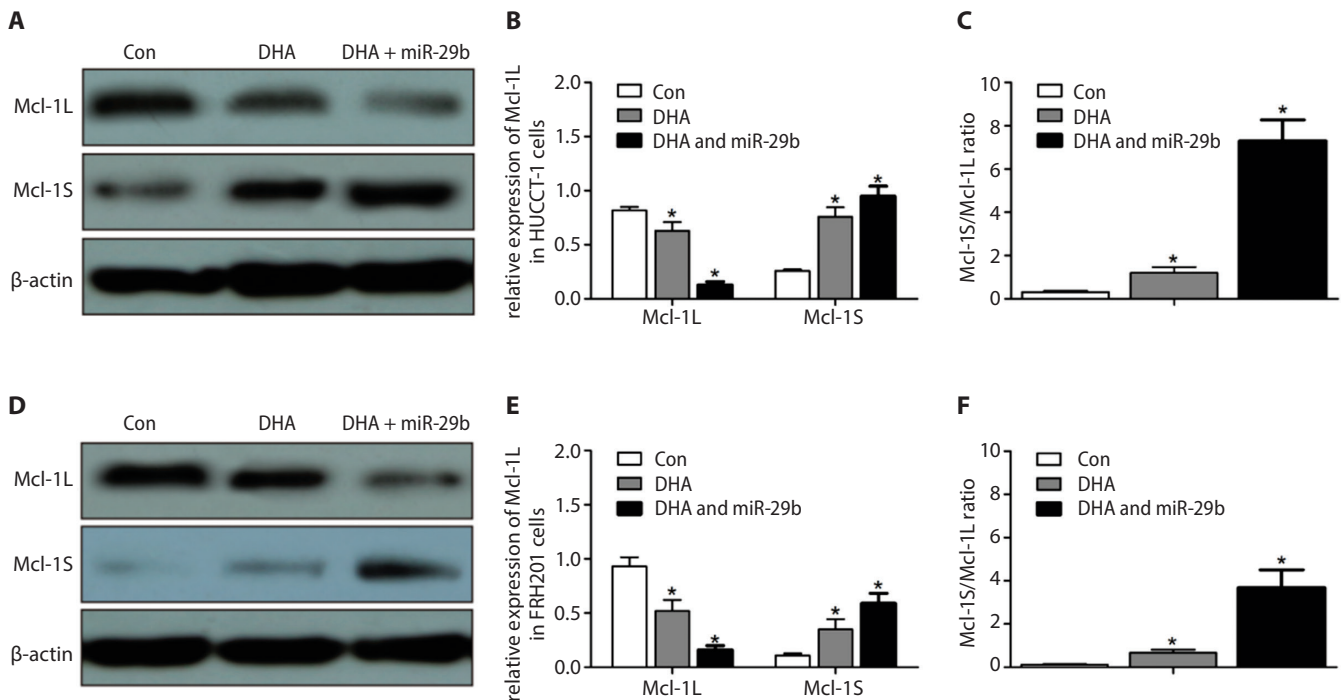


Fig. 5. A and B. Effects of DHA therapy and DHA+*miR-29b* combination therapy on Mcl-1L and Mcl-1S protein expression. C. Changes in Mcl-1S:Mcl-1L ratio. D and E. Effects of DHA therapy and DHA+*miR-29b* combination therapy on Mcl-1L and Mcl-1S protein expression. F. Changes in Mcl-1S:Mcl-1L ratio

\*  $p < 0.05$  vs control group.

tumor cells, the expression of Mcl-1L is higher than that of Mcl-1S. Therefore, Mcl-1L is also known as Mcl-1. The ratio between Mcl-1S and Mcl-1L determines the fate of Mcl-1-expressing cells.<sup>22-24</sup>

The anti-apoptotic protein Mcl-1 is highly expressed in cholangiocarcinoma cells, suggesting that the development of cholangiocarcinoma is closely correlated with the dysregulated expression of Mcl-1.<sup>25</sup> In our previous study, we found that DHA induced apoptosis of QBC939 cells by affecting the apoptosis-related protein Mcl-1; as a result, the proportion of Mcl-1S in Mcl-1 was significantly higher. Meanwhile, the proliferation of QBC939 cells was markedly suppressed and apoptosis was enhanced. It was speculated that the occurrence of QBC939 apoptosis could be attributed to abnormal Mcl-1 protein expression due to the effect of DHA, and the proportion of Mcl-1L and Mcl-1S proteins in cells determines the fate of cells.<sup>16</sup>

The Mcl-1 mRNA expression profile was also affected by the intervention. The mRNA for the synthesis of the Mcl-1S protein was significantly higher in the DHA-treated cholangiocarcinoma cells, along with a significant increase in the Mcl-1S protein expression level. As a result, the proportion of Mcl-1S in Mcl-1 was significantly higher. It was therefore speculated that DHA might induce the apoptosis of cholangiocarcinoma cells by upregulating the proportion of Mcl-1S in Mcl-1.<sup>16</sup> To rule out experimental error in a single cell line, to validate whether DHA has a definite pro-apoptotic effect on cholangiocarcinoma cells, and to confirm whether the changes in Mcl-1-related

expression promote apoptosis, in the current study, we used 2 cholangiocarcinoma cell lines: HUCCT-1 and FRH0201. Our experiments confirmed that DHA had potent growth-inhibiting and apoptosis-promoting effects on these 2 cholangiocarcinoma cell lines; meanwhile, DHA therapy significantly increased Mcl-1S expression in these 2 cell lines. These findings were consistent with our previous study on QBC939 cells.

Mott et al. reported that the expression of *miR-29b* was higher in a human immortalized, non-malignant cholangiocyte H69 cell line, but was decreased in a malignant cholangiocarcinoma KMCH cell line.<sup>14</sup> When *miR-29b* was overexpressed in KMCH cells, the protein expression of Mcl-1, an anti-apoptotic Bcl-2 family member, was significantly lower, along with increased sensitivity to tumor necrosis factor (TNF)-related apoptosis-inducing ligand (TRAIL). Many studies have confirmed that the downregulated expression of *miR-29b* in malignant cholangiocarcinoma cells is directly associated with the high expression of anti-apoptotic Mcl-1 protein in tumor cells. The *miR-29b* can also directly exert its effect on Mcl-1 gene 3'-UTR, whose overexpression, however, has no obvious effect on Mcl-1 mRNA.<sup>12</sup> The expression of *miR-29b* is low in normally growing tumor cells. Many studies have shown that the expression of Mcl-1 is controlled by the small endogenous RNA molecule miR-29, and that the high expression of miR-29 markedly decreases the expression of Mcl-1L in cholangiocarcinoma cells. In our current study, we applied *miR-29b* to transfect the DHA-treated cholangiocarcinoma cells and found that

DHA+*miR-29b* combination therapy markedly affected the mRNA expression profiles of Mcl-1 in both cell lines. More specifically, it significantly increased the expression level of mRNA, directing the synthesis of the Mcl-1S protein and thus increasing the Mcl-1S:Mcl-1L ratio. Flow cytometry revealed that DHA therapy and DHA+*miR-29b* combination therapy significantly increased the apoptosis of cholangiocarcinoma cells in a time-dependent manner. The pro-apoptotic effect was more prominent in the combination therapy group than in the DHA therapy group. Our experiment also showed that the inhibitory effects of DHA and DHA+*miR-29b* on the proliferation of cholangiocarcinoma cells were achieved by inducing apoptosis, and that the pro-apoptotic effect could be enhanced after combination therapy with *miR-29b*.

In summary, our study confirmed that DHA and *miR-29b* have a pro-apoptotic effect on cholangiocarcinoma cells, which may be because the DHA/*miR-29b*/Mcl-1 pathway changes the Mcl-1 gene expression profile by upregulating the expression of the pro-apoptotic protein Mcl-1S, thus increasing the proportion of Mcl-1S protein among the total Mcl-1 protein. However, due to the complexity of the cancer cell signaling pathways and their regulatory mechanisms, more relevant studies from different perspectives are warranted.

#### ORCID iDs

Kezhou Li  <https://orcid.org/0000-0002-5340-1129>  
 Hui Hu  <https://orcid.org/0000-0002-2772-7387>  
 Zongding Wang  <https://orcid.org/0000-0002-1952-546X>  
 Chunlu Tan  <https://orcid.org/0000-0002-1440-0430>  
 Xubao Liu  <https://orcid.org/0000-0002-6266-7519>  
 Hao Zhang  <https://orcid.org/0000-0003-1912-6036>

#### References

- Lunsford KE, Court C, Lee YS, et al. Propensity-matched analysis of patients with mixed hepatocellular-cholangiocarcinoma and hepatocellular carcinoma undergoing liver transplantation. *Liver Transpl*. 2018;24(10):1384–1397.
- Kato A, Shimizu H, Ohtsuka M, et al. Surgical resection after down-sizing chemotherapy for initially unresectable locally advanced biliary tract cancer: A retrospective single-center study. *Ann Surg Oncol*. 2013;20(1):318–324.
- Yan X, Li P, Zhan Y, et al. Dihydroartemisinin suppresses STAT3 signaling and Mcl-1 and survivin expression to potentiate ABT-263-induced apoptosis in non-small cell lung cancer cells harboring EGFR or RAS mutation. *Biochem Pharmacol*. 2018;150:72–85.
- Bergquist A, von Seth V. Epidemiology of cholangiocarcinoma. *Best Pract Res Clin Gastroenterol*. 2015;9(2):221–232.
- Wallender E, Vucicevic K, Jagannathan P, et al. Predicting optimal dihydroartemisinin-piperaquine regimens to prevent malaria during pregnancy for human immunodeficiency virus-infected women receiving efavirenz. *J Infect Dis*. 2018;217(6):964–972.
- Feng MX, Hong JX, Wang Q, et al. Dihydroartemisinin prevents breast cancer-induced osteolysis via inhibiting both breast cancer cells and osteoclasts. *Sci Rep*. 2016;6:19074.
- Qin G, Zhao C, Zhang L, et al. Dihydroartemisinin induces apoptosis preferentially via a Bim-mediated intrinsic pathway in hepatocarcinoma cells. *Apoptosis*. 2015;20(8):1072–1086.
- Chen SS, Hu W, Wang Z, Lou X-E, Zhou H-J. p8 attenuates the apoptosis induced by dihydroartemisinin in cancer cells through promoting autophagy. *Cancer Biol Ther*. 2015;16(5):770–779.
- Hu W, Chen SS, Zhang JL, Lou X-E, Zhou H-J. Dihydroartemisinin induces autophagy by suppressing NF- $\kappa$ B activation. *Cancer Lett*. 2014;343(2):239–248.
- Morciano G, Giorgi C, Balestra D, et al. Mcl-1 involvement in mitochondrial dynamics is associated with apoptotic cell death. *Mol Biol Cell*. 2016;27(1):20–34.
- de Necochea-Campion R, Diaz Osterman CJ, Hsu HW, et al. AML sensitivity to YM155 is modulated through AKT and Mcl-1. *Cancer Lett*. 2015;366(1):44–51.
- Nijhuis A, Curciarello R, Mehta S, et al. MCL-1 is modulated in Crohn's disease fibrosis by miR-29b via IL-6 and IL-8. *Cell Tissue Res*. 2017;368(2):325–335.
- Escudero S, Zaganjor E, Lee S, et al. Dynamic regulation of long-chain fatty acid oxidation by a noncanonical interaction between the MCL-1 BH3 helix and VLCAD. *Mol Cell*. 2018;69(5):729–743.
- Mott JL, Kobayashi S, Bronk SF, Gores GJ. miR-29 regulates Mcl-1 protein expression and apoptosis. *Oncogene*. 2007;26(42):6133–6140.
- Okamoto K, Miyoshi K, Murawaki Y. miR-29b, miR-205 and miR-221 enhance chemosensitivity to gemcitabine in HuH28 human cholangiocarcinoma cells. *PLoS One*. 2013;8(10):e77623.
- Hu H, Tan C, Liu X, Luo F, Li K. Upregulation of the MCL-1S protein variant following dihydroartemisinin treatment induces apoptosis in cholangiocarcinoma cells. *Oncol Lett*. 2015;10(6):3545–3550.
- Livak KJ, Schmittgen TD. Analysis of relative gene expression data using real-time quantitative PCR and the 2(-delta delta C(T)) method. *Methods*. 2001;25(4):402–408.
- Schmittgen TD, Livak KJ. Analyzing real-time PCR data by the comparative C(T) method. *Nat Protoc*. 2008;3(6):1101–1108.
- Tian F, Chen J, Zheng S, et al. miR-124 targets GATA6 to suppress cholangiocarcinoma cell invasion and metastasis. *BMC Cancer*. 2017;17(1):175.
- Renault TT, Teijido O, Antonsson B, Dejean LM, Manon S. Regulation of Bax mitochondrial localization by Bcl-2 and Bcl-x(L): Keep your friends close but your enemies closer. *Int J Biochem Cell Biol*. 2013;45(1):64–67.
- Liu D. Effects of procyanidin on cardiomyocyte apoptosis after myocardial ischemia reperfusion in rats. *BMC Cardiovasc Disord*. 2018;18(1):35.
- Palve V, Mallick S, Ghaisa G, Kannan S, Teni T. Overexpression of Mcl-1L splice variant is associated with poor prognosis and chemoresistance in oral cancers. *PLoS One*. 2014;9(11):e111927.
- Haydn T, Metzger E, Schuele R, Fulda S. Concomitant epigenetic targeting of LSD1 and HDAC synergistically induces mitochondrial apoptosis in rhabdomyosarcoma cells. *Cell Death Dis*. 2017;8(6):e2879.
- Chen S, Dai Y, Pei XY, Grant S. Bim upregulation by histone deacetylase inhibitors mediates interactions with the Bcl-2 antagonist ABT-737: Evidence for distinct roles for Bcl-2, Bcl-xL, and Mcl-1. *Mol Cell Biol*. 2009;29(23):6149–6169.
- Rizvi S, Yamada D, Hirsova P, et al. A hippo and fibroblast growth factor receptor autocrine pathway in cholangiocarcinoma. *J Biol Chem*. 2016;291(15):8031–8047.



# The quality of life after transnasal microsurgical and endoscopic resection of nonfunctioning pituitary adenoma

Maciej Bryl<sup>1,A–D</sup>, Jowita Woźniak<sup>2,B–D</sup>, Krzysztof Dudek<sup>3,C</sup>, Bogdan Czapiga<sup>4,A,C,E,F</sup>, Paweł Tabakow<sup>2,A,C–F</sup>

<sup>1</sup> Department of Neurosurgery and Neurooncology, Medical University of Lodz, Barlicki University Hospital, Poland

<sup>2</sup> Department of Neurosurgery, Wrocław Medical University, Poland

<sup>3</sup> Faculty of Natural Sciences and Technology, Karkonosze College, Jelenia Góra, Poland

<sup>4</sup> Department of Nervous System Diseases, Faculty of Health Sciences, Wrocław Medical University, Poland

A – research concept and design; B – collection and/or assembly of data; C – data analysis and interpretation; D – writing the article; E – critical revision of the article; F – final approval of the article

Advances in Clinical and Experimental Medicine, ISSN 1899–5276 (print), ISSN 2451–2680 (online)

*Adv Clin Exp Med.* 2020;29(8):921–928

## Address for correspondence

Maciej Bryl  
E-mail: bryl.maciej@gmail.com

## Funding sources

None declared

## Conflict of interest

None declared

Received on March 9, 2020  
Reviewed on March 31, 2020  
Accepted on June 2, 2020

Published online on August 3, 2020

## Cite as

Bryl M, Woźniak J, Dudek K, Czapiga B, Tabakow P.  
The quality of life after transnasal microsurgical and endoscopic resection of nonfunctioning pituitary adenoma.  
*Adv Clin Exp Med.* 2020;29(8):921–928.  
doi:10.17219/acem/123351

## DOI

10.17219/acem/123351

## Copyright

© 2020 by Wrocław Medical University  
This is an article distributed under the terms of the  
Creative Commons Attribution 3.0 Unported (CC BY 3.0)  
(<https://creativecommons.org/licenses/by/3.0/>)

## Abstract

**Background.** A pituitary tumor can be reached by a transsphenoidal approach with the use of a microscope or an endoscope. The impact of the surgical technique on the patient's quality of life (QOL) is of great interest to us. Currently, the development of both surgical techniques, especially the endoscopic one, is very rapid. Treatment outcomes are extremely important, especially in terms of patients' QOL after pituitary tumor resection, irrespective of the technical aspects.

**Objectives.** To compare the quality of life between patients who had undergone either transsphenoidal microscopic (MTS) or endoscopic (ETS) non-functioning pituitary adenoma resection.

**Material and methods.** The study population consisted of 32 consecutive patients (21 for the endoscopic and 11 for the microscopic method) who had undergone pituitary adenoma resection. Their QOL was evaluated using the World Health Organization's Quality of Life assessment tool (WHOQOL-BREF), the Sino-Nasal Outcome Test (SNOT-22) and the Visual Functioning Questionnaire (VFQ-25). Questionnaires were collected before and after surgery during the patients' hospital stay and 3 months after the surgery.

**Results.** The patients in the 2 groups did not differ significantly in terms of age, sex, tumor size, length of hospital stay, or QOL before the surgery. Vision-related QOL (VR-QOL) significantly improved in patients undergoing endoscopic surgery ( $p < 0.001$ ). There were no statistically significant differences in QOL between the study groups at any stage of the trial ( $p > 0.05$ ). Significantly more patients had improved QOL after endoscopic surgery according to the WHOQOL-BREF ( $p = 0.005$ ) and the VFQ-25 ( $p = 0.002$ ).

**Conclusions.** The novel observation in this study is the significant improvement of VR-QOL in patients after endoscopic non-functioning pituitary adenoma resection in comparison to patients having microscopic resection. The microscopic method does not exacerbate rhinological symptoms more than the endoscopic one. Endoscopic surgery seems to be more beneficial for patients with pituitary adenoma, which deteriorates VR-QOL.

**Key words:** pituitary adenoma, health-related quality of life, neuroendoscopy, transsphenoidal approach, microsurgery



## Introduction

In 1907, the transsphenoidal approach to pituitary lesions was adopted by Schoffler. Harvey Cushing performed his first transsphenoidal operation on a patient with acromegaly using a modified form of Schoffler's method.<sup>1</sup> The first direct endonasal approach was described by Griffith and Veerapen in 1987.<sup>2</sup> It is thought that the microscopic transsphenoidal approach is highly invasive and that the deeper the operating field is, the less invasive the surgery will be, due to a better angle of attack. There are 2 techniques for introducing the microscope into the anterior wall of the sphenoid sinus: 1) microscopic sublabial, with a wide angle of attack thanks to the nasal septum not being in the way; and 2) microscopic endonasal, which involves fitting a speculum under the mucosa of the nasal septum and is therefore considered to have a narrow angle of attack. In contrast, the endoscopic technique allows for the minimally invasive transsphenoidal approach, but the deeper the operating field, the higher the invasiveness due to the uncomfortable angle of attack. Again, 2 techniques can be performed – endoscopic endonasal binostril or uninostril – both with slightly different angles of attack, though the binostril technique is favored due to the contralateral location of the pivot point. Furthermore, the microscope or endoscope can be introduced submucosally or extramucosally, which is of great importance in regard to the patient's post-operative complaints. The development of both surgical techniques, especially the endoscopic one, has been rapid. Long-term treatment outcomes are important, especially in terms of the quality of life (QOL) of patients after pituitary tumor resection, irrespective of the technical aspects.

One of the most common symptoms of pituitary adenoma is visual field defect, occurring in 9–32% of patients.<sup>3</sup> It is crucial for such a patient (and for the surgeon as well) to improve the vision-related quality of life (VR-QOL). Nowadays, it is standard procedure to perform transsphenoidal pituitary tumor resection in more than 95% of such cases (when the tumor mass can be reached from the bottom through the sphenoid recess).<sup>3</sup> Such a procedure (with instruments within the nasal cavity) can cause a deterioration in QOL related to ear, nose and throat complaints. Furthermore, we believe that there are many other QOL aspects which are affected during or after the surgical treatment of pituitary masses.

## Objectives

Little has been written about the comprehensive assessment of overall QOL with a view to analyzing rhinology-specific quality of life (RS-QOL) and VR-QOL in patients undergoing transsphenoidal microscopic and endoscopic non-functioning pituitary adenoma (NFPA) resection. The objective of this study was to fill the gap in the research and to juxtapose the results with the results of other authors.

## Material and methods

The study initially involved 35 consecutive patients, but 3 of them were excluded due to the different surgical technique applied (a transcranial pterional approach). Ultimately, the study included 32 patients, aged 22–82 years (mean: 58 years; standard deviation (SD) = 14.7), among them 17 men (53%) and 15 women (47%). Informed consent was obtained from all individual participants of the study. All patients were operated on for an NFPA between July 2012 and February 2014 at the Department of Neurosurgery in Wroclaw Medical University Hospital, Poland. They were allocated into 2 groups: the endoscopic group (group E) and the microscopic group (group M), depending on the surgical method used. Both surgical techniques were applied by 2 experienced surgeons of similar experience; one of them specialized only in the microscopic surgery of pituitary lesions, while the other one only in endoscopic procedures. Both the researchers and the participants knew which treatment method would be used. An intention-to-treat (ITT) analysis was performed and dropouts were considered in the analysis. The navigation system manufactured by Medtronic (Minneapolis, USA) was used in both techniques. Patients from group M underwent a submucosal paraseptal sphenoidotomy approach to the sella turcica, while patients from group E received a submucosal binostril anterior sphenoidotomy approach. The endoscopic transsphenoidal surgery (ETS) was performed in 21 patients (12 men and 9 women; mean age: 61 years; mean tumor diameter: 2.46 × 2.66 × 2.44 cm), while the microscopic transsphenoidal surgery (MTS) was used in 11 patients (5 men and 6 women; mean age: 59 years; mean tumor diameter: 2.66 × 2.45 × 2.70 cm).

Health-related QOL (HR-QOL) was assessed using 3 questionnaires: 1) the Polish version of the World Health Organization's Quality of Life assessment tool (WHOQOL-BREF) to evaluate overall QOL<sup>4,5</sup>; 2) the Sino-Nasal Outcome Test 22 (SNOT-22) to assess RS-QOL<sup>6</sup>; and 3) the Visual Functioning Questionnaire 25 (VFQ-25) to evaluate VR-QOL.<sup>7</sup> The WHOQOL-BREF is comprised of 26 items measuring the following broad domains: physical health, psychological health, social relationships, and the environmental aspect (every domain is scored from 0% to 100% and higher results indicate better QOL). The SNOT-22 contains 22 questions on chronic rhinosinusitis-related symptoms, where the symptom severity is graded from 0 to 5, with 0 indicating no problem at all and 5 indicating the worst possible situation (a scale ranging from 0 to 110 points); high scores indicate a greater severity of rhinology-specific symptoms. The VFQ-25 consists of 25 vision-targeted questions representing 11 vision-related constructs and an additional single-item general health rating question. The VFQ-25 generates the following vision-targeted sections: general health and vision (0–21 points), difficulty with activities (0–83 points) and response to vision problems (0–45 points). Lower results indicate less severe vision

problems. The questionnaires were administered 3 times to each patient: before the surgery, after the surgery (during their hospital stay, between the 3<sup>rd</sup> and 6<sup>th</sup> day after surgery) and 3 months after discharge. In case of any condition that could interfere with a result of a single questionnaire (e.g., upper respiratory tract infections may increase the SNOT-22 score), distribution of the questionnaire was postponed until the symptoms were resolved. Both groups of patients were compared in terms of age, sex, hospital stay after surgery, tumor size, and QOL. Better QOL was defined as a better result of the questionnaire collected after the surgery.

The normality of the distribution of variables was verified by means of the Shapiro–Wilk test. A p-value <0.05 was considered statistically significant. Variables with normal distribution are presented in the tables as means and standard deviation (SD). The variables whose distribution was significantly different from the normal distribution are presented as medians and interquartile ranges (IQR). Categorical variables emerge as numbers and fractions (percentage). When comparing the ratings for 3 consecutive

periods, a non-parametric Friedman test was used for dependent variables. To compare quantitative variables in the 2 groups, the Mann–Whitney U test and Student's t-test were used. The interdependence of the qualitative variables was verified using Pearson's  $\chi^2$  test or Fisher's exact test. The statistics program package for STATISTICA v. 10 (StatSoft, Inc., Tulsa, USA) was used in calculations and graph creation.

## Results

The age, sex and tumor size of the study groups are presented in Table 1. Both groups of patients were homogeneous in terms of age, sex and tumor diameter ( $p > 0.05$ ).

Tables 2 and 3 present the statistical analysis of the WHOQOL-BREF, SNOT-22 and VFQ-25 results as medians and IQR. In group M, there was no statistically significant improvement in QOL according to the WHOQOL-BREF, SNOT-22 and VFQ-25. In group E, we observed statistically significant improvement in QOL as assessed

Table 1. Age, sex and tumor size of study groups

Variable	Total n = 32	Group		E vs M p-value
		endoscopic n = 21	microscopic n = 11	
Age [years]				
median (IQR)	60.5 (13.5)	61 (14)	59 (19)	0.463 <sup>a</sup>
range	22–82	22–82	22–74	
Sex				
male	17 (53.1%)	12 (57.1%)	5 (45.4%)	0.398 <sup>b</sup>
female	15 (46.9%)	9 (42.9%)	6 (54.6%)	0.412 <sup>b</sup>
Tumor diameter [cm]				
transverse	2.53 ±0.96	2.46 ±0.90	2.66 ±1.09	0.571 <sup>c</sup>
cranio-caudal	2.59 ±1.12	2.66 ±1.14	2.45 ±1.13	0.612 <sup>c</sup>
antero-posterior	2.53 ±0.87	2.44 ±0.78	2.70 ±1.05	0.429 <sup>c</sup>

<sup>a</sup> Mann–Whitney U test; <sup>b</sup> Fisher's exact test; <sup>c</sup> Student's t-test; IQR – interquartile range.

Table 2. Statistical analysis of the median results of WHOQOL-BREF, SNOT-22 and VFQ-25 for group E

Questionnaire	Preoperative	Postoperative	After 3 months	ANOVA <sup>a</sup> p-value
WHOQOL-BREF (broad domain)				
Physical, median (range)	63.19 (44–88)	50.19 (19–69)	63.70 (38–75)	0.267
Psychological, median (range)	63.13 (44–88)	69.9 (19–94)	69.60 (25–81)	0.350
Social, median (range)	75.25 (44–100)	75.25 (25–100)	75.25 (25–100)	0.703
Environment, median (range)	69.25 (25–88)	75.18 (25–94)	75.25 (25–88)	0.397
SNOT-22 (broad domain)				
Median (range)	35.28 (8–64)	42.17 (1–65)	22.21 (3–64)	0.097
VFQ-25 (broad domain)				
General, median (range)	11.40 (7–17)	10.40 (6–17)	8.30 (7–19)	0.010
Everyday, median (range)	30.20 (13–52)	22.18 (13–45)	16.13 (13–43)	<0.001
Response, median (range)	22.18 (9–42)	18.20 (9–46)	11.14 (9–44)	0.023

<sup>a</sup> Friedman ANOVA; ANOVA – analysis of variance; WHOQOL-BREF – World Health Organization's Quality of Life assessment tool; SNOT-22 – Sino-Nasal Outcome Test; VFQ-25 – Visual Functioning Questionnaire.

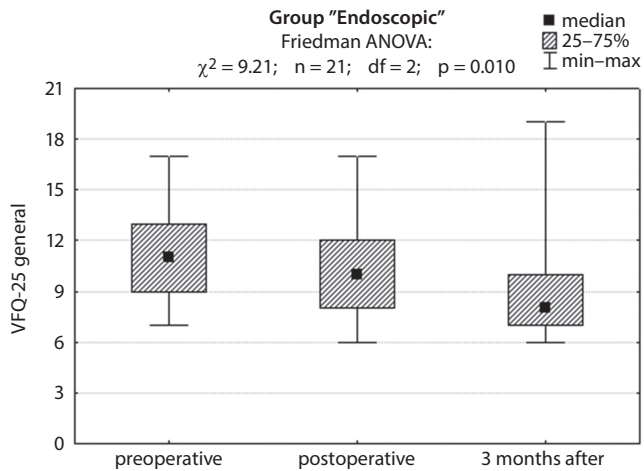


Fig. 1. Comparison of the VR-QOL self-assessment in VFQ-25 (GENERAL HEALTH AND VISION) and results of Friedman ANOVA test throughout the study (endoscopic group)

using the VFQ-25 (Fig. 1). Moreover, some improvement was observed as indicated by the WHOQOL-BREF and the SNOT-22, although the differences were not statistically significant ( $p > 0.05$ ).

Tables 4–6 compare quality of life in both groups before and after surgery and 3 months after discharge. There were no statistically significant differences between the groups in those 3 time points ( $p > 0.05$ ).

The mean length of hospital stay for group E was 6.5 days, and for group M 8.5 days. The difference in duration of hospital stay was not statistically significant (Fig. 2).

An improvement in QOL was frequently observed among patients who underwent ETS (Table 7). It was statistically significant ( $p < 0.05$ ) in all domains of the WHOQOL-BREF and in difficulty with activities and response to vision problems from the VFQ-25.

Better outcomes in the physical domain from the WHOQOL-BREF were observed in 12 patients (57%) who

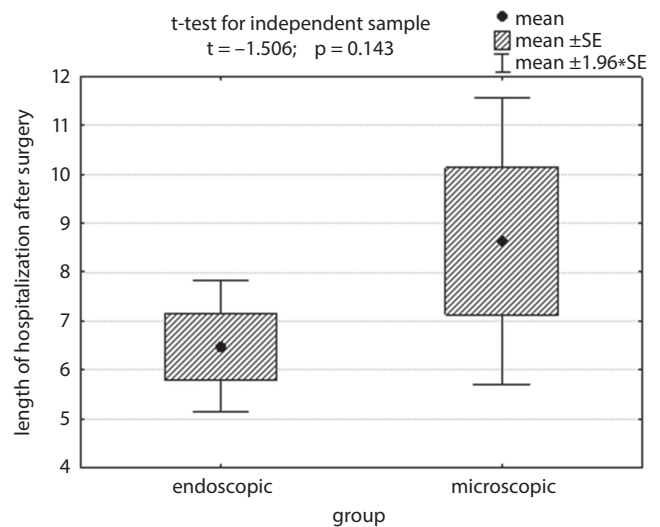


Fig. 2. Comparison of the length of hospitalization after surgery and results of t-test

had received ETS as compared with 2 patients (18%) who had received MTS ( $p = 0.039$ ); in the psychological domain, improvements were noted in 11 patients (52%) after ETS compared to 1 patient (9%) after MTS ( $p = 0.018$ ); in the social and environmental domains, the results were statistically significant. Better outcomes, as assessed using SNOT-22, were observed in 12 patients (57%) after ETS in comparison with 5 patients (45%) after MTS, although the outcomes were not statistically significant ( $p = 0.398$ ). According to the VFQ-25, better outcomes in difficulty with everyday activities were observed in 16 patients (76%) after ETS compared with 2 patients (18%) after MTS ( $p = 0.003$ ). With regard to response to vision problems, better results were obtained in 14 patients (67%) after ETS compared to 1 patient (9%) after MTS ( $p = 0.002$ ).

Furthermore, comparing the difference between the mean results of questionnaires before and 3 months after

Table 3. Statistical analysis of the median results of WHOQOL-BREF, SNOT-22 and VFQ-25 for group M

Questionnaire	Preoperative	Postoperative	After 3 months	ANOVA <sup>a</sup> p-value
WHOQOL-BREF (broad domain)				
Physical, median (range)	63.19 (38–69)	56.25 (38–81)	56.28 (13–81)	0.862
Psychological, median (range)	63.25 (31–81)	69.13 (31–81)	63.22 (19–81)	0.368
Social, median (range)	75.31 (31–100)	69.25 (31–100)	78.25 (31–81)	0.232
Environment, median (range)	63.38 (44–94)	63.12 (50–81)	72.38 (31–94)	0.554
SNOT-22 (broad domain)				
Median (range)	20.28 (0–61)	32.38 (0–73)	17.23 (0–70)	0.150
VFQ-25 (broad domain)				
General, median (range)	13.60 (4–17)	10.60 (4–16)	8.80 (4–16)	0.119
Everyday, median (range)	33.19 (13–48)	29.20 (13–44)	21.23 (13–48)	0.168
Response, median (range)	13.21 (9–41)	17.22 (9–39)	10.18 (9–36)	0.751

<sup>a</sup> Friedman ANOVA; ANOVA – analysis of variance; WHOQOL-BREF – World Health Organization's Quality of Life assessment tool; SNOT-22 – Sino-Nasal Outcome Test; VFQ-25 – Visual Functioning Questionnaire.



**Table 4.** Comparison of mean values and SD of the quality of life questionnaire results in both groups before surgery

Questionnaire	Endoscopic group	Microscopic group	Mann–Whitney U test p-value
WHOQOL-BREF (broad domain)			
Physical	54.8 ±14.5	58.9 ±12.9	0.242
Psychological	64.7 ±10.0	62.5 ±18.0	0.921
Social	71.4 ±16.6	72.6 ±22.7	0.827
Environment	63.5 ±17.7	73.8 ±17.6	0.751
SNOT-22 (broad domain)			
Median	33.4 ±15.8	25.6 ±21.0	0.197
VFQ-25 (broad domain)			
General	11.6 ±3.1	10.6 ±4.2	0.706
Everyday	30.4 ±11.4	28.5 ±12.8	0.968
Response	22.9 ±11.8	14.1 ±9.3	0.234

SD – standard deviation; WHOQOL-BREF – World Health Organization’s Quality of Life assessment tool; SNOT-22 – Sino-Nasal Outcome Test; VFQ-25 – Visual Functioning Questionnaire.

**Table 5.** Comparison of mean values and SD of the quality of life questionnaire results in both groups after surgery

Questionnaire	Endoscopic group	Microscopic group	Mann–Whitney U test p-value
WHOQOL-BREF (broad domain)			
Physical	51.4 ±15.2	56.4 ±12.0	0.620
Psychological	63.9 ±17.6	61.8 ±16.9	0.766
Social	73.2 ±19.9	71.0 ±24.4	0.796
Environment	69.0 ±16.4	69.0 ±11.1	0.372
SNOT-22 (broad domain)			
Median	35.3 ±14.2	37.0 ±21.3	0.706
VFQ-25 (broad domain)			
General	10.3 ±3.0	9.1 ±3.8	1.000
Everyday	25.7 ±10.5	25.0 ±9.2	0.552
Response	21.1 ±12.5	15.5 ±8.6	0.796

SD – standard deviation; WHOQOL-BREF – World Health Organization’s Quality of Life assessment tool; SNOT-22 – Sino-Nasal Outcome Test; VFQ-25 – Visual Functioning Questionnaire.

discharge, the p-values confirmed the benefit of ETS over MTS in obtaining greater improvement in patient VR-QOL, but no significant difference in RS-QOL (Table 8).

## Discussion

It must be noted that the literature lacks research which juxtaposes 2 surgical methods of NFPA treatment in the context of comprehensively assessing the patients’ QOL. According to the WHO, QOL is defined as an individual’s perception of their position in life in the context of the culture and value systems in which they live

**Table 6.** Comparison of mean values and SD of the quality of life questionnaire results in both groups 3 months after discharge

Questionnaire	Endoscopic group	Microscopic group	Mann–Whitney U test p-value
WHOQOL-BREF (broad domain)			
Physical	58.8 ±9.2	54.8 ±21.9	0.770
Psychological	63.2 ±14.2	58.6 ±19.7	0.626
Social	75.0 ±18.7	67.9 ±19.5	0.608
Environment	68.8 ±16.4	69.8 ±23.1	0.770
SNOT-22 (broad domain)			
Median	26.3 ±16.9	20.6 ±22.6	0.272
VFQ-25 (broad domain)			
General	9.7 ±3.6	9.5 ±4.6	0.575
Everyday	21.6 ±9.6	27.1 ±13.4	0.283
Response	18.4 ±12.1	16.9 ±12.1	0.367

SD – standard deviation; WHOQOL-BREF – World Health Organization’s Quality of Life assessment tool; SNOT-22 – Sino-Nasal Outcome Test; VFQ-25 – Visual Functioning Questionnaire.

**Table 7.** Comparison of the number of patients whose quality of life outcome was higher

Questionnaire	Total n = 32	Group		E vs M p-value
		endoscopic n = 21	microscopic n = 11	
WHOQOL-BREF (broad domain)				
Physical	14 (43.8%)	12 (57.1%)	2 (18.2%)	0.039 <sup>a</sup>
Psychological	12 (37.5%)	11 (52.4%)	1 (9.1%)	0.018 <sup>a</sup>
Social	10 (31.2%)	10 (47.6%)	0 (0.0%)	0.005 <sup>a</sup>
Environment	11 (34.4%)	10 (47.6%)	1 (9.1%)	0.033 <sup>a</sup>
SNOT-22 (broad domain)				
Median	17 (53.1%)	12 (57.1%)	5 (45.4%)	0.398 <sup>a</sup>
VFQ-25 (broad domain)				
General	16 (50.0%)	12 (57.1%)	4 (36.4%)	0.229 <sup>a</sup>
Everyday	18 (56.2%)	16 (76.2%)	2 (18.2%)	0.003 <sup>a</sup>
Response	15 (46.9%)	14 (66.7%)	1 (9.1%)	0.002 <sup>a</sup>

<sup>a</sup> Fisher’s test; WHOQOL-BREF – World Health Organization’s Quality of Life assessment tool; SNOT-22 – Sino-Nasal Outcome Test; VFQ-25 – Visual Functioning Questionnaire.

and in relation to their goals, expectations, standards, and concerns.<sup>4</sup> The authors analyzed patients’ QOL regarding both ETS and MTS before and after the surgery (during the hospital stay) and 3 months after discharge. The choice of a three-month postoperative period was due to a study by Little et al., which showed that RS-QOL after ETS improves 3 months after a procedure; also, Okamoto et al. used a three-month period in their VR-QOL assessment.<sup>3,8</sup>

Similar research methods to those used in our study have been reported by other authors. Dekkers et al. examined the QOL in patients with NFPA in remission during long-term follow-up after MTS using 4 tests: the Hospital

**Table 8.** Comparison of differences between the mean results before and 3 months after surgery in both groups

Questionnaire	Endoscopic group		Microscopic group	
	mean $\pm$ SD	p-value	mean $\pm$ SD	p-value
WHOQOL-BREF (broad domain)				
Physical	4.0 $\pm$ 13.0	0.168	-4.1 $\pm$ 15.4	0.474
Psychological	-1.5 $\pm$ 12.7	0.601	-3.9 $\pm$ 6.4	0.132
Social	3.7 $\pm$ 23.8	0.488	-4.8 $\pm$ 7.4	0.113
Environment	5.3 $\pm$ 18.9	0.214	-4.0 $\pm$ 11.0	0.338
SNOT-22 (broad domain)				
Median	-7.1 $\pm$ 15.8	0.051	-5.0 $\pm$ 14.6	0.365
VFQ-25 (broad domain)				
General	-1.9 $\pm$ 3.4	0.022	-1.1 $\pm$ 1.7	0.108
Everyday	-8.8 $\pm$ 9.3	<0.001	-1.4 $\pm$ 4.8	0.448
Response	-4.5 $\pm$ 6.5	0.005	2.8 $\pm$ 8.2	0.374

SD – standard deviation; WHOQOL-BREF – World Health Organization's Quality of Life assessment tool; SNOT-22 – Sino-Nasal Outcome Test; VFQ-25 – Visual Functioning Questionnaire.

Anxiety and Depression Scale (HADS), the Multidimensional Fatigue Index (MFI-20), the Nottingham Health Profile (NHP), and Short Form 36 (SF-36). Their conclusion was that QOL is considerably lower in patients after successful treatment of NFPA.<sup>9</sup> Wolf et al. used the Headache Impact Test (HIT-6) and the SF-36 to assess QOL – preoperatively and at 6 weeks and 6 months after ETS for pituitary adenoma. The results of their study confirmed that surgery can significantly decrease headaches in patients with pituitary adenomas by 6 months postoperatively, particularly in younger patients, whose preoperative QOL is usually deteriorated.<sup>10</sup> Tanemura et al. evaluated QOL in patients with NFPA after ETS using the SF-36, the General Health Questionnaire 30 (GHQ30) and the Numerical Rating Scale (NRS) for pain, administering them at 3 time points: immediately before surgery, and 1 month and 6 months postoperatively. The SF-36 baseline value of visual function-impaired NFPA patients was lower than that in a normal population. On the SF-36 and GHQ30, mental summary scores generally increased 1 month after the surgery and remained stable for 6 months. It was found that the strongest factor related to QOL was visual function.<sup>11</sup> Fathalla et al. evaluated QOL in patients after ETS for acromegaly. They collected the RAND-36, the Center for Epidemiologic Studies Depression Scale (CES-D) and the Pituitary QOL validated questionnaires from 20 patients with acromegaly who had undergone ETS. Clearly, transsphenoidal surgery improves QOL in acromegaly. Additionally, the authors demonstrated the important role of the patient–physician relationship in QOL and the need to measure QOL along with the traditional measures of outcome.<sup>12</sup> Karppinen et al. examined 137 patients after transsphenoidal surgery for NFPA and compared their QOL with that of a healthy population. They demonstrated that overall HR-QOL was near-normal

after medium-term follow-up and that the most impaired domains were vision and sexual activity. Comorbidities are strong predictors of impaired HR-QOL.<sup>13</sup> In the available literature, we found publications in which the authors examined QOL in patients with pituitary tumors compared to a healthy population – e.g., following the SF-36 questionnaire, Johnson et al. proved that patients with a pituitary adenoma had significantly lower QOL than a normal population in terms of physical and mental status.<sup>14</sup> Goudakos et al. used a literature review and meta-analysis, including their own experience, and analyzed the efficacy and safety of ETS in comparison with MTS. There were no significant differences in regards to the remission rate of hormone hypersecretion or cerebrospinal fluid (CSF) leaks, but postoperative diabetes insipidus and other complications were less frequent in patients after ETS.<sup>15</sup> The ETS is clearly superior to MTS, which was also confirmed in the literature reviews conducted by Rotenberg et al.<sup>16</sup> and Schaberg et al.<sup>17</sup>

In the available literature reporting on sino-nasal disorders in patients operated on for pituitary tumors, the most commonly found assessment tool is the SNOT-22, which is widely used as a means of evaluating ear, nose and throat disorders in patients with pituitary tumors. Graham et al. used this test to assess RS-QOL in a group of 71 patients with pituitary tumors who had undergone ETS and 122 consecutive patients who had had an open procedure. For ETS, it was found that the mean hospital stay was shorter (4.1 days compared with 6 days for open procedures) and the overall complication rate was lower (33.5% compared to 43.4% for open procedures); while cerebrospinal fluid leaks were more frequent in the endoscopy group, the mean SNOT-22 score was lower for patients in the endoscopy group. Patients in the endoscopy group had a significantly lower rhinology-specific mean score, and more patients who had presented with visual deterioration showed improvement after ETS.<sup>18</sup> In our opinion, comparing the QOL between patients undergoing a transcranial approach with patients undergoing an endonasal approach is pointless because the indications for these procedures are vastly different; therefore, the neurosurgeon has to deal with 2 differing pituitary tumors, which are incomparable. Little et al. compared RS-QOL and health status in 218 patients undergoing MTS (111 patients) or ETS (107 patients). They used 3 tests: 1) the Anterior Skull Base Nasal Inventory-12 (ASK Nasal-12) to evaluate postoperative rhinology-specific symptoms; 2) the SF-36; and 3) the European Quality of Life Questionnaire (EQ-5D) to evaluate overall QOL. Patients from the ETS group were more likely to have postoperative nasal deterioration. Three months after the surgery, patients undergoing ETS reported statistically better RS-QOL than patients undergoing MTS.<sup>19</sup> McCoul et al. found that the ETS to the skull base can result in an increased intranasal area without a detrimental effect on rhinology-specific symptoms.<sup>20</sup> Hong et al. carried out a study of olfactory function and

RS-QOL after pituitary tumor ETS and MTS. There was no significant difference in subjective olfaction in the Cross-Cultural Smell Identification Test (CC-SIT) or in scores on the Butanol Threshold Test (BTT) between the ETS and MTS groups.<sup>21</sup> Olfactory disorders may persist for at least 4 months after pituitary MTS.<sup>22</sup> In our study, the results of RS-QOL in both groups were comparable. McCoull et al. analyzed QOL in 81 patients after endoscopic endonasal resection of pituitary tumors. The patients filled out the Anterior Skull Base Questionnaire (ASBQ) and the SNOT-22 preoperatively, and then at regular intervals after the surgery. The endoscopic resection of a pituitary adenoma is associated with long-term improvement in site-specific QOL and stability in RS-QOL when assessed pre- and postoperatively with validated instruments, yet partial resection correlated with worse QOL. In turn, extrasellar tumor extension, visual disturbances, intraoperative CSF leakage, and the reconstruction technique during surgery did not influence postoperative QOL.<sup>23</sup>

Okamoto et al. described the use of the National Eye Institute's VFQ-25 to evaluate VR-QOL in 74 patients with pituitary adenoma before and 3 months after MTS. The authors showed that MTS can significantly improve VR-QOL in pituitary adenoma, and that the preoperative VFQ-25 composite score and visual field defect in the better-seeing eye are particularly important predictors associated with the postoperative VR-QOL. The VFQ-25 proved to be a useful tool in the assessment of patients admitted for surgical treatment of pituitary tumors.<sup>3</sup>

In our study, ETS proved to have a greater impact on patients' QOL; in the literature, ETS has gained a clear advantage over MTS. In our opinion, the reason for better outcomes after ETS is primarily the better visibility of the operation field provided by the endoscope, which goes hand in hand with a more efficient decompression of the optic chiasm and better visual control of the pituitary gland, which is almost always visible and therefore remains undamaged. Moreover, an endoscope facilitates extended approaches to the skull base lesions (suprasellar, retrosellar and parasellar), which is beyond the abilities of the microscope. It should also be pointed out that the choice of method does not affect RS-QOL, which we did not expect when planning the research. Despite different invasive methods, this aspect of QOL was similar.

Rudmik et al. demonstrated an interesting approach to pituitary tumor surgery in studying the cost-effectiveness of endoscopic compared to pituitary MTS. It was found that ETS is a more cost-effective intervention than MTS.<sup>24</sup> The unusual perspective of this subject was also demonstrated by Little et al., who examined the inpatient resource utilization for patients undergoing pituitary ETS or MTS. The authors demonstrated that the use of ETS for pituitary lesions does not adversely affect the utilization of resources for inpatients; however, the primary factors of hospital charges, in order of importance, were length of stay, a diagnosis of Cushing's disease and – to a lesser

extent – the use of ETS.<sup>25</sup> Yadav et al. stressed the role of the cooperation between a neurosurgeon and an otolaryngologist, cadaveric dissection, practice on models, and observation of live surgeries in pituitary ETS. The ETS, according to the authors, is a superior surgical option in most pituitary adenomas.<sup>26</sup> Strychowsky et al. also found that ETS of pituitary adenomas seems to be safe and efficacious when compared to the traditional MTS and may offer some benefits.<sup>27</sup> On the other hand, Iwai et al. compared a single surgeon's experience operating on pituitary tumors with the use of MTS compared to ETS. They analyzed the results of treatment in a group of 100 patients (124 procedures) treated through the sublabial transsphenoidal approach and 45 patients (54 procedures) treated with binostril ETS performed by a single surgeon. The patients who underwent ETS had less statistically significant intraoperative blood loss, experienced less pain and presented less need for postoperative hormone replacement therapy.<sup>28</sup> Zaidi et al. investigated the impact of the surgeon's experience on the outcome after surgery. In their study, patients had been treated either by a less experienced surgeon (100 independent cases) who practices fully endoscopic surgery exclusively or by a very experienced surgeon (1,800 independent cases) who practices microscopic surgery exclusively. The authors concluded that a less experienced surgeon using ETS was able to achieve outcomes similar to those of an experienced surgeon using MTS in a cohort of patients with NFPA smaller than 60 cm<sup>3</sup>.<sup>29</sup>

The results of our study showed that ETS is more favorable to patients in the case of pituitary tumor surgery, which corresponds with the findings of other articles. The patients in this study who underwent ETS achieved considerably greater improvement in the overall quality of life, as assessed with the WHOQOL-BREF and in VR-QOL, as assessed with the VFQ-25. Many studies have confirmed that ETS is currently preferred to MTS of a pituitary tumor, especially in the context of VR-QOL, a view which is also validated by the results of our study. Although few studies have proven that ETS is associated with less severe outcome in RS-QOL, our study does not confirm these findings.

It should be mentioned that this study had several limitations that may have potentially affected the results and led to bias. One of them is the small sample population of the study. Additionally, objective assessment of patients' QOL is virtually obsolete, taking into account that pituitary adenomas occur in different volumes, configurations and microscopic appearance, and that every patient has different anatomical conditions within the nasal cavity and different expectations regarding the effectiveness of treatment. In this study, both groups of patients were homogenous with regard to age, sex and adenoma size, and the conclusions are based on the differences in questionnaire results collected before and after the surgery, thereby avoiding other conditions that may affect the results of a single questionnaire.

## Conclusions

The novel observation from this study is the significant improvement in VR-QOL of patients after pituitary ETS in comparison to patients undergoing MTS. The MTS does not deteriorate RS-QOL more than ETS. Endoscopic surgery seems to be more beneficial for patients with pituitary adenoma, which can deteriorate VR-QOL.

### ORCID iDs

Maciej Bryl  <https://orcid.org/0000-0001-5300-2788>  
 Jowita Woźniak  <https://orcid.org/0000-0002-5536-961X>  
 Krzysztof Dudek  <https://orcid.org/0000-0002-9442-989X>  
 Bogdan Czapiga  <https://orcid.org/0000-0002-9819-2455>  
 Paweł Tabakow  <https://orcid.org/0000-0001-8638-3871>

### References

- Cohen-Gadol AA, Liu JK, Laws ER Jr. Cushing's first case of transsphenoidal surgery: The launch of the pituitary surgery era. *J Neurosurg.* 2005;103(3):570–574.
- Fatemi N, Dusick JR, de Paiva Neto MA, Kelly DF. The endonasal microscopic approach for pituitary adenomas and other parasellar tumors: A 10-year experience. *Neurosurgery.* 2008;63(4):244–256.
- Okamoto Y, Okamoto F, Yamada S, Honda M, Hiraoka T, Oshika T. Vision-related quality of life after transsphenoidal surgery for pituitary adenoma. *Invest Ophthalmol Vis Sci.* 2010;51(7):3405–3410.
- The WHOQOL Group: Development of the World Health Organization WHOQOL-BREF quality of life assessment. *Psychol Med.* 1998;28(3):551–558.
- Wołowicka L, Jaracz K. Polska wersja WHOQOL – WHOQOL 100 i WHOQOL-BREF [In:] *Jakość życia w naukach medycznych.* Poznań, Poland: Wydawnictwo Akademii Medycznej w Poznaniu; 2001: 235–280.
- Morley AD, Sharp HR. A review of sinonasal outcome scoring systems: Which is best? *Clin Otolaryngol.* 2006;31(2):103–109.
- Mangione CM, Lee PP, Gutierrez PR, Spritzer K, Berry S, Hays RD; National Eye Institute Visual Function Questionnaire Field Test Investigators. Development of the 25-item National Eye Institute Visual Function Questionnaire. *Arch Ophthalmol.* 2001;119(7):1050–1058.
- Little AS, Kelly D, Milligan J, et al. Predictors of sinonasal quality of life and nasal morbidity after fully endoscopic transsphenoidal surgery. *J Neurosurg.* 2001;122(6):1458–1465.
- Dekkers OM, van der Klaauw AA, Pereira AM, et al. Quality of life is decreased after treatment for nonfunctioning pituitary macroadenoma. *J Clin Endocrinol Metab.* 2006;91(9):3364–3369.
- Wolf A, Goncalves S, Salehi F, et al. Quantitative evaluation of headache severity before and after endoscopic transsphenoidal surgery for pituitary adenoma. *J Neurosurg.* 2016;124(6):1627–1633.
- Tanemura E, Nagatani T, Aimi Y, Kishida Y, Takeuchi K, Wakabayashi T. Quality of life in nonfunctioning pituitary macroadenoma patients before and after surgical treatment. *Acta Neurochir.* 2012;154(10): 1895–1902.
- Fathalla H, Cusimano MD, Alsharif OM, Jing R. Endoscopic transsphenoidal surgery for acromegaly improves quality of life. *Can J Neurol Sci.* 2014;41(6):735–741.
- Karppinen A, Ritvonen E, Roine R, et al. Health-related quality of life in patients treated for non-functioning pituitary adenomas during the years 2000–2010. *Clin Endocrinol (Oxf).* 2016;84(4):532–539. doi:10.1111/cen.12967
- Johnson MD, Woodburn CJ, Vance ML. Quality of life in patients with a pituitary adenoma. *Pituitary.* 2003;6(2):81–87.
- Goudakos JK, Markou KD, Georgalas C. Endoscopic versus microscopic trans-sphenoidal pituitary surgery: A systematic review and meta-analysis. *Clin Otolaryngol.* 2011;36(2):212–220.
- Rotenberg B, Tam S, Ryu WHA, Duggal N. Microscopic versus endoscopic pituitary surgery: A systematic review. *Laryngoscope.* 2010;120(7):1292–1297.
- Schaberg MR, Vijay KA, Schwartz TH, Cobb W. Microscopic versus endoscopic transnasal pituitary surgery. *Curr Opin Otolaryngol Head Neck Surg.* 2010;18(1):8–14.
- Graham SM, Iseli TA, Karnell LH, Clinger JD, Hitchon PW, Greenlee JDW. Endoscopic approach for pituitary surgery improves rhinologic outcomes. *Ann Otol Rhinol Laryngol.* 2009;118(9):630–635.
- Little AS, Kelly DF, Milligan J, et al. Comparison of sinonasal quality of life and health status in patients undergoing microscopic and endoscopic transsphenoidal surgery for pituitary lesions: A prospective cohort study. *J Neurosurg.* 2015;123(3):799–807.
- McCoul ED, Patel AS, Bedrosian JC, Anand VK, Schwartz TH. Intranasal cross-sectional area and quality of life changes following endoscopic transsphenoidal skull base surgery. *Int Forum Allergy Rhinol.* 2015;5(12):1124–1128. doi:10.1002/alr.21602
- Hong SD, Nam H, Seol HJ, et al. Endoscopic binostril versus transnasal transeptal microscopic pituitary surgery: Sinonasal quality of life and olfactory function. *Am J Rhinol Allergy.* 2015;29(3):221–225.
- Wang S, Chen Y, Li J, Wei L, Wang R. Olfactory function and quality of life following microscopic endonasal transsphenoidal pituitary surgery. *Medicine (Baltimore).* 2015;94(4):e465. doi:10.1097/MD.0000000000000465
- McCoul ED, Bedrosian JC, Akselrod O, Anand VK, Schwartz TH. Preservation of multidimensional quality of life after endoscopic pituitary adenoma resection. *J Neurosurg.* 2015;123(3):813–820.
- Rudmik L, Starreveld YP, Vandergrift WA, Banglawala SM, Soler ZM. Cost-effectiveness of the endoscopic versus microscopic approach for pituitary adenoma resection. *Laryngoscope.* 2015;125(1):16–24.
- Little AS, Chapple K, Jahnke H, White WL. Comparative inpatient resource utilization for patients undergoing endoscopic or microscopic transsphenoidal surgery for pituitary lesions. *J Neurosurg.* 2014;121(1):84–90.
- Yadav Y, Sachdev S, Parihar V, Namdev H, Bhatlele PR. Endoscopic endonasal trans-sphenoid surgery of pituitary adenoma. *J Neurosci Rural Pract.* 2012;3(3):328–337.
- Strychowsky J, Nayan S, Reddy K, Farrokhyar F, Sommer D. Purely endoscopic transsphenoidal surgery versus traditional microsurgery for resection of pituitary adenomas: Systematic review. *J Otolaryngol Head Neck Surg.* 2011;40(2):175–185.
- Iwai Y, Yoshimura M, Terada A, Yamanaka K, Koshimo N. Transsphenoidal surgery for pituitary tumors from microsurgery to the endoscopic surgery: Single surgeon's experience [in Japanese]. *No Shinkei Geka.* 2011;39(2):141–147.
- Zaidi HA, Awad AW, Bohl MA, et al. Comparison of outcomes between a less experienced surgeon using a fully endoscopic technique and a very experienced surgeon using a microscopic transsphenoidal technique for pituitary adenoma. *J Neurosurg.* 2015;16:1–9.



# MicroRNA-24 inhibits CDX1 expression in decidual tissues of recurrent spontaneous abortion mice to reduce the abortion risk

Shuyan Wang<sup>1,A–D</sup>, Shishan Guo<sup>2,C,E</sup>, Xiaoyan Hou<sup>1,A,B,D–F</sup>

<sup>1</sup> Department of Clinical Laboratory, Maternity and Child Health Care Hospital of Zaozhuang, China

<sup>2</sup> Department of Blood Transfusion, Maternity and Child Health Care Hospital of Zaozhuang, China

A – research concept and design; B – collection and/or assembly of data; C – data analysis and interpretation; D – writing the article; E – critical revision of the article; F – final approval of the article

Advances in Clinical and Experimental Medicine, ISSN 1899–5276 (print), ISSN 2451–2680 (online)

*Adv Clin Exp Med.* 2020;29(8):929–936

## Address for correspondence

Xiaoyan Hou

E-mail: [houxiaoyan4d7k@163.com](mailto:houxiaoyan4d7k@163.com)

## Funding sources

None declared

## Conflict of interest

None declared

Received on January 13, 2020

Reviewed on February 5, 2020

Accepted on May 8, 2020

Published online on August 21, 2020

## Abstract

**Background.** Recurrent spontaneous abortion (RSA), presenting as one of the difficult clinical diseases, has a high incidence rate among women of reproductive age, with a rising trend in recent years.

**Objectives.** To confirm a target relationship between miR-24 and CDX1. This study aimed to explore miR-24 expression in decidual tissue under recurrent spontaneous abortion (RSA) and its mechanism of regulating downstream gene *CDX1*.

**Material and methods.** Female CBA/J mice were mated with male BALB/C mice to establish normal pregnancy models, and mated with male DBA/2 mice to establish RSA models. Recurrent spontaneous abortion model mice were randomized into 5 groups: a model group, a NC group, a miR-24 mimic group, a CDX1 vector group, and a miR-24 mimic+CDX1 vector group. Expressions of miR-24, CDX1, VEGF, cleaved caspase-3, Fas, and FasL, as well as apoptosis in decidual tissues, embryonic development and embryo loss rate were compared.

**Results.** Compared with the normal group, the embryo loss rate, apoptosis rate, and the expressions of cleaved caspase-3, Fas and CDX1 in decidual tissue in other groups were significantly increased, and the expressions of miR-24, VEGF, and FasL were significantly decreased (all  $p < 0.05$ ). The miR-24 mimic group showed the opposite changes when compared with the model group (all  $p < 0.05$ ). However, CDX1 overexpression can significantly block the protective effect of miR-24 overexpression on embryonic development ( $p < 0.05$ ).

**Conclusions.** MiR-24 can inhibit CDX1 expression in decidual tissue of RSA mice, thus improving the embryonic development of the mice and reducing the RSA risk.

**Key words:** spontaneous abortion, caudal-type homeobox protein 1, microRNA-24

## Cite as

Wang S, Guo S, Hou X. MicroRNA-24 inhibits CDX1 expression in decidual tissues of recurrent spontaneous abortion mice to reduce the abortion risk.

*Adv Clin Exp Med.* 2020;29(8):929–936.

doi: [10.17219/acem/122173](https://doi.org/10.17219/acem/122173)

## DOI

[10.17219/acem/122173](https://doi.org/10.17219/acem/122173)

## Copyright

© 2020 by Wrocław Medical University

This is an article distributed under the terms of the Creative Commons Attribution 3.0 Unported (CC BY 3.0) (<https://creativecommons.org/licenses/by/3.0/>)

## Introduction

Recurrent spontaneous abortion (RSA) is defined as 3 consecutive pregnancy losses in a woman of reproductive age in the setting of 1 identical sexual partner.<sup>1,2</sup> Recurrent spontaneous abortion, presenting as a difficult clinical disease, has a high incidence rate among women of reproductive age, with a rising trend in recent years.<sup>3,4</sup> Exploration on the mechanism of RSA can enrich the theoretical basis in clinical treatment and thus may provide new critical ideas for RSA treatment.

We found that caudal-type homeobox 1 (CDX1) was significantly overexpressed in RSA through preliminary experiments. No research at present has confirmed the mechanism of CDX1 affecting RSA. One research study showed that the expression of enhancer of zeste homologue 2 (EZH2) was significantly downregulated in RSA, and 1 other research study through chromatin immunoprecipitation assay confirmed that EZH2 was obviously bound with CDX1, and through dual-luciferase reporter gene assay verified that EZH2 could negatively regulate CDX1 expression.<sup>5,6</sup> Therefore, we speculated that CDX1 may be a crucial target in RSA. However, the deeper significance and potential mechanism of CDX1 in RSA are still unclear. To date, many studies have reported microRNA expression regulation in RSA.<sup>7–11</sup> Some studies have shown that miR-24 expression is downregulated in decidual NK cells.<sup>12–14</sup> MiR-24 regulates post-transcriptional expressions mainly by targeting downstream genes. Collectively, miR-24 may also serve as an important regulatory factor affecting RSA. As a result, we screened the downstream target genes of miR-24 and found that there was a binding site between CDX1 and miR-24. Therefore, we further speculated that miR-24 may highly possibly serve as the upstream regulatory component of CDX1 in RSA.

In this study, we constructed RSA mouse models and conducted overexpression on miR-24 and CDX1 in order to explore the expression regulation relationship between miR-24 and CDX1 in the decidual tissues of RSA model as well as its effect on RSA.

## Methods

### Animals

One hundred and twenty specific pathogen-free female CBA/J mice, 10 male BALB/C mice and 50 male DBA/2 mice at 6–8 weeks of age were selected in this study. The mice were raised in animal rooms at suitable temperature, under a 12/12-hour dark/light cycle with ad libitum access to standard rodent diet and water throughout the study. All procedures were approved by the Animal Care and Use Committee and conformed to the revised (1996) Guide for the Care and Use of Laboratory Animals published by the US National Institutes of Health (NIH). This study was reviewed and approved by the local ethics committee.

## Animal modeling and grouping

The normal pregnancy models were constructed by mating CBA/J female mice with BALB/C male ones, while RSA models were made by mating CBA/J female mice with DBA/2 male ones. Twenty CBA/J female mice and 10 BALB/C male ones were mated in a ratio of 2:1, while 100 CBA/J female mice and 50 DBA/2 male ones were mated in the same ratio.<sup>15,16</sup> The presence of a vaginal plug marked that day as embryonic day 0 in a pregnant mouse, and finally 20 normal pregnancy model mice and 100 RSA model mice were obtained.

The RSA model mice were randomized into 5 groups on average, the model group (RSA mice without other treatment), the NC group (RSA mice with injection of miR-24 NC and transfection reagent through caudal vein), miR-24 mimic group (RSA mice with infection of miR-24 mimic and transfection reagent through caudal vein), the CDX1 vector group (RSA mice with injection of pcDNA3.1-CDX1 overexpression vector), and the miR-24 mimic+CDX1 vector group (RSA mice with injection of miR-24 mimic and pcDNA3.1-CDX1 overexpression vector). MiR-24 mimic NC, miR-24 mimic and pcDNA3.1-CDX1 were all purchased from Guangzhou RiboBio Co., Ltd., Guangzhou, China. MiR-24 mimic NC, NC vector, miR-24 mimic, and pcDNA3.1-CDX1 were mixed with 50  $\mu$ L culture medium and with 50  $\mu$ L Entranster<sup>TM</sup>-in vivo transfection reagent. According to the grouping, the mixed solutions were injected into the corresponding mice through the caudal vein at a dose of 2 mg/kg. The first intravenous injection was carried out at the time of mating in the cage; then, the same injection was performed at three-day intervals until the 14<sup>th</sup> day after conception. The mice were sacrificed at day 14 after conception, and the uteri of the mice were then removed out for observation on the embryonic development and the calculation on the embryo loss rate.

## Quantitative reverse-transcriptase PCR

Decidual tissues of the mice in each group were taken and ground into homogenate for quantitative reverse-transcriptase polymerase chain reaction (qRT-PCR) analysis. Total RNA in the decidual tissues was extracted using TRIzol<sup>®</sup> reagent (Invitrogen, Carlsbad, USA). The extracted RNA was reversely transcribed into cDNA by the TaqMan<sup>®</sup> MicroRNA Reverse Transcription Kit (4427975; Applied Biosystems, Foster City, USA). The reverse transcription reaction volume was set as 25  $\mu$ L. The reaction was performed at 37°C for 30 min, and the inactivation reaction was done at 85°C for 5 s. Primers designed for miR-24, CDX1, GAPDH, and U6 were synthesized by Beijing Tsingke Biotechnology Co., Ltd., Beijing, China (Table 1). Reverse-transcriptase quantitative PCR was processed using ABI7500 real-time quantitative PCR instrument (Thermo Fisher Scientific, Waltham, USA). The reaction conditions were as follows: pre-denaturation at 95°C for 10 min, denaturation at 95°C for 10 s, annealing at 60°C for 20 s, and lastly extension at 72°C for 2 min,

Table 1. Primer sequences

Gene	Primer sequence (5'-3')
miR-24	F: GGGTGGCTCAGTTCAGCAG
	R: GTGCAGGTCGAGGT
U6	F: CTCGCTTCGGCAGCACATA
	R: AACGATTACGAATTTGCGT
CDX1	F: GATGGCCTCAATGGGTACAAG
	R: TCGTTGTTGTTGATGTCACAGT
GAPDH	F: TGGCCTCCGTGTTCTCTAC
	R: GAGTTGCTGTTGAAGTCGCA

F – forward; R – reverse; CDX1 – caudal type homeobox 1.

with 35 cycles. The PCR system was set as 20  $\mu$ L, containing 0.8  $\mu$ L of qPCR forward primer (10  $\mu$ M), 0.8  $\mu$ L of qPCR reverse primer (10  $\mu$ M), 0.4  $\mu$ L of ROX reference dye II, 10  $\mu$ L of SYBR<sup>®</sup> Premix Ex Taq<sup>™</sup> II (Thermo Fisher Scientific), 2.0  $\mu$ L of cDNA template, and 6.0  $\mu$ L of sterilized distilled water. The U6 and GAPDH were used as internal controls for the relative expression of miR-24 and CDX1 mRNA, respectively. The relative expression level of each target gene was calculated with  $2^{-\Delta\Delta Ct}$  method, where  $\Delta\Delta Ct = \Delta Ct_{\text{experimental group}} - \Delta Ct_{\text{GAPDH}}$ , in which  $\Delta Ct = Ct_{\text{target gene}} - Ct_{\text{internal control}}$ . Ct referred to the amplification cycles.

## Dual-luciferase reporter gene assay

The binding sites of miR-24 to CDX1 gene within the 3'-UTR were analyzed through the bioinformatics prediction website (<https://cm.jefferson.edu/rna22/>). The target relationship between miR-24 and CDX1 was verified using dual-luciferase reporter gene assay. The 3' UTR of CDX1 gene and the 3' UTR of mutated CDX1 gene were respectively inserted into the dual-luciferase reporter gene vector pGL3-Basic, and 2 vectors were named as PGL3-CDX1 wt and PGL3-CDX1 mut, respectively. Renilla plasmid and the 2 reporter gene vectors were respectively co-transfected with miR-24 mimic and miR-24 mimic NC into human embryonic kidney (HEK) 293T cells. After 24 h of cell transfection, dual-luciferase activity was detected using the dual-luciferase reporter gene assay. The cells of each group were lysed and then centrifuged at 12,000 rpm for 1 min, and the supernatant was collected. The dual-luciferase reporter assay kit was purchased from Promega (Boston, USA) and luciferase activity was measured according to the instructions of the kit.

## Western blotting

Western blotting was used to detect the expression levels of cleaved caspase-3, Fas, FasL, and VEGF in decidual tissues of the mice. Decidual tissue homogenate was again prepared for western blotting. Protein extraction was performed using RIPA cell lysis reagent (BB-3209; BestBio Technology, Co., Ltd., Shanghai, China). The proteins were

separated with SDS-PAGE and transferred to polyvinylidene difluoride (PVDF) membrane at a constant voltage of 80 V. After being sealed by blocking solution for 1 h, the membrane was incubated with anti-rabbit primary antibodies against cleaved caspase-3 (1: 500; ab49822; Abcam, Cambridge, UK), Fas (1: 1,000; ab15285; Abcam), FasL (1: 1,000; ab15285; Abcam), VEGF (1: 1,000; Ab27278; Abcam) and GAPDH (1: 2,500; ab9485; Abcam), and sealed for incubation with shaking overnight at 4°C. Then, the membrane was incubated with horseradish peroxidase (HRP)-labeled goat anti-rabbit IgG (1: 2,000; ab205718; Abcam) with shaking at 37°C for 2 h. The PVDF membrane was color-developed and photographed. The relative expression of a target protein = the gray value of the target band/the gray value of the internal control band.

## TUNEL fluorescence assay

TUNEL fluorescence detection kit (Roche, Basel, Switzerland) was used to detect the cell apoptosis of decidual tissues in all mice. Paraffin blocks of fixed decidual tissues of all mice were made and sliced into serial sections. Then, the sections were mounted onto glass slides and numbered in sequence. Subsequently, the slices with sections were dewaxed and hydrated, and reacted with cell permeabilization reagent for 8 min, followed by washing with phosphate-buffered saline (PBS) twice. The 50  $\mu$ L TUNEL reaction mixture was added to the slides for 1 h in a wet box at room temperature, followed by 3 washes with PBS. The treated slides were observed under a Nikon eclipse TE2000-U fluorescence microscope (Nikon, Tokyo, Japan). The average number of TUNEL positive cells was observed using Image-Pro Plus v. 6.0 software by randomly selecting 5 visual fields under a light microscope.

## Immunofluorescent assay

The decidual tissue sections of all the mice were made and then mounted onto glass slides. Slices were sealed with primary antibody mouse anti-VEGF (1: 100; ab205; Abcam), incubated at room temperature for 1 h and sealed by FITC conjugated goat anti-mouse IgG antibody (1: 200; ab150117; Abcam) for 30 min. Then, the nucleus was stained by Invitrogen<sup>™</sup> Molecular Probes<sup>™</sup> DAPI (4',6-diamidino-2-phenylindole, dihydrochloride) for 10 min. After ten-minute staining, the slides were washed 3 times with 1  $\times$  PBS for 10 min each time to prevent fluorescence quenching agent from entering the sealed sections. The slides were observed under a fluorescence microscope (XSP-BM22AY; Shanghai Optical Instrument Factory, Shanghai, China).

## Statistical analysis

Data analyses were performed with the SPSS v. 21.0 software package (IBM Corp., Armonk, USA). All measurement data were expressed as mean  $\pm$  standard deviation

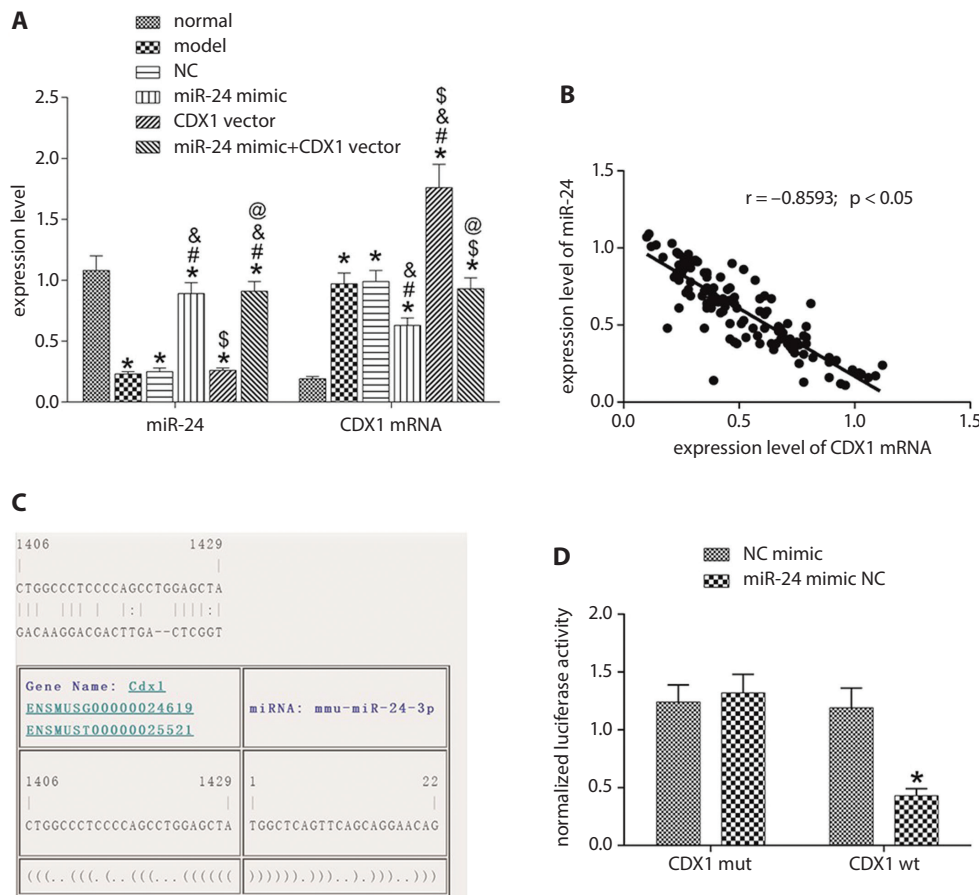


**Fig. 1.** MiR-24 can negatively regulate CDX1 expression. A. The expressions of miR-24 and CDX1 in decidual tissues of the mice through qRT-PCR; compared with the normal group, \* $p < 0.05$ ; compared with the model group, # $p < 0.05$ ; compared with the NC group, @ $p < 0.05$ ; compared with the miR-24 mimic group,  $\delta p < 0.05$ ; compared with CDX1 vector group,  $\epsilon p < 0.05$ ; B. Correlation analysis between miR-24 and CDX1; C. The targeted relationship between miR-24 and CDX1 through dual-luciferase reporter gene assay; D. The results of dual-luciferase reporter gene assay. Compared with NC mimic, \* $p < 0.05$

CDX1 – caudal type homeobox 1.

(SD). Pairwise comparisons among groups were conducted with one-way analysis of variance (ANOVA) test combined with Bonferroni post hoc test. A value of  $p < 0.05$  was considered statistically significant.

## Results

### MiR-24 can negatively regulate CDX1 expression

The expressions of miR-24 and CDX1 in decidual tissues of the mice detected using qRT-PCR are shown in Fig. 1A. Compared with the normal group, miR-24 expression level significantly decreased but CDX1 significantly increased in other groups (all  $p < 0.05$ ). Compared with the model group, miR-24 expression level in miR-24 mimic group was significantly increased, with significant decrease in CDX1 expression; miR-24 expression level in the miR-24 mimic+CDX1 vector group was significantly increased ( $p < 0.05$ ), but with no significant change in CDX1 expression level ( $p > 0.05$ ); CDX1 expression level in the CDX1 vector group was significantly increased ( $p < 0.05$ ), but with no significant change in miR-24 expression level ( $p > 0.05$ ).

We found a significant negative correlation between miR-24 and CDX1 in 120 female mice as shown in Fig. 1B. Since a binding site between miR-24 and CDX1 was predicted

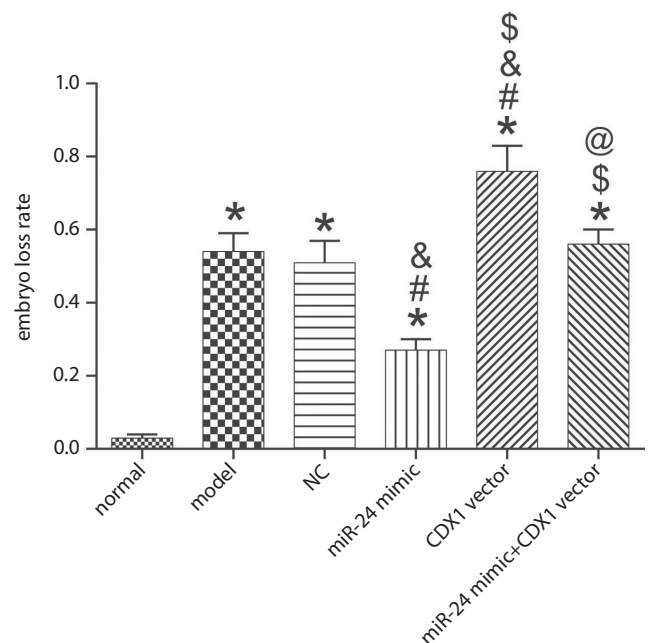


**Fig. 2.** Comparisons between groups of mice in embryonic loss rate. Compared with the normal group, \* $p < 0.05$ ; compared with the model group, # $p < 0.05$ ; compared with the NC group, @ $p < 0.05$ ; compared with the miR-24 mimic group,  $\delta p < 0.05$ ; compared with the CDX1 vector group,  $\epsilon p < 0.05$

CDX1 – caudal type homeobox 1.



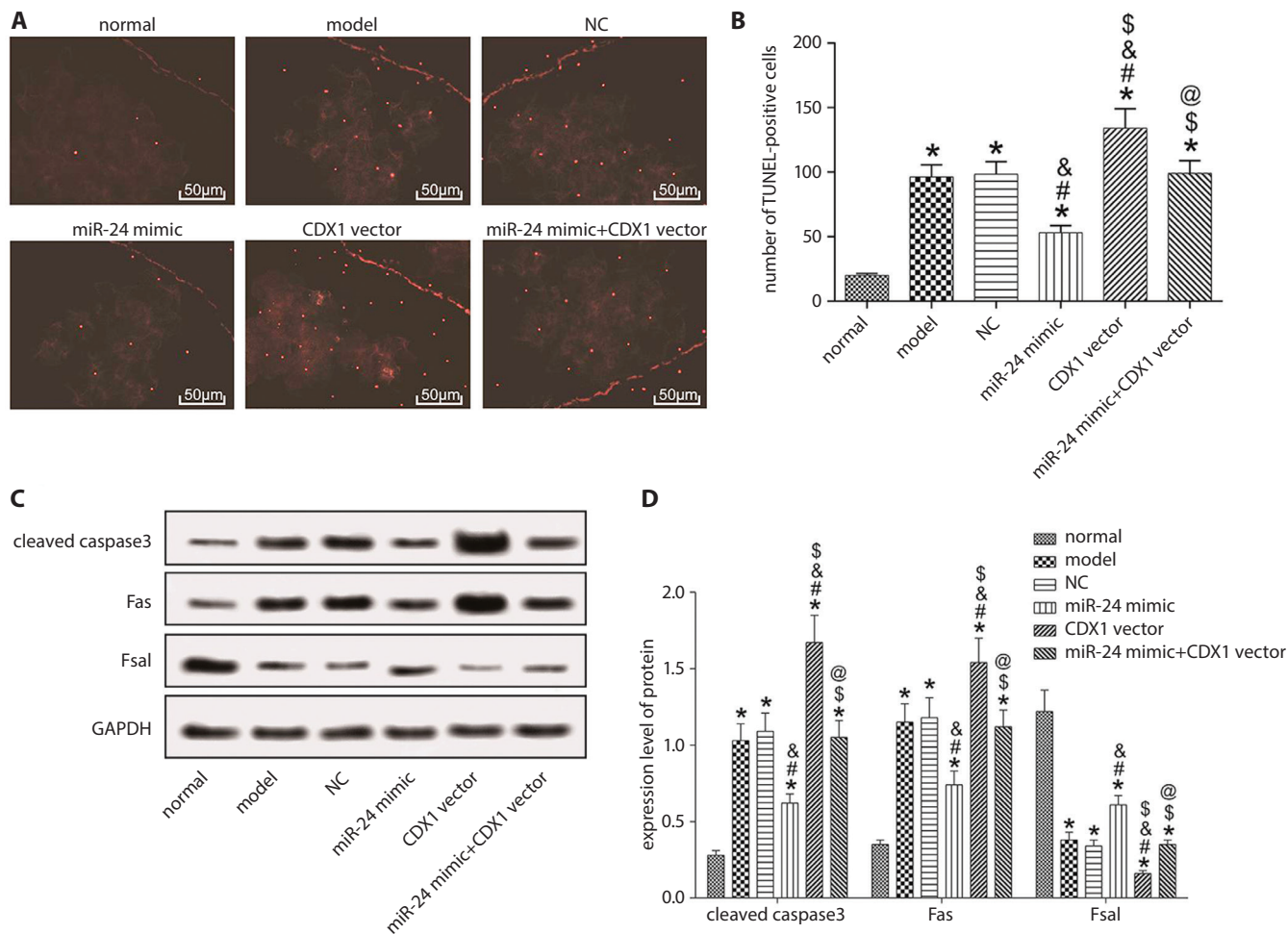


**Fig. 3.** Analysis of apoptosis in decidual tissues of the mice. The apoptosis (A) and the numbers of apoptotic cells (B) in decidual tissue of the mice through TUNEL fluorescence assay; C. Western blot bands; D. Detection results of apoptosis-related factors. Compared with the normal group, \* $p < 0.05$ ; compared with the model group, # $p < 0.05$ ; compared with the NC group, @ $p < 0.05$ ; compared with the miR-24 mimic group, § $p < 0.05$ ; compared with the CDX1 vector group, @ $p < 0.05$

CDX1 – caudal type homeobox 1.

by RNA22, we hypothesized that miR-24 may act as an upstream regulatory element regulating CDX1 expression, so we performed gene assay using a dual-luciferase reporter to test binding sites. The results in Fig. 1C and 1D showed that luciferase activity was significantly decreased after co-transformation of wild-type CDX1 reporter plasmid and miR-24 mimic ( $p < 0.05$ ), indicating that miR-24 can targetedly and negatively regulate CDX1 expression.

### Embryonic development of the mice

The mice were sacrificed at day 14 after pregnancy, and the uteri were then removed for observation for the embryonic development of all mice to obtain the embryo loss rate (Fig. 2). A higher embryo loss rates was observed in other groups when compared to that in the normal group (all  $p < 0.05$ ). Additionally, when compared with the model group, opposite results occurred in the miR-24 mimic group, while similar results were obtained in the CDX1 vector group (both  $p < 0.05$ ).

### Cell apoptosis of decidual tissues of the mice

Cell apoptosis of decidual tissues may be one of the causes contributing to mouse embryo death and RSA. We detected the cell apoptosis of decidual tissues in all mice using TUNEL fluorescence assay, and the results are shown in Fig. 3A and 3B. The normal group has significantly more TUNEL positive cells than other groups. The number of TUNEL positive cells significantly decreased in miR-24 mimic group, but significantly increased in CDX1 vector group when compared to that in the model group, which was significantly elevated in the miR-24 mimic+CDX1 vector group when compared with that in the miR-24 mimic group, while significantly decreased in the miR-24 mimic+CDX1 vector group when compared to that in the CDX1 vector group ( $p < 0.05$ ). Additionally, we detected the expression levels of apoptosis-related factors, cleaved caspase-3, Fas and FasL, through western blotting. The results in Fig. 3C and 3D show that

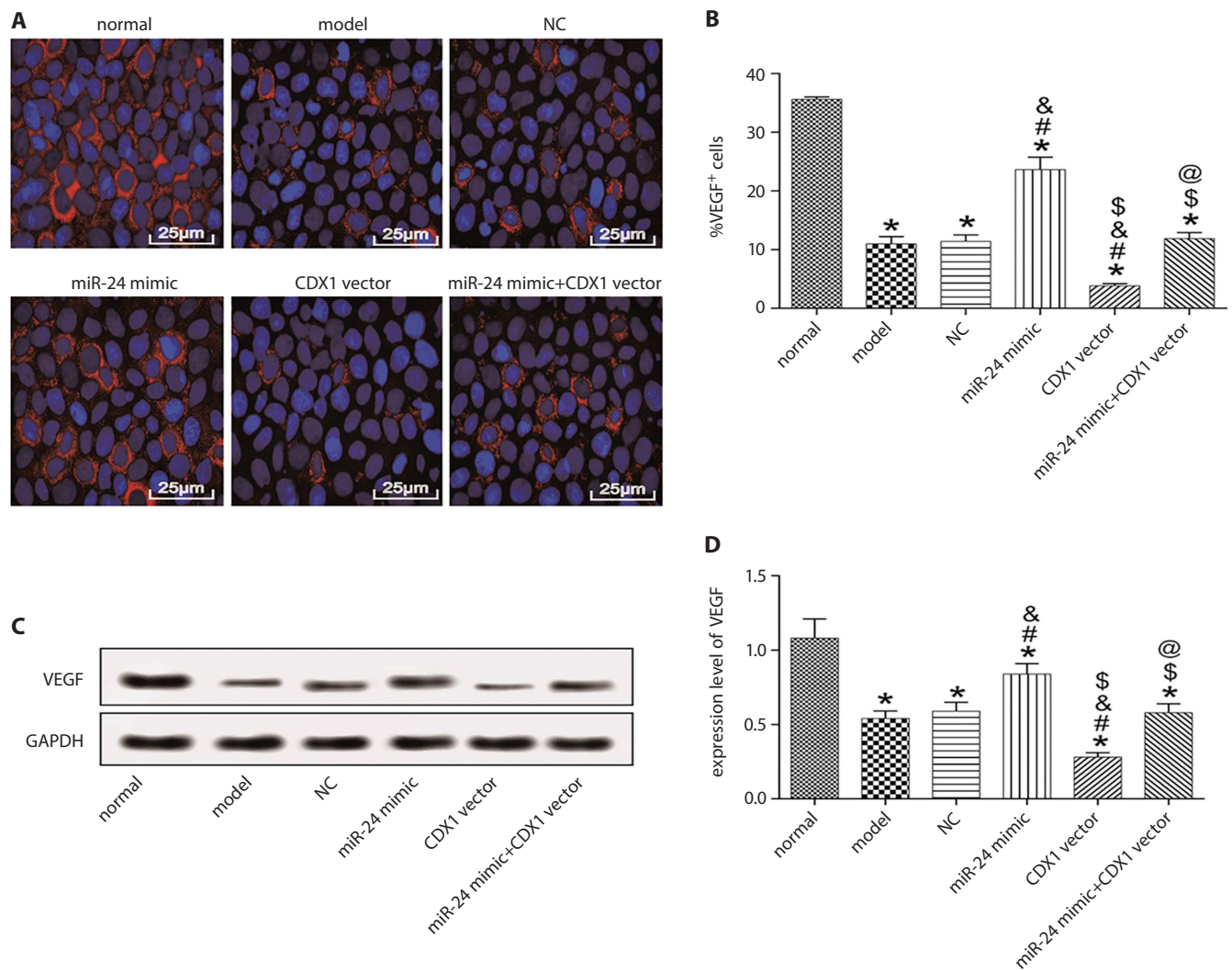


**Fig. 4.** Immunohistochemical results of rats in all groups. **A.** Microscopic image of immunohistochemical staining ( $\times 400$  magnification). **B.** Statistical analysis of the number of VEGF-positive cells in all groups; **C.** Western blot bands; **D.** Statistical analysis of VEGF protein expression. Compared with the normal group, \* $p < 0.05$ ; compared with the model group, # $p < 0.05$ ; compared with the NC group, & $p < 0.05$ ; compared with the miR-24 mimic group, \$ $p < 0.05$ ; compared with the CDX1 vector group, @ $p < 0.05$

CDX1 – caudal type homeobox 1; GAPDH – glyceraldehyde-3-phosphate dehydrogenase.

overexpression of miR-24 could inhibit the expressions of cleaved caspase-3 and Fas, and promote the expression of FasL, while CDX1 overexpression showed the opposite changes. These results comprehensively confirmed that miR-24 overexpression can significantly reduce the cell apoptosis of decidual tissue, while overexpression of CDX1 can promote the apoptosis of decidual tissues in mice; moreover, CDX1 overexpression can block the inhibitory effect of miR-24 overexpression on the apoptosis of decidual tissues in mice.

### VEGF expression of decidual tissues of the mice

The expression of VEGF in decidual tissues was detected with immunofluorescence assay, and the results are shown in Fig. 4A and 4B. The normal group has significantly higher fluorescence expression levels of VEGF in decidual

tissues than other groups ( $p < 0.05$ ). The VEGF fluorescence expression was significantly higher in miR-24 mimic group, while significantly lower in CDX1 vector group when compared to that in the model group ( $p < 0.05$ ). Additionally, we detected the protein expression of VEGF using western blotting (Fig. 4C,D), and the results were consistent with expression trend in the immunofluorescence assay.

## Discussion

Recurrent spontaneous abortion presents high incidence among pregnant women, with high difficulty in treatment and cure. The mechanism of RSA under exploration may serve as a crucial guiding role in clinical treatment.<sup>17,18</sup> In this study, we mainly focused on decidual tissue, which plays a vital role in the occurrence and maintenance of a pregnancy.<sup>19</sup>

Initially, we found that CDX1 may be overexpressed in RSA through preliminary experiments. Meanwhile, some literatures showed that CDX1 may have aggravating effect on the condition of RSA. Therefore, we constructed RSA mouse models and detected the expression of CDX1 in normal pregnant mice and RSA mice, and the results were consistent with the results of the bioinformatics prediction. Thus, we performed overexpression on CDX1 in RSA mice. The results showed that the fatality rate of treated mouse embryos increased significantly, suggesting that the development of mouse embryos evidently deteriorated after overexpression of CDX1. Additionally, we detected the apoptosis of decidual tissues and found that the apoptosis rate of decidual tissues in the mice increased significantly after CDX1 overexpression. VEGF plays a highly favorable role in the auxoaction for vascular remodeling of endometrium tissue, thus further facilitating differentiation of trophoblastic cells of mouse embryo and embryo implantation, conclusively promoting mouse embryo development.<sup>20–22</sup> We found that the expression level of VEGF after overexpression of CDX1 decreased significantly. Based on the above experiments, we speculate that CDX1 overexpression in the RSA mice may not only lead to apoptosis of decidual tissue and instability of embryo development during pregnancy, but also cause inhibition on VEGF expression and embryo implantation, thus hindering the development of mouse embryo and giving rise to further occurrence of RSA.

The bioinformatics prediction website also found a binding site between miR-24 and CDX1. We also detected the expression of miR-24 in normal pregnant mice and RSA mice, and verified the binding relationship between miR-24 and CDX1 using dual-luciferase reporter gene assay. The results show that miR-24 expression was downregulated in RSA mice, and miR-24 could target CDX1 and inhibit its expression. The phenotypic results in RSA mice receiving overexpression on miR-24 were opposite to those receiving overexpression on CDX1. In addition, compared with the RSA mice receiving miR-24 overexpression, the apoptosis ratio of decidual tissue in the RSA mice treated with overexpression on both miR-24 and CDX1 was significantly elevated, with significant reduction on VEGF expression. Based on the above results, we speculate that miR-24 overexpression can reduce apoptosis of decidual tissue and increase VEGF expression by inhibiting CDX1 expression in RSA mice, thus improving mouse embryo development and lowering abortion rate.

However, the causes of RSA are complex, and contributors also include endocrine disorders, body immunity and prethrombotic state apart from the effects of decidual tissue and uterus implantation.<sup>23–28</sup> However, this study mainly aimed to explore the effects of miR-24 and CDX1 on apoptosis of decidual tissue and VEGF expression, and it is not clear whether miR-24 and CDX1 have regulatory effects on endocrine, immune function and prethrombotic state of pregnant mice.


## Conclusions

We confirmed the expressions of miR-24 and CDX1 in decidual tissues of RSA mice and also the expression regulation relationship between them, which further enriches the mechanism of RSA, potentially providing a new idea for clinical treatment on RSA.

### ORCID iDs

Shuyan Wang  <https://orcid.org/0000-0003-1629-5176>

Shishan Guo  <https://orcid.org/0000-0001-7119-9641>

Xiaoyan Hou  <https://orcid.org/0000-0002-0645-8018>

### References

1. Karim S, Jamal HS, Rouzi A, et al. Genomic answers for recurrent spontaneous abortion in Saudi Arabia: An array comparative genomic hybridization approach. *Reprod Biol.* 2017;17(2):133–143.
2. Sun Q, Zhang XL. Research on apoptotic signaling pathways of recurrent spontaneous abortion caused by dysfunction of trophoblast infiltration. *Eur Rev Med Pharmacol Sci.* 2017;21(3 Suppl):12–19.
3. Al-Azawi IH, Khaleel SH, Al-Khafaji GK. Using PCR assay for detection and subtyping of *Ureaplasma parvum* in women with recurrent abortion. *Rev Med Microbiol.* 2017;28(1):26–29.
4. Yang HL, Zhou WJ, Gu CJ, et al. Pleiotropic roles of melatonin in endometriosis, recurrent spontaneous abortion, and polycystic ovary syndrome. *Am J Reprod Immunol.* 2018;80(1):e12839.
5. Ling Y, Huang Y, Chen C, Mao J, Zhang H. Low dose cyclosporin A treatment increases live birth rate of unexplained recurrent abortion: Initial cohort study. *Clin Exp Obstet Gynecol.* 2017;44(2):230–235.
6. Huang XJ, Wang X, Ma X, et al. EZH2 is essential for development of mouse preimplantation embryos. *Reprod Fertil Dev.* 2014;26(8):1166–1175.
7. Dong X, Yang L, Wang H. miR-520 promotes DNA-damage-induced trophoblast cell apoptosis by targeting PARP1 in recurrent spontaneous abortion (RSA). *Gynecol Endocrinol.* 2017;33(4):274–278.
8. Zhao L, Li J, Huang S. Patients with unexplained recurrent spontaneous abortion show decreased levels of miR-146a-5p in the decidua. *Ann Clin Lab Sci.* 2018;48(2):177–182.
9. Chen H, Yang Q, Chen K, et al. Integrated microRNA and transcriptome profiling reveals a miRNA-mediated regulatory network of embryo abortion under calcium deficiency in peanut (*Arachis hypogaea* L.). *BMC Genomics.* 2019;20(1):392.
10. Lu XY, Chen D, Gu XY, et al. Predicting value of *ALCAM* as a target gene of miR-483-5p in patients with early recurrence in hepatocellular carcinoma. *Front Pharmacol.* 2017;8:973.
11. Zhu Y, Lu H, Huo Z, et al. MicroRNA-16 inhibits fetomaternal angiogenesis and causes recurrent spontaneous abortion by targeting vascular endothelial growth factor. *Sci Rep.* 2016;6:35536.
12. Li D, Li J. Association of miR-34a-3p/5p, miR-141-3p/5p, and miR-24 in decidual natural killer cells with unexplained recurrent spontaneous abortion. *Med Sci Monit.* 2016;22:922–929.
13. Wang X, Li B, Wang J, et al. Evidence that miR-133a causes recurrent spontaneous abortion by reducing HLA-G expression. *Reprod Biomed Online.* 2012;25(4):415–424.
14. Yuan Y, Kluiver J, Koerts J, et al. miR-24-3p is overexpressed in Hodgkin lymphoma and protects Hodgkin and Reed–Sternberg cells from apoptosis. *Am J Pathol.* 2017;187(6):1343–1355.
15. Sadighi-Moghaddam B, Salek Farrokhi A, Namdar Ahmadabad H, Barati M, Moazzeni SM. Mesenchymal stem cell therapy prevents abortion in CBA/J x DBA/2 mating. *Reprod Sci.* 2018;25(8):1261–1269.
16. Amsalem H, Kwan M, Hazan A, et al. Identification of a novel neutrophil population: Proangiogenic granulocytes in second-trimester human decidua. *J Immunol.* 2014;193(6):3070–3079.
17. Lv S, Wang N, Lv H, et al. The attenuation of trophoblast invasion caused by the downregulation of EZH2 is involved in the pathogenesis of human recurrent miscarriage. *Mol Ther Nucleic Acids.* 2019;14:377–387.
18. Park DW, Lee HJ, Park CW, Hong SR, Kwak-Kim J, Yang KM. Peripheral blood NK cells reflect changes in decidual NK cells in women with recurrent miscarriages. *Am J Reprod Immunol.* 2010;63(2):173–180.

19. Ahn JH, Park HR, Park CW, Park DW, Kwak-Kim J. Expression of TWIST in the first-trimester trophoblast and decidual tissue of women with recurrent pregnancy losses. *Am J Reprod Immunol*. 2017;78(2). doi:10.1111/aji.12670
20. Su MT, Tsai PY, Tsai HL, Chen YC, Kuo PL. miR-346 and miR-582-3p-regulated EG-VEGF expression and trophoblast invasion via matrix metalloproteinases 2 and 9. *Biofactors*. 2017;43(2):210–219.
21. Zhi Z, Yang W, Liu L, Jiang X, Pang L. Early missed abortion is associated with villous angiogenesis via the HIF-1alpha/VEGF signaling pathway. *Arch Gynecol Obstet*. 2018;298(3):537–543.
22. Xia S, Zhen Y, Ma H, Wang A. Abnormal expression of microRNA-575 leads to missed abortion through regulating apoptosis and angiogenesis. *Exp Ther Med*. 2017;14(5):3993–4000.
23. Starchenko, II, Vitko YN, Prylutskyi OK, Bilokon SO, Vynnyk NI. Morphological and immunohistochemical characteristics of human trigeminal ganglion neurons in the prenatal period of development. *Wiad Lek*. 2017;70(3 Pt 2):561–565.
24. Yang J, Wang Y, Wang XY, Zhao YY, Wang J, Zhao YY. Adverse pregnancy outcomes of patients with history of first-trimester recurrent spontaneous abortion. *Biomed Res Int*. 2017;2017:4359424.
25. Feli A, Jazayeri S, Bitaraf MA, Solaymani Dodaran M, Parastouei K, Hosseinzadeh-Attar MJ. Combination therapy with low copper diet, penicillamine and gamma knife radiosurgery reduces VEGF and IL-8 In patients with recurrent glioblastoma. *Asian Pac J Cancer Prev*. 2017; 18(7):1999–2003.
26. Zhu L, Chen H, Liu M, et al. Treg/Th17 cell imbalance and IL-6 profile in patients with unexplained recurrent spontaneous abortion. *Reprod Sci*. 2017;24(6):882–890.
27. Stavrou S, Gratz M, Tremmel E, et al. TAAR1 induces a disturbed GSK-3beta phosphorylation in recurrent miscarriages through the ODC. *Endocr Connect*. 2018;7(2):372–384.
28. Gao Y, Hong X, Wang Z, Zhu Y. Endometrial receptivity and conception outcome among women with light menstrual bleeding of unidentified etiology. *Int J Gynaecol Obstet*. 2018;140(1):37–41.



# Introducing enhanced recovery after surgery protocol in pediatric surgery

Anna Modrzyk<sup>A–D</sup>, Michał Jerzy Pasierbek<sup>D,E</sup>, Wojciech Korlacki<sup>E,F</sup>, Andrzej Grabowski<sup>C</sup>

Department of Children's Developmental Defects Surgery and Traumatology, Medical University of Silesia, Zabrze, Poland

A – research concept and design; B – collection and/or assembly of data; C – data analysis and interpretation; D – writing the article; E – critical revision of the article; F – final approval of the article

Advances in Clinical and Experimental Medicine, ISSN 1899–5276 (print), ISSN 2451–2680 (online)

*Adv Clin Exp Med.* 2020;29(8):937–942

## Address for correspondence

Michał Jerzy Pasierbek  
E-mail: [michal.pasierbek@sum.edu.pl](mailto:michal.pasierbek@sum.edu.pl)

## Funding sources

None declared

## Conflict of interest

None declared

Received on February 26, 2020

Reviewed on March 7, 2020

Accepted on May 1, 2020

Published online on August 21, 2020

## Abstract

**Background.** Enhanced recovery after surgery (ERAS) is a holistic perioperative care protocol created to improve treatment outcomes. Implementation of new rules radically changed the perioperative care of adult patients. The protocol refers to the preoperative, intraoperative and postoperative periods.

**Objectives.** To describe a novel pediatric ERAS protocol designed for reverse stoma surgery and to compare a group of patients with implemented ERAS protocol to a group of patients from pre-ERAS period.

**Material and methods.** A retrospective comparative review was performed which included 14 patients from pre-ERAS period (2016–2017) and 13 patients in the ERAS period (2018–2019). Total parenteral nutrition (TPN) time, time to oral fluid intake, time to regular diet, time to stooling, and length of stay (LOS) were analyzed.

**Results.** In the ERAS period, the LOS decreased from 8.64 to 6.08 days, time to oral fluid intake decreased from 4.36 to 1 postoperative day, time to regular diet decreased from 6.14 to 3.23 postoperative day. Total parenteral nutrition decreased from 5.14 in the pre-ERAS period to 1.69 days in the ERAS period. With the progress of implementation of ERAS protocol, TPN was gradually withdrawn.

**Conclusions.** The implementation of the pediatric ERAS in children undergoing reverse stoma surgery is safe, reduces patient's metabolic stress and improves treatment outcomes. However, further research is needed.

**Key words:** pediatric surgery, total parenteral nutrition, enhanced recovery after surgery, length of stay, enhanced recovery after surgery

## Cite as

Modrzyk A, Pasierbek MJ, Korlacki W, Grabowski A. Introducing enhanced recovery after surgery protocol in pediatric surgery. *Adv Clin Exp Med.* 2020;29(8):937–942. doi: 10.17219/acem/121931

## DOI

10.17219/acem/121931

## Copyright

© 2020 by Wrocław Medical University  
This is an article distributed under the terms of the Creative Commons Attribution 3.0 Unported (CC BY 3.0) (<https://creativecommons.org/licenses/by/3.0/>)



## Introduction

In 1999, Henrik Kehlet described the first attempts to improve adult perioperative care for patients undergoing open sigmoidectomy.<sup>1</sup> In this paper, Kehlet described various factors impacting the length of stay (LOS) and proposed a multimodal rehabilitation program, which helped to reduce LOS after colonic surgery from 5–10 days to 2 days without increasing complications. In further works, Kehlet indicated the importance of preoperative patient information, as well as thoracic epidural anesthesia in open colonic surgery.<sup>2</sup> In 2001, members of the working group, including Olle Ljungqvist and Henrik Kehlet, analyzed many more research works in the field of perioperative care and “fast track” programs, and identified a few other factors in the patient’s treatment which have an impact on surgical complications.<sup>3</sup> The extended “fast track” program was formally named as enhanced recovery after surgery (ERAS) protocol. Such protocols have been adopted relatively slowly in both adult and pediatric surgery, and Kehlet in one of his recent works provides an interesting discussion about the reasons for that,<sup>4</sup> with encouragement to move forward.

Enhanced recovery after surgery gathers a set of preoperative, intraoperative and postoperative guidelines. The core part of the protocol is aimed at maintaining physiologic homeostasis by reducing metabolic stress caused by a surgical procedure.<sup>5,6</sup> Recently, ERAS protocol have been published not only for colorectal surgery, but also for many other adult procedures, such as cardiac surgery, gynecologic/oncology, lung and liver surgery, esophagectomy, breast reconstruction, major head and neck cancer surgery with free flap reconstruction, bariatric surgery, pancreaticoduodenectomy, radical cystectomy for bladder cancer, and gastrectomy.<sup>7</sup>

Many studies in the field of ERAS suggest that the protocol adopted for adult patients is feasible, safe and effective.<sup>8</sup> So far, there have been few published works dealing with ERAS for children, and many of those are theoretical discussions.

In this paper, we presented a novel, pediatric enhanced recovery after surgery (pediatric ERAS) protocol implemented for children undergoing reverse stoma surgery at our department since January 2018.

## Material and methods

### Study design

Various types of elective procedures performed in our department in the pre-ERAS period were analyzed from January 2016 to December 2017 by a team of surgeons, anesthesiologists and nurses. Perioperative treatment was assessed and compared with ERAS protocol assumptions. A group of patients assigned for reverse stoma surgery was

selected. This group had been treated with varying classic perioperative procedures, especially with respect to ERAS protocol, and therefore it was possible to perform a wide and thorough study of how various stages of ERAS impact the patient’s overall convalescence.

A retrospective review was performed of 14 patients in the pre-ERAS period from January 2016 to December 2017 and 13 patients in the ERAS period from January 2018 to May 2019. In most cases, stoma was performed in the neonatal period, mainly as a result of necrotizing enterocolitis (NEC), anal atresia and meconium ileus (MI). The distribution of illnesses leading to stoma are shown in Fig. 1. The types of stoma are shown in Fig. 2

The parameters of total parenteral nutrition (TPN) time, time to oral fluid intake, time to regular diet, time to stool, and LOS were analyzed.

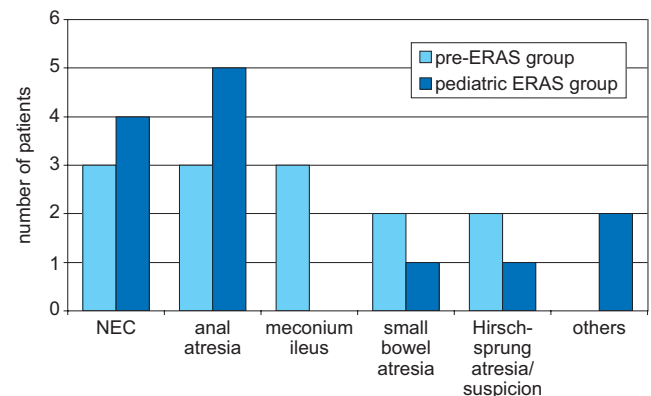


Fig. 1. Illnesses being reasons for performing stoma

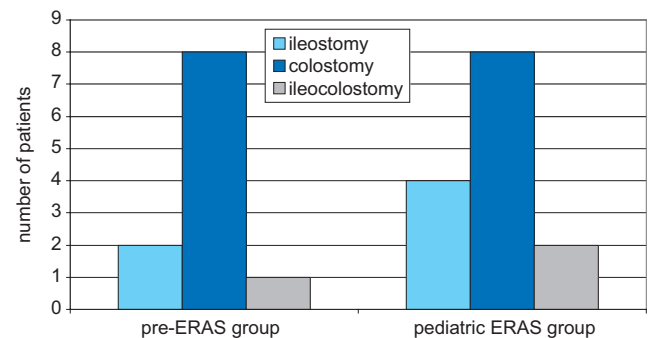


Fig. 2. Analyzed group of patients (reverse stoma surgery)

## Pediatric ERAS protocol development

After the analyzed group of patients had been revised, the development of the ERAS protocol suitable for our patients was launched. Classic ERAS for adult patients was the reference; however, an evaluation of each stage of the original protocol was done, assessing the safeness and benefits for children, as well as the possibility of practical implementation in our hospital. As a result of this thorough process, pediatric ERAS consisting of 16 steps was prepared as shown in Table 1.

Table 1. Comparison of pre-ERAS and pediatric ERAS procedures

ERAS procedures	Pre-ERAS treatment	Pediatric ERAS treatment
Preoperative		
1. Preadmission preparation	not included	included
2. Oral nutrition support 2 weeks in advance	not included	included
3. Zero-residue diet 3 days in advance	not included	included
4. Intravenous antibiotics only (cephalosporin 3 <sup>rd</sup> generation + metronidazole)	not included	included
5. No prolonged preoperative fasting	not included	included
6. Supply of non-opiate preoperative analgesic medications	included	included
Intraoperative		
7. Intraoperative tasks for anesthesiologists	included	included
8. TAP-block	not included	not included
9. Avoid nasogastric tubes and peritoneal cavity drainage after anastomosis	included	included
10. Early removal of urinary catheter	included	included
Postoperative		
11. Avoid fluids and salt overload	not included	included
12. Non-opioid analgesia for postoperative pain management	included	included
13. Early oral intake with clears in the postoperative day 0	not included	included
14. Early oral nutrition in the postoperative day 1	not included	included
15. Early mobilization	included	included
16. Audit of compliance and outcomes	not included	included

TAP – transversus abdominis plane.

Some of the procedures were performed even before pediatric ERAS protocol. These are indicated in the 2<sup>nd</sup> column in Table 1. According to the ERAS protocol, perioperative care can be improved only when protocol guidelines for each patient are implemented to their fullest and the importance of multi-specialist cooperation is taken into account. Intraoperative tasks for anesthesiologists consist of 5 recommendations.

Restrictive fluid therapy and avoiding sodium overloading helps prevent the most common complication after reverse stoma surgery, such as paralytic ileus. Maintaining normothermia reduces the risk of postoperative wound infection. The use of dexamethasone and ondansetron during surgery prevents postoperative nausea and vomiting (PONV). The last guideline recommends the use of multimodal analgesia, which together with regional

anesthesia techniques, such as infiltration and transversus abdominis plane (TAP)-block, reduces the stress associated with surgical procedure. An additional limitation of opioids is reduced time to regaining correct bowel function.

## Protocol implementation

The implementation of pediatric ERAS was methodologically and logistically challenging. Understanding the physiological base of the protocol was key in changing the rules of the patient's treatment, which had been practiced for years and considered as canonical in pediatric surgery.

Doctor-patient-parent conversation following ERAS Society recommendations was introduced and information materials about preoperative nutrition were also provided. For every ERAS patient, assessment of the nutritional status using body mass index (BMI) score, percentile meshes, and check of albumin level was performed. As part of pre-admission assessment, morphology parameters (to exclude anemia) were also checked, and, if required, consultations with other specialists were ordered. With respect to non-prolonged preoperative fasting, zero-residue diet up to 6 h and supply of clears, including supply of preoperative oral carbohydrate liquid (10 mL/kg up to a maximum 200 mL up to 2 h before surgery) were allowed. Before preparations for surgery, all parents had agreed to undergo the pediatric ERAS protocol. The parents were also educated about discharge criteria, i.e., 100% tolerance of regular diet and fluids, successful defecation, patient's mobilization adequate to age, and pain control with oral medications.

Pediatric ERAS protocol was started in January 2018. The 16 steps proposed for pediatric ERAS protocol are shown in Table 1. Gradually, the new 9 steps of pediatric ERAS were introduced, in addition to 6 procedures that had been performed thus far. Finally, 15 points were successfully implemented. The only procedure that we have not managed to introduce in the analyzed group is TAP-block regional anesthesia.

## Results

The level of confidence for the procedures and the conviction that ERAS is safe for young patients have been improving with each patient along with surgeons' efficiency. Initially, 8 stages of the protocol were enabled, whereas for the last patients 14–15 procedures were successfully introduced. The progress in introducing pediatric ERAS in our group of 13 patients is shown in Fig. 3. From the 13 planned reverse stoma surgeries, 12 were performed as scheduled. For 1 of the patients, pediatric ERAS pre-admission preparation revealed microcytic anemia; therefore, oral treatment was applied, which delayed the operation. Once the patient's morphology parameters had improved, surgery was performed successfully.

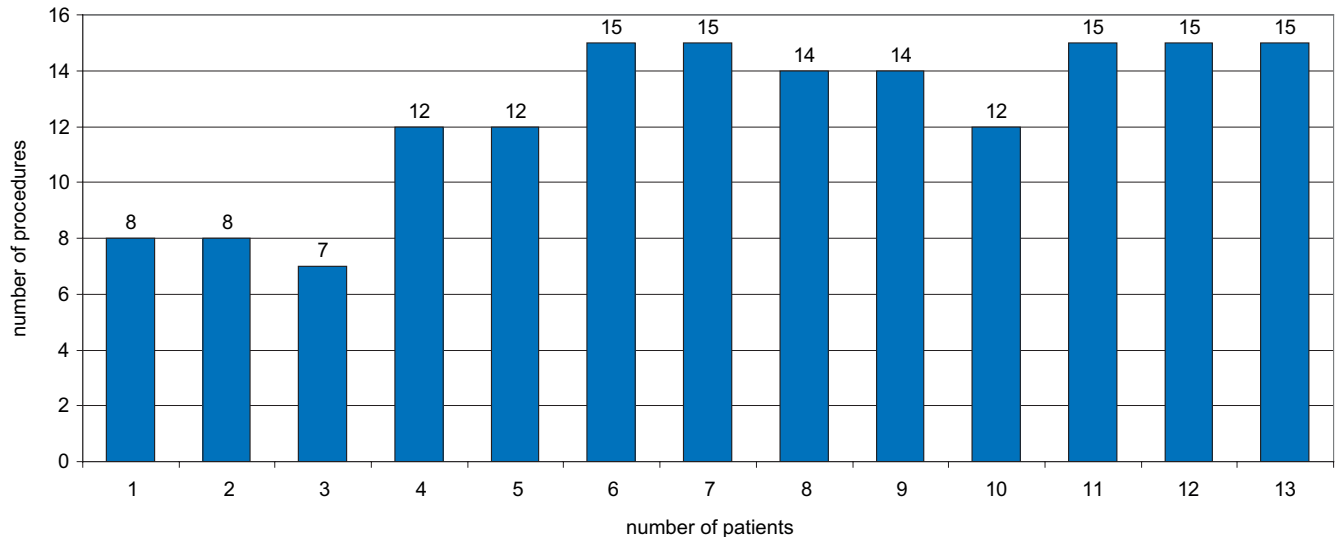


Fig. 3. Successfully introduced pediatric ERAS procedures per each pediatric patient

The average patient age in the pre-ERAS group was 0.9 years, with the age across the group ranging from 8 to 15 months. In the ERAS group, the average age was 2.05 years, with the youngest and oldest patient's age of 8 months and 8.17 years, respectively. The LOS in the ERAS group decreased from  $8.64 \pm 2.4$  days to  $6.08 \pm 2.6$  days in the period of 2016–2019. In the pre-ERAS group, TPN lasted for  $5.14 \pm 2.3$  days, oral fluid intake was introduced in  $4.36 \pm 1.9$  postoperative day and full tolerance for regular diet was achieved in  $6.14 \pm 2$  postoperative day. In the ERAS group, time to oral fluid intake was reduced to  $1.0 \pm 1.5$  postoperative day and time to regular diet was reduced to  $3.23 \pm 1.8$  postoperative days. Total parenteral nutrition decreased to  $1.69 \pm 2.5$  days (averaged numbers with standard deviation (SD)). However, during the implementation of the pediatric ERAS protocol, TPN was gradually withdrawn, i.e., initially applied to 4 patients for 5.5 days on average, and then completely withdrawn for the remaining 10 patients (time of TPN = 0). The withdrawal of TPN resulted in the introduction of a regular diet in the  $2.22 \pm 1.1$  postoperative days and in shortening the average LOS to  $5.33 \pm 1.2$  days. Furthermore, the reduction of time to stooling was observed, from  $3.5 \pm 1.9$  to  $2.23 \pm 0.9$  postoperative days (averaged numbers with SD). Comparative summary of the results achieved for the pre-ERAS and pediatric ERAS patients can be found in Table 2.

In the ERAS group, the only important complication was vomiting which occurred in 3 patients – in 2 patients after colostomy reversal (1 patient treated for Hirschsprung's disease and 1 with gastroschisis with colon atresia) vomiting was observed on the 1<sup>st</sup> postoperative day, and in 1 girl after Bishop–Koop stoma reversal (treated for gastroschisis with short bowel syndrome/SBS/and partial parenteral nutrition) vomiting lasted for 4 postoperative days and stopped after erythromycin was introduced in prokinetic

Table 2. Pre-ERAS and pediatric ERAS treatment outcomes

Observed parameter	Classic perioperative treatment (pre-ERAS)	Pediatric ERAS treatment
Time to oral fluid intake (postoperative day, $\pm$ SD)	$4.36 \pm 1.9$	$1.0 \pm 1.5$
Time to regular diet (postoperative day, $\pm$ SD)	$6.14 \pm 2.0$	$3.23 \pm 1.8$
Time to stooling (postoperative day, $\pm$ SD)	$3.5 \pm 1.9$	$2.23 \pm 0.9$
Total parenteral nutrition time (postoperative day, $\pm$ SD)	$5.14 \pm 2.3$	$1.69 \pm 2.5$
Length of stay (day, $\pm$ SD)	$8.64 \pm 2.4$	$6.08 \pm 2.6$

doses. For the remaining ERAS patients, no complications were observed during hospitalization. None of the ERAS patients required readmission within 30 days and reoperation within 90 days.

## Discussion

A thorough review of the current literature for pediatric ERAS can be found in research conducted by Shinnick et al.<sup>9</sup> and Pearson et al.<sup>10</sup> The former<sup>9</sup> noticed that there is a paucity of high-quality literature evaluating pediatric ERAS, and observes in the review that in 5 studies regarding pediatric ERAS, the mean number of adopted elements was only 5.6 (the maximum 11 was presented in the review by Pearson et al.<sup>10</sup>) in comparison to over 23 procedures on average adopted in adults. From this perspective, our implementation of 15 procedures is a very good outcome. What is interesting, Pearson et al.<sup>10</sup> also noticed that no implementation of preoperative carbohydrate load was an important exception from adult ERAS. This element

was adopted in our study. Pearson et al.<sup>10</sup> also referred to 2 studies which showed no reduction of costs. However, in our opinion, introducing pediatric ERAS with a reduction of LOS also reduced patient costs (less laboratory tests, less imaging examinations such as X-ray, ultrasound, no central venous catheter, less intravenous fluids and analgesic drugs). In terms of practical implementation, Short et al.<sup>11</sup> in their interesting work presented the so-called pediatric-specific enhanced recovery protocol (ERP) developed for pediatric ileocectomy, partial/total colectomy, proctectomy/J-pouch and pediatric ileostomy reversal. Based on available literature, the authors<sup>11</sup> noticed that the assessment of individual elements used in ERAS (regional and non-opioid analgesia, the omission of a mechanical bowel preparation and usage of urinal catheters, early mobilization, the use of dexamethasone and ondansetron, early enteral nutrition) are safe in children, yet according to Rove et al.<sup>12</sup> the synchronous study of entire protocols is of great interest. Also, Bernhard Haid et al.<sup>13</sup> applied ERAS protocol for children undergoing augmentation and diversion surgery using small bowel, showing the protocol to be safe. However, applying ERAS protocols to infants, children and adolescents seems to be less challenging than in the case of neonates. Gibb and Crosby<sup>14</sup> proposed neonatal ERAS guidelines, with new elements of care, for intestinal resection surgery.

We analyzed developed and implemented pediatric ERAS protocol for children undergoing reverse stoma surgery. Based on the treatment results, we observed a visible improvement in the general condition of the patients. During this short period of implementation of pediatric ERAS, vomiting was the only complication in 3 children. One patient with Hirschsprung's disease, after reversal colostomy, vomited once. In a nine-month old boy vomiting occurred after each attempt of oral fluid intake on the 1<sup>st</sup> postoperative day; however, it lasted for 1 day and stopped after conservative treatment. In an eight-month old girl with partial parenteral nutrition, undergoing reversal of Bishop–Koop stoma, vomiting lasted for 4 postoperative days. On the 5<sup>th</sup> day, we introduced erythromycin in prokinetic doses, and the breakthrough was observed as she started to tolerate oral fluid intake and diet. However, we do not know what actually helped the return of correct bowel function, but we found out that last 2 patients mentioned above had a common feature, which was gastroschisis in the neonatal period. We suspected that the described problems were caused by the immaturity of the intestines. As mentioned above, none of the ERAS patients required readmission within 30 days and reoperation within 90 days, which confirmed the observations of Short et al.<sup>11</sup>

In our comparative study of 14 pre-ERAS and 13 pediatric ERAS patients, the following key parameters were observed: the length of stay, total parenteral nutrition time, time to oral fluid intake, time to regular diet, and time to defecation. For our team, early oral fluid intake

and nutrition were the most important aspects. Time to oral fluid intake was reduced from  $4.36 \pm 1.9$  days to  $1.0 \pm 1.5$  day and time to regular diet from  $6.14 \pm 2$  days to  $3.23 \pm 1.8$  days, which was in agreement with other studies shown in the review by Shinnick et al.<sup>9</sup> Furthermore, the length of stay was also decreased from  $8.64 \pm 2.4$  days to  $6.08 \pm 1.9$  days in our study, which was confirmed in other surveys mentioned in the aforementioned review.<sup>9</sup> Historically, in our department, postoperative care was more conservative with zero diet lasting several days after surgery and intravenous hydration, as well as total parenteral nutrition applied to all the patients. What is more, children undergoing reverse stoma surgery quite often presented postoperative paralytic ileus, sometimes demanding diagnostic imaging to distinguish their condition from mechanical bowel obstruction. However, this was improved, as time to stooling decreased from  $3.5 \pm 1.9$  days to  $2.23 \pm 0.9$  days; however, we were unable to eliminate paralytic ileus in all ERAS patients. Nevertheless, we hope this can be achieved with greater experience gained with the protocol. Furthermore, the application of the pediatric ERAS enabled us to withdraw the parenteral nutrition, thereby allowing us to completely avoid the risk of complications caused by TPN.

Another important outcome of our study was considerable increase of patients and parents' comfort, as well as trust in medical staff. We observed that stress level of ERAS patients and their parents was significantly lower when compared with pre-ERAS patients, and they went through the overall hospitalization with much less trauma, which is particularly important for some patients undergoing multiple medical procedures due to serious disease. In our opinion, this lower stress and better comfort came from that fact that parents were well informed of and very engaged in the respective phases of the treatment; they knew how to prepare their children for surgery and had detailed knowledge of discharge criteria. Our conclusions in that the aspects of perioperative care were aligned with the outcomes of researched performed by Heiss and Raval, where they studied patient engagement to enhance recovery for children undergoing surgery.<sup>15</sup>

All the positive outcomes of pediatric ERAS described by the other authors<sup>10,11,13</sup> together with our experience of handling unexpected postoperative complications give us confidence that this innovative protocol is feasible, safe and effective for children. Therefore, we are encouraged to continuously expand our skills in improving multimodal pain therapy. A good example of this is the application of TAP-block, which we hope to introduce in the near future, and which will further reduce the amount of oral and intravenous analgesic medicines. Our ultimate goal of using TAP-block is to accelerate the mobilization of patients after operations.

The limitation of our study was that the group of patients in our survey was very heterogeneous, which made the evaluation of every aspect difficult in a matter




of unification. What is more, there is still room for improvement in antibiotic therapy. Specifically, our pediatric ERAS protocol did not incorporate guidelines for preoperative antibiotic prophylaxis. At the moment, full antibiotic therapy is employed. Furthermore, the other elements from adult ERAS, such as the use of insulin and thromboembolism prophylaxis, need more attention and further review. Thus, we are of the opinion that more studies in the field of ERAS applicable to children, as well as elaboration of clear and consistent rules of treatment dedicated for pediatric patients are needed.

## Conclusions

We described the development and implementation of pediatric ERAS for children undergoing reverse stoma surgery at our Department of Children's Developmental Defects Surgery and Traumatology. The proposed pediatric ERAS protocol was feasible, safe and effective. Early introduction of oral fluid intake and nutrition in the implemented protocol allowed us to completely eliminate TPN in our treatment. Also, the time to stooling and LOS parameters were reduced. We considered the protocol outcomes to be positive, but more studies are needed in the field of pediatric ERAS.

### ORCID iDs

Anna Modrzyk  <https://orcid.org/0000-0001-5828-4171>  
 Michał Jerzy Pasierbek  <https://orcid.org/0000-0003-1215-2776>  
 Wojciech Korlacki  <https://orcid.org/0000-0002-2632-3567>  
 Andrzej Grabowski  <https://orcid.org/0000-0002-5162-3043>

## References

1. Kehlet H, Mogen T. Hospital stay of 2 days after open sigmoidectomy with a multimodal rehabilitation programme. *Br J Surg.* 1999;86(2): 227–230.
2. Kehlet H. Fast-track colorectal surgery. *Lancet.* 2008; 371(9615):791–793.
3. Kłęk S, Pędzwiatr M, Matłok M. Historia i motywy powstania protokołu ERAS, który zmieni opiekę okołoperacyjną. *Med Prakt.* 2014;4: 69–77. <https://www.mp.pl/eras/wytyczne/103312,historia-i-motywy-powstania-protokolu-eras-ktory-zmieniil-opieke-okolooperacyjna>. Accessed September 22, 2018.
4. Kehlet H. ERAS implementation: Time to move forward. *Ann Surg.* 2018;267(6):998–999.
5. Kehlet H. Multimodal approach to control postoperative pathophysiology and rehabilitation. *Br J Anaesth.* 1997;78(5):606–617.
6. Ljungqvist O, Jonathan E. Rhoads lecture 2011: Insulin resistance and enhanced recovery after surgery. *J Parent Enteral Nutr.* 2014;36(4): 389–398.
7. ERAS Society. List of Guidelines <http://erassociety.org/guidelines/list-of-guidelines/>. Accessed September 15, 2019.
8. Liu VX, Rosas E, Hwang J, et al. Enhanced recovery after surgery program implementation in 2 surgical populations in an integrated health care delivery system. *JAMA Surg.* 2017;52(7):e171032.
9. Shinnick JK, Short HL, Heiss KF, Santore MT, Blakely ML, Raval MV. Enhancing recovery in pediatric surgery: A review of the literature. *J Surg Res.* 2016;202(1):165–176.
10. Pearson KL, Hall NJ. What is the role of enhanced recovery after surgery in children? A scoping review. *Pediatr Surg Int.* 2017;33:43–51.
11. Short HL, Heiss KF, Burch K, et al. Implementation of an enhanced recovery protocol in pediatric colorectal surgery. *J Pediatr Surg.* 2017; 53(4):688–692.
12. Rove KO, Brockel MA, Saltzman AF, et al. Prospective study of enhanced recovery after surgery protocol in children undergoing reconstructive operations. *J Pediatr Urol.* 2018;14(3):252.
13. Haid B, Karl A, Koen M, Mottl W, Haid A, Oswald J. Enhanced recovery after surgery (ERAS) protocol, pediatric urologic augmentation and diversion surgery using small bowel. *J Urol.* 2018;200(5):1100–1106.
14. Gibb ACN, Crosby MA, McDiarmid C, et al. Creation of an enhanced recovery after surgery (ERAS) guideline for neonatal intestinal surgery patients: A knowledge synthesis and consensus generation approach and protocol study. *BMJ Open.* 2018;8(12):e02365.
15. Heiss KF, Raval MV. Patient engagement to enhance recovery for children undergoing surgery. *Semin Pediatr Surg.* 2018;27(2):86–91.



# Evaluation of serum human epididymis protein 4 in patients with relapsing-remitting multiple sclerosis

Bożena Adamczyk<sup>1,A–D</sup>, Robert Partyka<sup>2,A,B</sup>, Monika Adamczyk-Sowa<sup>1,E,F</sup>,  
Krzysztof Wierzbicki<sup>1,A</sup>, Paweł Sowa<sup>3,A</sup>, Danuta Kokocińska<sup>2,A</sup>

<sup>1</sup> Department of Neurology in Zabrze, School of Medicine with the Division of Dentistry in Zabrze, Medical University of Silesia, Katowice, Poland

<sup>2</sup> Department of Anesthesiology, Intensive Care and Emergency Medicine Ward, St. Barbara's Provincial Specialist Hospital in Sosnowiec, Medical University of Silesia, Katowice, Poland

<sup>3</sup> Department of Laryngology in Zabrze, School of Medicine with the Division of Dentistry in Zabrze, Medical University of Silesia, Katowice, Poland

A – research concept and design; B – collection and/or assembly of data; C – data analysis and interpretation;

D – writing the article; E – critical revision of the article; F – final approval of the article

Advances in Clinical and Experimental Medicine, ISSN 1899–5276 (print), ISSN 2451–2680 (online)

*Adv Clin Exp Med.* 2020;29(8):943–948

## Address for correspondence

Bożena Adamczyk

E-mail: bozena.m.adamczyk@gmail.com

## Funding sources

None declared

## Conflict of interest

None declared

Received on November 17, 2019

Reviewed on March 9, 2020

Accepted on April 24, 2020

Published online on August 13, 2020

## Cite as

Adamczyk B, Partyka R, Adamczyk-Sowa M, Wierzbicki K, Sowa P, Kokocińska D. Evaluation of serum human epididymis protein 4 in patients with relapsing-remitting multiple sclerosis. *Adv Clin Exp Med.* 2020;29(8):943–948. doi:10.17219/acem/121006

## DOI

10.17219/acem/121006

## Copyright

© 2020 by Wrocław Medical University

This is an article distributed under the terms of the Creative Commons Attribution 3.0 Unported (CC BY 3.0) (<https://creativecommons.org/licenses/by/3.0/>)

## Abstract

**Background.** So far, little is known about the properties of human epididymis protein 4 (HE4) in multiple sclerosis (MS). This type 4 glycoprotein belongs to a family of genes encoding proteins whose expression is associated with the process of spermatogenesis in the epididymis. The biological function of HE4 is not fully understood. Overexpression of HE4 has been found in several malignant tumors, particularly in ovarian cancer, as well as in mesothelioma, lung, endometrial, breast, and kidney cancers.

**Objectives.** To evaluate serum HE4 in patients with relapsing-remitting multiple sclerosis (RRMS) as compared to healthy controls.

**Material and methods.** Fifty patients with RRMS undergoing first-line immunomodulatory treatment were enrolled in the prospective study. We analyzed correlations between serum HE4 levels and gender, age, disease duration, the Expanded Disability Status Scale (EDSS), annualized relapse rate (ARR), and magnetic resonance imaging (MRI) lesions.

**Results.** The patients from the study group had higher concentrations of HE4 than the subjects from the control group. Patients with EDSS > 2 had significantly higher concentrations of HE4. Positive correlations were found between HE4 concentrations and age as well as between HE4 concentrations and disease duration. No significant correlations were found between HE4 concentrations and EDSS or between HE4 concentrations and ARR.

**Conclusions.** The results of the study indicate a novel aspect of the HE4 protein in the pathomechanisms of MS.

**Key words:** multiple sclerosis, autoimmune diseases, biomarker, human epididymis protein 4, relapsing-remitting multiple sclerosis

## Introduction

Serum human epididymis protein 4 (HE4) antigen was discovered by Kirchhoff et al. in 1991.<sup>1</sup> Its usefulness as a potential tumor marker of ovarian cancer was described by Schummer et al. in 1999<sup>2</sup> and confirmed by Hellström et al. in 2003.<sup>3</sup> This type 4 glycoprotein belongs to a family of gene-encoding proteins containing whey-acidic-protein (WAP) motifs, whose expression is associated with the process of spermatogenesis in the epididymis.<sup>4</sup> The HE4 is a protein from the group of small thermostable molecules involved in inhibiting the activity of proteases. Since it is released into the circulation, it is possible to determine its concentration in blood serum.

The biological function of this protein is not fully understood. It is known that HE4 promotes tumor growth and the migration and adhesion of ovarian cancer cells. Overexpression of this protein has been found in several malignant tumors, particularly in ovarian cancer, as well as in mesothelioma, lung, endometrial, breast, and kidney cancers.<sup>5,6</sup> Compared with cancer antigen 125 (CA-125), its increase in benign lesions and non-neoplastic diseases is much less common in premenopausal women (8% vs 29%).<sup>7</sup>

Reviewing the literature on HE4, it can be seen that HE4 has been analyzed from many perspectives. The most recent reports have assessed its usefulness as a marker in ovarian cancer and pulmonary tuberculosis, or investigated the relationship between HE4 and renal function and diabetic kidney disease in patients with type 2 diabetes mellitus.<sup>8</sup> Furthermore, Gasiorowska et al. analyzed the level of HE4 in blood serum in relation to smoking and age; they suggested that permanent inflammation caused by smoking may induce an increase in HE4.<sup>9</sup> Other authors have indicated an association between HE4 and an increase in myocardial injury expressed by N-terminal pro-b-type natriuretic peptide (NT-proBNP) and troponin T.<sup>10</sup>

It is known that autoimmune and chronic inflammatory processes are involved in the pathomechanism of multiple sclerosis (MS). However, it seems that oxidative stress (OS) is also crucial to cancer development, and recent studies have demonstrated that some drugs effective in MS (e.g., fingolimod (FG)) may also be helpful in cancer treatment.<sup>11</sup> It seems that in light of this, the assessment of HE4 in MS may provide new information, particularly due to the fact that diagnostic and prognostic markers are constantly being sought in MS.<sup>12</sup>

We have found no reports that analyzed HE4 in patients with MS. The aim of this study was to evaluate serum HE4 in MS patients compared to a control group.

## Material and methods

We assessed serum HE4 in MS patients in relation to gender, age, disease duration, degree of disability in the Expanded Disability Status Scale (EDSS), annualized relapse rate (ARR), and MRI Gd + lesions.

The study involved 50 patients diagnosed with relapsing-remitting multiple sclerosis (RRMS) according to the 2010 McDonald criteria, who were treated mainly with first-line immunomodulatory therapy. The study also involved 26 healthy volunteers as a control group. Among the patients, 54.28% (19) were being treated with interferon  $\beta$ -1a (IFN $\beta$ -1a) (30 ug intramuscularly (i.m.) weekly or 44 ug s.c. 3 times weekly); 31.43% (11) with IFN $\beta$ -1b (250 ug every second day s.c.); 11.43% (4) with glatiramer acetate (20 mg/daily s.c.); and 2.86% (1) with fingolimod (FG) (0.5 mg/daily p.o.). Only FG is approved as second-line therapy.

The inclusion criteria for the study group were as follows: age  $\geq$ 18 years, RRMS diagnosed according to the 2010 McDonald criteria, no relapse, and written informed consent for participation in the study. The exclusion criteria were refusal to give written informed consent to participate in the study and confirmed cancer or other severe disease.

The inclusion criteria for the control group were as follows: generally healthy individuals (treatment of hypertension was not a contraindication) and written informed consent to participate; the exclusion criteria for the controls were the same as for the patient group.

A 10 mL venous blood sample was obtained from all participants, taken a minimum of 4 h after the MS patients were administered their medications. After centrifugation of the blood samples, the obtained serum was frozen at  $-20^{\circ}\text{C}$ . In all the samples, HE4 concentration was determined using chemiluminescence commercial kits (Abbott Laboratories, Abbott Park, USA). Concentrations below 22 pg/mL were considered normal.

Demographic data, disease duration, clinical disease onset, the clinical form of MS, the type of treatment, the degree of disability in the EDSS, ARR and lesions on magnetic resonance imaging (MRI) were obtained from medical databases from Department of Neurology at the Medical University of Silesia (Zabrze, Poland).

STATISTICA v. 9.1 software (StatSoft Inc, Tulsa, USA) was used for the statistical analysis. P-value  $<0.05$  was considered statistically significant. The normality of the distribution was checked using the Shapiro–Wilk test. Demographic characteristics and all the results were expressed as the number (n), the arithmetic mean, standard deviation (SD), and percentage (%). The homogeneity of continuous variables between the groups was analyzed using the parametric analysis of variance (ANOVA) test (for normally distributed variables) or the non-parametric Kruskal–Wallis ANOVA (for variables whose distribution was not normal). Post hoc analysis using Tukey's test with the Bonferroni correction was conducted in the case of statistically significant differences. Student's t-test and the non-parametric Mann–Whitney U test were used to compare the 2 groups. The relationships between the attributes were evaluated using the nonlinear Spearman correlation. The results were stored in a database prepared specifically for this purpose in Microsoft Excel (Microsoft Corp., Redmond, USA).

## Results

Table 1 presents the characteristics of the study groups. The mean age of the MS group was  $38.66 \pm 8.24$  years, and of the control group  $37.69 \pm 8.64$  years. The number of female patients was higher than the number of males (Table 1).

Table 2 shows an analysis of the study group considering the clinical and radiological indicators of disease activity, such as disease duration, EDSS, ARR, and T2 MRI lesions. The patients were mainly treated with IFN $\beta$ . The mean disease duration in the MS group was  $8.91 \pm 5.52$  years.

Patients from the MS group had higher concentrations of HE4 than the subjects from the control group. A post hoc analysis was conducted for women and men in both groups. No differences were found between male and

female MS patients' concentrations of HE4. The women and men with MS had higher concentrations of HE4 than the women and men in the control group (Fig. 1).

A comparison was made between patients with and without a relapse within the last year, and the analysis did not show any differences in the serum HE4 concentrations of these patients. However, patients with EDSS > 2 had significantly higher concentrations of HE4 than those with lower EDSS scores (Table 3).

No significant correlations were found for gadolinium-enhancing (Gd+) lesions or ARR. A moderate negative correlation was revealed between Gd+ and HE4. Among the women with MS, a positive correlation was found between HE4 and EDSS scores. No significant correlations were noted for men with MS (Table 4).

## Discussion

Multiple sclerosis is a biphasic disease.<sup>13</sup> Initially, neuro-inflammation is prevalent,<sup>14</sup> which induces OS in the nervous tissue, leading to impaired oxidative/antioxidant balance,<sup>12</sup> a loss of blood–brain barrier integrity,<sup>15–17</sup> demyelination, and neurodegeneration.<sup>12</sup> The ultimate mechanism for the development of MS is not known. Due to the development of novel methods of MS treatment, the timing of a switch to more aggressive treatment is of great importance. An ongoing search for new markers is underway, with the aim of helping to assess the prognosis. In the future, HE4 could be used as a new indicator of disease progression, as it is in ovarian cancer, endometrial cancer, renal failure,<sup>18–20</sup> and other diseases.

The WAP four-disulfide core domain protein 2 gene (WFDC2) encodes HE4. *WFDC2* gene expression has been discovered in the epididymis, vas deferens, the epithelium of the female genital tract, the breast, respiratory epithelium, intestines, salivary glands, and distal renal tubules.<sup>6,21</sup> Studies of the expression of the HE4 protein in the central nervous system (CNS) have not yet been

Table 1. General characteristics of the groups

Group	MS group	Control group	p-value
n	35	26	–
Age [years]	$38.66 \pm 8.24$	$37.69 \pm 8.64$	0.7
Gender (% of females)	74.28	61.54	–

MS group – multiple sclerosis group; statistical significance at  $p < 0.05$ .

Table 2. Clinical characteristics of the study group

Group	MS group
Type of treatment in I-line:	
IFN $\beta$ 1a (%)	54.28 (19)
IFN $\beta$ 1b (%)	31.43 (11)
glatiramer acetate (%)	11.43 (4)
II line treatment:	
fingolimod (%)	2.86 (1)
Disease duration [years]	$8.91 \pm 5.52$
EDSS (score)	$2.24 \pm 1.13$
T2 MRI lesions (N)	$19.16 \pm 2.80$

MS group – multiple sclerosis group; IFN $\beta$  – interferon beta; EDSS – Expanded Disability Status Scale; ARR – annualized relapse rate.

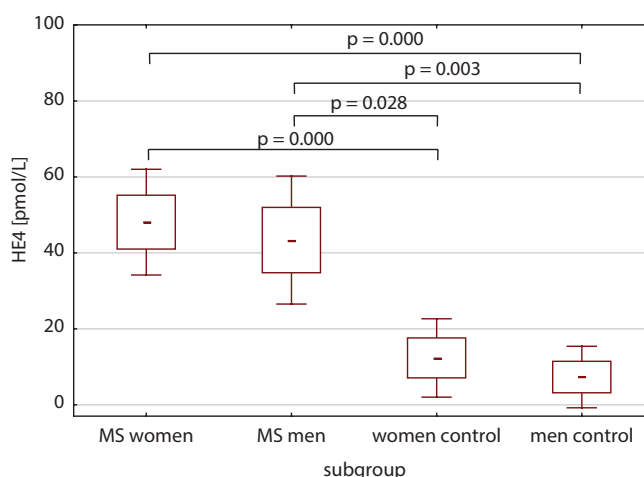
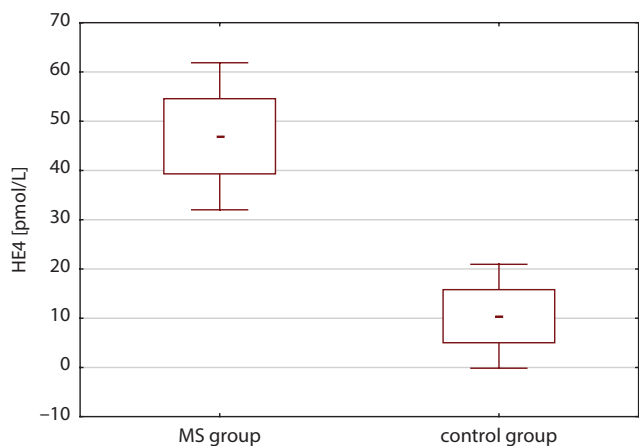


Fig. 1. A comparison of the study group and control group in terms of HE4 and an analysis in subgroups by gender (means and SD)

conducted. It is difficult to assess whether the observed increase in HE4 in MS patients is a result of increased HE4 expression outside the CNS or other mechanisms, including the involvement of nervous tissue. In the future, studies should aim at assessing the effect of the HE4 protein on the integrity of the blood–brain barrier. The aim of our paper was to provide a preliminary assessment of the concentrations of HE4 in MS patients. Due to the fact that no studies assessing HE4 among MS patients have been conducted, the conclusions from our study have to be treated with caution.

Significantly higher concentrations of HE4 were observed in the patients with MS compared to the controls. Patients with a worse course of the disease (EDSS > 2) had higher HE4 concentrations than patients with EDSS ≤ 2. Those with EDSS > 2 did not differ in terms of age from those with lower EDSS scores (data not shown).

The concentration of HE4 did not increase with the age or disease duration. The lack of age dependence among healthy individuals may be due to their younger age and smaller SD, with insufficient numbers to reach statistical significance. It appears that HE4 levels may be age-related, because HE4 is an essential marker of ovarian and endometrial cancer in premenopausal women<sup>22</sup> and pregnant women.<sup>23</sup>

Our study did not find any differences between male and female MS patients' HE4 levels. The group of men was smaller, and a study with a larger cohort is necessary. Women are more often affected by MS, which may result from hormonal predispositions<sup>24,25</sup> and various additional factors. One study revealed that the concentrations of HE4 in women with ovarian cancer were generally higher than those in our patients with MS.<sup>18</sup> The highest

concentrations were found in epithelial ovarian cancer, which may suggest the involvement of epithelial tissue in HE4 production.<sup>18,26</sup>

The involvement of hormonal disorders may play a key role in the increase in HE4 among women with MS compared to healthy women. However, this conclusion should be treated with caution. No studies have been performed to assess the relationship between HE4 and hormonal disorders in women with MS. It is known that the HE4 protein causes the resistance of ovarian cancer cells to anti-estrogens (e.g., tamoxifen); it has been found that HE4 interacts with estrogen receptor  $\alpha$  (ER- $\alpha$ ), and the overexpression of HE4 reduces the expression of ER- $\alpha$  in ovarian cancer cells.<sup>27</sup>

Another analysis of the dependence of HE4 on gender indicated that the protein has been recognized as one of the most important prognostic markers not only in ovarian cancer but also in endometrial cancer.<sup>18</sup> Higher concentrations of the protein have been found among women with atypical endometrial hyperplasia compared to women without this condition.<sup>19</sup> Studies on HE4 indicate that it has multi-directional effects in men as well. The protein plays a key role in fertilization, especially in sperm maturation, motility and capacity.<sup>28</sup>

In our study, HE4 concentration was increased in women with EDSS ≥ 2. This suggests that EDSS and HE4 concentration can be prognostic factors, but further studies are needed to confirm this.

Among the limitations of our study are the small sample size and the lack of complete homogeneity between the groups in terms of age and gender. However, the results suggest that the protein could be involved in the pathomechanism of MS in both women and men. In the literature, HE4 is most often discussed in terms of ovarian cancer, but it should be borne in mind that it also plays a significant role in spermatogenesis.<sup>4</sup> Currently, OS is postulated in spermatogenic disorders<sup>29</sup> and in the development of tumors and MS. An analysis of the relationship between the functions of HE4 and OS could be useful in further research.

The role of this unique protein is increasingly being discussed in relation to many diseases. The HE4 is a useful marker for differentiating between lupus nephritis and systemic lupus erythematosus.<sup>30</sup> A study has shown that the participation of HE4 in autoimmune diseases may be

**Table 3.** Analysis of selected factors of disease activity in the study group in relation to HE4

Group	With relapse	With no relapse	p-value
N	9	26	–
HE4 [pmol/L]	47.44 ± 7.65	46.15 ± 7.75	0.66
Group	EDSS ≤ 2	EDSS > 2	p-value
N	21	12	–
HE4 [pmol/L]	44.66 ± 6.13	50.96 ± 8.54	0.019

HE4 – human epididymis protein 4; EDSS – Expanded Disability Status Scale.

**Table 4.** Analysis of the most important correlations for the MS group in relation to gender

Parameter	Age [years]	Disease duration [years]	ARR	EDSS	Gd+ MRI lesions (N)	Group
HE4	NS	NS	NS	NS	R = –0.390 P = 0.024	MS group
HE4	NS	NS	NS	R = 0.56 P = 0.003	NS	women with MS
HE4	NS	NS	NS	NS	NS	men with MS

HE4 – human epididymis protein 4; MS group – multiple sclerosis group; EDSS – Expanded Disability Status Scale; ARR – annualized relapse rate; NA – non-applicable; R – Spearman linear correlation coefficient.



significant: The protein modified the functions of the immune system, for instance, with rendering ovarian tumors undetectable by immune surveillance.<sup>31</sup>

Explaining the role of HE4 and the immune system in the formation of cancer seems to be essential. It is known that many molecules such as programmed cell death protein 1 (PD-1), cytotoxic T-lymphocyte-associated protein 4 (CTLA4), and T-cell immunoglobulin help tumor cells escape immune targeting and elimination.<sup>32</sup> Nivolumab, a monoclonal antibody that binds to PD-1, prevents tumor spread.<sup>33</sup> Shen et al. showed the possibility of using a high-affinity monoclonal antibody against HE4.<sup>34</sup> Monoclonal antibodies are also widely used in autoimmune diseases. The role of HE4 could be explained by searching for similarities between the development of MS and cancer. Many of the same factors may have different key functions in the body depending on the type of activation. This mechanism is common among tumors, e.g., the action of dual specificity phosphatase 6 (DUSP6) may depend on the type and stage of cancer and may enhance or block tumor growth.<sup>32</sup>

The participation of HE4 in the development of ovarian cancer is better understood. It is known that an increase in HE4 is associated with a worse prognosis because this protein induces tumor growth, metastasis, proliferation, anti-estrogen resistance, and chemoresistance.<sup>32</sup> James et al. explained the effect of HE4 on the development of ovarian cancer: In their study, DUSP6 was found to be upregulated by recombinant human HE4 treatment in CD8<sup>+</sup> T and CD56<sup>+</sup> NK cell subsets of human peripheral blood mononuclear cells, which enhanced tumorigenesis in ovarian cancer.<sup>32</sup>

One study revealed that HE4 could be a significant biomarker of decreased kidney function and renal fibrosis in kidney transplant recipients. Furthermore, serum HE4 concentrations increased with disease severity, the severity of fibrosis and HE4 tissue expression in renal biopsies.<sup>20</sup> In the future, post-mortem examinations of MS patients' brain tissue should be conducted to determine the concentration of HE4.

Wang et al. suggested that HE4 could be a potential biomarker of kidney damage in acute and chronic renal dysfunction.<sup>35</sup> Other authors did not find any association between HE4 and liver fibrosis or cirrhosis.<sup>36</sup>

Another limitation of our study was that HE4 concentrations were evaluated only in the serum, which may not reflect the concentrations in the CNS. Additionally, we did not perform a comparative analysis of patients with more advanced forms of MS (i.e., primary progressive MS or secondary progressive MS). However, as already mentioned, no other studies have been conducted assessing the importance of HE4 among women and men with MS. Our study is innovative since it aims to provide an initial analysis of the MS population relative to HE4.

In the future, HE4 could be used as a new indicator of disease progression in MS as in other diseases.


The mechanism responsible for the increase in HE4 protein in MS patients remains unknown. Female hormones could be involved in the concentration of the protein, as in ovarian cancer. Studies on HE4 have also indicated its multi-directional effect in men. Currently, OS is postulated in spermatogenesis disorders; an analysis of the relationship between the functions of HE4 and OS could probably be useful in further research.

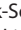
## Conclusions


It is possible that among patients with more severe MS, especially in women, HE4 may be a prognostic factor. Further studies on the importance of the HE4 protein in MS are warranted. This protein could be involved in the pathomechanism of MS and could become a novel target of treatment.


### ORCID iDs


Bożena Adamczyk  <https://orcid.org/0000-0003-1641-5350>

Robert Partyka  <https://orcid.org/0000-0002-0136-2914>

Monika Adamczyk-Sowa  <https://orcid.org/0000-0002-6894-9891>

Krzysztof Wierzbicki  <https://orcid.org/0000-0001-5019-581X>

Paweł Sowa  <https://orcid.org/0000-0001-6179-2572>

Danuta Kokocińska  <https://orcid.org/0000-0002-0453-7900>

### References

- Kirchhoff C, Habben I, Ivell R, Krull N. A major human epididymis-specific cDNA encodes a protein with sequence homology to extracellular proteinase inhibitors. *Biol Reprod.* 1991;45(2):350–357.
- Schummer M, Ng WV, Bumgarner RE, et al. Comparative hybridization of an array of 21,500 ovarian cDNAs for the discovery of genes overexpressed in ovarian carcinomas. *Gene.* 1999;238(2):375–385.
- Hellström I, Raycraft J, Hayden-Ledbetter M, et al. The HE4 (WFDC2) protein is a biomarker for ovarian carcinoma. *Cancer Res.* 2003;63(13):3695–3700.
- Jia LT, Zhang YC, Li J, Tian Y, Li JF. The role of human epididymis protein 4 in the diagnosis of epithelial ovarian cancer. *Clinical Transl Oncol.* 2016;18(3):233–239.
- Li J, Chen H, Mariani A, et al. HE4 (WFDC2) promotes tumor growth in endometrial cancer cell lines. *Int J Mol Sci.* 2013;14(3):6026–6043.
- Galgano MT, Hampton GM, Frierson HF Jr. Comprehensive analysis of HE4 expression in normal and malignant human tissues. *Mod Pathol.* 2006;19(6):847–853.
- Moore RG, Miller MC, Steinhoff MM, et al. Serum HE4 levels are less frequently elevated than CA125 in women with benign gynecologic disorders. *Am J Obstet Gynecol.* 2012;206(4):351.e1–e8.
- Zhang M, Zhao B, Xie J, Liang Y, Yang Z. Serum human epididymis protein 4 is associated with renal function and diabetic kidney disease in patients with type 2 diabetes mellitus. *Biomed Res Int.* 2019;2019:4831459.
- Gasiorowska E, Kluz T, Lipski D, Warchol W, Tykarski A, Nowak-Markwitz E. Human epididymis protein 4 (HE4) reference limits in Polish population of healthy women, pregnant women, and women with benign ovarian tumors. *Dis Markers.* 2019;2019:3890906.
- Piek A, Meijers WC, Schrotten NF, Gansevoort RT, de Boer RA, Sillje HH. HE4 serum levels are associated with heart failure severity in patients with chronic heart failure. *J Card Fail.* 2017;23(1):12–19.
- Takasaki T, Hagihara K, Satoh R, Sugiura R. More than just an immunosuppressant: The emerging role of FTY720 as a novel inducer of ROS and apoptosis. *Oxid Med Cell Longev.* 2018;2018:4397159.
- Adamczyk B, Adamczyk-Sowa M. New insights into the role of oxidative stress mechanisms in the pathophysiology and treatment of multiple sclerosis. *Oxid Med Cell Longev.* 2016;2016:1973834.



13. Fiorini A, Koudriavtseva T, Bucaj E, et al. Involvement of oxidative stress in occurrence of relapses in multiple sclerosis: The spectrum of oxidatively modified serum proteins detected by proteomics and redox proteomics analysis. *PLoS One*. 2013;8(6):e65184.
14. Mossakowski AA, Pohlan J, Bremer D, et al. Tracking CNS and systemic sources of oxidative stress during the course of chronic neuroinflammation. *Acta Neuropathol*. 2015;130(6):799–814.
15. van Horsen J, Witte ME, Schreibelt G, de Vries HE. Radical changes in multiple sclerosis pathogenesis. *Biochim Biophys Acta*. 2011;1812(2):141–150.
16. Witherick J, Wilkins A, Scolding N, Kemp K. Mechanisms of oxidative damage in multiple sclerosis and a cell therapy approach to treatment. *Autoimmune Dis*. 2010;2011:164608.
17. Dringen R. Oxidative and antioxidative potential of brain microglial cells. *Antioxid Redox Signal*. 2005;7(9–10):1223–1233.
18. Brenk A, Bodzek P, Balis M, Barbachowska A, Janosz I, Olejek A. Usefulness of HE4 protein in differentiation of pelvic masses in woman. *Prz Menopauzalny*. 2019;18(1):27–32.
19. Li X, Gao Y, Tan M, et al. Expression of HE4 in endometrial cancer and its clinical significance. *Biomed Res Int*. 2015;2015:437468 [Erratum in: Corrigendum to "Expression of HE4 in endometrial cancer and its clinical significance". Li X, Gao Y, Tan M, Zhuang H, et al. *Biomed Res Int*. 2018;2018:6795629. doi:10.1155/2018/6795629].
20. Luo J, Wang F, Wan J, et al. Serum human epididymis secretory protein 4 as a potential biomarker of renal fibrosis in kidney transplantation recipients. *Clin Chim Acta*. 2018;483:216–221.
21. Nowak M, Janas L, Stachowiak G, Stetkiewicz T, Wilczynski JR. Current clinical application of serum biomarkers to detect ovarian cancer. *Prz Menopauzalny*. 2015;14(4):254–259.
22. Dong C, Liu P, Li C. Value of HE4 combined with cancer antigen 125 in the diagnosis of endometrial cancer. *Pak J Med Sci*. 2017;33(4):1013–1017.
23. Uslu B, Dogan S, Ozdem S, Simsek T. Serum concentrations of HE4 and Ca125 in uncomplicated pregnancies: A longitudinal study. *J Obstet Gynaecol*. 2020;40(1):70–76.
24. Avila M, Bansal A, Culbertson J, Peiris AN. The role of sex hormones in multiple sclerosis. *Eur Neurol*. 2018;80(1–2):93–99.
25. Neto LO, Gromisch ES, Sloan J, Tyry T, Foley FW. Sex differences in predictors of illness intrusiveness in persons with multiple sclerosis. *Qual Life Res*. 2019;28(2):389–397.
26. Dewan R, Dewan A, Jindal M, Bhardawaj M. Diagnostic performance of serum human epididymis protein 4 (HE4) for prediction of malignancy in ovarian masses. *Asian Pac J Cancer Prev*. 2019;20(4):1103–1108.
27. Lokich E, Singh RK, Han A, et al. HE4 expression is associated with hormonal elements and mediated by importin-dependent nuclear translocation. *Sci Rep*. 2014;4:5500.
28. Kant K, Tomar AK, Sharma P, Kundu B, Singh S, Yadav S. Human epididymis protein 4 quantification and interaction network analysis in seminal plasma. *Protein Pept Lett*. 2019;26(6):458–465.
29. Nowicka-Bauer K, Lepczynski A, Ozgo M, et al. Sperm mitochondrial dysfunction and oxidative stress as possible reasons for isolated asthenozoospermia. *J Physiol Pharmacol*. 2018;69(3). doi:10.26402/jpp.2018.3.05
30. Ren Y, Xie J, Lin F, et al. Serum human epididymis protein 4 is a predictor for developing nephritis in patients with systemic lupus erythematosus: A prospective cohort study. *Int Immunopharmacol*. 2018;60:189–193.
31. James NE, Cantillo E, Oliver MT, et al. HE4 suppresses the expression of osteopontin in mononuclear cells and compromises their cytotoxicity against ovarian cancer cells. *Clin Exp Immunol*. 2018;193(3):327–340.
32. James NE, Oliver MT, Ribeiro JR, et al. Human epididymis secretory protein 4 (HE4) compromises cytotoxic mononuclear cells via inducing dual specificity phosphatase 6. *Front Pharmacol*. 2019;10:216.
33. Volpe VO, Klufas DM, Hegde U, Grant-Kels JM. The new paradigm of systemic therapies for metastatic melanoma. *J Am Acad Dermatol*. 2017;77(2):356–368.
34. Shen Y, Wang Y, Jiang X, et al. Preparation and characterization of a high-affinity monoclonal antibody against human epididymis protein-4. *Protein Expr Purif*. 2018;141:44–51.
35. Wang L, Sun Y, Cai X, Fu G. The diagnostic value of human epididymis protein 4 as a novel biomarker in patients with renal dysfunction. *Int Urol Nephrol*. 2018;50(11):2043–2048.
36. Zhang M, Yuan L, Yao F, et al. Human epididymis protein 4 concentration is not associated with liver fibrosis and cirrhosis in a case control study. *Clin Chim Acta*. 2018;484:213–217.

# The effect of 3-bromopyruvate on the properties of cathepsin B in the aspect of metastatic potential of colon cancer cells

Izabela Szczuka<sup>A-F</sup>, Jerzy Wiśniewski<sup>B,C</sup>, Irena Kustrzeba-Wójcicka<sup>E,F</sup>, Grzegorz Terlecki<sup>A,C-F</sup>

Department of Medical Biochemistry, Wrocław Medical University, Poland

A – research concept and design; B – collection and/or assembly of data; C – data analysis and interpretation; D – writing the article; E – critical revision of the article; F – final approval of the article

Advances in Clinical and Experimental Medicine, ISSN 1899–5276 (print), ISSN 2451–2680 (online)

Adv Clin Exp Med. 2020;29(8):949–957

## Address for correspondence

Izabela Szczuka

E-mail: izabela.szczuka@umed.wroc.pl

## Funding sources

None declared

## Conflict of interest

None declared

## Acknowledgements

The authors would like to thank the Foundation of Wrocław Medical University (FUM) and its Board Chairmen for financing the purchase of HCT 116 cell line.

Received on April 28, 2020

Reviewed on May 24, 2020

Accepted on June 7, 2020

Published online on August 21, 2020

## Cite as

Szczuka I, Wiśniewski J, Kustrzeba-Wójcicka I, Terlecki G.

The effect of 3-bromopyruvate on the properties of cathepsin B in the aspect of metastatic potential of colon cancer cells. *Adv Clin Exp Med.* 2020;29(8):949–957. doi:10.17219/acem/123622

## DOI

10.17219/acem/123622

## Copyright

© 2020 by Wrocław Medical University

This is an article distributed under the terms of the Creative Commons Attribution 3.0 Unported (CC BY 3.0) (<https://creativecommons.org/licenses/by/3.0/>)

## Abstract

**Background.** Cathepsin B (CTSB, EC 3.4.22.1) is a protease that physiologically resides in lysosomes and whose biosynthesis, cell surface location, intracellular distribution, and enzymatic activity undergo changes during the pathogenesis of cancer; it plays an important role in metastasis. Due to its active center structure, it is theoretically susceptible to the action of 3-bromopyruvate – an analogue of pyruvic acid and an alkylator that has been studied in depth in recent years for its anti-cancer activity, mainly through the inhibition of glycolytic enzymes.

**Objectives.** To investigate the effects of 3-bromopyruvate on the tumor cell properties in selected colorectal carcinoma cell lines that are widely attributed to the dysregulation of CTSB. Moreover, the effect of direct action of 3-bromopyruvate on the CTSB molecule was investigated in vitro.

**Material and methods.** The research on the effect of 3-bromopyruvate on Caco-2/HCT 116 cells and purified human CTSB included a scratch/wound healing assay, a cell invasion assay, spectrofluorimetric measurements of enzymatic activity of cathepsin B, indirect immunofluorescence and flow cytometry, zymography, and liquid chromatography/mass spectrometry methods.

**Results.** 3-bromopyruvate reduced the activity and secretion of active CTSB and lowered the motility and invasiveness of Caco-2/HCT 116 human colorectal cancer cells. It decreased the exposure of CTSB on the outer surface of the cell membrane in both cell lines. 3-bromopyruvate inhibited the activity of CTSB reversibly and did not alkylate the molecule of the enzyme.

**Conclusions.** This is the first report on the effect of 3-bromopyruvate directly on CTSB and indirectly on the mechanisms leading to its distinct pathophysiological properties, resulting in increased metastatic potential of cancer cells, among others. Although detailed mechanisms of the interaction between 3-bromopyruvate and the active site of CTSB require further research, the results provide a new perspective from which to study the antitumor effect of 3-bromopyruvate.

**Key words:** cathepsin B, protease inhibitor, 3-bromopyruvate, Caco-2 cells, HCT 116 cells

## Introduction

Cathepsin B (CTSB; EC 3.4.22.1) is a cysteine protease physiologically occurring within the lysosomes of eukaryotic cells. Under physiological conditions it is controlled on many levels, including through the activation of zymogen or the action of endogenous inhibitors.<sup>1</sup> It is extensively studied due to its role in cancer pathogenesis and metastasis, when its biosynthesis, intracellular distribution, location on the cell surface, and enzyme activity are altered.<sup>2,3</sup> This enzyme plays an important role in the metastasis process by directly degrading extracellular matrix (ECM) proteins (such as fibrinogen, type IV collagen and laminin<sup>4</sup>) and intensifying the proteolytic cascade by inactivating the tissue inhibitors of metalloproteinases (TIMP).<sup>5</sup> The mechanism of CTSB enzymatic catalysis is based on the interaction of 3 amino acid residues within the active center of the enzyme (forming the catalytic triad): Cys29, His199 and Asn219.<sup>6</sup> Altered levels of CTSB expression and activity, as well as different locations and distribution, are related to the occurrence of various pathological conditions, particularly neoplastic diseases,<sup>7</sup> neurodegenerative diseases<sup>8</sup> and inflammatory diseases of the nervous system.<sup>9</sup> Mitrović et al. proved that the suppression of endo- and exopeptidase activity of CTSB limits ECM degradation and the invasiveness of tumor cells.<sup>10</sup> The role of CTSB in pre-cancer processes and the development, metastasis and invasiveness<sup>11–13</sup> of colon cancer cells has also been demonstrated. It was found that an elevated level of CTSB correlates positively with the increased mortality of patients with colon cancer.<sup>14</sup> Higher immunoreactivity of this protein has also been found in cancerous tissues and elevated concentrations have been found in the urine and serum of patients with metastatic changes.<sup>15,16</sup> Van Noorden et al. demonstrated in a rat model that the selective inhibition of CTSB reduces the probability of metastases occurring from the colon to the liver.<sup>17</sup>

Many inhibitors of CTSB have already been discovered or synthesized, with different types and modes of inhibition, selectivity or reversibility of the reaction.<sup>18</sup> Although some of them were promising, the possibilities of conducting research in clinical practice with these compounds turned out to be very limited. The compound tested in this study for the inhibition of CTSB was 3-bromopyruvate (3-BrPA). It is a synthetic, structural analogue of pyruvic and lactic acids, entering eukaryotic cells through MCT1 monocarboxylic acid transporters.<sup>19</sup> It is intensively studied because it is thought to have an antitumor effect, mainly via alkylation of key glycolytic enzymes in tumor cells.<sup>20,21</sup> To date, 2 cases of clinically applying this compound in the treatment of advanced cancers have been reported.<sup>22,23</sup> Studies on the effect of 3-BrPA on CTSB have not yet been conducted, so this is the first attempt in the literature to explore this subject.

## Material and methods

### Material

3-bromopyruvate (purity  $\geq 97\%$ ) was purchased from Sigma-Aldrich (St. Louis, USA). Human liver CTSB (purity  $\geq 95\%$  by SDS-PAGE) was obtained from Calbiochem (Sigma-Aldrich). The specific fluorogenic substrate for CTSB, Z-Arg-Arg-AMC hydrochloride salt, was supplied by Bachem AG (Bubendorf, Switzerland). Human colorectal adenocarcinoma Caco-2 cells (ATCC<sup>®</sup> HTB-37<sup>™</sup>) and human colorectal carcinoma HCT 116 cells (ATCC<sup>®</sup> CCL-247<sup>™</sup>) were purchased from ATCC (Manassas, USA). Primary monoclonal IgG rat anti-human CTSB antibodies were purchased from R&D Systems (Minneapolis, USA). Secondary IgG (H+L) goat anti rat antibodies conjugated with Alexa Fluor 633 dye were purchased from Invitrogen (Carlsbad, USA). All other reagents were of analytical, LC/MS or other grade suitable for cell culturing.

### Methods

#### Cell culture

The human colorectal adenocarcinoma Caco-2 cells (ATCC<sup>®</sup> HTB-37<sup>™</sup>) and human colorectal carcinoma HCT 116 cells (ATCC<sup>®</sup> CCL-247<sup>™</sup>) were cultured at 37°C in 95% air with 5% CO<sub>2</sub> in CELCULTURE<sup>®</sup> CCL-170B-8 incubator (Esco, Singapore) with EMEM (Eagle's Minimum Essential Medium; BioWhittaker<sup>®</sup>, Lonza, Basel, Switzerland), supplemented with 2 mmol/L L-glutamine, 10% (v/v) fetal bovine serum (FBS), 100 U/mL penicillin, 100 µg/mL streptomycin, and 0.25 µg/mL amphotericin B (Gibco, Thermo Fisher Scientific). The medium was renewed every 3 days. Cells were harvested with TrypLE<sup>™</sup> Express (Gibco, Thermo Fisher Scientific) after rinsing with Dulbecco's Phosphate Buffered Saline solution (DPBS; Gibco, Thermo Fisher Scientific). The cells were counted with Countess<sup>™</sup> Automated Cell Counter (Invitrogen) after staining with 0.4% trypan blue solution (Invitrogen).

#### Scratch/wound healing assay

Seventy microliters of cell suspension containing  $5 \times 10^4$  cells was added to each well of the two-well culture insert (Ibidi, Gräfelfing, Germany), placed into a 24-well cell culture plate and cultured for 24 h. Subsequently, the inserts were removed from the wells and the wells were rinsed with DPBS, followed by the addition of EMEM with or without 10 µM or 30 µM of 3-BrPA. The closure of the insert-created gap (wound, initially 500 µm) was observed after 0 h, 24 h, and 48 h under a CKX41 inverted microscope with a SC30 camera (Olympus, Tokyo, Japan). The gap area was measured using the MRI Wound Healing Tool macro for ImageJ software (National Institutes of Health, Bethesda, USA).

## Cell invasion assay

For cell invasiveness testing, the cells were cultured in standard conditions until 80% confluence was achieved; then, the medium was changed to EMEM 0% FBS and the culture was incubated for 24 h, followed by harvesting with TrypLE™ Express reagent and centrifugation in EMEM 5% bovine serum albumin (BSA). The cell suspensions were diluted in EMEM 0% FBS to a concentration of  $5 \times 10^5$  cells/mL.

3-bromopyruvate in EMEM 0% FBS was added (up to 50  $\mu$ M for Caco-2 and up to 30  $\mu$ M for HCT 116) to the cell suspensions to obtain the concentration of the compound used in the experiment, while the controls were supplemented with the appropriate volume of EMEM 0% FBS. The cell suspensions were gently placed on a QCM™ Cell Invasion Assay 96-well plate (Chemicon, Merck, Darmstadt, Germany) prepared according to the manufacturer's instructions, based on the Boyden chamber principle. The experiment was carried out according to the manufacturer's recommendations. The following controls were also performed for each cell line: cells without 3-BrPA and a medium without chemoattractant in the wells in which the insert was placed. Fluorescence was measured using a CLARIOstar® (BMG Labtech, Offenburg, Germany) microplate reader with values of  $\lambda_{ex} = 480$  nm and  $\lambda_{em} = 520$  nm.

## Fluorescent microplate assay for cancer-cell-associated CTSB

The assay used in our study was a modified version of the method published by Hulkower et al.<sup>24</sup> In brief,  $5 \times 10^4$  Caco-2/HCT 116 cells per well were seeded into a 96-well plate and cultured (37°C; 5% CO<sub>2</sub>) for 24 h, then the medium was changed to EMEM 0% FBS with or without 3-BrPA and incubated for 1 h, after which the culture medium was replaced with a fresh one (0% FBS). The culture was carried out for a further 24 h to obtain 80% confluence. The medium was then collected from the cell layer and identical volumes were transferred to empty wells on the plate. The cell layer was washed with sterile DPBS solution and then incubated for 30 min with pericellular assay buffer (PAB) I (Hank's Balanced Salt Solution) without sodium bicarbonate, 0.6 mM of CaCl<sub>2</sub>, 0.6 mM of MgCl<sub>2</sub>, 25 mM of PIPES, and 2 mM of L-cysteine (pH 7.0)) under the abovementioned conditions. After the incubation time, the PAB I was removed. Subsequently, PAB II (Hank's Balanced Salt Solution without sodium bicarbonate, 0.6 mM of CaCl<sub>2</sub>, 0.6 mM of MgCl<sub>2</sub>, 25 mM of PIPES, and 2 mM of L-cysteine (pH 7.0)) containing 100 mM of Z-Arg-Arg-AMC substrate was added to the wells containing cells and previously collected post-culture media. In half of the wells containing cells, the composition of PAB II also included 0.1% aqueous solution of Triton X-100 in order to obtain the lysis effect of cell membranes, thereby visualizing

the total cellular activity of CTSB. In the half of the wells with cells where the detergent was not added, the activity of CTSB at the cell surface was evaluated. Spectrofluorimetric evaluation of the reaction product gain per minute was performed on a CLARIOstar® microplate reader with values of  $\lambda_{ex} = 380$  nm and  $\lambda_{em} = 460$  nm.

## Indirect immunofluorescence and flow cytometry analysis

Cells for flow cytometry analysis were seeded in six-well plates at  $1 \times 10^6$  cells per well under standard conditions. After obtaining 80% confluence, the medium was changed to EMEM 0% FBS with 30  $\mu$ M 3-BrPA (test samples) or EMEM 0% FBS (control samples) for 1 h. Subsequently, the medium was replaced with fresh EMEM 0% FBS. The culture was carried out for 24 h, followed by medium removal, mechanical culture harvesting in PBS 2% FBS, centrifugation, resuspension of cell pellets in PBS 2% FBS, and centrifugation. The resulting pellets were suspended in PBS buffer with primary rat anti-human CTSB monoclonal antibodies at a concentration of 2.5  $\mu$ g/mL and incubated for 30 min at room temperature. Afterwards, the suspensions were centrifuged, the pellets were washed with PBS, centrifuged again, resuspended in a PBS solution containing secondary goat anti rat IgG (H + L) antibodies conjugated with Alexa Fluor 633 dye (1:200 dilution ratio), and incubated in the dark for 30 min, followed by 2 cycles of washing in PBS. The analysis of the results showing the presence of the antigen (CTSB) on the outer surface of the cell membrane was performed using a CytoFLEX flow cytometer (Beckman Coulter, Indianapolis, USA) equipped with CytExpert v. 2.1 software (Beckman Coulter). The fluorescence emission of used fluorochrome (Alexa Fluor 633) was evaluated (channel: FL6, laser: 635 nm, wavelength: corresponding to allophycocyanin). The results were developed using Kaluza Analysis Software (Beckman Coulter) v. 2.0. The number of cells subjected to flow cytometry analysis differed between samples (due to the way they were prepared), so we present the data showing the relative fluorescence intensity of fluorochrome per cell, as a result of dividing the mean of relative fluorochrome fluorescence intensity of a given population by the number of cells present within it.

## Cathepsin B spectrofluorimetric enzymatic activity assay

The assay used in our research was a modified version of the method published by Barrett.<sup>25</sup> Samples consisting of 0.75 nM of purified human liver CTSB, the desired concentrations of 3-BrPA, deionized water, reaction buffer I (0.4 M of phosphate buffer and 4 mM of EDTA (pH 6.0)), and 0.1% Brij 35P were subjected to 10 min of preincubation at 37°C. The enzyme reaction was started by adding



100  $\mu\text{M}$  of Z-Arg-Arg-AMC substrate in reaction buffer II (0.4 M of phosphate buffer, 8 mM of L-cysteine, and 4 mM of EDTA (pH 6.0)). The reaction was carried out at 37°C for 15 min. Fluorescence was measured with a CLARIOstar® (BMG Labtech) microplate reader at  $\lambda_{\text{ex}} = 380 \text{ nm}$  and  $\lambda_{\text{em}} = 460 \text{ nm}$ .

## Zymography

Samples consisting of 130 nM of purified human liver CTSB (positive control) and 50–5000  $\mu\text{M}$  of 3-BrPA were incubated for 10 min at 37°C, after which the samples were electrophoresed on 8% lithium dodecyl sulfate (LDS) polyacrylamide gel containing 0.1% porcine skin gelatin. The buffering system and staining/destaining procedures followed the protocol described by Klose et al.<sup>26</sup> The resulting zymogram was documented using Gel-Doc™ EZ (Bio-Rad, Hercules, USA) and the results were analyzed with Image Lab v. 5.2.1 (Bio-Rad).

## Liquid chromatography/mass spectrometry analysis

The tested samples, consisting of 2  $\mu\text{M}$  of CTSB with 500  $\mu\text{M}$  of 3-BrPA in 50 mM of acetate buffer (with 1 mM of EDTA; pH 5.0) and control samples (2  $\mu\text{M}$  of CTSB in 50 mM of acetate buffer (with 1 mM of EDTA; pH 5.0)) were incubated for 10 min at 37°C prior to separation. Mass spectrometric studies were conducted using a Nano-Acquity UPLC Q-TOF/MS (Waters, Milford, USA) system. The chromatograph was equipped with an Acquity UPLC HSS C18 analytical column (1 mm  $\times$  100 mm; 1.8  $\mu\text{m}$ ) with the flow-rate maintained at 50  $\mu\text{L}/\text{min}$  and the injection volume at 3  $\mu\text{L}$ . The separation was held for 15 min at 35°C. The mobile phase constituents were solvent A – 0.1% formic acid in water – and solvent B, 0.1% formic acid in acetonitrile. The elution took place in a gradient system: 0–1 min: 15% B; 2 min: 25% B; 8 min: 60% B; 10 min: 85% B; 11 min: 85% B; 11.5 min: 15% B; 15 min: 15% B. The eluted CTSB was analyzed using Xevo G2-Q-TOF (Waters) mass spectrometer with an electrospray ionization source in positive ionization mode (ESI+). The capillary voltage was set at 3.0 kV, and the cone voltage for CTSB was set at 40 V. The cone gas flow was maintained at 80 L/h, and the source temperature was set at 100°C. Leucine Enkephalin (Waters) was used as the lock mass solution. Data was collected from  $m/z$  200 to  $m/z$  2000. The mass spectra were deconvoluted with MaxEnt 1 (Waters).

## Statistical analysis

The results of the scratch/wound healing assay and zymography are a representative set of photographs from 1 of the 3 experiments conducted. The gap area ratios for scratch/wound healing assay were calculated using a comparison of 2 ratios (the ratio of a gap area at a given time

point to the gap area at 0 h for treated cells, compared to the ratios of their untreated counterparts). The results of the cell invasiveness and proteolytic activity experiments are presented as a mean value  $\pm$  standard deviation (SD) of 3 independent experiments, analyzed using the t-test for one mean. A p-value  $<0.05$  was considered statistically significant. Statistical analysis was conducted using MedCalc Statistical Software v. 19.2 (MedCalc Software Ltd, Ostend, Belgium).

## Results

### Effect of 3-bromopyruvate on colon cancer cells and properties of CTSB from colon cancer cells

#### Cell motility

A scratch/wound healing assay was used to evaluate the effect of 3-BrPA treatment on the migratory properties of Caco-2 and HCT 116 colon cancer cells. Stimulation with 3-BrPA visibly decreased the motility of cells from both of the studied cancer cell lines in a dose-dependent manner (Fig. 1).

#### Cell invasiveness

The cell invasion assay was used to evaluate the effect of 3-BrPA treatment on the invasiveness of Caco-2 and HCT 116 colon cancer cells. The Caco-2 cells (Fig. 2A), as a result of 3-bromopyruvate treatment, showed reduced levels of invasiveness compared to the untreated control cells (10% FBS) in a dose-dependent manner. Fifty microliters of 3-BrPA reduced the invasiveness of the tested cells by more than 60% in comparison to the untreated positive control samples. The HCT 116 cells (Fig. 2B) also showed decreased invasiveness, but the response was weaker than in the Caco-2 cells, reaching up to 25% decreased invasion compared to the controls.

#### Cathepsin B proteolytic activity in cells and post-culture media

The fluorescent microplate assay for cancer-cell-associated CTSB was used to evaluate the effect of 3-BrPA on CTSB proteolytic activity in Caco-2 and HCT 116 colon cancer cells and post-culture media. In Caco-2 cells (Fig. 3A) the total cellular activity of CTSB decreased in a dose-dependent manner, reaching 76% and 66% of the control value for 3-BrPA concentrations of 10  $\mu\text{M}$  and 30  $\mu\text{M}$ , respectively. The activity of CTSB in post-culture media was also reduced, though it was similar for both 3-BrPA concentrations used, amounting to about 75% of the control value. 3-bromopyruvate did not affect the total cellular activity of CTSB in HCT 116 cells (Fig. 3B):



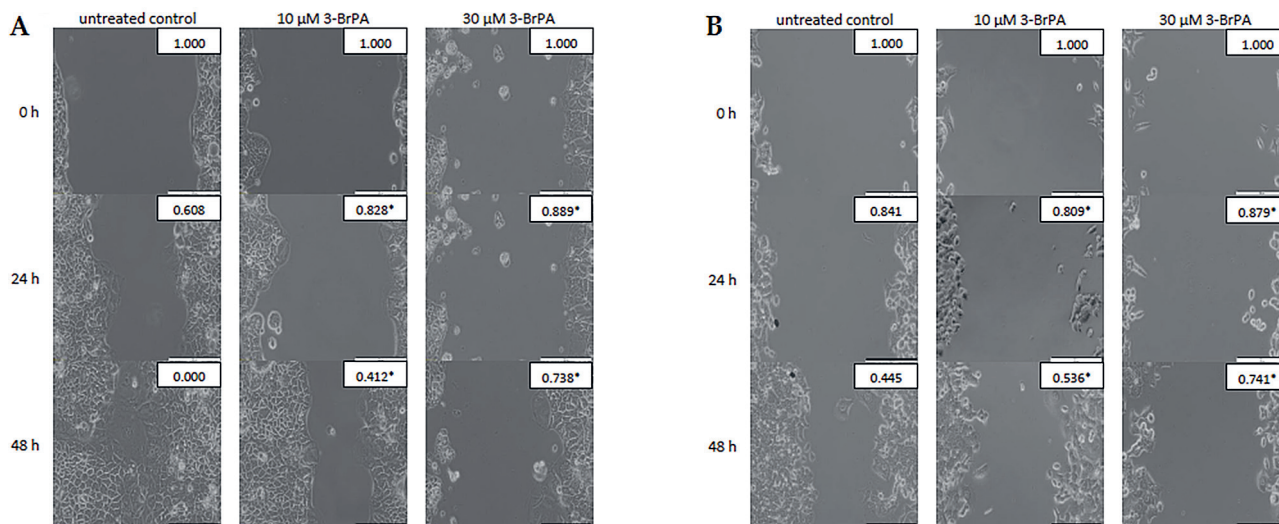


Fig. 1. The impact of one-hour 3-BrPA (10 μM and 30 μM) stimulation on the motility of Caco-2 (A) and HCT 116 (B) colon cancer cells at 0 h, 24 h and 48 h (representative data). Scale bars (200 μm) appear in the lower right corner of each photograph; the numeric data in the upper right corner of each photograph indicates the gap area ratio at a given time point to the gap area at 0 h. The ratios in treated cells significantly different ( $p < 0.05$ ) from their untreated counterparts are marked with asterisks

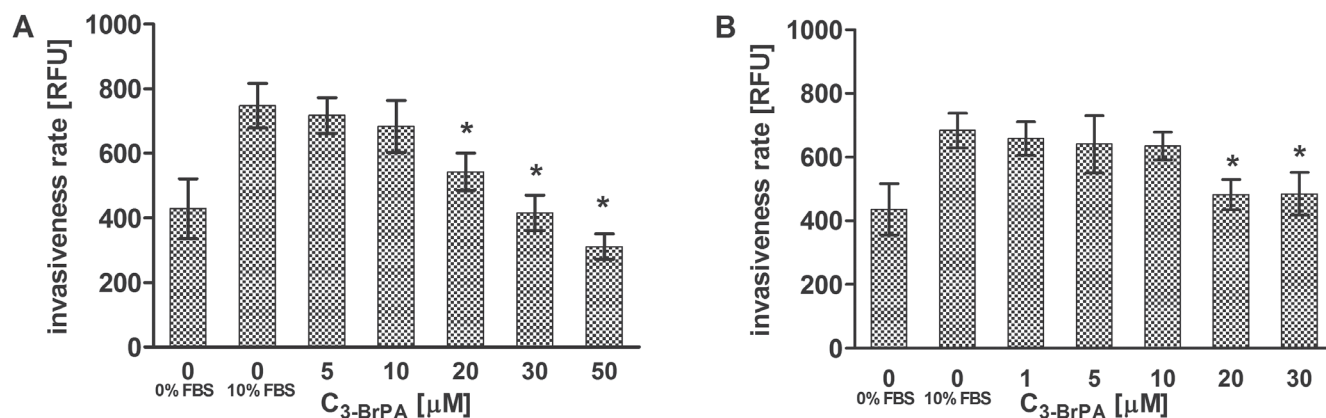


Fig. 2. The impact of 3-BrPA stimulation on the invasiveness of Caco-2 (A) and HCT 116 (B) colon cancer cells. Columns represent the level of cell invasiveness presented as mean fluorescence intensity of the CyQuant GR® dye that stained (previously lysed) the invasive cells. The serum-free medium in the lower chamber was used as negative controls; 10% FBS medium in the lower chamber was used as positive controls. Statistically significant differences ( $p < 0.05$ ) in the treated cells compared to their respective controls are marked with asterisks

RFU – relative fluorescence units.

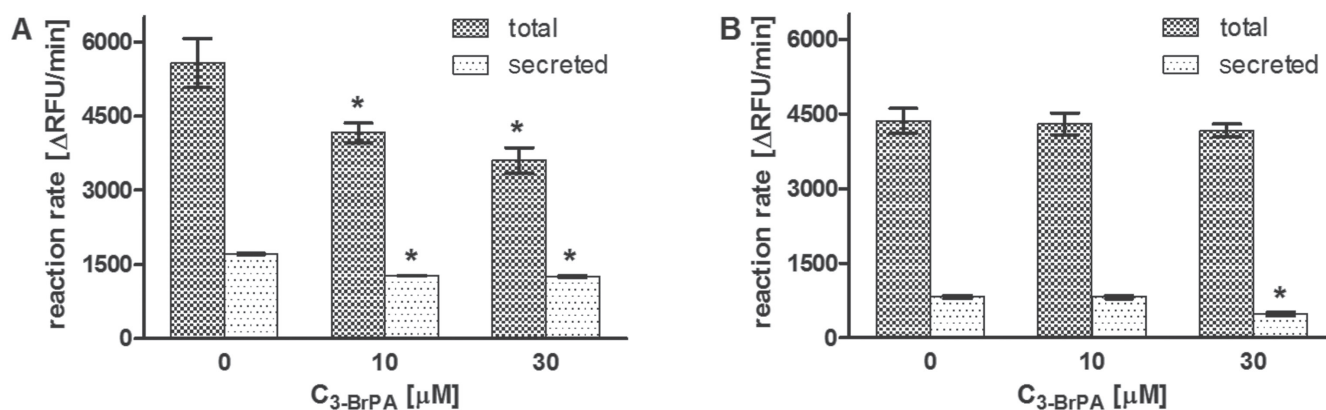


Fig. 3. The effect of 3-BrPA on proteolytic activity of CTSB in Caco-2 (A) and HCT 116 (B) colon cancer cells and post-culture media. Columns represent reaction rates (as a mean of 3 independent experiments  $\pm$ SD); statistically significant differences ( $p < 0.05$ ) are marked with asterisks

total – cathepsin B activity in lysed cells; secreted – cathepsin B activity in post-culture media; RFU – relative fluorescence units.

the fluorescence intensity values for the tested samples were about 96–98% of the control value for this parameter. However, a significant decrease in CTSB activity in HCT 116 post-culture media was observed in the 30- $\mu\text{M}$  3-BrPA samples. The activity decreased to about 58% of the control value. No measurable CTSB activity was detected on the cell surface.

### Cathepsin B exposure on surface of the outer membrane of the cells

Indirect immunofluorescence and flow cytometry analysis was used to evaluate CTSB exposure on the surface of the outer membrane after 3-BrPA treatment. The results presented in Fig. 4 show that 3-BrPA treatment caused a considerable decrease CTSB exposure on the outer surface of the cell membrane in both of the examined colorectal cancer lines, but CTSB exposure in control cells and its loss in treated cells was much broader in Caco-2 cells.

### Effect of 3-bromopyruvate on properties of purified human CTSB

#### Proteolytic activity

As shown in Fig. 5, 3-BrPA decreased the activity of CTSB in a dose-dependent manner, reaching  $\text{IC}_{50}$  at 750  $\mu\text{M}$ ; therefore, it cannot be considered a potent CTSB inhibitor.

#### Type of inhibition

The reversibility of CTSB inhibition by 3-BrPA was determined with gelatin zymography, in which CTSB aliquots were incubated with 3-BrPA prior to gel electrophoresis. The results shown in Fig. 6 indicate that 3-BrPA, irrespective of the concentration in the sample, dissociated from the molecule of the enzyme during migration in the gel, allowing cathepsin to restore its activity in the following stages of zymography. The bands on the zymogram representing the proteolytic activity of the tested samples against gelatin were comparable to the control. This result indicates that the inhibition of CTSB by 3-BrPA is reversible.

	A	B	C	D	E
3-BrPA [ $\mu\text{M}$ ]	0	50	500	1000	5000

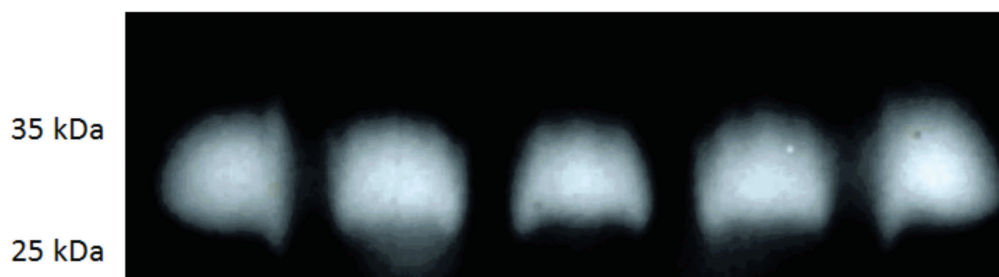


Fig. 6. Zymographic investigation of the reversibility of CTSB inhibition by 3-BrPA. Transparent bands represent CTSB activity of (A) positive controls (130 nM of CTSB) and (B–E) 130 nM of CTSB incubated for 10 min at 37°C with 3-BrPA prior to electrophoresis

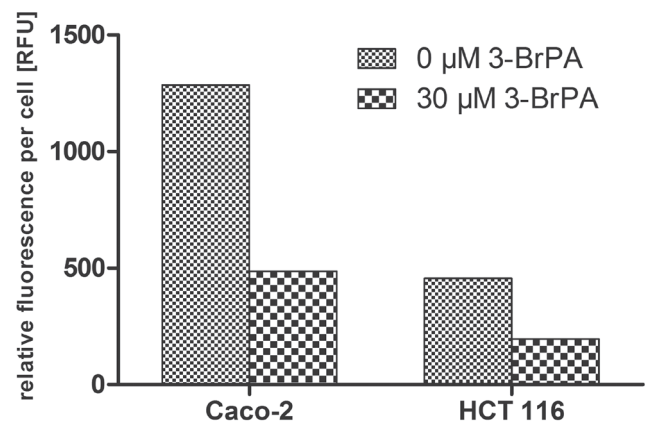


Fig. 4. The effect of 3-BrPA on CTSB exposure on the surface of the outer membrane of the cells in Caco-2 and HCT 116 colon cancer cells. Columns represent relative fluorescence of Alexa Fluor 633 dye per cell

RFU – relative fluorescence units.

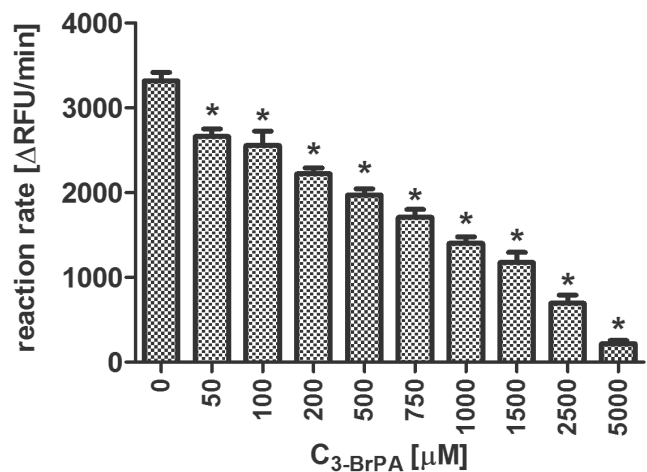


Fig. 5. The effect of 3-BrPA on purified human CTSB activity evaluated with spectrofluorimetric assay. Columns represent reaction rates (as a mean of 3 independent experiments  $\pm$ SD); statistically significant differences ( $p < 0.05$ ) are marked with asterisks

RFU – relative fluorescence units.

### Modifications of the protein molecule

To confirm that 3-BrPA does not bind covalently to the molecule of CTSB, a liquid chromatography/mass spectrometry analysis was performed. As shown in Fig. 7,





the mass spectrum of the test sample (Fig. 7B,D) and the mass spectrum of the control (Fig. 7A,C) showed no notable differences, a finding which proves a lack of covalent modifications within the CTSB molecule caused by 3-BrPA.

## Discussion

Much of the research on the antitumor effects of 3-BrPA focuses on its alkylating action on the enzymes of the glycolytic pathway and the respiratory chain; therefore, we decided to look at this compound from a different perspective and examine how it affects the metastasis process by acting on the enzyme CTSB. Cell lines selected for the purposes of this study have been used in research on both 3-BrPA<sup>27</sup> and CTSB.<sup>12,24,28</sup> Our studies based on cancer cell cultures included a one-hour incubation of cells with 3-BrPA. The choice of this incubation time was dictated by the half-life of 3-BrPA (about 77 min at a pH of ~7<sup>29</sup>). The selected 3-BrPA concentrations in the experiments did not significantly decrease cell viability (checked with sulforhodamine B assay, data not shown). Being based on the above assumptions, the results cannot be compared with those of studies by Lea et al. and Ho et al., who used a 72-hour incubation time with 3-BrPA, obtaining IC<sub>50</sub> values for this compound of 50  $\mu\text{M}$ <sup>27</sup> and 37  $\mu\text{M}$ <sup>30</sup> for the Caco-2 cell line and 25  $\mu\text{M}$ <sup>27</sup> and 23  $\mu\text{M}$ <sup>30</sup> for the HCT 116 cell line. These studies reported lower sensitivity of the Caco-2 cells to 3-BrPA compared to HCT 116 cells. This may be due to a different baseline level of glutathione (GSH), the main cellular antioxidant, in both cell lines: higher in Caco-2 and lower in HCT 116.<sup>31</sup> 3-BrPA reduces the level of GSH<sup>32</sup> and stimulates the production of free radicals, increasing oxidative stress in the cell.<sup>33</sup>

Research presented by El Sayed et al., Xu et al. and Tomizawa et al. on the inhibitory effect of 3-BrPA on cell motility confirmed our observations, but these studies were carried out on human C6 glioma,<sup>34</sup> U87 and CD133 + U87,<sup>35</sup> and HCC hepatocellular carcinoma<sup>36</sup> cell lines. The results from the invasiveness assay indicated an overall higher invasiveness of Caco-2 cells than the HCT 116 line and a greater susceptibility of the former to stimulating invasion in the presence of a chemoattractant (10% FBS). As expected, both cell lines displayed decreased invasiveness after 3-BrPA treatment, with Caco-2 exhibiting a clearer effect dependent on the concentration of the compound. This effect may be caused by the inhibition of proteolytic enzymes by 3-BrPA – especially CTSB, which is responsible for the degradation of protein components present in the ECMatrix<sup>TM</sup> layer – and the effect of this compound on cellular mechanisms of synthesis and secretion of proteolytic enzymes. These assumptions have been confirmed by Bian et al., who proved with an analogous method that the treatment of colorectal cancer cells with CTSB-specific inhibitor CA-074 significantly reduces their invasiveness in vitro. A similar effect was observed after reducing CTSB expression in the tested cells.<sup>12</sup>

The tests on the proteolytic activity of CTSB in cells and post-culture media indicated a higher total activity of CTSB in the cells (determined after lysis of cell membranes with Triton X-100 detergent) and in post-culture media in the Caco-2 cell line than in the HCT 116 cell line, which is in agreement with the results presented by Bian et al.<sup>12</sup> The inhibitory effect of 3-BrPA on the total cellular activity of CTSB in a dose-dependent manner was visible only in Caco-2 cells, suggesting that this compound probably acts on the cellular mechanisms responsible for CTSB processing in those cells, in contrast to HCT 116. The negative effect of 3-BrPA on the secretion of CTSB was visible in both cell lines, suggesting that it may interfere with the intracellular distribution and secretion of this enzyme, in addition to the above effects. The mechanisms underlying these observations require further research. In the interpretation of results obtained with indirect immunofluorescence and flow cytometry analysis, we used fluorescence per cell as a parameter. It presents comparable values between 2 lines and between samples within a line. Our research demonstrated that the cells of both tested lines have CTSB on the outer surface of the cell membrane, which has been confirmed by the studies of both lines obtained by Hulkower et al.<sup>24</sup> and of the HCT 116 line published by Cavallo-Medved et al.<sup>28</sup> 3-bromopyruvate, incubated with cells for 1 h on the day preceding the measurement, caused an average twofold decrease in CTSB exposure on the cell surface of both lines compared to the control cells, with a higher exposure for the Caco-2 line. These observations, supported by the spectrofluorimetric experiments described above, may suggest that 3-bromopyruvate affects the mechanisms of CTSB distribution and the interaction of this protein with the membrane in colorectal cancer cells. Studies on a cellular model did not provide an opportunity to reveal the mechanism of 3-BrPA action on the enzyme. Therefore, we conducted further experiments on the purified protein.

In our research, we used 2 enzymatic methods: spectrofluorimetry and gelatin zymography, which have been successfully applied for CTSB enzymatic activity evaluation.<sup>37</sup> The relatively high concentrations of 3-BrPA inhibiting CTSB activity, particularly in comparison with the concentrations of irreversible inhibitors of this enzyme presented in an article by Frlan and Gobec,<sup>18</sup> raised our concerns as to the validity of attributing the effects of 3-BrPA–CTSB interaction to its alkylating effect and, consequently, also the question of reversing this inhibition. The analysis of the zymogram produced in this study indicated that the inhibition of CTSB by 3-BrPA would be reversible. During the electrophoresis process, 3-BrPA dissociated from the enzyme molecule, allowing CTSB to restore its activity in subsequent stages of zymography. Such an effect would not be possible if there was an alkylation reaction between these molecules (in which the inhibitor covalently binds to the enzyme). We confirmed this observation by mass spectrometry/liquid chromatography analysis, as the increase in molecular weight expected in the case

of 3-BrPA-mediated alkylation should amount +86 Da, and the mass spectra of CTSB and CTSB incubated with 3-BrPA in our study showed no such differences. Although detailed mechanisms of the interaction between 3-BrPA and CTSB require further research, these results provide a new perspective from which to study the antitumor and antimetastatic effect of 3-BrPA.

### ORCID iDs

Izabela Szczuka  <https://orcid.org/0000-0001-7311-9633>

Jerzy Wiśniewski  <https://orcid.org/0000-0003-2831-7643>

Irena Kustrzeba-Wójcicka  <https://orcid.org/0000-0001-5551-4445>

Grzegorz Terlecki  <https://orcid.org/0000-0001-8242-0866>

### References

- Turk V, Turk B, Turk D. Lysosomal cysteine proteases: Facts and opportunities. *EMBO J*. 2001;20(17):4629–4633. doi:10.1093/emboj/20.17.4629
- Gondi CS, Rao JS. Cathepsin B as a cancer target. *Expert Opin Ther Targets*. 2013;17(3):281–291. doi:10.1517/14728222.2013.740461
- Mohamed MM, Sloane BF. Cysteine cathepsins: Multifunctional enzymes in cancer. *Nat Rev Cancer*. 2006;6(10):764–775. doi:10.1038/nrc1949
- Koblinski JE, Ahram M, Sloane BF. Unraveling the role of proteases in cancer. *Clin Chim Acta*. 2000;291(2):113–135. doi:10.1016/S0009-8981(99)00224-7
- Kostoulas G, Lang A, Nagase H, Baici A. Stimulation of angiogenesis through cathepsin B inactivation of the tissue inhibitors of matrix metalloproteinases. *FEBS Lett*. 1999;455(3):286–290. doi:10.1016/S0014-5793(99)00897-2
- Musil D, Zucic D, Turk D, et al. The refined 2.15 Å X-ray crystal structure of human liver cathepsin B: The structural basis for its specificity. *EMBO J*. 1991;10(9):2321–2330.
- Aggarwal N, Sloane BF. Cathepsin B: Multiple roles in cancer. *Proteomics Clin Appl*. 2014;8(5–6):427–437. doi:10.1002/prca.201300105
- Ii K, Ito H, Kominami E, Hirano A. Abnormal distribution of cathepsin proteinases and endogenous inhibitors (cystatins) in the hippocampus of patients with Alzheimer's disease, parkinsonism-dementia complex on Guam, and senile dementia and in the aged. *Virchows Arch A Pathol Anat Histopathol*. 1993;423(3):185–194. doi:10.1007/BF01614769
- Nagai A, Murakawa Y, Terashima M, et al. Cystatin C and cathepsin B in CSF from patients with inflammatory neurological diseases. *Neurology*. 2000;55(12):1828–1832. doi:10.1212/WNL.55.12.1828
- Mitrović A, Mirković B, Sosić I, Gobec S, Kos J. Inhibition of endopeptidase and exopeptidase activity of cathepsin B impairs extracellular matrix degradation and tumour invasion. *Biol Chem*. 2016;397(2):165–174. doi:10.1515/hsz-2015-0236
- Abdulla MH, Valli-Mohammed MA, Al-Khayal K, et al. Cathepsin B expression in colorectal cancer in a Middle East population: Potential value as a tumor biomarker for late disease stages. *Oncol Rep*. 2017. doi:10.3892/or.2017.5576
- Bian B, Mongrain S, Cagnol S, et al. Cathepsin B promotes colorectal tumorigenesis, cell invasion, and metastasis. *Mol Carcinog*. 2016;55(5):671–687. doi:10.1002/mc.22312
- Hazen LGM, Bleeker FE, Lauritzen B, et al. Comparative localization of cathepsin B protein and activity in colorectal cancer. *J Histochem Cytochem*. 2000;48(10):1421–1430. doi:10.1177/002215540004801012
- Campo E, Muñoz J, Miquel R, et al. Cathepsin B expression in colorectal carcinomas correlates with tumor progression and shortened patient survival. *Am J Pathol*. 1994;145(2):301–309.
- Hirano T, Manabe T, Takeuchi S. Serum cathepsin B levels and urinary excretion of cathepsin B in the cancer patients with remote metastasis. *Cancer Lett*. 1993;70(1):41–44. doi:10.1016/0304-3835(93)90072-H
- Hirai K, Yokoyama M, Asano G, Tanaka S. Expression of cathepsin B and cystatin C in human colorectal cancer. *Hum Pathol*. 1999;30(6):680–686. doi:10.1016/S0046-8177(99)90094-1
- Van Noorden CJF, Jonges TGN, Van Marle J, et al. Heterogeneous suppression of experimentally induced colon cancer metastasis in rat liver lobes by inhibition of extracellular cathepsin B. *Clin Exp Metastasis*. 1998;16(2):159–167. doi:10.1023/A:1006524321335
- Frlan R, Gobec S. Inhibitors of cathepsin B. *Curr Med Chem*. 2006;13(19):2309–2327. doi:10.2174/092986706777935122
- Birsoy K, Wang T, Possemato R, et al. MCT1-mediated transport of a toxic molecule is an effective strategy for targeting glycolytic tumors. *Nat Genet*. 2013;45(1):104–108. doi:10.1038/ng.2471
- Cardaci S, Desideri E, Ciriolo MR. Targeting aerobic glycolysis: 3-bromopyruvate as a promising anticancer drug. *J Bioenerg Biomembr*. 2012;44(1):17–29. doi:10.1007/s10863-012-9422-7
- Shoshan MC. 3-bromopyruvate: Targets and outcomes. *J Bioenerg Biomembr*. 2012;44(1):7–15. doi:10.1007/s10863-012-9419-2
- El Sayed SM, Mohamed WG, Hassan Seddik MA, et al. Safety and outcome of treatment of metastatic melanoma using 3-bromopyruvate: A concise literature review and case study. *Chin J Cancer*. 2014;33(7):356–364. doi:10.5732/cjc.013.10111
- Ko YH, Verhoeven HA, Lee MJ, Corbin DJ, Vogl TJ, Pedersen PL. A translational study “case report” on the small molecule “energy blocker” 3-bromopyruvate (3BP) as a potent anticancer agent: From bench side to bedside. *J Bioenerg Biomembr*. 2012;44(1):163–170. doi:10.1007/s10863-012-9417-4
- Hulkower KI, Butler CC, Linebaugh BE, et al. Fluorescent microplate assay for cancer cell-associated cathepsin B. *Eur J Biochem*. 2000;267(13):4165–4170. doi:10.1046/j.1432-1327.2000.01458.x
- Barrett AJ. Fluorimetric assays for cathepsin B and cathepsin H with methylcoumarylamide substrates. *Biochem J*. 1980;187(3):909–912. doi:10.1042/bj1870909
- Klose A, Zigrino P, Denhoyer R, Mauch C, Hunzelmann N. Identification and discrimination of extracellularly active cathepsins B and L in high-invasive melanoma cells. *Anal Biochem*. 2006;353(1):57–62. doi:10.1016/j.ab.2006.01.037
- Lea MA, Qureshi MS, Buxhoeveden M, Gengel N, Kleinschmit J, Desbordes C. Regulation of the proliferation of colon cancer cells by compounds that affect glycolysis, including 3-bromopyruvate, 2-deoxyglucose and biguanides. *Anticancer Res*. 2013;33(2):401–407.
- Cavallo-Medved D, Rudy D, Blum G, Bogyo M, Caglic D, Sloane BF. Live-cell imaging demonstrates extracellular matrix degradation in association with active cathepsin B in caveolae of endothelial cells during tube formation. *Exp Cell Res*. 2009;315(7):1234–1246. doi:10.1016/j.yexcr.2009.01.021
- Glick M, Biddle P, Jantzi J, Weaver S, Schirch D. The antitumor agent 3-bromopyruvate has a short half-life at physiological conditions. *Biochem Biophys Res Commun*. 2014;452(1):170–173. doi:10.1016/j.bbrc.2014.08.066
- Ho N, Morrison J, Silva A, Coomber BL. The effect of 3-bromopyruvate on human colorectal cancer cells is dependent on glucose concentration but not hexokinase II expression. *Biosci Rep*. 2016;36(1):e00299. doi:10.1042/BSR20150267
- Kim AD, Zhang R, Han X, et al. Involvement of glutathione and glutathione metabolizing enzymes in human colorectal cancer cell lines and tissues. *Mol Med Rep*. 2015;12(3):4314–4319. doi:10.3892/mmr.2015.3902
- Qin JZ, Xin H, Nickoloff BJ. 3-bromopyruvate induces necrotic cell death in sensitive melanoma cell lines. *Biochem Biophys Res Commun*. 2010;396(2):495–500. doi:10.1016/j.bbrc.2010.04.126
- Kim JS, Ahn KJ, Kim JA, et al. Role of reactive oxygen species-mediated mitochondrial dysregulation in 3-bromopyruvate induced cell death in hepatoma cells: RROS-mediated cell death by 3-BrPA. *J Bioenerg Biomembr*. 2008;40(6):607–618. doi:10.1007/s10863-008-9188-0
- El Sayed SM, El-Magd RMA, Shishido Y, et al. 3-bromopyruvate antagonizes effects of lactate and pyruvate, synergizes with citrate and exerts novel anti-glioma effects. *J Bioenerg Biomembr*. 2012;44(1):61–79. doi:10.1007/s10863-012-9409-4
- Xu DQ, Tan XY, Zhang BW, et al. 3-bromopyruvate inhibits cell proliferation and induces apoptosis in CD133+ population in human glioma. *Tumor Biol*. 2016;37(3):3543–3548. doi:10.1007/s13277-015-3884-2
- Tomizawa M, Shinozaki F, Motoyoshi Y, Sugiyama T, Yamamoto S, Ishige N. Suppressive effects of 3-bromopyruvate on the proliferation and the motility of hepatocellular carcinoma cells. *Oncol Rep*. 2016;35(1):59–63. doi:10.3892/or.2015.4370
- Kezdior M, Sereďyński R, Godzik U, et al. Inhibition of cathepsin B activity by 2,3,7,8-tetrachlorodibenzo-p-dioxin. *Environ Sci Pollut Res*. 2015;22(1):721–732. doi:10.1007/s11356-014-3482-7





# Effect of matrine on JAK2/STAT3 signaling pathway and brain protection in rats with cerebral ischemia-reperfusion

Jixing Chen<sup>1,A–D</sup>, Cuiqin Huang<sup>2,B,C</sup>, Lichao Ye<sup>1,D</sup>, Boxin Yao<sup>1,E</sup>, Meili Yang<sup>1,E</sup>, Qiankun Cai<sup>1,E</sup>

<sup>1</sup> Department of Neurology, The Second Affiliated Hospital of Fujian Medical University, Quanzhou, China

<sup>2</sup> Department of Neurology, Quanzhou Hospital of Traditional Chinese Medicine, China

A – research concept and design; B – collection and/or assembly of data; C – data analysis and interpretation; D – writing the article; E – critical revision of the article; F – final approval of the article

Advances in Clinical and Experimental Medicine, ISSN 1899–5276 (print), ISSN 2451–2680 (online)

*Adv Clin Exp Med.* 2020;29(8):959–966

## Address for correspondence

Jixing Chen

E-mail: chenjixing08djf@163.com

## Funding sources

This work was supported by the Project of the Science and Technology Bureau of Quanzhou for Effect of early tirofiban administration on cerebral blood perfusion and endothelial function in Acute Ischemic Stroke patients treated with mechanical thrombectomy (grant No. 2017Z003).

## Conflict of interest

None declared

Received on December 1, 2019

Reviewed on April 14, 2020

Accepted on June 2, 2020

Published online on August 21, 2020

## Abstract

**Background.** Ischemic encephalopathy is a common clinical disease. The main treatment goal is to achieve vascular recanalization. However, after vascular recanalization, the reperfusion of fresh blood can change local cell metabolism, thus adversely affecting cell structure and function, which can result in reperfusion injury.

**Objectives.** To explore the effect of matrine intervention of different concentrations on JAK2/STAT3 signaling pathway and brain protection in rats with cerebral ischemia-reperfusion.

**Material and methods.** Healthy male Sprague Dawley rats were divided into a blank control group (20 rats), a model group (80 rats) and a sham group (20 rats). In the model group, the middle cerebral artery was occluded with suture method to establish cerebral ischemia-reperfusion model rats, which were subdivided into cerebral ischemia-reperfusion group, and 5, 10 and 20 mg/kg matrine groups, with 20 rats in each group. Indicators including neurological function score, brain infarct size, brain water content, lactic dehydrogenase activity, protein expressions of p-JAK2 and p-STAT3, as well as superoxide dismutase activity and malondialdehyde content were evaluated.

**Results.** Compared with cerebral ischemia-reperfusion group, all the indicators were significantly improved in the 3 matrine treatment groups in a dose-dependent manner, and protein expressions of p-JAK2 and p-STAT3 in the brain tissue and brain cell apoptosis rate were decreased with the increase of matrine concentration (all  $p < 0.05$ ).

**Conclusions.** Matrine can significantly ameliorate the neurological function and brain edema of rats with cerebral ischemia-reperfusion, and improve superoxide dismutase, malondialdehyde and lactic dehydrogenase levels in the brain tissue and brain cell apoptosis rate. The mechanism of matrine may be related to the inhibition of abnormal JAK2/STAT3 signaling pathway activation.

**Key words:** ischemia-reperfusion injury, motor function, JAK2/STAT3 signaling pathway, neurological function, matrine cerebral

## Cite as

Chen J, Huang C, Ye L, Yao B, Yang M, Cai Q. Effect of matrine on JAK2/STAT3 signaling pathway and brain protection in rats with cerebral ischemia-reperfusion. *Adv Clin Exp Med.* 2020;29(8):959–966. doi:10.17219/acem/123352

## DOI

10.17219/acem/123352

## Copyright

© 2020 by Wrocław Medical University

This is an article distributed under the terms of the Creative Commons Attribution 3.0 Unported (CC BY 3.0) (<https://creativecommons.org/licenses/by/3.0/>)

## Introduction

Reperfusion injury is common in ischemic encephalopathy.<sup>1,2</sup> After the occurrence of cerebral ischemia-reperfusion, brain cells will gradually die in the form of apoptosis; the occurrence of cerebral ischemia-reperfusion also leads to neuron necrosis and neurological deficit.<sup>3,4</sup>

Matrine is a kind of monomeric compound extracted from *Sophora flavescens*, a legume plant. It not only has anti-tumor and anti-oxidation effect, but also protects the cardiocerebral vascular system from injuries to some extent.<sup>5,6</sup> A previous study in rats has revealed that matrine can suppress myocardial injury induced by septic shock by inhibiting JAK2/STAT3 signaling pathway activation.<sup>7</sup> As for the effect of matrine on cerebral ischemia-reperfusion, some studies suggested that matrine could exert a protective effect on neurons of rats with cerebral ischemia-reperfusion by activating cannabinoid receptor type 2.<sup>8</sup>

Janus kinase – signal transducer and activator transcription (JAK/STAT) signaling pathway is closely related to the occurrence of cerebral ischemia-reperfusion injury.<sup>9</sup> A recent study has shown that the inhibition of JAK2/STAT3 signaling pathway activation can inhibit neuron apoptosis, thereby alleviating cerebral ischemia-reperfusion injury.<sup>10</sup> However, there is no report on whether matrine could protect brain damage through JAK2/STAT3 signaling pathway in cerebral ischemia-reperfusion rat models.

Therefore, to further explore the neuroprotective effect of matrine in cerebral ischemia-reperfusion and its potential regulatory mechanism, we investigated the effect of different concentrations of matrine on JAK2/STAT3 signaling pathway in cerebral ischemia-reperfusion rat models.

## Material and methods

### Animals and material

A total of 120 healthy male SD rats, aged 8 weeks and weighed 170.68 ± 7.39 g, were obtained from the Laboratory Animal Center of Hebei Medical University (certificate No. 712065). Rats were housed in a plastic case with bedding on the solid bottom at a constant temperature of 22°C and a relative humidity of 50~65% in a normal day and night circle of 12/12 h. Rats were provided free access to food and water. The operation in the modeling process conformed to the standards of the Experimental Animal Ethics Committee of our hospital, by which this study was approved.

Matrine was purchased from the Ningxia Zijinhua Pharmaceutical Co., Ltd., Wuzhong, China (batch No. 90161019; purity ≥ 99%). The 0.9% sodium chloride injection was purchased from the Hunan Kelun Pharmaceutical Co., Ltd., Chengdu, China (batch No. 2A16030602). TUNEL apoptosis detection kit was purchased from the Wuhan Boster

Biological Technology Co., Ltd., Wuhan, China (batch No. BAO621). Primary antibodies JAK2, p-JAK2, STAT3, p-STAT3 and β-actin were purchased from the Shanghai Anyan Trade Co., Ltd., Shanghai, China. Goat anti-rabbit secondary antibody was purchased from the Abcam (Shanghai, China) Trade Co., Ltd., China (1:2,000, batch No. ab6721). Paraffin embedding center and rotary microtome were purchased from the Leica Biosystems Inc., Wetzlar, Germany. Optical microscope and microscope imaging analysis system were purchased from the Olympus Optical Co., Ltd., Tokyo, Japan. Lactic dehydrogenase (LDH), superoxide dismutase (SOD) and malondialdehyde (MDA) detection kits were purchased from the Wuhan MSK Biotechnology Co., Ltd., Wuhan, China.

### Modeling

Rats were divided into a model group (80 rats), a sham group (20 rats) and a blank control group (20 rats). Rats in the blank control group were fed routinely without intervention. Rats in the model group were used to establish the model of cerebral ischemia-reperfusion. The specific modeling process was as follows. Rats were firstly anesthetized with 3 mL/kg 10% chloral hydrate. Then, the anesthetized rats were fixed on the operating table in the supine position. After routine skin preparation and disinfection, the skin was cut open lengthways through the middle of the neck, and the common carotid artery, external carotid artery and internal carotid artery were separated. Then, the common carotid artery and internal carotid artery were occluded using silk sutures. A small incision was cut on the wall of the external carotid artery at 3 mm from the arterial intersection. A nylon thread was inserted into the incision and pushed slowly towards the internal carotid artery until encountering resistance at a push-in depth of about 20 mm. At this moment, the nylon thread reached into the anterior cerebral artery and blocked the blood supply to the middle cerebral artery. Then, the external carotid artery was tightened, and the skin was sutured. Two hours later, the nylon thread was pulled outwards to the external carotid artery to develop cerebral ischemia-reperfusion. After the rats were revived, they were sent back to the cage for continuous feeding. Rats that walked towards the contralateral side or circled to their tails after operation indicated successful modeling. In the sham group, the artery of the rat was separated only without subsequent artery ligation, nylon thread insertion, etc., and other procedures, such as skin suture, were the same as in the model group.

Rats in the model group were subdivided into cerebral ischemia-reperfusion group, 5 mg/kg matrine group, 10 mg/kg matrine group, and 20 mg/kg matrine group, with 20 rats in each group. In the 3 matrine groups, matrine solutions (concentrations of 5 mg/kg, 10 mg/kg and 20 mg/kg) were intraperitoneally injected into the rats

30 min before ischemia and 2 h after ischemia.<sup>11</sup> Rats in the cerebral ischemia-reperfusion group, the sham group and the blank control group were intraperitoneally injected with the same amount of normal saline at same time points.

## Neurological function scoring

Neurological function was scored by Longa method 24 h after operation.<sup>12</sup> Detailed scoring rules were as follows: no neurological function deficit was scored as 0; mild neurological function deficit (contralateral fore limbs could not be fully outstretched) was scored as 1; moderate neurological function deficit (rats circled to the contralateral side) was scored as 2; severe neurological function deficit (rats toppled towards the contralateral side) was scored as 3; the symptom that rats could not walk and had clouding of consciousness was scored as 4.

## Brain infarct size calculation

After neurological function evaluation, 5 rats were randomly selected and euthanatized by cervical dislocation. The brain tissue was taken out and frozen in a refrigerator at  $-20^{\circ}\text{C}$  for 10 min. The infarct area was cut into sections from the coronal plane of anterior and posterior optic chiasma, with a thickness of 2 mm. Serial sections were incubated away from light in 1% 2,3,5-triphenyl-tetrazolium chloride (TTC) solution at  $37^{\circ}\text{C}$  for 20 min. The percentage of brain infarct size was calculated. Percentage of brain infarct size (%) = brain infarct size/total size of brain infarct section \* 100%.

## Detection of brain water content

Five rats in each group were randomly selected and sacrificed. Wet weight of the brain was weighed after removal of the olfactory bulb, cerebellum and lower brain stem. Then the brain was baked at  $108^{\circ}\text{C}$  for 72 h. Dry weight of the brain was weighed. Brain water content (%) = (wet weight – dry weight)/wet weight \* 100%.

## Detection of SOD activity, MDA content and LDH activity in the brain tissue

Five rats were randomly selected and sacrificed 24 h after model establishment. A part of the brain tissue was taken out and ground. The ground brain tissues were put into a test tube with the addition of 25% trypsin and incubated in a water bath at  $37^{\circ}\text{C}$ . After digestion, the solution was blown with a pipette to be homogeneous and centrifuged at 1,000 r/min for 5 min. The supernatant was collected and washed with phosphate-buffered saline (PBS) to prepare tissue suspension. LDH activity, SOD activity and MDA content in the brain tissue were measured with chemical colorimetry method, xanthine oxidase method and thiobarbituric acid method, respectively.

## Detection of brain cell apoptosis rate with TUNEL method

Additional 5 rats were randomly selected. The brain infarct area was cut into sections to prepare specimens. Proteins of the brain tissue were digested at room temperature with 20  $\mu\text{g}/\text{mL}$  protease K and rinsed 4 times with distilled water. Then, the section was incubated with TUNEL reaction mixture for 50 min and incubated with anti-fluorescein-dUTP. 3'-diaminobenzidine (DAB) coloration was performed. Five different visual fields on the infarct area were randomly selected under a light microscope to observe and count apoptotic cells. The brownish yellow showed positive apoptotic cells. Apoptosis rate (%) = number of apoptotic cells/total number of cells \* 100%.

## Detection of JAK2, p-JAK2, STAT3, and p-STAT3 protein expressions measured with western blot

Partial tissue suspension prepared during the detection of SOD activity, MDA content and LDH activity in the brain tissue was lysed with RIPA lysis buffer and mixed on the ice. The mixture was centrifuged at 1,300 r/min for 10 min. Then, the proteins were separated using 10% SDS-PAGE and transferred to polyvinylidene difluoride (PVDF) membranes. The membrane was sealed with 5% skim milk overnight at  $4^{\circ}\text{C}$ . Then the membrane was incubated with primary antibodies JAK2 (1:1,000), p-JAK2 (1:1,000), STAT3 (1:1,000), p-STAT3 (1:1,000), and  $\beta$ -actin (1:1,000) overnight at  $4^{\circ}\text{C}$  and horseradish peroxidase (HRP)-labeled goat anti-rabbit immunoglobulin (2<sup>nd</sup> antibody, 1:1,200) at room temperature for 1 h. The membrane was rinsed with PBS and color development was carried out using ECL developer. The results were expressed as gray value of the target band/gray value of the internal reference.

## Statistical analysis

SPSS v. 19.0 software (IBM Corp., Armonk, USA) was adopted to analyze the collected data. The measurement data was expressed as mean  $\pm$  standard deviation (SD). Comparison among groups was performed with one-way analysis of variance (ANOVA) followed by post hoc pairwise comparison using Least Significant Difference (LSD)/t test. A  $p < 0.05$  indicated that the difference was statistically significant.

## Results

### Neurological function scores

Neurological function scores at 24 h after operation in the blank control group, the sham group, the cerebral ischemia-reperfusion group, the 5 mg/kg matrine group,

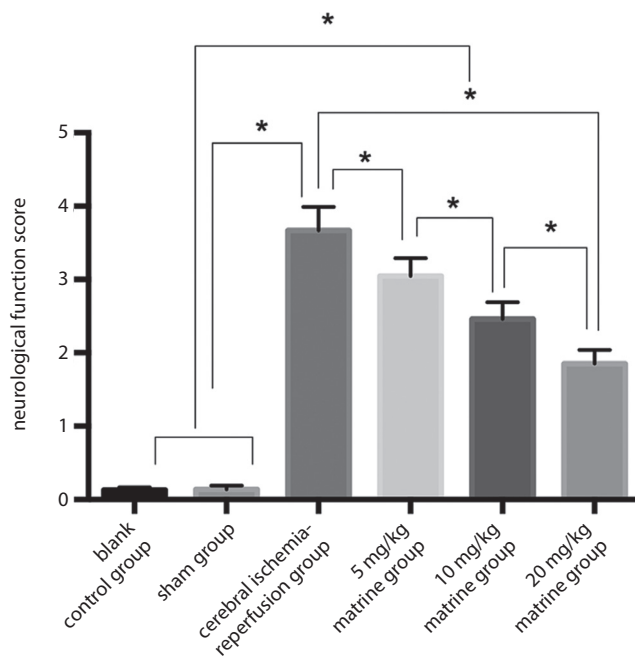
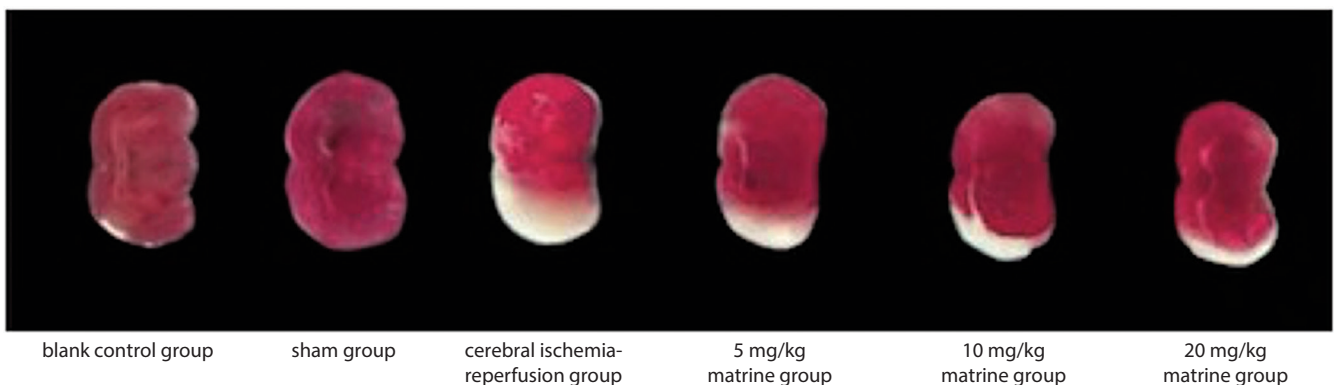


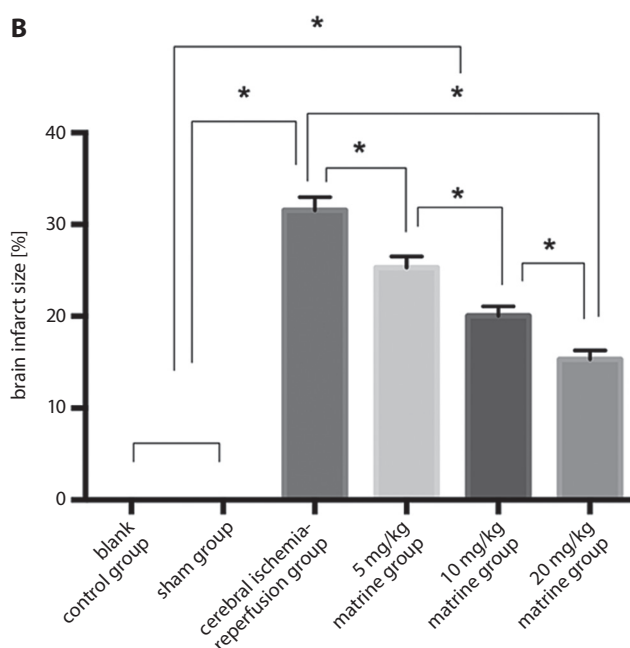
Fig. 1. Neurological function score

\* $p < 0.05$ .

A



B



the 10 mg/kg matrine group, and the 20 mg/kg matrine group were  $0.13 \pm 0.04$ ,  $0.14 \pm 0.05$ ,  $3.67 \pm 0.32$ ,  $3.05 \pm 0.24$ ,  $2.46 \pm 0.23$ , and  $1.85 \pm 0.19$  scores, respectively; there were no significant differences in neurological function scores between the blank control group and the sham group ( $p > 0.05$ ). Neurological function scores in cerebral ischemia-reperfusion group were significantly higher than those in the sham group, the blank control group, the 5 mg/kg matrine group, the 10 mg/kg matrine group, and the 20 mg/kg matrine group. Neurological function scores were the highest in the 5 mg/kg matrine group, followed by the 10 mg/kg matrine group and the 20 mg/kg matrine group (all  $p < 0.05$ , Fig. 1).

### Brain infarct size

Brain infarct size at 24 h after operation in the blank control group, the sham group, the cerebral ischemia-reperfusion group, the 5 mg/kg matrine group, the 10 mg/kg matrine group and the 20 mg/kg matrine group was 0%, 0%,  $(31.54 \pm 1.45)\%$ ,  $(25.32 \pm 1.21)\%$ ,  $(20.06 \pm 1.02)\%$ , and  $(15.33 \pm 0.97)\%$ , respectively. Brain infarct size in cere-

Fig. 2. Brain infarct size

A – picture of brain infarct; B – brain infarct size comparison; \* $p < 0.05$ .

bral ischemia-reperfusion group was significantly larger than that in the sham group, the blank control group, the 5 mg/kg matrine group, the 10 mg/kg matrine group, and the 20 mg/kg matrine group. Rats in the 20 mg/kg matrine group had the smallest brain infarct size, followed by the 10 mg/kg matrine group and the 5 mg/kg matrine group (all  $p < 0.05$ , Fig. 2).

### Brain water content

Brain water content at 24 h after operation in the blank control group, the sham group, cerebral ischemia-reperfusion group, the 5 mg/kg matrine group, the 10 mg/kg matrine group, and the 20 mg/kg matrine



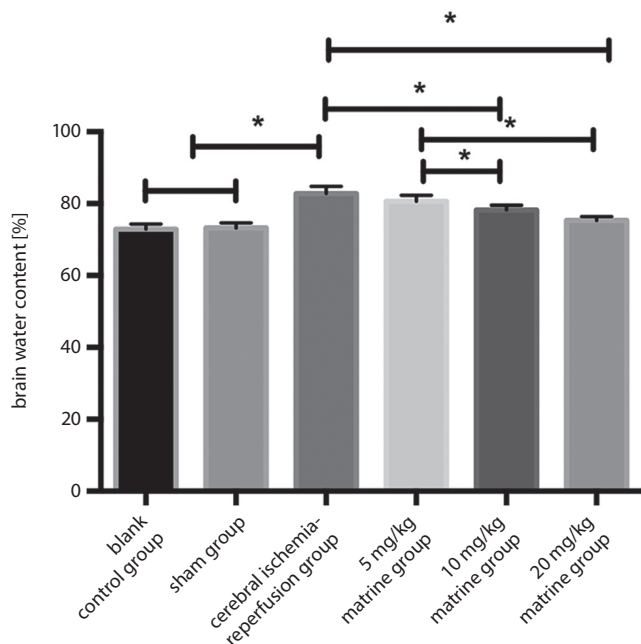


**Fig. 3.** Brain water content. Brain water content in cerebral ischemia-reperfusion group was significantly higher than that in sham group, blank control group, 10 mg/kg matrine group, and 20 mg/kg matrine group. Brain water content in 5 mg/kg matrine group was significantly higher than that in 10 mg/kg matrine group and 20 mg/kg matrine group

group was (72.87 ± 1.39)%, (73.21 ± 1.42)%, (82.76 ± 2.03)%, (80.64 ± 1.66)%, (78.21 ± 1.34)%, and (75.26 ± 1.15)%, respectively; brain water content at 24 h after operation in the cerebral ischemia-reperfusion group was significantly higher than that in the sham group and the blank control group (both  $p < 0.05$ ). Brain water content of rats treated with matrine was reduced in dose-dependent manner; brain water content in the 10 mg/kg matrine group and the 20 mg/kg matrine group was significantly lower than that in the cerebral ischemia-reperfusion group (both  $p < 0.05$ , Fig. 3).

### SOD, MDA and LDH levels in the brain tissue

Rats in the sham group had significantly lower MDA and LDH levels and higher SOD level than cerebral ischemia-reperfusion group (all  $p < 0.05$ ). Compared with cerebral ischemia-reperfusion group, SOD, MDA and LDH levels in the 5 mg/kg matrine group, the 10 mg/kg matrine group and the 20 mg/kg matrine group were significantly improved, and the improvement was more significant with the increase of matrine concentration (all  $p < 0.05$ , Table 1).

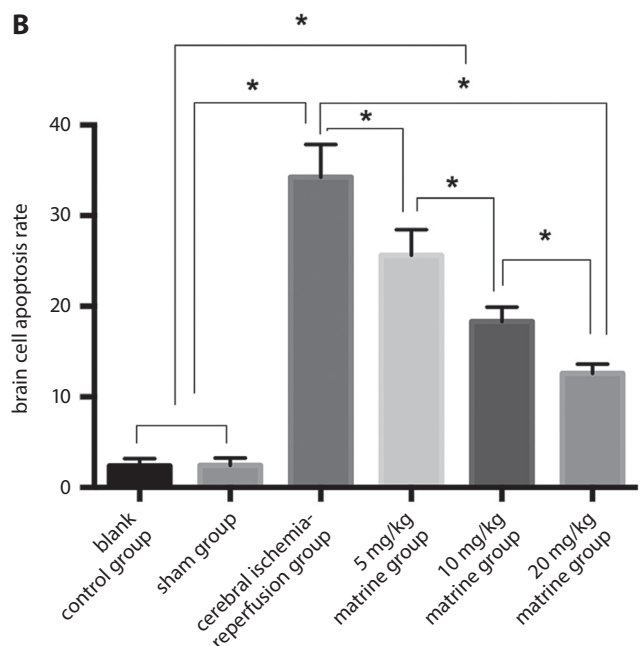
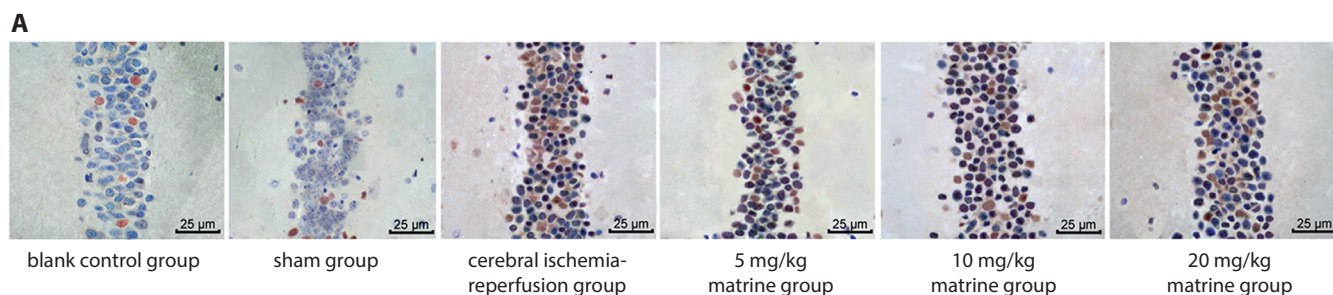


**Fig. 4.** Brain cell apoptosis rate

A – brain cell apoptosis diagram using TUNEL; B – histogram of brain cell apoptosis rate; \* $p < 0.05$ .

### Brain cell apoptosis rate

Brain cell apoptosis rate at 24 h after operation in the blank control group, the sham group, the cerebral ischemia-reperfusion group, the 5 mg/kg matrine group, the 10 mg/kg matrine group, and the 20 mg/kg matrine group was (2.39 ± 0.78)%, (2.45 ± 0.81)%, (34.26 ± 3.59)%, (25.61 ± 2.85)%, (18.33 ± 1.59)%, and (12.57 ± 1.04)%, respectively. Brain cell apoptosis rate in cerebral ischemia-reperfusion group was significantly higher than in the sham group, the blank control group, the 5 mg/kg matrine group, the 10 mg/kg matrine group, and the 20 mg/kg matrine group. Rats in the 20 mg/kg matrine group had the lowest brain cell apoptosis rate, followed by the 10 mg/kg matrine group and the 5 mg/kg matrine group (all  $p < 0.05$ , Fig. 4).

\* $p < 0.05$ .

**Table 1.** SOD, MDA and LDH levels in the brain tissue

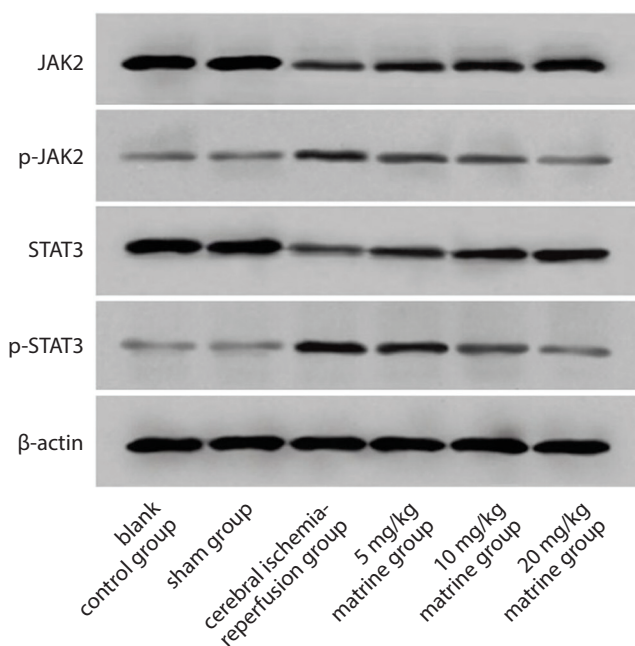
Variable	SOD [U/mg]	MDA [nmol/mg]	LDH [U/mg]
Blank control group (n = 5)	91.65 ±18.97	0.82 ±0.11	2210.957 ±273.65
Sham group (n = 5)	91.76 ±19.33	0.84 ±0.12	2215.97 ±276.81
Cerebral ischemia-reperfusion group (n = 5)	41.27 ±14.65*#	1.79 ±0.35*#	7268.25 ±341.63*#
5 mg/kg matrine group (n = 5)	61.32 ±12.48*#&	1.48 ±0.29*#&	6738.46 ±295.68*#&
10 mg/kg matrine group (n = 5)	69.79 ±13.39*#&@	1.26 ±0.23*#&@	4395.77 ±285.35*#&@
20 mg/kg matrine group (n = 5)	78.86 ±12.28*#&@ <sup>§</sup>	1.09 ±0.13*#&@ <sup>§</sup>	3859.45 ±288.86*#&@ <sup>§</sup>
F	7.89	14.17	271.3
p-value	<0.001	<0.001	<0.001

SOD – superoxide dismutase; MDA – malondialdehyde; LDH – lactic dehydrogenase; \*p < 0.05 – compared with blank control group; #p < 0.05 – compared with sham group; &p < 0.05 – compared with cerebral ischemia-reperfusion group; @p < 0.05 – compared with 5 mg/kg matrine group; §p < 0.05 – compared with 10 mg/kg matrine group.

**Table 2.** JAK2, STAT3, p-JAK2, and p-STAT3 protein expressions in the brain tissue

Variable	JAK2	STAT3	p-JAK2	p-STAT3
Blank control group (n = 5)	1.15 ±0.13	1.13 ±0.12	0.20 ±0.08	0.12 ±0.03
Sham group (n = 5)	1.14 ±0.12	1.12 ±0.10	0.21 ±0.09	0.13 ±0.02
Cerebral ischemia-reperfusion group (n = 5)	0.38 ±0.07*#	0.29 ±0.04*#	0.41 ±0.06*#	0.60 ±0.09*#
5 mg/kg matrine group (n = 5)	0.45 ±0.05*#&	0.41 ±0.06*#&	0.35 ±0.08*#&	0.47 ±0.06*#&
10 mg/kg matrine group (n = 5)	0.58 ±0.06*#&@	0.57 ±0.06*#&@	0.29 ±0.07*#&@	0.34 ±0.05*#&@
20 mg/kg matrine group (n = 5)	0.71 ±0.07*#&@	0.69 ±0.07*#&@ <sup>§</sup>	0.25 ±0.03*#&@ <sup>§</sup>	0.22 ±0.04*#&@ <sup>§</sup>
F	72.221	99.293	6.734	65.662
p-value	<0.001	<0.001	<0.001	<0.001

\*p < 0.05 – compared with blank control group; #p < 0.05 – compared with sham group; &p < 0.05 – compared with cerebral ischemia-reperfusion group; @p < 0.05 – compared with 5 mg/kg matrine group; §p < 0.05 – compared with 10 mg/kg matrine group.

**Fig. 5.** Protein bands in western blot

## Protein expressions of JAK2, p-JAK2, STAT3, and p-STAT3 in the brain tissue

Rats in the cerebral ischemia-reperfusion group had significantly greater p-JAK2 and p-STAT3 protein expressions and lower JAK2 and STAT3 protein expressions than the blank control group and the sham group (all  $p < 0.05$ ). In the 5 mg/kg matrine group, the 10 mg/kg matrine group and the 20 mg/kg matrine group, p-JAK2 and p-STAT3 protein expressions were significantly decreased, and JAK2 and STAT3 protein expressions were significantly elevated, compared with the cerebral ischemia-reperfusion group; p-JAK2 and p-STAT3 protein expressions dropped with the increase of matrine concentration, and JAK2 and STAT3 protein expressions ascended with the increase of matrine concentration (all  $p < 0.05$ , Table 2, Fig. 5).

## Discussion

In this study, cerebral ischemia-reperfusion rat models were established using suture method and matrine intervention was administrated to rats at different concentrations to explore the curative effect of matrine on cerebral

ischemia-reperfusion and its possible mechanism. The results of neurological function evaluation indicated that rats with cerebral ischemia-reperfusion suffered from significant neurological function deficit, while matrine could relieve cerebral ischemia-reperfusion injuries in rats.

Neurons are poorly tolerant to hypoxia ischemia. Therefore, cerebral ischemia-reperfusion causes neuron necrosis and further leads to neurological function deficit.<sup>13,14</sup> The results in this study found that matrine could improve neurological function deficit of rats with cerebral ischemia-reperfusion to some extent.

In addition, brain infarct size and brain water content of rats treated with matrine were lowered with the increase of matrine concentration, suggesting that cerebral ischemia-reperfusion in rats not only caused cerebral infarction, but also resulted in brain edema. Results of some studies indicated that matrine could decrease the degree of brain edema caused by middle cerebral artery occlusion in rats and effectively lessen brain infarct size of rats in cerebral infarction rat models,<sup>15,16</sup> which were consistent with the results of our study, indicating that matrine could reduce the degree of cerebral edema and cerebral infarction in rats with cerebral ischemia-reperfusion.

In addition, we found that matrine can increase the activity of SOD, reduce the content of MDA, improve energy metabolism, and inhibit the increase of LDH content and the apoptosis of nerve cells caused by brain injury. When cerebral ischemia-reperfusion occurs, uncoupling of oxidative phosphorylation takes place in the mitochondria, and a great number of free radicals are generated.<sup>17</sup> The SOD can catalyze and scavenge the disproportionated reaction of free radicals, while the change of MDA content can indirectly reflect the change of oxygen radicals; cerebral ischemia leads to the release of a large number of intracellular LDHs, which further induces brain cell damage.<sup>18,19</sup> After the occurrence of cerebral ischemia-reperfusion, the death procedure of brain cells is activated, mainly manifesting in neuron apoptosis.<sup>20,21</sup> These findings were in line with the results of our study, indicating that matrine can reduce the neuronal apoptosis of rats after cerebral ischemia and reperfusion to protect the rat brain tissue.

When cerebral ischemia-reperfusion occurs, the expressions of phosphorylated JAKs and STATs in the brain tissue are significantly increased.<sup>22,23</sup> The results in our study showed that the abnormal activation of JAK2/STAT3 signaling pathway and the phosphorylation of JAK2 and STAT3 proteins in model rats might play an important role in cerebral ischemia-reperfusion injuries. Besides, after matrine intervention, rats had decreased p-JAK2 and p-STAT3 protein expressions and increased JAK2 and STAT3 protein expressions in the brain tissue, and the decrease of p-JAK2 and p-STAT3 protein expressions was more significant with the increase of matrine concentration. A study reported that inhibiting the activation of JAK2/STAT3 signaling pathway could restrain the inflammatory response induced by cerebral ischemia-reperfusion injuries and

thereby lessen neuron apoptosis.<sup>24</sup> Therefore, we hypothesize that the neuroprotective effect of matrine on cerebral ischemia-reperfusion model rats might be exerted by the activation of JAK2/STAT3 signaling pathway and the inhibition of JAK2 and STAT3 protein phosphorylation. However, we have not explored other potential mechanisms in this study. Thus, our results remain to be further verified in the future.

## Conclusions

Matrine can significantly improve neurological function and brain edema of rats with cerebral ischemia-reperfusion and ameliorate SOD, MDA and LDH levels as well as apoptosis rate in the brain tissue by inhibiting abnormal activation of JAK2/STAT3 signaling pathway.

### ORCID iDs

Jixing Chen  <https://orcid.org/0000-0001-8073-9638>  
 Cuiqin Huang  <https://orcid.org/0000-0002-0676-2351>  
 Lichao Ye  <https://orcid.org/0000-0001-5748-1077>  
 Boxin Yao  <https://orcid.org/0000-0002-3634-5364>  
 Meili Yang  <https://orcid.org/0000-0002-9912-2774>  
 Qiankun Cai  <https://orcid.org/0000-0001-8725-1934>

### References

- Li Y, Liu S. The effect of dexmedetomidine on oxidative stress response following cerebral ischemia-reperfusion in rats and the expression of intracellular adhesion molecule-1 (ICAM-1) and S100B. *Med Sci Monit.* 2017;23:867–873.
- Che N, Ma Y, Xin Y. Protective role of fucoidan in cerebral ischemia-reperfusion injury through inhibition of MAPK signaling pathway. *Biomol Ther (Seoul).* 2017;25(3):272–278.
- Lu H, Wang B. SIRT1 exerts neuroprotective effects by attenuating cerebral ischemia/reperfusion-induced injury via targeting p53/microRNA-22. *Int J Mol Med.* 2017;39(1):208–216.
- Duan S, Wang T, Zhang J, et al. Huatuo Zaizao pill promotes functional recovery and neurogenesis after cerebral ischemia-reperfusion in rats. *BMC Complement Altern Med.* 2017;17:19.
- Chen L, Wang F, Han Z. Effects of matrine on inflammatory cytokines for rats with cerebral ischemia reperfusion injury. *Journal of Emergency in Traditional Chinese Medicine.* 2010;19:2098–2099.
- Meng FR, Wang YJ, Kong YM, Wang D, Chen C. Matrine alleviated incomplete cerebral ischemia-reperfusion injury in mice. *Journal of Liaoning University.* 2011;4:350–352.
- Zhang M, Wang X, Wang X, et al. Oxymatrine protects against myocardial injury via inhibition of JAK2/STAT3 signaling in rat septic shock. *Mol Med Rep.* 2013;7(4):1293–1299.
- Tang M, Dong Z, Cai JH, et al. Pharmacology DO. Neuroprotective effects of matrine by activating cannabinoid 2 receptor on focal cerebral ischemia-reperfusion injury in rats. *Chinese Journal of New Drugs & Clinical Remedies.* 2014;33:311–316.
- Hu GQ, Du X, Li YJ, Gao XQ, Chen BQ, Yu L. Inhibition of cerebral ischemia/reperfusion injury-induced apoptosis: Nicotiflorin and JAK2/STAT3 pathway. *Neural Regen Res.* 2017;12(1):96–102.
- Chang C, Zhao Y, Song G, She K. Resveratrol protects hippocampal neurons against cerebral ischemia-reperfusion injury via modulating JAK/ERK/STAT signaling pathway in rats. *J Neuroimmunol.* 2018;315:9–14.
- Li P, Lei J, Hu G, Chen X, Liu Z, Yang J. Matrine mediates inflammatory response via gut microbiota in TNBS-induced murine colitis. *Front Physiol.* 2019;10:28.
- Liu YZ, Wang C, Wang Q, et al. Role of fractalkine/CX3CR1 signaling pathway in the recovery of neurological function after early ischemic stroke in a rat model. *Life Sci.* 2017;184:87–94.

13. Singh V, Krishan P, Shri R. Improvement of memory and neurological deficit with *Ocimum basilicum* L. extract after ischemia reperfusion induced cerebral injury in mice. *Metab Brain Dis*. 2018;33(4):1111–1120.
14. Min L, Xiangjian Z, Lili C, et al. The neuroprotection of oxymatrine in cerebral ischemia/reperfusion is related to nuclear factor erythroid 2-related factor 2 (nrf2)-mediated antioxidant response: Role of nrf2 and hemeoxygenase-1 expression. *Biol Pharm Bull*. 2011;34(5):595–601.
15. Hu ZL, Tan YX, Zhang JP, Qian DH. Effects of inhibitor of protein kinase C on brain edema formation evoked by experimental cerebral ischemia in gerbils and rats. *Acta Pharmaceutica Sinica*. 1996;31:886.
16. Liu Z, He D, Zhang X, et al. Neuroprotective effect of early and short-time applying sophoridine in pMCAO rat brain: Down-regulated TRAF6 and up-regulated p-ERK1/2 expression, ameliorated brain infarction and edema. *Brain Res Bull*. 2012;88(4):379–384.
17. Wang SY, Xiao-Jiang W, Jin WZ, Tong CL, Yao LI. Effect of ginkgo biloba extract on SOD activity of and MDA level after cerebral ischemia reperfusion in rat [in Chinese]. *Heilongjiang Medicine and Pharmacy*. 2004;27(6):29.
18. Wang XY, Zhang YY, Wan HT, et al. Protective effect of Shenxiong injection on cerebral ischemia/reperfusion injury of rats. *China J Chin Mater Med*. 2014;39:503–506.
19. Jiang CP, Liu F, Yi LI, et al. Effect of Shenfu injection on MDA, SOD, TXB<sub>2</sub> and 6-keto-PGF<sub>1α</sub> after cerebral ischemia/reperfusion injury in rats. *J China Med Univ*. 2012;41:124–127.
20. Gao XJ, Xie GN, Liu L, Fu ZJ, Zhang ZW, Teng LZ. Sesamol attenuates oxidative stress, apoptosis and inflammation in focal cerebral ischemia/reperfusion injury. *Exp Ther Med*. 2017;14(1):841–847.
21. Zhao P, Zhou RU, Zhu XY, et al. Matrine attenuates focal cerebral ischemic injury by improving antioxidant activity and inhibiting apoptosis in mice. *Int J Mol Med*. 2015;36(3):633–644.
22. Zhu H, Zou L, Tian J, Du G, Gao Y. SMND-309, a novel derivative of salvianolic acid B, protects rat brains ischemia and reperfusion injury by targeting the JAK2/STAT3 pathway. *Eur J Pharmacol*. 2013;714(1–3):23–31.
23. Xie HF, Ru-Xiang XU, Wei JP, Jiang XD. P-JAK2 and p-STAT3 protein expression and cell apoptosis following focal cerebral ischemia-reperfusion injury in rats [in Chinese]. *Nan Fang Yi Ke Da Xue Xue Bao*. 2007;27(2):208–211,218.
24. Li L, Li H, Li M. Curcumin protects against cerebral ischemia-reperfusion injury by activating JAK2/STAT3 signaling pathway in rats. *Int J Clin Exp Med*. 2015;8(9):14985.

# The application of the percutaneous suturing technique in thoracoscopic repair of congenital diaphragmatic hernia

Bartosz Bogusz<sup>1,A–D,F</sup>, Adam Mol<sup>1,B,C,E</sup>, Oskar Zgraj<sup>2,A,D,E</sup>, Wojciech Górecki<sup>3,B,E,F</sup>

<sup>1</sup> Department of Pediatric Surgery, University Children's Hospital, Jagiellonian University Medical College, Kraków, Poland

<sup>2</sup> Department of Pediatric Surgery, St. Luke Regional Hospital, Tarnów, Poland

<sup>3</sup> Department of Pediatric Surgery, University Children's Hospital, Jagiellonian University Medical College, Kraków, Poland

A – research concept and design; B – collection and/or assembly of data; C – data analysis and interpretation;

D – writing the article; E – critical revision of the article; F – final approval of the article

Advances in Clinical and Experimental Medicine, ISSN 1899–5276 (print), ISSN 2451–2680 (online)

*Adv Clin Exp Med.* 2020;29(8):967–970

## Address for correspondence

Bartosz Bogusz

E-mail: [bjbart@poczta.onet.pl](mailto:bjbart@poczta.onet.pl)

## Funding sources

None declared

## Conflict of interest

None declared

Received on February 12, 2020

Reviewed on March 15, 2020

Accepted on May 14, 2020

Published online on September 1, 2020

## Abstract

**Background.** Thoracoscopic surgery of congenital diaphragmatic hernia (CDH) is connected with a higher incidence of recurrence than open repair is. This is usually caused by the dehiscence of sutures in the lateral part of the defect. This area is characterized by increased tension on proximate tissues and difficult thoracoscopic suturing. For more effective repair, the authors adopted a variant of percutaneous internal ring suturing (PIRS) technique.

**Objectives.** To present and evaluate the efficacy of the PIRS technique for the repair of CDH.

**Material and methods.** The study is based on retrospective analysis of the medical data of patients with CDH treated in the Department of Pediatric Surgery of the Jagiellonian University Medical College (Kraków, Poland) from January 2013 to July 2019. The PIRS technique was applied when thoracoscopic repair under acceptable tension appeared impossible.

**Results.** Fifty-one patients were identified. Of these, 11 children died before surgery and 1 after, leaving 39 (76%) who were operated on and survived. Thoracoscopy was used in 27 cases (69%), with 3 conversions. The recurrence rate in patients who underwent thoracoscopic closure of the defect with intermittent sutures was 27% (3 out of 11 children), while in the group that underwent thoracoscopic repair with the additional use of percutaneous suturing, the recurrence rate was 6.25% (1 out of 16 patients). The follow-up periods ranged from 4 months to 6 years.

**Conclusions.** The applied PIRS technique permits safe and effective closure of intermediate-size diaphragmatic defects under acceptable tension. The method is feasible and can be listed among countermeasures against recurrence.

**Key words:** hernia, congenital, thoracoscopy, diaphragmatic, suturing

## Cite as

Bogusz B, Mol A, Zgraj O, Górecki W. The application of the percutaneous suturing technique in thoracoscopic repair of congenital diaphragmatic hernia. *Adv Clin Exp Med.* 2020;29(8):967–970. doi:10.17219/acem/122396

## DOI

10.17219/acem/122396

## Copyright

© 2020 by Wrocław Medical University

This is an article distributed under the terms of the Creative Commons Attribution 3.0 Unported (CC BY 3.0) (<https://creativecommons.org/licenses/by/3.0/>)



## Introduction

The classical surgical approach to the repair of a congenital diaphragmatic hernia (CDH) is transverse subcostal laparotomy. The first case of successful laparoscopic repair of this pathology was reported in 1995,<sup>1</sup> while the thoracoscopic approach was first described in 2001.<sup>2</sup> Nowadays, thoracoscopic access presents a popular strategy of surgical treatment in children with CDH. However, numerous authors report a higher incidence of recurrence in patients with CDHs following thoracoscopic repair, as compared to open surgery.<sup>3,4</sup> Most of those complications result from the dehiscence of sutures within the most lateral part of the defect.

The pathology of CDH presents a wide spectrum of defects ranging from small, oval or cigar-shaped lesions to those involving over 90% of the hemi-diaphragm. In 2014, the Congenital Diaphragmatic Hernia Study Group (CDHSG) developed a staging system to describe the variability of diaphragmatic defects.<sup>5</sup> This system has been shown to correlate strongly with mortality in patients with CDH.<sup>6</sup> Depending on their size, diaphragmatic defects in CDH were divided into 4 groups (A–D). From the surgical perspective, the defects classified as groups C and D qualify for mesh repair. Small group A defects require a primary repair with interrupted sutures.

Patients classified as group B present with an intermediate-size defect. Intraoperatively, following the reduction of the viscera into the abdomen, these do not usually warrant a mesh repair. However, poor development of the posterior rim of the diaphragm and the resulting increased stretch of the approximated edges of the defect produce an increased risk of recurrence. Moreover, thoracoscopic suturing is usually less feasible in the costodiaphragmatic recess, which presents another important risk of suture line dehiscence. To cope with this problem, the authors decided to adopt a variant of the percutaneous internal ring suturing (PIRS) technique described by Patkowski et al.<sup>7</sup>

The aim of this study was to present the efficacy and feasibility of the PIRS technique in the treatment of CDH in children, with particular emphasis on avoiding hernia recurrence.

## Material and methods

A retrospective analysis was performed, reviewing the medical data of 51 patients with CDH treated between January 2013 and July 2019 in the Department of Pediatric Surgery at the University Children's Hospital of Jagiellonian University Medical College in Kraków (Poland).

The percutaneous method of suturing has been used in this department since January 2016, in cases when, in the surgeon's opinion, the completion of the thoracoscopic repair of the diaphragmatic defect with simple interrupted sutures was possible, but resulted in excessive

tension in the part adjacent to the chest wall. In these patients, the diaphragmatic defects were recognized as group B according to the CDHSG classification criteria.

## Surgical technique

Thoracoscopies were performed in the lateral decubitus position. Single-lung ventilation was not utilized. We prefer to use 3–5 mm ports. After the reduction of the herniated viscera, the size of the defect was evaluated and the course of action was determined. Defects qualifying as CDHSG groups C and D were repaired with mesh, employing thoracoscopic access or laparotomy. Small group A-type defects were repaired with interrupted 2.0 non-absorbable braided sutures after delineation and scarification of the edges. Intermediate-size group B defects were characterized by poor development or the complete absence of a significant portion of the postero-lateral diaphragmatic rim. Even after careful mobilization of this structure, there was excessive tension on the antero-medial margin of the diaphragm. This resulted in an increased risk of tearing the diaphragmatic muscle during its approximation to the hypoplastic postero-lateral edge and the chest wall. For these patients, the authors decided to adopt the PIRS technique developed by D. Patkowski for single port laparoscopic repair of an inguinal hernia.<sup>7</sup> The first step was the scarification of the pleura covering the selected rib and the free margin of the diaphragmatic flap. The medial part of the defect was repaired with interrupted non-absorbable braided 2.0 sutures. In the lateral part of the defect, where the postero-lateral edge of the diaphragm was hypoplastic or absent, a percutaneous suturing technique similar to the PIRS method was applied, in order to facilitate fixation and reduce tension on the suture line. The percutaneous suturing technique is presented in Fig. 1. We used non-absorbable braided 2-0 sutures, introduced through an 18G injection needle. The tip of the needle was slightly curved to facilitate its manipulation within tissues. The puncture sites on the skin were closed with strips, leaving almost no scar. A single skin incision was used to create up to 3 percutaneous sutures. One of the 2 puncture sites of each suture was above the selected rib, while the other was below it.

## Results

The retrospective analysis identified the medical records of 51 patients with CDH treated at our center. Of these, 11 died before surgical intervention and 1 died after surgery because of a generalized Gram-negative infection. Thirty-nine (76%) were operated on and survived. Thoracoscopy was applied in 27 of them (69%). In 3 children (13%), conversion to laparotomy was necessary because of the size of the defect and the need for mesh repair.

The recurrence rate in the group of patients operated on by thoracoscopic access was 15% (4 patients). There were

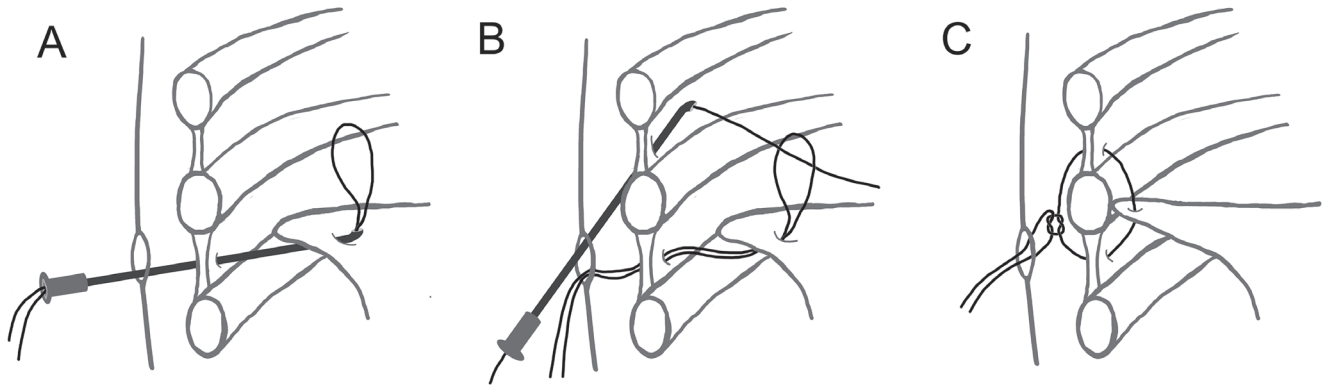


Fig. 1. Technique of percutaneous suturing in CDH, adopted from the PIRS method

no recurrences in the patients who underwent open repair. In all patients, the cause of recurrence was disruption of the suture line within the costodiaphragmatic recess.

In the group of patients who underwent thoracoscopic repair with the use of simple intermittent sutures (11 patients), the recurrence rate was very high, reaching 27% (3 children). All of these recurrences occurred in children operated on between January 2013 and December 2015, and were managed using transverse subcostal laparotomy. None of the patients with recurrent CDH required mesh repair during the re-do.

Among the 16 patients who underwent thoracoscopic closure with the use of percutaneous sutures, there was only 1 case of hernia recurrence (6.25%), diagnosed in 2017.

The group of patients subjected to thoracoscopic repair with the application of percutaneous sutures included 13 newborns operated on between the 2<sup>nd</sup> and 5<sup>th</sup> day of life, and 3 children with late presentations of the pathology at the ages of 8 and 15 months. Intraoperatively, these defects were all categorized as group B defects according to the CDHSG classification. The only recurrence in this group consisted in herniation of the greater omentum between the sutures anchoring the diaphragmatic muscle to the chest wall. This complication was diagnosed during routine ultrasound examination on the 5<sup>th</sup> day after surgery. The problem was repaired immediately through thoracoscopic access (Fig. 2). The intervention consisted in the addition of percutaneous stitches introduced through the points on the skin used during the first operation. The patient's further clinical course was uneventful. No other complications related to the operative technique were observed. The follow-up period varied from 4 months to 6 years.

## Discussion

Since the first reports, published in 2001,<sup>2</sup> thoracoscopic repair has become a very popular strategy for surgical treatment in children with CDH. Minimally invasive techniques offer numerous advantages, such as improved

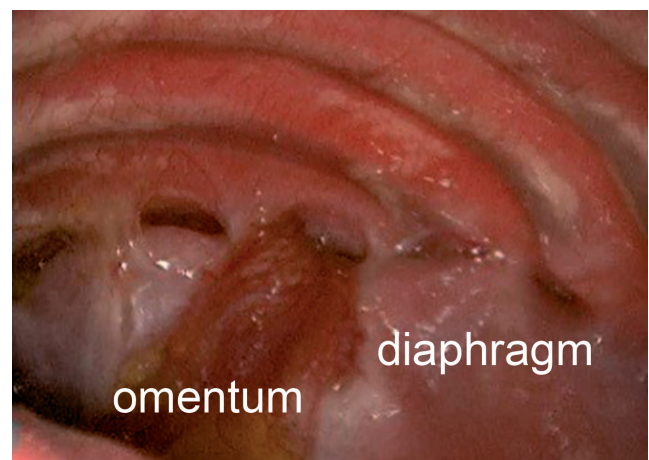


Fig. 2. CDH recurrence after thoracoscopic repair

visualization, reduction of postoperative opioid intake, shorter length of intubation, and improved cosmesis.<sup>8</sup> Nevertheless, the main goal of CDH treatment is a durable repair.

Studies consistently report a higher recurrence rate in patients who have undergone thoracoscopic CDH interventions.<sup>3,8–11</sup> Initial five-year experience of our institution with thoracoscopic treatment of CDH also showed a high percentage of recurrent herniation. According to the available clinical data, the higher risk of recurrence in children who have undergone thoracoscopic procedures cannot be explained by demographic data, the severity of illness or nonsurgical therapeutic procedures before and/or after surgery.<sup>4,11</sup>

Gander et al. presented a list of technical difficulties that can be responsible for a high relapse percentage in children who have undergone a thoracoscopic CDH correction.<sup>4</sup> In cases of intermediate and large defects, the posterolateral part of the diaphragm is usually atrophic or hypoplastic and vulnerable, especially after its mobilization by partial dissection from the chest wall. Thoracoscopic suturing at this site is not feasible, which, in combination with the tension on proximate structures, can increase the risk of disruption.

In our patients, all cases of recurrent herniation were caused by a relatively small dehiscence of diaphragmatic sutures in the most lateral part of the defect. Therefore, we decided to focus on effective and feasible methods that allow anchoring the well-developed antero-medial margin of the defect directly to the adjacent rib. Several literature reports have been published about various methods of percutaneous suturing that allow these structures to be fixed in a safe and effective way.<sup>12,13</sup> Because of our previous experience with the PIRS method, we decided to adopt it in this procedure in order to achieve solid fixation of the lateral section of the diaphragmatic defect to the chest wall. We observed only 1 recurrence in 16 patients (all with group B defects according to CDHSG) who had undergone thoracoscopic repair with the use of percutaneous suturing. The different outcomes observed over the whole period of this study between the groups of patients treated thoracoscopically with and without the application of the percutaneous suturing technique could be explained by both the effect of the learning curve, and by the feasibility and efficacy of percutaneous diaphragm fixation. Starting from 2015, we also adopted a lower threshold for utilization of mesh repair in larger diaphragmatic defects (CDHSG groups C and D). We believe that these 2 factors combined allowed the reduction of the overall number of recurrences in patients with CDHs within the period from January 2015 to July 2019 (8%, 2 patients).

In the light of the relatively high recurrence rate after thoracoscopic repair of CDH, the controversies concerning the optimal treatment method remain unsolved.<sup>4,14,15</sup> Nevertheless, in our opinion, the benefits of thoracoscopic intervention outweigh the potential risk of recurrence, which can easily be detected and managed with the same method.

## Conclusions


The technique of percutaneous suturing allows for the safe and effective closure of the posterolateral part of diaphragmatic defects in CDH. It permits a feasible repair under acceptable tension, and can be listed among countermeasures against recurrence. The technique should be considered in CDHSG group A and B cases where simple interrupted suturing does not ensure an uneventful recovery because of the size or morphology of the defect.

## ORCID iDs

Bartosz Bogusz  <https://orcid.org/0000-0002-8763-0990>

Adam Mol  <https://orcid.org/0000-0001-9378-549X>

Oskar Zgraj  <https://orcid.org/0000-0003-1738-2482>

Wojciech Górecki  <https://orcid.org/0000-0003-4907-0520>

## References

1. Zee DCVD, Bax NMA. Laparoscopic repair of congenital diaphragmatic hernia in a 6-month-old child. *Surg Endosc*. 1995;9(9):1001–1003. doi:10.1007/bf00188460
2. Becmeur F, Jamali R, Moog R, et al. Thoracoscopic treatment for delayed presentation of congenital diaphragmatic hernia in the infant. *Surg Endosc*. 2001;15(10):1163–1166. doi:10.1007/s004640090064
3. Lansdale N, Alam S, Losty PD, Jesudason EC. Neonatal endosurgical congenital diaphragmatic hernia repair. *Ann Surg*. 2010;252(1):20–26. doi:10.1097/sla.0b013e3181dca0e8
4. Gander JW, Fisher JC, Gross ER, et al. Early recurrence of congenital diaphragmatic hernia is higher after thoracoscopic than open repair: A single institutional study. *J Pediatr Surg*. 2011;46(7):1303–1308. doi:10.1016/j.jpedsurg.2010.11.048
5. Harting MT, Lally KP. The Congenital Diaphragmatic Hernia Study Group registry update. *Semin Fetal Neonatal Med*. 2014;19(6):370–375. doi:10.1016/j.siny.2014.09.004
6. Putnam LR, Harting MT, Tsao K, et al. Congenital diaphragmatic hernia defect size and infant morbidity at discharge. *Pediatrics*. 2016; 138(5):e20162043. doi:10.1542/peds.2016-2043
7. Patkowski D, Czernik J, Chrzan R, Jaworski W, Apoznański W. Percutaneous internal ring suturing: A simple minimally invasive technique for inguinal hernia repair in children. *J Laparoendosc Adv Surg Tech A*. 2006;16(5):513–517. doi:10.1089/lap.2006.16.513
8. Kim AC, Bryner BS, Akay B, Geiger JD, Hirschl RB, Mychaliska GB. Thoracoscopic repair of congenital diaphragmatic hernia in neonates: Lessons learned. *J Laparoendosc Adv Surg Tech A*. 2009;19(4):575–580. doi:10.1089/lap.2009.0129
9. McHoney M, Giacomello L, Nah SA, et al. Thoracoscopic repair of congenital diaphragmatic hernia: Intraoperative ventilation and recurrence. *J Pediatr Surg*. 2010;45(2):355–359. doi:10.1016/j.jpedsurg.2009.07.072
10. Gourlay DM, Cassidy LD, Sato TT, Lal DR, Arca MJ. Beyond feasibility: A comparison of newborns undergoing thoracoscopic and open repair of congenital diaphragmatic hernias. *J Pediatr Surg*. 2009;44(9): 1702–1707. doi:10.1016/j.jpedsurg.2008.11.030
11. Lao OB, Crouthamel MR, Goldin AB, Sawin RS, Waldhausen JH, Kim SS. Thoracoscopic repair of congenital diaphragmatic hernia in infancy. *J Laparoendosc Adv Surg Tech A*. 2010;20(3):271–276. doi:10.1089/lap.2009.0150
12. Chen B, Wang Q, Li B, Wang B. Thoracoscopic repair of diaphragmatic hernia in infants: A new modification of the technique. *Eur J Pediatr Surg*. 2015;26(06):519–523. doi:10.1055/s-0035-1568996
13. Boo Y, Rohleder S, Muensterer O. A novel technique of posterolateral suturing in thoracoscopic diaphragmatic hernia repair. *Eur J Pediatr Surg Rep*. 2017;05(1):e26–e28. doi:10.1055/s-0037-1604049
14. Inoue M, Uchida K, Otake K, et al. Thoracoscopic repair of congenital diaphragmatic hernia with countermeasures against reported complications for safe outcomes comparable to laparotomy. *Surg Endosc*. 2015;30(3):1014–1019. doi:10.1007/s00464-015-4287-6
15. Jancelewicz T, Langer JC, Chiang M, Bonnard A, Zamakhshary M, Chiu PP. Thoracoscopic repair of neonatal congenital diaphragmatic hernia (CDH): Outcomes after a systematic quality improvement process. *J Pediatr Surg*. 2013;48(2):321–325. doi:10.1016/j.jpedsurg.2012.11.012

# Comparative analysis of clinical features and risk factors of severe pneumonia development in pediatric patients hospitalized with seasonal influenza or swine-origin influenza infection

Ling Jin<sup>1,B–F</sup>, En-Mei Liu<sup>2,B,C,E,F</sup>, Xiao-Hong Xie<sup>2,C,E,F</sup>, Ying Hu<sup>1,C,F</sup>, Wei Liao<sup>1,A,C,E,F</sup>

<sup>1</sup> Department of Pediatrics, First Affiliated Hospital (Southwest Hospital) of The Third Military Medical University, Chongqing, China

<sup>2</sup> Respiratory Center of the Affiliated Children's Hospital of Chongqing Medical University, China

A – research concept and design; B – collection and/or assembly of data; C – data analysis and interpretation;

D – writing the article; E – critical revision of the article; F – final approval of the article

Advances in Clinical and Experimental Medicine, ISSN 1899–5276 (print), ISSN 2451–2680 (online)

*Adv Clin Exp Med.* 2020;29(8):971–977

## Address for correspondence

Wei Liao

E-mail: 540696970@qq.com

## Funding sources

This study was granted by China Special Grant for the Prevention and Control of Infection Diseases (grant No. 2009ZX10004-204), 2016 Military Medical Science and Technology Innovation Program (SWH2016LCYB-15).

## Conflict of interest

None declared

Received on September 21, 2017

Reviewed on November 20, 2017

Accepted on April 30, 2020

Published online on August 13, 2020

## Cite as

Jin L, Liu EM, Xie XH, Hu Y, Liao W. Comparative analysis of clinical features and risk factors of severe pneumonia development in pediatric patients hospitalized with seasonal influenza or swine-origin influenza infection. *Adv Clin Exp Med.* 2020;29(8):971–977. doi:10.17219/acem/121520

## DOI

10.17219/acem/121520

## Copyright

© 2020 by Wrocław Medical University

This is an article distributed under the terms of the Creative Commons Attribution 3.0 Unported (CC BY 3.0) (<https://creativecommons.org/licenses/by/3.0/>)

## Abstract

**Background.** The influenza A virus is the most important human pathogen affecting respiratory tract in children and has been prevalent for more than a century.

**Objectives.** To describe epidemiological and clinical features in hospitalized children with acute respiratory infection caused by a novel swine-origin influenza virus (S-OIV) and seasonal influenza virus A (IVA).

**Material and methods.** A total of 1,074 nasopharyngeal aspirate (NPA) samples were collected from children hospitalized with acute respiratory tract infections. The RNAs of S-OIV and seasonal IVA in the samples were examined using real-time polymerase chain reaction (RT-PCR).

**Results.** The presence of IVA was detected in 105 samples (9.8%), including S-OIV in 15 samples (1.4%) and seasonal IVA in the remaining samples (8.4%). The incidence of both viral infections was lower in autumn and winter. The rates of severe pneumonia in patients with S-OIV and seasonal IVA were 6.7% and 15.6%, respectively. In total, 14 out of 90 seasonal IVA-positive cases were categorized as severe pneumonia and 1 out of 15 S-OIV-positive cases as severe bronchiolitis. Five samples were found to have single S-OIV infection among 15 S-OIV-positive cases, while other respiratory viruses were detected in the other 9 samples. Twenty-one samples were found to be single seasonal-IVA-positive among the 90 seasonal-IVA-positive cases. Underlying heart conditions (odds ratio (OR) = 13.60), wheezing (OR = 6.82) and co-infection with adenovirus (OR = 6.21) were risk factors for developing severe pneumonia in seasonal IVA patients.

**Conclusions.** Children younger than 2 years appeared to be susceptible to both kinds of viral infection. Diagnoses of non-severe respiratory tract infection were mainly made for patients with S-OIV and IVA infection. Underlying heart conditions, wheezing and co-infection with adenovirus increase the risk of developing severe pneumonia in seasonal IVA patients.

**Key words:** children, swine-origin influenza virus, seasonal influenza virus A, acute respiratory tract infection



## Introduction

Influenza A virus (IVA) is the most important pathogen of respiratory tract infection in children and has been prevalent for more than a century. The flu has caused epidemics every year and erupts into a global pandemic at intervals of about 40 years.<sup>1</sup> The most common symptoms of flu pediatric patients include fever, cough and sputum.<sup>2</sup> Because of the antigenic drift or antigenic shift of the hemagglutinin and neuraminidase glycoproteins of the influenza viruses, the clinical features vary from year to year. Such is the case with the swine-origin influenza A (H1N1) virus (S-OIV).<sup>3</sup>

In April 2009, the first infection of S-OIV in humans was reported in Mexico, and the virus has rapidly spread across the world, affecting mainly young adults and children. The S-OIV probably resulted from the reassortment of recent North American H3N2 and H1N2 swine viruses (that is, avian/human/swine 'triple' reassortant viruses) with Eurasian avian-like swine viruses.<sup>4</sup> The main presentation of S-OIV was fever, cough, runny nose, nausea, poor feeding, and labored breathing in children,<sup>5</sup> which was more obvious in gastrointestinal symptoms than seasonal influenza. Because of the risk of emerging epidemics and pandemics, influenza always attracts the attention of patients, physicians, health organizations, and the media.<sup>6</sup> Information on the clinical course of children infected with H1N1 is still emerging.<sup>7,8</sup>

In this study, the purpose was to describe the clinical features, laboratory examination results and risk factors of severe pneumonia development in children after seasonal influenza or S-OIV infection, with the respiratory infectious pediatric patients admitted to Children's Hospital of Chongqing Medical University (China) serving as the test subjects.

## Material and methods

### Participants and clinical methods

The study population consisted of 1,074 children under the age of 16 years who were admitted to the Division of Respiratory Medicine at Children's Hospital of Chongqing Medical University between June 1, 2009 and May 31, 2011. During the two-year study period, out of 1,074 pediatric patients, 90 had a confirmed IVA infection and 15 had confirmed S-OIV infection. These 105 pneumonia patients with IVA or S-OIV infection were divided into a severe pneumonia group and a non-severe pneumonia group. The demographic, clinical and laboratory data extracted from medical records for the study included complete blood count, respiratory tract immune fluorescence, sputum culture for bacteria, radiological findings, and epidemiological data, using a standardized datasheet. Subjective symptoms such as headache, sore throat and

myalgia were also assessed, but only in children older than 5 years. The diagnosis of pneumonia and severe pneumonia were mainly based on the guidelines from the Pediatrics Branch Respiratory Study Group of the Chinese Medical Association.<sup>9</sup> The comparison was done between severe pneumonia patients and non-severe pneumonia patients. Clinical and laboratory data was compared between patients with seasonal influenza and those with S-OIV.

All patients or their legal guardians gave informed consent to participate in this study. The study was carried out in accordance with the Helsinki Declaration.

### Laboratory confirmation

All specimens were collected using nasopharyngeal aspirates (NPAs) method. The NPAs were stored at 4°C for a short duration (4–6 h) in the hospital ward; then, they were transported on ice to the Lab for Pediatric Respiratory Medicine of the Children's Hospital of Chongqing, where they were divided into centrifuge tubes and stored at –80°C. DNA and RNA were co-extracted from 200-µL NPA samples using QIAamp® MinElute Virus Spin Kits (Qiagen, Hilden, Germany) according to the manufacturer's instructions, and the samples were eluted in 62 µL of RNase-free water. Then, cDNA was synthesized using a SuperScript® First-Strand Synthesis System for real-time polymerase chain reaction (RT-PCR; Invitrogen, Carlsbad, USA). The RT-PCR was used to detect IVA and S-OIV. Nested PCR assays – providing a higher sensitivity than non-nested PCR – detected parainfluenza viruses (PIVs), respiratory syncytial virus (RSV), human metapneumovirus (hMPV), and Netherlands human coronavirus (HCoV); the PCR method was used to detect Aleutian disease virus (ADV).<sup>9–13</sup> The primers used in the experiments are listed in Table 1.

Table 1. Primers and probes for RT-PCR

Primers and probes	Sequence (5'-3')	Working concentration
IVA forward	AAAGCGAATTCAGTGTGAT	0.2 µM
IVA reverse	GAAGGCAATGTGAGATTT	0.2 µM
IVA probe	GAAAGCCCGGTCCCTCTT	0.1 µM
S-OIV forward	GCACGGTCAGCACTTATYCTRAG	0.2 µM
S-OIV reverse	GTGRGCTGGGTTTTCATTTGGTC	0.2 µM
S-OIV probe	CYACTGCAAGCCCA**ACACACAAGCAGGCA	0.1 µM

IVA – seasonal influenza virus A; S-OIV – swine-origin influenza virus.

### Statistical analysis

Statistical analyses were performed using SPSS v. 17.0 software (SPSS Inc., Chicago, USA). Data is expressed as mean ± standard deviation (SD), median, percentage, or frequency. The  $\chi^2$  test was used to compare categorical



variables, with Fisher’s correction when needed. The t-test was used for comparing continuous variables. To analyze for the risk factors of severe pneumonia, we used multivariate logistic regression. Odds ratios (ORs) and 95% confidence intervals (95% CIs) were calculated. A two-tailed p-value of less than 0.05 was considered statistically significant.

## Results

During the two-year study period, out of 1,074 pediatric patients, 90 had confirmed IVA infections and 15 had confirmed S-OIV infections. The age of the IVA patients ranged from 1 to 135 months (median age: 9 months) while the age of the S-OIV patients ranged from 1 to 63 months (median age: 9 months). Of note, there were significantly

more males than females, at a ratio of 2:1 and 4:1 for IVA and S-OIV infections, respectively. Most patients (76.6% and 79.9%, respectively) were younger than 2 years. Approximately 40% of both had an underlying medical condition, such as premature labor, previous respiratory infection ( $\geq 3$ ), asthma, or congenital heart disease. Meanwhile, there were no significant differences regarding demographic characteristics between the IVA and S-OIV groups ( $p > 0.05$ ; Table 2).

The clinical manifestations of IVA or S-OIV infection in the hospitalized pediatric patients are listed in Table 3. The results indicate that there were no significant differences in the symptoms, signs and blood parameters between the IVA and S-OIV groups ( $p > 0.05$ ; Table 3). The most common symptoms of IVA or S-OIV patients at admission were mainly cough (94.4% and 100.0%,

**Table 2.** Demographic characteristics of 90 patients hospitalized with IVA and 15 patients with S-OIV

Characteristic	IVA (n = 90)	S-OIV (n = 15)	p-value
Sex	male, 60 (66.7%) female, 30 (33.3%)	male, 12 (80%) female, 3 (20%)	>0.05
Age groups	>5 years, 7 (7.8%) 2–5 years, 14 (15.6%) <2 years, 79 (76.6%)	>5 years, 1 (6.7%) 2–5 years, 2 (13.4%) <2 years, 12 (79.9%)	>0.05
Median age (range)	9 months (1–135)	9 months (1–63)	>0.05
Underlying medical conditions	34 (37.8%)	6 (40.0%)	>0.05
premature (<37 weeks)	8 (8.9%)	2 (13.3%)	>0.05
previous respiratory infection ( $\geq 3$ )	13 (14.4%)	4 (26.7%)	>0.05
asthma	10 (11.1%)	2 (13.3%)	>0.05
congenital heart disease	7 (7.8%)	0 (0.0%)	>0.05

IVA – seasonal influenza virus A; S-OIV – swine-origin influenza virus.

**Table 3.** Clinical features of 90 IVA patients and 15 S-OIV patients

Clinical feature	IVA (n = 90)	S-OIV (n = 15)	p-value
Symptom			
Cough	85 (94.4%)	15 (100.0%)	0.455
Sputum	63 (70.0%)	7 (46.7%)	0.076
Fever	54 (60.0%)	10 (66.7%)	0.425
Wheezing	29 (32.2%)	5 (33.3%)	0.574
Dyspnea	12 (13.3%)	1 (6.7%)	0.412
Fatigue	6 (6.7%)	0 (0.0%)	0.387
Sore throat	1 (1.1%)	0 (0.0%)	0.857
Headache	2 (2.2%)	0 (0.0%)	0.734
Chest pain	1 (1.1%)	0 (0.0%)	0.857
Abdominal pain	2 (2.2%)	0 (0.0%)	0.734
Sign			
Moist	64 (71.1%)	9 (60.0%)	0.300
Wheeze	39 (43.3%)	5 (33.3%)	0.307
Hemanalysis			
WBC [ $/mm^3$ ]	9926 $\pm$ 4170	9611 $\pm$ 5224	0.915
CRP [mg/dL]	8.569 $\pm$ 27.93	15.83 $\pm$ 38.66	0.483

IVA – seasonal influenza virus A; S-OIV – swine-origin influenza virus; WBC – white blood cell count; CRP – C-reactive protein level.

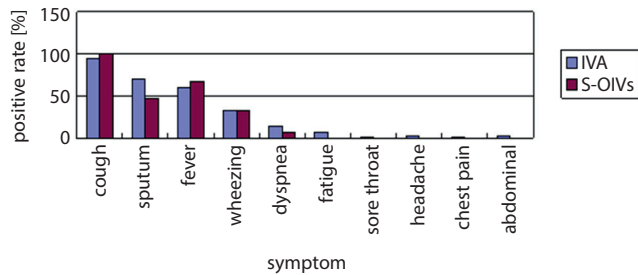


Fig. 1. The symptoms in IVA and S-OIV infection

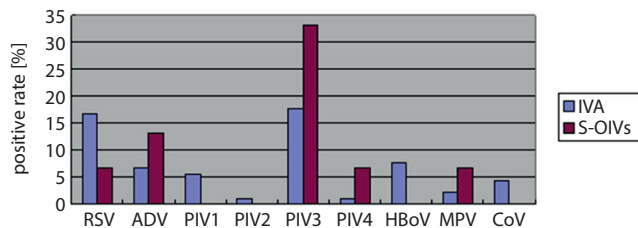


Fig. 2. Viral co-infection in IVA and S-OIV infection

respectively), fever (60.0% and 66.7%, respectively) and sputum (70.0% and 46.7%, respectively). The symptoms of fatigue, sore throat, headache, abdominal pain, and chest pain were rare in both groups of patients (Fig. 1). Physical examination at admission found moist (71.7% and 60.0%, respectively) and wheezing (43.3% and 33.3%, respectively). Detailed blood test results were collected within 24 h of admission. The white blood cell (WBC) count was almost normal, while the C-reactive protein (CRP) level was higher than average, especially in the S-OIV patients.

Out of the 90 IVA-positive cases, 39 (43.3%) had co-infection with other common respiratory viruses, while 9 (60.0%) S-OIV-positive cases had co-infection. The most common co-infection for both was PIVs (25.6% and 40.0%, respectively) – especially PIV3 (17.8% and 33.3%, respectively) – followed by RSV (16.7% and 6.7%, respectively) and ADV (6.7% and 13.3%, respectively). Co-infection with hMPV or HCoV was relatively rare. However, there is a selective bias because S-OIV prefers to mix with ADV, PIV<sub>3</sub>, PIV<sub>4</sub>, and MPV (Fig. 2). Sputum culture was positive in *Streptococcus pneumoniae* (12.2% and 26.7%, respectively), *Hemophilus influenzae* (6.7% and 0.0%, respectively), *Escherichia coli* (6.7% and 0.0%, respectively), and *Klebsiella pneumoniae* (6.7% and 0.0%, respectively) (Table 4). The *S. pneumoniae* co-infection in the IVA group was significantly less common than in the S-OIV group (Table 4;  $p < 0.05$ ). All other concrete data is presented in Table 4.

In order to understand the difference of illness severity between IVA infection and S-OIV infection, we compared the indicators of average inpatient course, number of dyspnea patients, number of severe pneumonia cases, temperatures, and respiratory rates (Table 5). The results revealed that the average inpatient course was significantly longer in the IVA group compared to the S-OIV group (Table 5;  $p < 0.05$ ). However, the other indicators were

Table 4. Co-infection of 90 IVA patients and 15 S-OIV patients

Co-infection	IVA (n = 90)	S-OIV (n = 15)	p-value
Virus			
RSV	6.715 (16.7%)	1 (6.7%)	0.209
ADV	6 (6.7%)	2 (13.3%)	0.491
PIV1	5 (5.6%)	0 (0.0%)	0.455
PIV2	1 (1.1%)	0 (0.0%)	0.320
PIV3	16 (17.8%)	5 (33.3%)	0.256
PIV4	1 (1.1%)	1 (6.7%)	0.424
hBoV	7 (7.8%)	0 (0.0%)	0.328
hMPV	2 (2.2%)	1 (6.7%)	0.526
hCoV	4 (4.4%)	0 (0.0%)	0.535
Sputum culture			
<i>E. coli</i>	6 (6.7%)	0 (0.0%)	0.387
<i>K. pneumoniae</i>	6 (6.7%)	0 (0.0%)	0.387
<i>H. influenzae</i>	6 (6.7%)	0 (0.0%)	0.387
<i>S. pneumoniae</i>	11 (12.2%)	4 (26.7%)	<0.05

IVA – seasonal influenza virus A; S-OIV – swine-origin influenza virus; PIV – parainfluenza viruses; RSV – respiratory syncytial virus; hMPV – human metapneumovirus; hCoV – human coronavirus; hBoV – human bocavirus; ADV – Aleutian disease virus; *E. coli* – *Escherichia coli*; *K. pneumoniae* – *Klebsiella pneumoniae*; *H. influenzae* – *Hemophilus influenzae*; *S. pneumoniae* – *Streptococcus pneumoniae*.

Table 5. Comparison of illness severity between IVA infection and S-OIV infection

Variable	Value		p-value
	IVA (n = 90)	S-OIV (n = 15)	
Average inpatient course [days]	7.73 ± 9.16	5.67 ± 1.29	0.042
Dyspnea case	12 (13.3%)	1 (6.7%)	0.666
Severe pneumonia cases	14 (15.6%)	1 (6.7%)	0.351
Temperature	37.11 ± 0.76	37.44 ± 0.92	0.180
Respiratory rate	42.51 ± 11.54	42.47 ± 10.89	0.857

IVA – seasonal influenza virus A; S-OIV – swine-origin influenza virus.

not significantly different, which does not fully explain whether there is a significant difference in illness severity between IVA infection and S-OIV infection (Table 5).

The patients with severe pneumonia had more co-infection with RSV or ADV, and a higher prevalence of *K. pneumoniae* than the patients with mild pneumonia (Table 6). Severe pneumonia was also more common in patients with underlying conditions, such as congenital heart disease. Patients with severe pneumonia were basically similar in their incidence of the symptoms of cough, fever, sputum, dyspnea, etc. (Table 6). There is no statistically significant difference in WBC counts and CRP levels between severe and mild pneumonia. Meanwhile, in the IVA group, the CHD rate was significantly higher and the incidence of sputum was significantly lower in the severe pneumonia group compared to that of the non-severe pneumonia group (Table 6;  $p < 0.05$ ).

**Table 6.** Risk factors associated with severe pneumonia due to IVA and S-OIV

Variable	S-OIV (n = 15)			IVA (n = 90)		
	severe pneumonia (n = 1)	non-severe pneumonia (n = 14)	p-value	severe pneumonia (n = 14)	non-severe pneumonia (n = 76)	p-value
Sex (male)	1 (100.0%)	11 (78.6%)	0.800	8 (57.1%)	52 (68.4%)	0.298
Age (<2 years)	1 (100.0%)	11 (78.6%)	0.800	13 (92.9%)	56 (73.7%)	0.107
Underlying medical conditions						
Premature labor	1 (100.0%)	2 (14.3%)	0.867	1 (7.1%)	7 (9.2%)	0.638
Previous respiratory infection (≥3)	1 (100.0%)	9 (64.3%)	0.667	7 (50.0%)	44 (57.9%)	0.770
Asthma	0 (0.0%)	2 (14.3%)	0.867	12 (85.7%)	68 (89.5%)	0.484
CHD	0 (0.0%)	0 (0.0%)	1.000	4 (28.6%)	3 (3.9%)	<0.05
Symptoms						
Cough	1 (100.0%)	14 (100.0%)	1.000	13 (92.9%)	72 (94.7%)	0.580
Sputum	0 (0.0%)	7 (50.0%)	0.533	13 (92.9%)	50 (65.8%)	<0.05
Fever	0 (0.0%)	0 (0.0%)	1.000	7 (50.0%)	47 (61.8%)	0.294
Wheezing	1 (100.0%)	4 (28.6%)	0.333	4 (28.6%)	25 (32.9%)	0.508
Dyspnea	0 (0.0%)	1 (7.1%)	0.933	4 (28.6%)	8 (10.5%)	0.088
Fatigue	0 (0.0%)	0 (0.0%)	1.000	1 (7.1%)	5 (6.6%)	0.649
Sore throat	0 (0.0%)	0 (0.0%)	1.000	0 (0.0%)	1 (1.3%)	0.844
Headache	0 (0.0%)	0 (0.0%)	1.000	0 (0.0%)	2 (2.6%)	0.712
Chest pain	0 (0.0%)	0 (0.0%)	1.000	0 (0.0%)	1 (1.3%)	0.844
Abdominal pain	0 (0.0%)	0 (0.0%)	1.000	1 (7.1%)	1 (1.3%)	0.288
Co-infection with virus						
RSV	1 (100.0%)	1 (7.1%)	0.133	5 (35.7%)	10 (13.2%)	0.245
ADV	1 (100.0%)	1 (7.1%)	0.133	2 (14.3%)	4 (5.3%)	0.233
PIV1	0 (0.0%)	0 (0.0%)	1.000	1 (7.1%)	4 (5.3%)	0.580
PIV2	0 (0.0%)	0 (0.0%)	1.000	0 (0.0%)	1 (1.3%)	0.844
PIV3	0 (0.0%)	5 (35.7%)	0.667	4 (28.6%)	12 (15.8%)	0.214
PIV4	0 (0.0%)	1 (7.1%)	0.933	0 (0.0%)	1 (1.3%)	0.844
HBoV	0 (0.0%)	0 (0.0%)	1.000	2 (14.3%)	5 (6.6%)	0.298
MPV	0 (0.0%)	1 (7.1%)	0.933	1 (7.1%)	1 (1.3%)	0.288
CoV	0 (0.0%)	0 (0.0%)	1.000	1 (7.1%)	3 (3.9%)	0.498

IVA – seasonal influenza virus A; S-OIV – swine-origin influenza virus; PIV – parainfluenza viruses; RSV – respiratory syncytial virus; hCoV – human coronavirus; hBoV – human bocavirus; ADV – Aleutian disease virus; CHD – coronary heart disease.

In multivariate analysis (Table 7), independent risk factors for the development of severe pneumonia were co-infection with RSV ( $p = 0.042$ ; OR = 4.245; 95% CI = 1.052–17.128), co-infection with ADV ( $p = 0.029$ ; OR = 7.336; 95% CI = 1.221–44.076), *K. pneumoniae*-positive sputum culture ( $p = 0.022$ ; OR = 7.763; 95% CI = 1.342–44.896), and basic condition of congenital heart diseases ( $p = 0.009$ ; OR = 9.577; 95% CI = 1.777–51.610).

## Discussion

This study compared the characteristics of pediatric patients with seasonal influenza to those with H1N1 infection and analyzed the risk factors for development of severe pneumonia.

Our findings are consistent with other reports in that the clinical features of S-OIV infection are generally similar to those of seasonal influenza infection.<sup>14,15</sup> The most common symptoms were cough, sputum and fever, while the symptoms of fatigue, sore throat, headache, abdominal pain, and chest pain were rare in pediatric patients. Young children cannot formulate complaints, which probably helps explain the less common symptoms.

Studies have previously indicated that many hospitalized patients during the peak periods of seasonal influenza were usually younger than 2 years or older than 65 years.<sup>16,17</sup> In our groups, patients under the age of 2 years represented 79 (76.6%) and 12 (79.9%) cases, suggesting that infants and children under 2 years are the most susceptible group for seasonal influenza and S-OIV in Chongqing.<sup>18</sup> The reason may be that infants and children less than 2 years old lack

Table 7. Multivariable analysis of risk factors associated with severe pneumonia

Variable	IVA (n = 90)		Model		
	severe pneumonia (n = 14)	non-severe pneumonia (n = 76)	OR	95% CI	p-value
Sex (male)	8 (57.1%)	52 (68.4%)	0.595	0.192–1.847	0.298
Age (<2 years)	13 (92.9%)	56 (73.7%)	5.141	1.742–48.430	0.107
CHD	4 (28.6%)	3 (3.9%)	9.577	1.777–51.610	<0.05
Symptoms					
Cough	13 (92.9%)	72 (94.7%)	0.138	0.007–2.755	0.580
Sputum	13 (92.9%)	50 (65.8%)	6.330	0.740–54.133	<0.05
Fever	7 (50.0%)	47 (61.8%)	1.321	0.345–5.066	0.294
Co-infection with virus					
RSV	5 (35.7%)	10 (13.2%)	2.360	0.345–16.137	0.245
ADV	2 (14.3%)	4 (5.3%)	1.736	0.136–22.167	0.233
PIV3	4 (28.6%)	12 (15.8%)	2.652	0.446–15.771	0.214
Sputum culture					
<i>E. coli</i>	2 (14.3%)	4 (5.3%)	1.025	0.078–13.405	0.985
<i>K. pneumoniae</i>	3 (21.4%)	3 (3.9%)	3.242	0.336–31.275	<0.05
<i>H. influenzae</i>	1 (7.1%)	5 (6.6%)	0.334	0.006–19.456	0.597
<i>S. pneumoniae</i>	1 (7.1%)	10 (13.2%)	0.299	0.020–4.523	0.383

OR – odds ratio; 95% CI – 95% confidence interval; CHD – coronary heart disease; PIV – parainfluenza viruses; RSV – respiratory syncytial virus; ADV – Aleutian disease virus; *E. coli* – *Escherichia coli*; *K. pneumoniae* – *Klebsiella pneumoniae*; *H. influenzae* – *Hemophilus influenzae*; *S. pneumoniae* – *Streptococcus pneumoniae*.

elastic tissue and mucus gland secretion and have poor cilia movement, which leads to a lower non-specific immune response.<sup>19</sup>

In the comparison of clinical characteristics between IVA and S-OIV patients, we find that the former group has a higher average inpatient course and more cases of dyspnea and severe pneumonia. Although these are not statistically significant, in view of the mere 15 S-OIV-positive cases, it cannot be completely excluded that there is a difference in illness severity between them. According to our data, there is a strong possibility that the pediatric patients with IVA infection have more severe cases than patients with S-OIV. Brundage and Shanks have reported that the replacement of amino acids in the PB2, NS1 and PB1-F2 proteins of the influenza virus has a direct impact on virus virulence.<sup>20</sup> S-OIV possesses fewer pathogenic amino acid sites in the PB2, NS1 and PB1-F2 proteins than IVA, which may be one explanation.

The study shows that the conditions of congenital heart disease, *K. pneumoniae*-positive sputum culture, and co-infection with RSV or ADV are risk factors for developing severe pneumonia. Other reports reveal that mixed IVA pneumonia is 3 times more prevalent than simple influenza pneumonia,<sup>21,22</sup> regardless of the seasonal flu or S-OIV in 2009. The most common bacteria in mixed pneumonia are *S. pneumoniae*, *H. influenzae* and *Staphylococcus aureus* – especially *S. pneumoniae*,<sup>23</sup> which is in accordance with our study.

Influenza pneumonia co-infection with *S. pneumoniae* easily develops into severe pneumonia and raises the mortality rate.<sup>23,24</sup> Two mechanisms for this phenomenon have

been reported. Firstly, animal experiments show that the H1N1 virus mixed with *S. pneumoniae* can induce a synergistic role in enhancing the expression of platelet-activating factor receptor; in consequence, *S. pneumoniae* is easier to adhere to and increases damage to the lungs.<sup>23</sup> Secondly, a mixed infection of the two can upregulate interleukin 1 (IL-1) expression, which reduces the macrophage clearance of *S. pneumoniae*.<sup>24</sup> However, our results suggest that the condition of *S. pneumoniae*-positive sputum culture is not a statistically significant factor, while a *K. pneumoniae*-positive sputum culture ( $p = 0.023$ ; OR = 7.250; 95% CI = 1.311–40.098) is one of the risk factors for the development of severe pneumonia in children hospitalized with respiratory tract IVA infections. This phenomenon has not yet been clearly reported in the literature: only 1 case report has been published in Taiwan, which found that IVA mixed with *K. pneumoniae* in nasopharyngeal carcinoma patients appear to pneumonia and progressive dyspnea.<sup>25,26</sup> In conclusion, the synergistic effect and its mechanism of IVA co-infection with *K. pneumoniae* require further study.

We recognize several limitations in our study. Notably, imaging data was not included, some laboratory values were missing and some symptoms may have been under-reported through poor clinical recognition. Furthermore, the S-OIV-positive cases were too few (only 15 cases) – the relationship between S-OIV and severe pneumonia requires a larger sample size for further study.

The IVA spreads throughout the year, and regional epidemics or worldwide pandemics occur frequently.

As it is one of the most common pathogens in children with respiratory tract infection, determining the prevalence, clinical characteristics and risk factors of severe pneumonia in children with ARIs in Chongqing can be important to its clinical diagnosis, treatment and vaccination.

Although the present study resulted in some interesting findings, there were also limitations. As it is well-known, many risk factors – such as current body weight, birth weight, anemia, and familial diseases – may lead to severe pneumonia in hospitalized pediatric patients. However, these risk factors were not discussed in this study. Therefore, in the following study, we would also investigate the effects of the above risk factors on severe pneumonia.

## Conclusions

The study indicated that the detection rates of S-OIV infection and seasonal IVA were 1.4% and 8.4%, respectively, in children hospitalized with acute airway respiratory infection in Chongqing. Children younger than 2 years appeared to be susceptible to both viruses. A diagnosis of non-severe respiratory tract infection was mainly presented in patients hospitalized with S-OIV and IVA infection in the respiratory medicine division of our hospital. Underlying heart conditions, wheezing and co-infection with adenovirus all increase the risk of developing severe pneumonia in patients with seasonal IVA infection.

## References

- Fouchier RA, Munster V, Wallesten A, et al. Characterization of a novel influenza A virus hemagglutinin subtype (H16) obtained from black-headed gulls. *J Virol*. 2005;79(5):2814–2822.
- Piyarat S, Kano KS, Pranee S, et al. Clinical and epidemiological characteristics of respiratory syncytial virus and influenza virus associated hospitalization in urban Thai infants. *J Med Assoc Thai*. 2011;94(Suppl 3):S164–S171.
- Taubenberger JK, Huhin JV, Morens DM. Discovery and characterization of the 1918 pandemic influenza virus in historical context. *Antivir Ther*. 2007;12(4 Pt B):581–591.
- Peiris JS, Poon LL, Guan Y. Emergence of a novel swine-origin influenza A (H1N1) virus in humans. *J Clin Virol*. 2009;45(3):169–173.
- Muhammad Ismail HI, Tan KK, Lee YL, et al. Characteristics of children hospitalized for pandemic (H1N1) 2009 in Malaysia. *Emerg Infect Dis*. 2011;17(4):708–710.
- Falagas ME, Kiriaze IJ. Reaction to the threat of influenza pandemic: The mass media and the public. *Crit Care*. 2006;10(1):408.
- Piekarska K, Zacharczuk K, Wolkowicz T, et al. Distribution of 16S rRNA methylases among different species of aminoglycoside-resistant *Enterobacteriaceae* in a tertiary care hospital Poland. *Adv Clin Exp Med*. 2017;25(3):539–544.
- Halasa NB. Update on the 2009 pandemic influenza A H1N1 in children. *Curr Opin Pediatr*. 2010;22(1):83–87.
- Wang C, Liu Y, Wang Y, et al. Adenovirus-mediated siRNA targeting CXCR2 attenuates titanium particle-induced osteolysis by suppressing osteoclast formation. *Med Sci Monit*. 2016;22(1):727–735.
- Xu W, McDonough MC, Erdman DD. Species-specific identification of human adenoviruses by a multiplex PCR assay. *J Clin Microbiol*. 2000;38(11):4114–4120.
- Allander T, Jartti T, Gupta S, et al. Human bocavirus and acute wheezing in children. *Clin Infect Dis*. 2007;44(7):904–910.
- Call SA, Vollenweider MA, Hornung CA, Simel DL, McKinney WP. Does this patient have influenza? *JAMA*. 2005;293(8):987–997.
- Cox NJ, Subbarao K. Influenza. *Lancet*. 1999;354(9186):1277–1282.
- Fiore AE, Shay DK, Broder K, et al; Centers for Disease Control and Prevention. Prevention and control of influenza: Recommendations of the Advisory Committee on Immunization Practices (ACIP). *MMWR Recomm Rep*. 2009;58(RR-8):1–52.
- Thompson WW, Shay DK, Weintraub E, et al. Influenza associated hospitalizations in the United States. *JAMA*. 2004;292(11):1333–1340.
- Monies M, Vicente D, Perez-Yarza E, Cilla G, Pérez-Trallero E. Influenza-related hospitalizations among children aged less than 5 years old in the Basque country, Spain: A 3-year study (July 2001–June 2004). *Vaccine*. 2005;23(34):4302–4306.
- Neuzil K, Zhu Y, Griffin M, et al. Burden of inter-pandemic influenza in children younger than 5 years: A 25-year prospective study. *Infect Dis*. 2002;185(1):147–152.
- Neumann G, Noda T, Kawaoka Y. Emergence and pandemic potential of swine-origin H1N1 influenza virus. *Nature*. 2009;459(7249):931–939.
- Morens DM, Taubenberger JK, Fauci AS. Predominant role of bacterial pneumonia as a cause of death in pandemic influenza: Implications for pandemic influenza preparedness. *J Infect Dis*. 2008;198(7):962–970.
- Brundage JF, Shanks GD. Deaths from bacterial pneumonia during the 1918–1919 influenza pandemic. *Emerg Infect Dis*. 2008;14(8):1193–1199.
- Wunderink RG. Influenza and bacterial pneumonia, constant companions. *Crit Care*. 2010;14(3):150.
- Chertow DS, Memoli MJ. Bacterial coinfection in influenza: A grand rounds review. *JAMA*. 2013;309(3):275–282.
- McCullers JA, Jerold ER. Lethal synergism between influenza virus and *Streptococcus pneumoniae*: Characterization of a mouse model and the role of platelet-activating factor receptor. *J Infect Dis*. 2002;186(3):341–350.
- Shigeki N, Kimberly MD, Jeffrey NW. Synergistic stimulation of type I interferons during influenza virus coinfection promotes *Streptococcus pneumoniae* colonization in mice. *J Clin Microbiol*. 2011;121(9):3657–3665.
- Lai CC, Lee PL, Tan CK, et al. Pneumonia due to pandemic (H1N1) 2009 influenza virus and *Klebsiella pneumoniae* capsular serotype K16 in a patient with nasopharyngeal cancer. *J Microbiol Immunol Infect*. 2011;45(5):382–384.
- Radzikowska E, Rozy A, Jagus P, et al. Clarithromycin decreases IL-6 concentration in serum and BAL fluid in patients with cryptogenic organizing pneumonia. *Adv Clin Exp Med*. 2016;25(5):871–878.





# The effect of unilateral carpal tunnel release on the non-operated contralateral hand

Andrzej Żyluk<sup>A,C-F</sup>, Paweł Dec<sup>B-D</sup>, Piotr Puchalski<sup>B,C</sup>

Clinic of General and Hand Surgery, Pomeranian Medical University in Szczecin, Poland

A – research concept and design; B – collection and/or assembly of data; C – data analysis and interpretation; D – writing the article; E – critical revision of the article; F – final approval of the article

Advances in Clinical and Experimental Medicine, ISSN 1899–5276 (print), ISSN 2451–2680 (online)

*Adv Clin Exp Med.* 2020;29(8):979–982

## Address for correspondence

Andrzej Żyluk  
E-mail: azyluk@hotmail.com

## Funding sources

None declared

## Conflict of interest

None declared

Received on July 15, 2019  
Reviewed on February 22, 2020  
Accepted on May 7, 2020

Published online on August 27, 2020

## Abstract

**Background.** Carpal tunnel syndrome (CTS) is often (60–90%) a bilateral condition. It has been suggested that patients with bilateral disease may benefit in the non-operated hand after unilateral surgery.

**Objectives.** To investigate the effect of unilateral carpal tunnel release on the non-operated contralateral hand.

**Material and methods.** In 186 patients with bilateral CTS, a number of measurements were performed prior to surgery. The patients were scheduled for surgery on the other hand operation 3 months after the first. Upon admission, the same measurements were performed on the still unoperated hand.

**Results.** All subjective variables were significantly better in the hand scheduled for operation as compared to the second one. Pain intensity was lower by a mean of 0.8 on a numeric rating scale (NRS); Levine symptom and function scores were lower by a mean of 0.7 and 0.3, respectively. Digital sensibility and grip strength were also better, but the changes were without clinical or statistical significance. Asked directly about the status of the non-operated hand, 109 patients (64%) reported improvement, 40 (23%) noted no change and 21 (13%) deterioration.

**Conclusions.** Regardless of the reasons for improvement, this study demonstrates that 64% of patients feel partial relief in the non-operated hand after unilateral carpal tunnel release.

**Key words:** outcome measures, carpal tunnel syndrome etiology, bilateral manifestation, carpal tunnel surgery

## Cite as

Żyluk A, Dec P, Puchalski P. The effect of unilateral carpal tunnel release on the non-operated contralateral hand. *Adv Clin Exp Med.* 2020;29(8):979–982. doi:10.17219/acem/122167

## DOI

10.17219/acem/122167

## Copyright

© 2020 by Wrocław Medical University  
This is an article distributed under the terms of the Creative Commons Attribution 3.0 Unported (CC BY 3.0) (<https://creativecommons.org/licenses/by/3.0/>)

## Introduction

Carpal tunnel syndrome (CTS) is the most common peripheral nerve neuropathy, affecting about 5–6% of women over 40 years of age.<sup>1–7</sup> Carpal tunnel syndrome is often (60–90%) a bilateral condition.<sup>8–13</sup> It has been suggested that patients with bilateral CTS may benefit in the non-operated hand after unilateral surgery.<sup>14–16</sup> It is, however, difficult to determine if the effect experienced by some patients in the non-operated hand is caused by the operation on the contralateral hand, or if it may rather be attributed to spontaneous recovery in some patients.<sup>17,18</sup> The postoperative clinical course of the non-operated contralateral hand in unilateral CTS is not well-documented. The prevalence of CTS in the general population makes the choices and timing for treatment a relevant issue. The objective of this study was to investigate the effect of unilateral carpal tunnel release on the non-operated contralateral hand.

## Material and methods

From 2016 to 2017, we recruited 186 patients, 155 women (83%) and 31 men (17%) with a mean age of 57 years, presenting to our department with bilateral CTS for carpal tunnel surgery. The study was approved by the medical

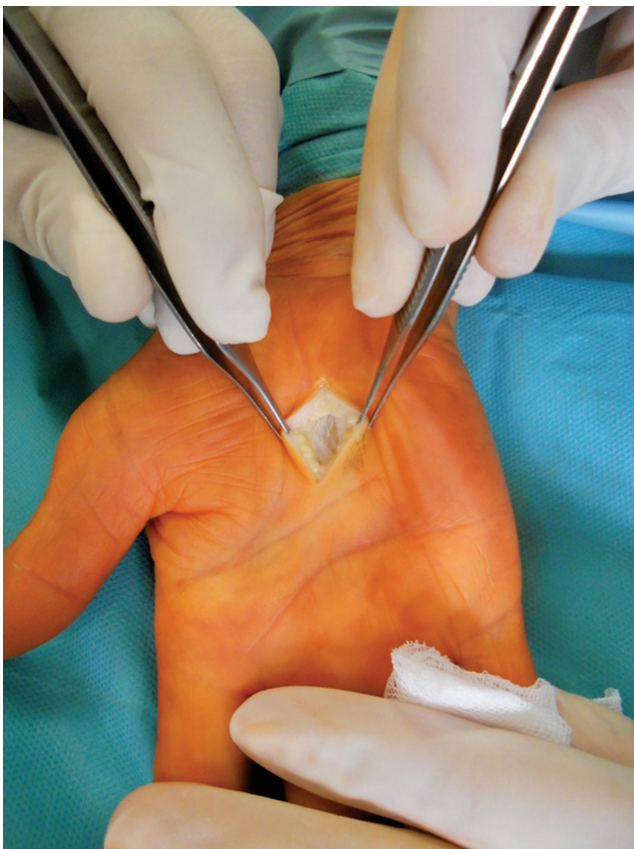


Fig. 1. Incision for mini-invasive carpal tunnel release



Fig. 2. View of the operation site after dissection of the flexor retinaculum. Note scissors inside the carpal tunnel

research and ethics committee of the Pomeranian Medical University in Szczecin, Poland. The diagnosis of CTS was made on the basis of clinical findings and the results of electrodiagnostic tests, which were positive in both hands of all the patients. Patients presenting with comorbidities such as diabetes, rheumatoid arthritis or a history of hypothyroidism were not excluded. The preoperative measurements included subjective pain intensity on a numeric rating scale (NRS), digital sensibility using Semmes–Weinstein filaments, grip strength with a Jamar dynamometer, and the Levine questionnaire. The objective measurements (digital sensibility and grip strength) were performed in both hands at the time of the 1<sup>st</sup> operation and 3 months later, before the 2<sup>nd</sup> operation. The patients underwent mini-invasive carpal tunnel release in one hand, under local anesthesia, with the use of a tourniquet (Fig. 1,2). Upon discharge, each patient's next hand operation was scheduled for a date 2–4 months after the first one (mean: 3 months). Of the 186 patients who underwent operation on one hand, 170 (91%) were admitted to the hospital for surgery to the other hand. The same measurements were performed as prior to the first operation. The results of these measurements were compared. The statistical significance of differences in outcomes was examined using the Mann–Whitney U test for non-normal distribution of variables.

## Results

All the subjective variables were significantly better in the hand which was scheduled for operation than the second one (Table 1). Pain intensity was lower by a mean of 0.8 on the NRS; the Levine symptom and function scores were lower by means of 0.7 and 0.3, respectively. The patients were also asked if they could feel any improvement in the second hand scheduled for operation. One hundred and nine patients (64%) reported improvement, 40 (23%) noted no change and 21 (13%) deterioration. Of the 16 patients who did not present for the 2<sup>nd</sup> operation, 11 were located and responded to the survey by telephone. Among them, 7 patients reported improvement in the non-operated hand and declined further surgery; 4 others postponed surgery for non-medical reasons.

A minimal clinically important difference (MCID) is the smallest change in an outcome measure that is clinically meaningful (relevant to the patient), and not simply statistically significant. Based on our systematic analysis of the literature, an improvement of (roughly) 1.0 point on both the symptom severity score (SSS) and functional system score (FSS) is considered a minimal clinically important difference.<sup>19</sup> Based on the mean values of the SSS scores in our study, the reductions of symptoms in the non-operated hand, although statistically significant, did not reach clinical relevance. However, 109 patients (64%) experienced and declared improvement in the non-operated hand at the time of admission for 2<sup>nd</sup> operation. Answering direct question, these 64% of the patients confirmed that the reduction in their symptoms was clinically relevant for them. However, none of them opted for splint or steroid injection, mostly because they considered this improvement transient.

## Discussion

The results of this study show spontaneous clinical improvement in the non-operated hand in 64% of patients suffering from bilateral CTS, after contralateral carpal tunnel release. This effect was detected at the time of the patients' admission to the hospital for surgery on the other hand,

at a mean of 3 months after the 1<sup>st</sup> operation. It was not clearly determined when after the operation the symptoms started to withdraw, but in 1 study this beneficial effect was observed as early as 2 days postoperatively.<sup>1</sup>

Literature about this phenomenon is very scarce. Yoon et al. reported that in 15 of 20 patients with bilateral CTS, symptoms in the non-operated hand subsided within 1 year following surgery; this, however, did not translate into improvement in electrodiagnostic studies.<sup>14</sup> Unno et al. reported significant reduction of pain, nocturnal symptoms and paresthesia on the non-operated side 6 months after the operation in 58 of 69 patients (84%). At 12 months, 51 (74%) of these patients reported minimal or no remaining symptoms in the non-operated hand. Only 13 of them (19%) had carpal tunnel surgery on the other hand during the observation period. Electrophysiological tests on the non-operated hand were not repeated.<sup>15</sup> Conversely, the authors of another study found no improvement in the non-operated hand 6 months after unilateral surgery.<sup>16</sup>

Several hypotheses have been proposed to explain this phenomenon.<sup>20–28</sup> The results of studies on animal models have suggested that chronic neuropathic pain might use different transmission patterns than acute, somatic pain. Nociceptive stimulation may be conducted diffusely, involving the somatosensory cortex bilaterally, and this may translate as perception of pain in the contralateral extremity.<sup>29</sup> The same mechanism may be responsible for an experience of pain cessation in both extremities after intervention performed on only one. "Immune activation" of peripheral nerves may also be involved in the development of pathological "mirror allodynia" in the contralateral extremity after experimental inflammatory neuritis was induced in an ipsilateral one. These animal models suggest that complex neuro-humoral and immune responses might regulate induction (and cessation) of nociceptive signals in a way that is still poorly understood.<sup>16,29</sup>

## Conclusions

Regardless of the reasons for improvement, this study demonstrates that 64% of patients feel partial relief in the non-operated hand. A weak point in this study

**Table 1.** Comparison of variables prior to operations on the first compared to the second hand

Parameter	First hand n = 186		Second hand n = 170		p-value
	mean	SD	mean	SD	
Pain intensity (NRS, range: 0–10)	6.4	3.0	5.6	3.0	0.01
Sensory Index (range: 1–5)	3.4	0.8	3.6	1.0	0.03
Total grip strength [kg]	17.7	10.4	18.5	10.0	0.34
Levine symptom score	3.2	0.6	2.5	0.8	0.001
Levine function score	3.2	0.7	2.9	0.8	0.007

SD – standard deviation; NRS – numeric rating scale.




is that the results of our measurements might be partially attributed to the patients' preference for having surgery on the more symptomatic hand first. Another possible explanation may include a reduction in activity and repetitive work done by the non-operated hand as an effect of functional improvement in the operated hand. In this study design, we cannot exclude influence of these factors.

### ORCID iDs

Andrzej Żyluk  <https://orcid.org/0000-0002-8299-4525>

Paweł Dec  <https://orcid.org/0000-0002-8514-3259>

Piotr Puchalski  <https://orcid.org/0000-0002-0865-1647>

### References

- Mitake T, Iwatsuki K, Hirata H. Differences in characteristics of carpal tunnel syndrome between male and female patients. *J Orthop Sci*. 2019;S0949-2658(19)30339-2. doi:10.1016/j.jos.2019.10.017
- Zyluk-Gadowska P, Zyluk A. Factors affecting the outcomes of carpal tunnel surgery: A review. *Handchir Mikrochir Plast Chir*. 2016;48:260–265.
- Zyluk A, Zyluk-Gadowska P, Kolodziej L, Szlosser Z. An analysis of patient's and disease related factors predictive of the outcomes of surgery for carpal tunnel syndrome. *Handchir Mikrochir Plast Chir*. 2020;52:11–17.
- Alimohammadi E, Bagheri SR, Hadidi H, Rizevandi P, Abdi A. Carpal tunnel surgery: Predictors of clinical outcomes and patients' satisfaction. *BMC Musculoskelet Disord*. 2020;21:51.
- Jenkins PJ, Watts AC, Duckworth AD, McEachan JE. Socioeconomic deprivation and the epidemiology of carpal tunnel syndrome. *J Hand Surg Eur Vol*. 2012;37(2):123–129.
- Zyluk A, Walaszek I, Szlosser Z. No correlation between sonographic and electrophysiological parameters in carpal tunnel syndrome. *J Hand Surg Eur Vol*. 2014;39(2):161–166.
- Zyluk A, Walaszek I. The effect of the involvement of the dominant or non-dominant hand on grip/pinch strengths and the Levine score in patients with carpal tunnel syndrome. *J Hand Surg Eur Vol*. 2012;37(5):427–431.
- Bagatur AE, Zorer G. The carpal tunnel syndrome is a bilateral disorder. *J Bone Joint Surg Br*. 2001;83(5):655–658.
- Dec P, Zyluk A. Bilateral carpal tunnel syndrome: A review. *Neurol Neurochir Pol*. 2018;52(1):79–83.
- Moser VL, Krimmer H, Lanz U. Bilateral carpal tunnel syndrome with familial accumulation. *Handchir Mikrochir Plast Chir*. 2005;37:176–178.
- Alford JW, Weiss AP, Akelman E. The familial incidence of carpal tunnel syndrome in patients with unilateral and bilateral disease. *Am J Orthop (Belle Mead NJ)*. 2004;33(8):397–400.
- Padua L, Padua R, Nazzaro M, Tonali P. Incidence of bilateral symptoms in carpal tunnel syndrome. *J Hand Surg Br*. 1998;23(5):603–606.
- Unglaub F, Wolf MB, Dragu A, Horch RE. Bilateral atypical muscles causing acute bilateral carpal tunnel syndrome in recreational climber. *Arch Orthop Trauma Surg*. 2010;130(1):37–40.
- Zhang D, Janssen SJ, Blazar P, Earp BE. Predictors of future contralateral carpal tunnel release at the time of unilateral surgery. *J Hand Surg Am*. 2019;44(9):e800–e809.
- Yoon ES, Kwon HK, Lee HJ, Ahn DS. The outcome for the non-operated contralateral hand in carpal tunnel syndrome. *Ann Plast Surg*. 2001;47(1):20–24.
- Unno F, Lucchina S, Bosson D, Fusetti C. Immediate and durable clinical improvement in the non-operated hand after contralateral surgery for patients with bilateral carpal tunnel syndrome. *Hand (N Y)*. 2015;10(3):381–387.
- Afshar A, Yekta Z, Mirzatoeuei F. Clinical course of the non-operated hand in patients with bilateral idiopathic carpal tunnel syndrome. *J Hand Surg Am*. 2007;32(8):1166–1170.
- Puchalski P, Zyluk A, Zyluk-Gadowska P. An analysis of the course of carpal tunnel syndrome before operation. *Acta Orthop Belg*. 2017;83(1):22–29.
- Rodrigues JN, Mabvuure NT, Nikkhah D, Shariff Z, Davis TR. Minimal important changes and differences in elective hand surgery. *J Hand Surg Eur Vol*. 2015;40(9):900–912.
- Fernández-de-las-Peñas C, de la Llave-Rincón AI, Fernández-Carnero J, Cuadrado ML, Arendt-Nielsen L, Pareja JA. Bilateral widespread mechanical pain sensitivity in carpal tunnel syndrome: Evidence of central processing in unilateral neuropathy. *Brain*. 2009;132(Pt 6):1472–1479.
- Zambelis T, Tsvigoulis G, Karandreas N. Carpal tunnel syndrome: Associations between risk factors and laterality. *Eur Neurol*. 2010;63(1):43–47.
- Mellet E, Mazoyer B, Leroux G, Joliot M, Tzourio-Mazoyer N. Cortical asymmetries during hand laterality task vary with hand laterality: A f-MRI study in 295 participants. *Front Hum Neurosci*. 2016;10:628.
- Fornander L, Nyman T, Hansson T, Brismar T, Engström M. Inter-hemispheric plasticity in patients with median nerve injury. *Neurosci Lett*. 2016;628:59–66.
- Maeda Y, Kettner N, Kim J, et al. Primary somatosensory/motor cortical thickness distinguishes paresthesia-dominant from pain-dominant carpal tunnel syndrome. *Pain*. 2016;157(5):1085–1093.
- Tecchio F, Padua L, Aprile I, Rossini PM. Carpal tunnel syndrome modifies sensory hand cortical somatotopy: A MEG study. *Hum Brain Mapp*. 2002;17(1):28–36.
- Druschky K, Kaltenhäuser M, Hummel C, et al. Alteration of the somatosensory cortical map in peripheral mononeuropathy due to carpal tunnel syndrome. *Neuroreport*. 2000;11(17):3925–3930.
- Dhond RP, Ruzich E, Witzel T, et al. Spatio-temporal mapping cortical neuroplasticity in carpal tunnel syndrome. *Brain*. 2012;135(10):3062–3073.
- Maeda Y, Kettner N, Holden J, et al. Functional deficits in carpal tunnel syndrome reflect reorganization of primary somatosensory cortex. *Brain*. 2014;137(6):1741–1752.
- Chacur M, Milligan ED, Gazda LS, et al. A new model of sciatic inflammatory neuritis (SIN): Induction of unilateral and bilateral mechanical allodynia following acute unilateral peri-sciatic immune activation in rats. *Pain*. 2001;94(3):231–244.



# Radiation dose and repeatability of aortic valve measurement by multidetector row computed tomography to assess eligibility for transcatheter aortic valve implantation

Bartłomiej Kędzierski<sup>1,A–D,F</sup>, Paweł Gać<sup>1,2,A–D,F</sup>, Martyna Głośna<sup>1,B,F</sup>, Rafał Poręba<sup>3,A,C,E,F</sup>, Krystyna Pawlas<sup>2,E,F</sup>

<sup>1</sup> Centre for Diagnostic Imaging, 4<sup>th</sup> Military Hospital, Wrocław, Poland

<sup>2</sup> Department of Hygiene, Wrocław Medical University, Poland

<sup>3</sup> Department of Internal Medicine, Occupational Diseases and Hypertension, Wrocław Medical University, Poland

A – research concept and design; B – collection and/or assembly of data; C – data analysis and interpretation; D – writing the article; E – critical revision of the article; F – final approval of the article

Advances in Clinical and Experimental Medicine, ISSN 1899–5276 (print), ISSN 2451–2680 (online)

*Adv Clin Exp Med.* 2020;29(8):983–992

## Address for correspondence

Paweł Gać

E-mail: pawelgac@interia.pl

## Funding sources

None declared

## Conflict of interest

None declared

Received on September 23, 2019

Reviewed on May 17, 2020

Accepted on June 7, 2020

Published online on August 27, 2020

## Abstract

**Background.** Aortic valve stenosis is among the most common valvular defects in developed countries. In the assessment of eligibility for transcatheter aortic valve implantation (TAVI), multidetector row computed tomography (MDCT) is performed to determine the precise dimensions of the aortic valve, the topography of the aortic ostium and the ability to use various arterial access routes.

**Objectives.** To evaluate the relationships between the radiation dose and the repeatability of measurements of dimensions of the aortic valve in MDCT performed before TAVI.

**Material and methods.** The study involved a group of 60 consecutive patients undergoing MDCT before TAVI. The radiation dose was expressed as computed tomography dose index volume (CTDIvol) and dose length product (DLP). The coefficient of variation (CV) of each measurement was defined as the standard deviation (SD) of the measurements/mean measurement  $\times$  100%, based on the measurements performed independently by 2 radiologists.

**Results.** A statistically significant negative linear correlation was observed between the DLP value of the MDCT before TAVI, and the CV of the measurement of the minimum dimension of the aortic annulus ( $r = -0.25$ ;  $p < 0.05$ ). Lower DLP doses of the MDCT before TAVI constitute an independent factor associated with a higher CV for the measurement of the minimum dimension of the aortic annulus.

**Conclusions.** It is proposed that tests using lower radiation doses should be followed by an assessment of the degree of repeatability of the aortic valve sizing.

**Key words:** aortic valve, coefficient of variation, radiation dose, TAVI, repeatability of measurement

## Cite as

Kędzierski B, Gać P, Głośna M, Poręba R, Pawlas K. Radiation dose and repeatability of aortic valve measurement by multidetector row computed tomography to assess eligibility for transcatheter aortic valve implantation. *Adv Clin Exp Med.* 2020;29(8):983–992. doi:10.17219/acem/123624

## DOI

10.17219/acem/123624

## Copyright

© 2020 by Wrocław Medical University

This is an article distributed under the terms of the Creative Commons Attribution 3.0 Unported (CC BY 3.0) (<https://creativecommons.org/licenses/by/3.0/>)

## Introduction

Aortic valve stenosis is among the most common valvular defects in developed countries.<sup>1</sup> The treatment of choice in patients with severe aortic stenosis is implantation of a prosthetic aortic valve.<sup>2</sup> For a large group of elderly patients with a significant burden of comorbidities, the risk of classic cardiosurgical aortic valve replacement is too high. The solution in these patients is transcatheter (transcatheter) aortic valve implantation (TAVI).<sup>3,4</sup> In the assessment of eligibility for TAVI, standard imaging tests are performed to determine the precise dimensions of the aortic valve, the topography of the aortic ostium and the ability to use various arterial access routes. Currently, the standard examination is multidetector row computed tomography (MDCT) of the heart and large vessels.<sup>5,6</sup>

Computed tomography (CT) scans expose patients to ionizing radiation. Due to a direct effect on the double DNA helix, and – as a result of water radiolysis – the formation of free oxygen radicals interacting with the DNA (i.e., an indirect effect), ionizing radiation causes modifications in the cellular genetic material that may be associated with deterministic and stochastic consequences.<sup>7</sup> Following the principles established by the International Commission on Radiological Protection (ICRP), no procedure involving radiation exposure should be performed unless it provides sufficient benefits to the exposed patients or society, outweighing the radiation-induced damage to the health related to this procedure. If the benefit-to-harm balance associated with procedures using ionizing radiation is positive, it is necessary to find a way to optimize the radiation dose.<sup>8</sup> Following the rules of radiological protection and the ALARA principle (as low as reasonably achievable), the ionizing radiation dose should preferably be reduced during those procedures using this form of radiation. An adequate level of quality for the diagnostic images should be maintained; however, if a minor loss of quality allows the radiation dose to be reduced, it is justified.<sup>9,10</sup>

Minimizing the radiation for those studies involving high doses, such as CT of the heart and large vessels during the assessment for TAVI, is particularly important, as there is a direct relationship between the radiation dose and the risk of stochastic consequences from the ionizing radiation.<sup>11</sup> However, the costs associated with reduced exposure due to the use of lower exposure doses increase disproportionately to the degree of effective dose reduction.<sup>12</sup> Therefore, it is not socially justified or economically profitable to avoid every small risk. Therefore, efforts should be focused on optimizing high and moderate doses.

It may be interesting to determine whether or not the attempt to decrease the dose used in MDCT studies during the assessment of eligibility for TAVI would result in an overly significant reduction in scan quality, in this case defined primarily as reduced repeatability of aortic valve sizing. To achieve this goal, the hypothesis

regarding the relationship between the ionizing radiation dose in standard MDCT examinations and the repeatability of aortic valve sizing needs to be verified.

## Study purpose

The aim of the study was to assess the relationships between the ionizing radiation dose and the repeatability of the aortic dimension measurements using MDCT, as part of a standard assessment of eligibility for TAVI.

## Material and methods

### Study group

The study involved a group of 60 consecutive patients, who received MDCT of the heart and large vessels as part of the eligibility assessment for TAVI in the years 2012–2016. The mean age of the subjects was  $79.60 \pm 9.17$  years, and mean body mass index (BMI) was  $27.85 \pm 3.99$  kg/m<sup>2</sup>. In the study, 63.3% of the subjects were males and 36.7% were females. Only 25.0% of the subjects had normal body weight, 51.7% were overweight and 23.3% were obese. The clinical characteristics of the study group are presented in Table 1.

### Study design

The study was part of the project “Possible optimization of ionizing radiation dose in computed tomography studies during the eligibility assessment for transcatheter aortic valve implantation”. The study protocol was approved by the local bioethics committee (approval No. KB 198/2018). Clinical data of all the subjects were collected, and all the patients received a MDCT examination of the heart and large vessels.

### Basic anthropometric parameters

The BMI was calculated using the following formula:  $BMI = \text{body weight [kg]} / \text{height [m]}^2$ . Body surface area (BSA) was derived on the basis of the DuBois formula:  $BSA = 0.007184 \times \text{body weight [kg]}^{0.425} \times \text{height [cm]}^{0.725}$ . Normal body weight was defined as  $BMI < 25$  kg/m<sup>2</sup>, overweight was defined as  $BMI 25–29.9$  kg/m<sup>2</sup> and obesity was defined as  $BMI \geq 30$  kg/m<sup>2</sup>.

### MDCT studies

All the MDCT examinations of the heart and large vessels during the eligibility assessment for TAVI were performed using a SOMATOM Definition Dual-Source CT scanner (Siemens Healthcare, Kemnath, Germany), following a standardized angiography protocol. The study protocol included a topogram, pre-monitoring and monitoring

**Table 1.** Clinical characteristics of the study group (n = 60)

Variable	X	Me	Min	Max	SD
Age [years]	79.60	82.00	44.00	95.00	9.17
Height [cm]	169.55	170.00	148.00	186.00	8.08
Body mass [kg]	80.10	80.00	52.00	112.00	12.84
BMI [kg/m <sup>2</sup> ]	27.85	28.32	19.27	37.38	3.99
BSA [m <sup>2</sup> ]	1.91	1.93	1.50	2.30	0.17
Gender, n (%)					
men			38 (63.3)		
women			22 (36.7)		
Body mass, n (%)					
normal body mass			15 (25.0)		
overweight			31 (51.7)		
obesity			14 (23.3)		

BMI – body mass index; BSA – body surface area; Max – maximum value; Min – minimum value; n – number of patients; SD – standard deviation; X – arithmetic mean.

at the level of tracheal bifurcation, with acquisition triggered by the required contrast enhancement of the region of interest (ROI) in the ascending aorta, an electrocardiography (ECG)-gated thoracic arterial phase angiography, and a non-ECG-gated angiography of the abdominal and pelvic arteries. The basic technical parameters of the angiographic phases included: craniocaudal direction of image acquisition, spiral method of image acquisition, study scope from the pulmonary apexes to half the length of the femoral shafts, layer collimation of 0.6 mm, exposure kilovoltage of 120 units, and variable mAs values. The examination involved an intravenous administration of a contrast medium at a volume determined by the patient's body weight. Between 90 mL and 120 mL of iodine-based, non-ionic contrast medium was administered using an automatic syringe into the veins in the cubital fossa with infusion rate of 4.0 mL/s. Reconstructions were performed in axial orientations, in layers of 3.0 mm and 0.75 mm, and secondary multi-planar reconstructions (MPRs) were obtained in the coronal and sagittal planes, using maximum intensity projection (MIP) and volume rendering technique (VRT) algorithms.

## Ionizing radiation dose

The ionizing radiation dose was determined by recording automated measurements performed using CT. The radiation dose was expressed as computed tomography dose index volume (CTDI<sub>vol</sub>) and dose length product (DLP) for the thoracic arterial phase MDCT.

## Aortic valve assessment

The CT scans of the heart and large vessels were analyzed in terms of assessing the aortic valve and aortic root sizing, topography of the aortic ostium and the possibility to use various arterial access routes during the TAVI procedure. The tests were evaluated following the recommendations of the Society of Cardiovascular Computed

Tomography expert consensus document on CT imaging before TAVI/transcatheter aortic valve replacement (TAVR).<sup>6</sup> For the purpose of this project, the tests were assessed independently by 2 radiologists with 7 and 10 years of experience in the assessment of CT heart scans, respectively. The assessment involved the following parameters of the aortic valve and root: type of valve (number of leaflets); maximum, minimum and mean dimension of the aortic annulus; maximum, minimum and mean dimension of the aortic root and its height; and distance between the left and the right coronary artery ostia and the aortic annulus (Fig. 1A–F). All the measurements were expressed in millimeters to an accuracy of 0.1 mm.

## Assessment of the repeatability of measurements

The analysis of repeatability of the measurements involved the following quantitative variables, calculated on the basis of the measurement of the aortic valve and aortic root parameters, performed independently by 2 radiologists experienced in the evaluation of the cardiovascular system: measurement mean (X), standard deviation (SD), absolute difference (AD), relative difference (RD), and coefficient of measurement variation (CV). The following mathematical formulas were used to calculate the above characteristics of measurement repeatability: AD = |measurement 1 – measurement 2|; RD = AD of the measurement/X of the measurement; CV = SD of the measurement/X of the measurement × 100%. Absolute difference was expressed in mm, RD had no unit, and CV was expressed as percentage.

## Subgroups

In the comparative analyses of the studied group of MDCT examinations conducted to assess eligibility for TAVI, the following subgroups were distinguished, based on the median CTDI<sub>vol</sub> and DLP values for



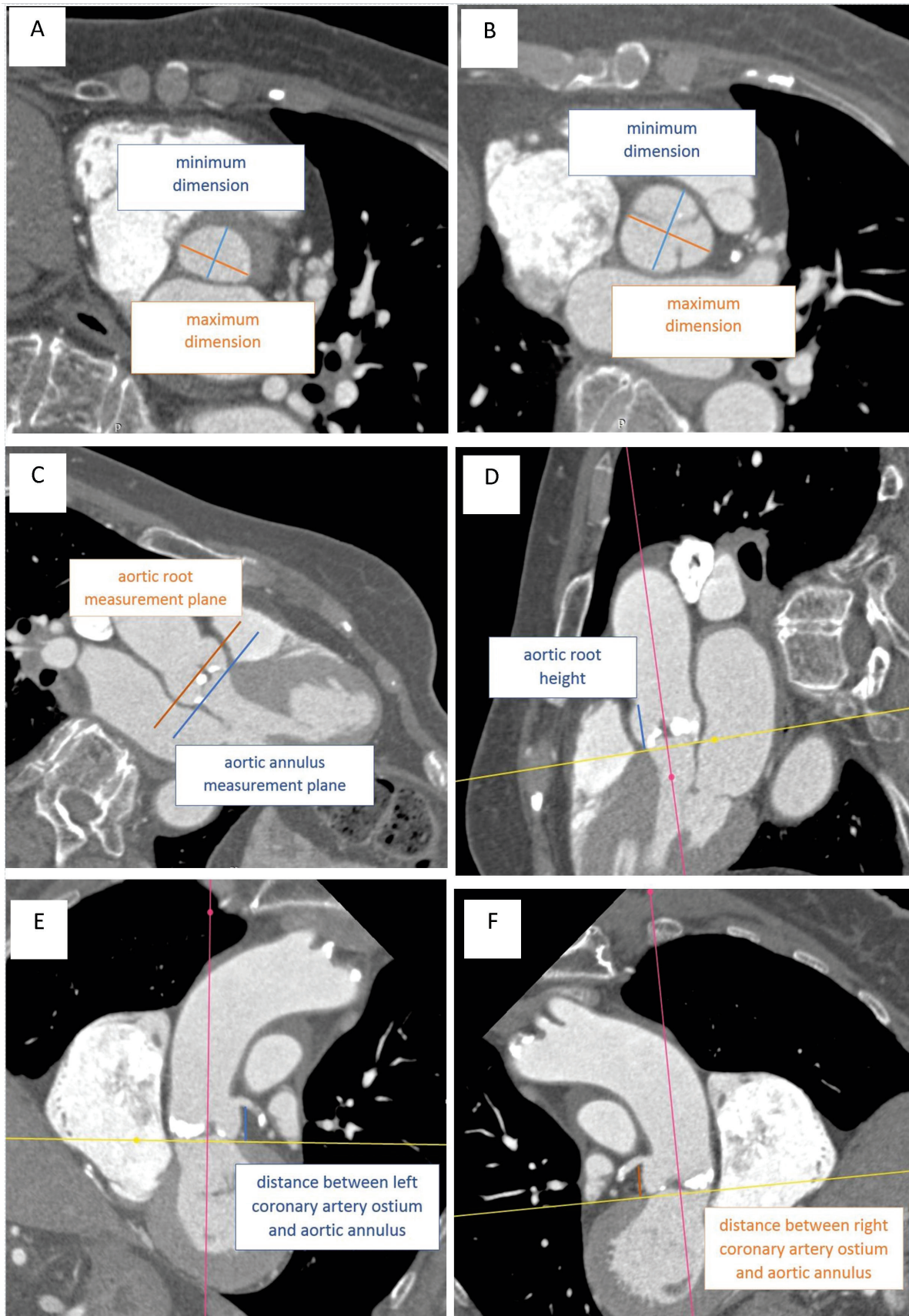


Fig. 1. Computed tomography aortic valve measurements: A) maximum and minimum dimension of the aortic annulus (mean dimension of the aortic annulus = (maximum dimension of the aortic annulus + minimum dimension of the aortic annulus)/2); B) maximum and minimum dimension of the aortic root (mean dimension of the aortic root = (maximum dimension of the aortic root + minimum dimension of the aortic root)/2); C) aortic annulus and aortic root measurement planes; D) height of the aortic root; E) distance between the left coronary artery ostium and the aortic annulus; F) distance between the right coronary artery ostium and the aortic annulus

the thoracic arterial phase of the MDCT. Based on the median CTDIvol (43.92 mGy), a low CTDIvol (CTDIvol < Me, n = 30) and a high CTDIvol (CTDIvol ≥ Me, n = 30) subgroup were identified. Considering the median DLP (1143.00 mGy), a low DLP (DLP < Me, n = 29) and a high DLP (DLP ≥ Me, n = 31) subgroup were identified.

## Statistical analysis

Statistical analyses were conducted using Dell Statistica v. 13 software (Dell Inc., Austin, USA). The quantitative variables were characterized with arithmetic means, medians, maximum and minimum values, and SD. The distribution of the variables was verified using the Shapiro–Wilk W test. Due to absence of normal distribution in comparative analyses, the Mann–Whitney U test was used. The results for qualitative variables were characterized by absolute values and percentages. In order to determine the relationships between the analyzed variables, both correlation analysis (2 variables) and multiple regression analyses (more than 2 variables) were conducted. Those results with  $p < 0.05$  were considered statistically significant.

## Results

The mean CTDIvol and DLP values for the thoracic arterial phase of the MDCT during the eligibility assessment for TAVI were  $48.71 \pm 20.33$  mGy and  $1319.98 \pm 613.58$  mGycm, respectively. In the studied population, 93.3%

of the patients had a tricuspid aortic valve, 5% had a bicuspid aortic valve and 1.7% had a quadricuspid aortic valve. The mean dimensions of the aortic annulus and the aortic root were  $24.44 \pm 2.50$  mm and  $32.20 \pm 3.95$  mm, respectively. The complete results of aortic valve assessment in the MDCT tests for TAVI in the studied group of patients are presented in Table 2.

The analysis of repeatability of aortic valve measurements in the MDCT tests assessing the eligibility for TAVI in the studied subjects showed the greatest absolute measurement difference in the distance between the left coronary artery ostium and the aortic annulus ( $1.77 \pm 0.96$  mm), whereas the smallest absolute measurement difference was found in the mean dimension of the aortic annulus ( $0.97 \pm 0.60$  mm). The greatest relative measurement difference and the highest CV was observed in the distance between the left coronary artery ostium and aortic annulus ( $0.13 \pm 0.07\%$  and  $9.24 \pm 5.17\%$ , respectively). The smallest relative measurement difference and the smallest CV were found in the mean dimension of the aortic root ( $0.03 \pm 0.02\%$  and  $2.39 \pm 1.72\%$ , respectively). The results of the analysis of aortic valve measurement repeatability in the MDCT tests for TAVI in the studied group of patients are presented in Table 3.

A comparative analysis did not reveal any statistically significant differences in the mean values of the parameters characterizing the repeatability of individual aortic valvular measurements between the groups identified based on the median CTDIvol in the thoracic arterial phase of the MDCT examination used to assess the eligibility for TAVI (Table 4).

**Table 2.** Aortic valve assessment in MDCT scans evaluating the eligibility for TAVI in the study group (n = 60)

Variable	n		%		
Number of aortic valve leaflets					
2	3		5.0		
3	56		93.3		
4	1		1.7		
Statistical variable	X	Me	Min	Max	SD
Aortic annulus					
maximum dimension [mm]	27.04	27.00	22.50	35.50	3.05
minimum dimension [mm]	21.84	21.50	17.50	31.00	2.83
mean dimension [mm]	24.44	23.88	20.00	31.50	2.50
Aortic root					
maximum dimension [mm]	33.95	33.75	27.50	45.00	4.16
minimum dimension [mm]	30.44	30.00	18.00	44.50	4.33
mean dimension [mm]	32.20	31.75	24.25	44.75	3.95
height [mm]	21.23	20.75	17.00	29.00	2.71
Distance between a coronary artery ostium and the aortic annulus					
left coronary artery [mm]	13.78	14.00	8.25	18.50	2.47
right coronary artery [mm]	15.06	15.00	10.50	20.50	2.51
Radiation dose					
CTDIvol [mGy]	48.71	43.92	24.60	99.14	20.33
DLP [mGycm]	1319.98	1143.00	420.00	2887.00	613.58

Aortic valve dimensions and distances: mean values of measurements conducted by 2 researchers; CTDIvol – computed tomography dose index volume; DLP – dose length product; Max – maximum value; Min – minimum value; n – number of patients; SD – standard deviation; X – arithmetic mean; TAVI – transcatheter aortic valve implantation; MDCT – multidetector row computed tomography.



**Table 3.** Analysis of repeatability of aortic valve measurements in MDCT scans evaluating the eligibility for TAVI in the study group (n = 60).

Variable	Measurement 1 [mm]	Measurement 2 [mm]	Measurement X [mm]	Measurement SD [mm]	Measurement AD [mm]	Measurement RD	Measurement CV [%]
Aortic annulus							
Maximum dimension	26.72 ±3.11	27.37 ±3.15	27.04 ±3.05	0.95 ±0.53	1.35 ±0.76	0.05 ±0.03	3.58 ±2.12
Minimum dimension	21.60 ±2.78	22.08 ±3.05	21.84 ±2.83	0.84 ±0.63	1.18 ±0.89	0.05 ±0.04	3.83 ±2.92
Mean dimension	24.16 ±2.57	24.73 ±2.53	24.44 ±2.50	0.68 ±0.42	0.97 ±0.60	0.04 ±0.02	2.81 ±1.74
Aortic root							
Maximum dimension	33.48 ±4.18	34.42 ±4.28	33.95 ±4.16	1.01 ±0.66	1.43 ±0.93	0.04 ±0.03	3.03 ±2.00
Minimum dimension	30.45 ±4.35	30.43 ±4.46	30.44 ±4.33	0.93 ±0.73	1.32 ±1.03	0.05 ±0.04	3.20 ±2.59
Mean dimension	31.97 ±3.98	32.43 ±4.01	32.20 ±3.95	0.74 ±0.49	1.04 ±0.69	0.03 ±0.02	2.39 ±1.72
Height	21.87 ±2.80	20.60 ±2.84	21.23 ±2.71	1.24 ±0.71	1.75 ±1.01	0.08 ±0.05	5.87 ±3.34
Distance between coronary artery ostium and aortic annulus							
Left coronary artery	14.43 ±2.73	13.12 ±2.44	13.78 ±2.47	1.25 ±0.68	1.77 ±0.96	0.13 ±0.07	9.24 ±5.17
Right coronary artery	14.47 ±2.58	15.65 ±2.73	15.06 ±2.51	1.24 ±0.79	1.75 ±1.11	0.12 ±0.07	8.29 ±5.22

Values are expressed as mean ± standard deviation (SD); AD – absolute difference; CV – coefficient of variation; RD – relative difference; X – arithmetic mean; TAVI – transcatheter aortic valve implantation; MDCT – multidetector row computed tomography.

**Table 4.** Analysis of repeatability of aortic valve measurements in MDCT scans evaluating the eligibility for TAVI in subgroups identified based on median CTDIvol

Variable		Low CTDIvol (CTDIvol < Me, n = 30)	High CTDIvol (CTDIvol ≥ Me, n = 30)	p-value
Aortic annulus				
Maximum dimension	measurement AD [mm]	1.33 ±0.76	1.37 ±0.76	0.866
	measurement RD	0.05 ±0.03	0.05 ±0.03	0.878
	measurement CV [%]	3.63 ±2.18	3.54 ±2.10	0.878
Minimum dimension	measurement AD [mm]	1.17 ±0.91	1.20 ±0.89	0.886
	measurement RD	0.05 ±0.04	0.06 ±0.04	0.801
	measurement CV [%]	3.73 ±2.92	3.93 ±2.96	0.801
Mean dimension	measurement AD [mm]	0.88 ±0.52	1.05 ±0.66	0.282
	measurement RD	0.04 ±0.02	0.04 ±0.03	0.290
	measurement CV [%]	2.57 ±1.50	3.05 ±1.95	0.290
Aortic root				
Maximum dimension	measurement AD [mm]	1.47 ±0.94	1.40 ±0.93	0.783
	measurement RD	0.05 ±0.03	0.04 ±0.03	0.458
	measurement CV [%]	3.22 ±2.19	2.83 ±1.81	0.458
Minimum dimension	measurement AD [mm]	1.40 ±0.93	1.23 ±1.14	0.537
	measurement RD	0.05 ±0.03	0.04 ±0.04	0.510
	measurement CV [%]	3.42 ±2.34	2.97 ±2.84	0.510
Mean dimension	measurement AD [mm]	1.17 ±0.75	0.92 ±0.62	0.163
	measurement RD	0.04 ±0.03	0.03 ±0.02	0.147
	measurement CV [%]	2.71 ±1.91	2.07 ±1.47	0.147
Height	measurement AD [mm]	1.87 ±1.05	1.63 ±0.96	0.374
	measurement RD	0.09 ±0.05	0.08 ±0.04	0.449
	measurement CV [%]	6.20 ±3.61	5.54 ±3.08	0.449
Distance between the coronary artery ostium and the aortic annulus				
Left coronary artery	measurement AD [mm]	1.82 ±0.97	1.72 ±0.97	0.691
	measurement RD	0.13 ±0.07	0.13 ±0.08	0.827
	measurement CV [%]	9.10 ±5.11	9.39 ±5.32	0.827
Right coronary artery	measurement AD [mm]	1.60 ±1.16	1.90 ±1.06	0.301
	measurement RD	0.11 ±0.08	0.13 ±0.07	0.234
	measurement CV [%]	7.48 ±5.35	9.10 ±5.04	0.234

Values are expressed as mean ± standard deviation (SD); AD – absolute difference; CTDIvol – computed tomography dose index volume; TAVI – transcatheter aortic valve implantation; MDCT – multidetector row computed tomography; CV – coefficient of variation; RD – relative difference.

**Table 5.** Analysis of repeatability of aortic valve measurements in MDCT scans evaluating the eligibility for TAVI in subgroups identified based on median DLP

Variable		Low DLP (DLP < Me, n = 29)	High DLP (DLP ≥ Me, n = 31)	p-value
Aortic annulus				
Maximum dimension	measurement AD [mm]	1.38 ±0.78	1.32 ±0.75	0.774
	measurement RD	0.05 ±0.03	0.05 ±0.03	0.782
	measurement CV [%]	3.66 ±2.23	3.51 ±2.06	0.782
Minimum dimension	measurement AD [mm]	1.38 ±0.98	1.00 ±0.77	0.100
	measurement RD	0.06 ±0.05	0.05 ±0.03	0.121
	measurement CV [%]	4.44 ±3.27	3.26 ±2.47	0.121
Mean dimension	measurement AD [mm]	0.97 ±0.63	0.97 ±0.58	0.989
	measurement RD	0.04 ±0.03	0.04 ±0.02	0.833
	measurement CV [%]	2.76 ±1.84	2.86 ±1.68	0.833
Aortic root				
Maximum dimension	measurement AD [mm]	1.41 ±0.87	1.45 ±0.99	0.876
	measurement RD	0.04 ±0.03	0.04 ±0.03	0.831
	measurement CV [%]	3.09 ±2.08	2.97 ±1.96	0.831
Minimum dimension	measurement AD [mm]	1.38 ±1.08	1.26 ±1.00	0.654
	measurement RD	0.05 ±0.04	0.04 ±0.03	0.600
	measurement CV [%]	3.38 ±2.77	3.02 ±2.44	0.600
Mean dimension	measurement AD [mm]	1.35 ±0.68	0.73 ±0.65	0.018 *
	measurement RD	0.05 ±0.03	0.02 ±0.02	0.020 *
	measurement CV [%]	2.90 ±1.81	1.88 ±1.49	0.020 *
Height	measurement AD [mm]	1.84 ±1.11	1.66 ±0.91	0.485
	measurement RD	0.09 ±0.05	0.08 ±0.04	0.441
	measurement CV [%]	6.22 ±3.73	5.55 ±2.97	0.441
Distance between the coronary artery ostium and the aortic annulus				
Left coronary artery	measurement AD [mm]	1.74 ±1.07	1.79 ±0.86	0.846
	measurement RD	0.12 ±0.07	0.14 ±0.07	0.430
	measurement CV [%]	8.69 ±5.26	9.76 ±5.12	0.430
Right coronary artery	measurement AD [mm]	1.69 ±1.07	1.81 ±1.17	0.689
	measurement RD	0.11 ±0.07	0.12 ±0.08	0.644
	measurement CV [%]	7.96 ±4.74	8.59 ±5.69	0.644

Values are expressed as mean ± standard deviation (SD); \*p < 0.05; AD – absolute difference; DLP – dose length product; CV – coefficient of variation; RD – relative difference; TAVI – transcatheter aortic valve implantation; MDCT – multidetector row computed tomography.

A comparative analysis of the mean values of the parameters characterizing the repeatability of various aortic valve measurements between the subgroups, based on the median DLP for the thoracic arterial phase of the MDCT examination in the assessment of eligibility for TAVI, revealed significant statistical differences regarding the measurement of the mean aortic root dimension. In the low DLP subgroup (DLP value < the median), the absolute measurement difference, the relative measurement difference and the CV in the case of the mean dimension of the aortic valve were significantly higher than in the high DLP subgroup (DLP value ≥ of the median) (Table 5).

A correlation analysis of the investigated group of tests demonstrated statistically significant negative linear correlations between the DLP value in the thoracic arterial phase of the MDCT during the assessment of eligibility for TAVI, and the AD, RD and CV of the measurement of the minimum dimension of the aortic annulus ( $r = -0.26$ ,  $r = -0.25$  and  $r = -0.25$ , respectively;  $p < 0.05$ ). In addition, positive linear correlations were presented between BMI and AD, RD and CV of the measurement of the minimum dimension of the aortic root ( $r = 0.28$ ,  $r = 0.31$  and  $r = 0.31$ , respectively;  $p < 0.05$ ), as well as between BMI and AD,

RD and CV of the distance between the left coronary artery ostium and the aortic annulus ( $r = 0.33$ ,  $r = 0.28$  and  $r = 0.28$ , respectively;  $p < 0.05$ ).

A multiple stepwise forward-regression analysis determined the relationships between the basic anthropological parameters (age, sex, BMI, and BSA) or the parameters characterizing the radiation dose in the thoracic arterial phase of the MDCT examination assessing the eligibility for TAVI (CTDIvol and DLP), and the CVs for the consecutive aortic valve measurements in these tests. The conducted estimations resulted in the following statistically significant models:

- CV of the measurement of the aortic annular minimum dimension =  $5.898 + 0.779$  female –  $0.001$  DLP;
- CV of the measurement of the aortic root minimum dimension =  $-1.789 + 0.206$  BMI +  $1.198$  female;
- CV of the measurement of the distance between the left coronary artery and the aortic annulus =  $4.948 + 0.394$  BMI +  $2.283$  female +  $0.102$  age.

The models obtained in the regression analysis indicate that female sex and lower DLP doses in the thoracic arterial phase of the MDCT used to assess the eligibility for TAVI are factors independently associated with a higher CV for

**Table 6.** Results of multiple regression analysis in the study group (n = 60)**A.** Model of relationship determining the independent predictors of higher CV of the measurement of the aortic annular minimum dimension

Model for: CV of the measurement of the aortic annular minimum dimension			
variable	intercept	female	DLP [mGycm]
Regression coefficient	5.898	0.779	-0.001
SEM of Rc	0.989	0.362	0.001
p-value	<0.001	0.009	0.042

DLP – dose length product; CV – coefficient of variation; SEM – standard error of the mean; Rc – regression coefficient.

**B.** Model of the relationship determining independent predictors of higher CV for the measurement of the aortic root minimum dimension

Model for: CV of the measurement of the aortic root minimum dimension			
variable	intercept	BMI [kg/m <sup>2</sup> ]	female
Regression coefficient	-1.789	0.206	1.198
SEM of Rc	1.262	0.079	0.552
p-value	0.043	0.012	0.041

CV – coefficient of variation; SEM – standard error of the mean; Rc – regression coefficient; BMI – body mass index.

**C.** Model of relationship determining independent predictors of higher CV of the measurement of the distance between the left coronary artery ostium and the aortic annulus

Model for: CV of the measurement of the distance between the left coronary artery ostium and the aortic annulus				
variable	intercept	BMI [kg/m <sup>2</sup> ]	female	age [years]
Regression coefficient	4.948	0.394	2.283	0.102
SEM of Rc	2.603	0.163	1.324	0.031
p-value	0.046	0.008	0.040	0.047

CV – coefficient of variation; SEM – standard error of the mean; Rc – regression coefficient; BMI – body mass index.

the measurement of the minimum dimension of the aortic annulus. Higher BMI and female sex are independently associated with a higher CV for the measurement of the minimal aortic root dimension, whereas higher BMI, female sex and older age are independently associated with a higher CV for the measurement of the distance between the left coronary artery and the aortic annulus. The results of the estimation for significant models obtained in the regression analysis are presented in Table 6.

## Discussion

In analyzing the results of this study, it is impossible to identify unequivocally a relationship between the ionizing radiation dose and repeatability of the aortic dimension measurements using MDCT performed for the standard assessment of eligibility for TAVI. The size of the radiation dose in routine MDCT tests to assess eligibility for TAVI did not affect the repeatability of the aortic valve measurements, which justifies the attempts to perform these tests using lower radiation doses. However, it is important to bear in mind the demonstrated individual statistically significant correlations, i.e., considerably higher absolute measurement difference, relative measurement difference and CV of the mean aortic valve diameter in the low DLP subgroup (DLP values < the median) compared

to the high DLP subgroup (DLP values  $\geq$  the median); statistically significant negative linear relationships between the DLP value and the absolute measurement difference, relative measurement difference and CV for the minimum aortic annular dimension; as well as a lower DLP dose as an independent factor associated with a higher CV for the minimum aortic annular dimension. Therefore, it is suggested that the MDCT tests using lower radiation doses in the assessment of eligibility for TAVI should be followed by a control of the degree of repeatability of the aortic valve sizing measurements. Based on the conducted studies, it is possible to identify groups of patients in which the variations in aortic valve sizing using MDCT may be higher. Regardless of the radiation dose, higher BMI, female sex, and elderly age affect the CV for individual measurements of the aortic valve. It seems that in these groups of patients, greater caution should be taken while performing MDCT tests using lower radiation doses in the assessment of eligibility for TAVI.

It is worth emphasizing that the presented study results are the first scientific attempt to find a relationship between the ionizing radiation dose and repeatability of aortic dimension measurements using MDCT performed for a standard assessment of eligibility for TAVI.

In the available literature, the problem of repeatability of aortic valve sizing using MDCT before a TAVI procedure was mentioned only occasionally. Schmidkonz et al.

demonstrated that MDCT offers repeatable measurements of aortic annulus and aortic root geometry in patients eligible for TAVI. They also revealed that the highest degree of concordance was obtained for the measurements of the aortic annulus diameter estimated secondarily on the basis of the aortic annulus circumference.<sup>13</sup> The study did not compare the repeatability of the aortic annulus circumference measurement; among the analyzed parameters, the highest concordance (the lowest CV) was obtained for the mean diameter of the aortic root.

The comparability of the aortic valve assessment was evaluated much more frequently using other diagnostic methods: echocardiography, CT and magnetic resonance imaging (MRI). A study by Bernhardt et al. compared the usefulness of aortic valve sizing prior to a TAVI procedure using non-contrast enhanced MRI with the gold standard, i.e., MDCT examination. In a group of 52 patients who underwent both tests, it was demonstrated that an MRI examination including a 3D steady-state free-precession sequence covering the entire ascending aorta was highly concordant with aortic annulus assessment using MDCT. The mean aortic annular circumference in the measurement with multi-slice computed tomography (MSCT) was 76.7 ± 6.9 mm, whereas in the MRI test it was 76.5 ± 6.7 mm, with a high correlation coefficient for the measurements ( $r = 0.93$ ,  $p < 0.0001$ ).<sup>14</sup> Husser et al. compared the results of aortic valve assessments in patients eligible for TAVI which had been obtained using 3D transesophageal echocardiography (3D-TEE) with the results obtained with the use of MDCT. Based on the comparison of results in a group of 57 patients, the aortic annular diameters and surface areas assessed using 3D-TEE are clearly lower than those obtained in MSCT, with the exception of diameters measured in the sagittal planes. Only in these planes did both methods determine the final size of the prosthesis with a similar accuracy.<sup>15</sup> Other studies by the same researchers compared the results of aortic valve sizing using 2D transesophageal echocardiography (2D-TEE) with 3D-TEE. They demonstrated that the mean aortic annulus diameters were significantly greater in 3D-TEE than in 2D-TEE, with a mean difference of 1.2 mm. The size of the prosthetic valvular implant was correctly determined based on 67% of 2D-TEE tests and 80% of 3D-TEE tests. Discrepancies between 2D-TEE and 3D-TEE test results were observed in 26% of the analyzed cases.<sup>16</sup> The presented study results seem to demonstrate that the use of TEE for the aortic valve sizing in patients eligible for TAVI is limited. The non-contrast enhanced MRI method is promising, but its accessibility is lower compared to MDCT, and the duration of the test is longer, which may be of key importance for patients with severe aortic stenosis. In this context, the authors believe that it is increasingly important to refine the MDCT method in the assessment of eligibility for TAVI.

In relation to the discussed parameters, the significance of the morphological type of the aortic valve should be

mentioned. In the studied group of patients, 93.3% had a tricuspid aortic valve, 5.0% had a bicuspid aortic valve and 1.7% had a quadricuspid aortic valve. The above distribution is similar to the literature data regarding the frequency of individual aortic valve types. Based on the epidemiological studies, the tricuspid aortic valve is considered to be the most common type (98–99.5% of individuals), the bicuspid valve is found in 0.5–2% of individuals and other types are observed only occasionally.<sup>17</sup> The bicuspid aortic valve is often associated with abnormalities, mainly with a predisposition for aortic stenosis.<sup>18,19</sup> The distribution obtained in the presented study, including 5.0% of patients with bicuspid valves in the group of patients diagnosed with aortic stenosis eligible for a valve replacement procedure, may be considered typical for the population.

This study has certain significant limitations, including a relatively low number of patients participating in the project, a lack of complete clinical characteristics of the patients, including cardiovascular comorbidities and risk factors, considerations related to tests performed using a single tomography scanner, a lack of tests conducted with reduced ionizing radiation doses, a lack of dose determination using size-specific dose estimate (SSDE), a lack of determination of intrapersonal repeatability of the measurements, and the subjective selection of the analyzed aortic valve dimensions. However, the authors believe that these limitations do not undermine the usefulness of the study, which may be considered in further research associated with the presented issue.

## Conclusions


The size of the radiation dose in routine MDCT tests assessing eligibility for TAVI essentially does not affect the repeatability of the aortic valve measurements, which justifies the attempts to perform these tests using lower radiation doses.


Due to the demonstrated individual correlations between the radiation dose in MDCT studies performed during the assessment of eligibility for TAVI and the repeatability of aortic valve sizing, it is proposed that tests at lower radiation doses should be followed by a control of the degree of repeatability of the aortic valve sizing.


### ORCID iDs

Bartłomiej Kędzierski  <https://orcid.org/0000-0002-9109-0368>

Paweł Gać  <https://orcid.org/0000-0001-8366-0239>

Martyna Głońska  <https://orcid.org/0000-0001-9271-7401>

Rafał Poręba  <https://orcid.org/0000-0002-5109-8023>

Krystyna Pawlas  <https://orcid.org/0000-0001-5485-7649>

### References

1. Thaden JJ, Nkomo VT, Enriquez-Sarano M. The global burden of aortic stenosis. *Prog Cardiovasc Dis.* 2014;56(6):565–571.
2. Bajona P, Suri RM, Greason KL, Schaff HV. Outcomes of surgical aortic valve replacement: The benchmark for percutaneous therapies. *Prog Cardiovasc Dis.* 2014;56(6):619–624.

3. Krasopoulos G, Falconieri F, Benedetto U, et al. European real world trans-catheter aortic valve implantation: Systematic review and meta-analysis of European national registries. *J Cardiothorac Surg.* 2016;11(1):159.
4. Davlourous PA, Mplani VC, Koniari I, Tsigkas G, Hahalıs G. Transcatheter aortic valve replacement and stroke: A comprehensive review. *J Geriatr Cardiol.* 2018;15(1):95–104.
5. Debonnaire P, Katsanos S, Delgado V. Computed tomography to improve TAVI outcomes. *EuroIntervention.* 2012;8(5):531–533.
6. Achenbach S, Delgado V, Hausleiter J, Schoenhagen P, Min JK, Leipsic JA. SCCT expert consensus document on computed tomography imaging before transcatheter aortic valve implantation (TAVI)/transcatheter aortic valve replacement (TAVR). *J Cardiovasc Comput Tomogr.* 2012;6(6):366–380.
7. Mettler FA. Medical effects and risks of exposure to ionising radiation. *J Radiol Prot.* 2012;32(1):N9–N13.
8. Vano E. Global view on radiation protection in medicine. *Radiat Prot Dosimetry.* 2011;147(1–2):3–7.
9. Newman B, Callahan MJ. ALARA (as low as reasonably achievable) CT 2011: Executive summary. *Pediatr Radiol.* 2011;41(Suppl 2):453–455.
10. Cohen MD. ALARA, image gently and CT-induced cancer. *Pediatr Radiol.* 2015;45(4):465–470.
11. Niwa O, Barcellos-Hoff MH, Globus RK, et al. ICRP Publication 131: Stem cell biology with respect to carcinogenesis aspects of radiological protection. *Ann ICRP.* 2015;44(3–4):347–357.
12. Kalra MK, Sodickson AD, Mayo-Smith WW. CT radiation: Key concepts for gentle and wise use. *Radiographics.* 2015;35(6):1706–1721.
13. Schmidkonz C, Marwan M, Klinghammer L, et al. Interobserver variability of CT angiography for evaluation of aortic annulus dimensions prior to transcatheter aortic valve implantation (TAVI). *Eur J Radiol.* 2014;83(9):1672–1678.
14. Bernhardt P, Rodewald C, Seeger J, et al. Non-contrast-enhanced magnetic resonance angiography is equal to contrast-enhanced multislice computed tomography for correct aortic sizing before transcatheter aortic valve implantation. *Clin Res Cardiol.* 2016;105(3):273–278.
15. Husser O, Holzamer A, Resch M, et al. Prosthesis sizing for transcatheter aortic valve implantation: Comparison of three dimensional transesophageal echocardiography with multislice computed tomography. *Int J Cardiol.* 2013;168(4):3431–3438.
16. Husser O, Rauch S, Endemann DH, et al. Impact of three-dimensional transesophageal echocardiography on prosthesis sizing for transcatheter aortic valve implantation. *Catheter Cardiovasc Interv.* 2012;80(6):956–963.
17. Ko SM, Song MG, Hwang HK. Bicuspid aortic valve: Spectrum of imaging findings at cardiac MDCT and cardiovascular MRI. *AJR Am J Roentgenol.* 2012;198(1):89–97.
18. Siu SC, Silversides CK. Bicuspid aortic valve disease. *J Am Coll Cardiol.* 2010;55(25):2789–2800.
19. Roberts WC, Ko JM. Frequency by decades of unicuspid, bicuspid, and tricuspid aortic valves in adults having isolated aortic valve replacement for aortic stenosis, with or without associated aortic regurgitation. *Circulation.* 2005;111(7):920–925.



# Clinical outcomes of continuous vs intermittent meropenem infusion for the treatment of sepsis: A systematic review and meta-analysis

Peng Chen<sup>1,A–F</sup>, Fuchao Chen<sup>2,F</sup>, Jiexin Lei<sup>3,F</sup>, Benhong Zhou<sup>1,F</sup>

<sup>1</sup> Department of Pharmacy, Renmin Hospital of Wuhan University, China

<sup>2</sup> Department of Pharmacy, Dongfeng Hospital, Hubei University of Medicine, Shiyan, China

<sup>3</sup> Department of Endocrinology, Renmin Hospital of Wuhan University, China

A – research concept and design; B – collection and/or assembly of data; C – data analysis and interpretation;

D – writing the article; E – critical revision of the article; F – final approval of the article

Advances in Clinical and Experimental Medicine, ISSN 1899–5276 (print), ISSN 2451–2680 (online)

*Adv Clin Exp Med.* 2020;29(8):993–1000

## Address for correspondence

Benhong Zhou

E-mail: benhongzh@whu.edu.cn

## Funding sources

None declared

## Conflict of interest

None declared

Received on September 22, 2018

Reviewed on October 19, 2018

Accepted on May 1, 2020

Published online on August 12, 2020

## Abstract

The antibiotic meropenem is commonly administered to patients with sepsis and septic shock. The aim of this study was to conduct a meta-analysis to evaluate the clinical efficacy and safety of continuous compared to intermittent meropenem infusion for the treatment of sepsis. Electronic databases such as PubMed, EMBASE, Cochrane Library, and China National Knowledge Infrastructure (CNKI) were researched to collect clinical trials comparing continuous and intermittent infusion of meropenem in patients with sepsis. After data extraction and quality assessment of the included studies, Stata v. 12.0 software (Stata Corporation LLC, College Station, USA) was used for a meta-analysis of mortality, clinical cure, microbiological eradication, and safety. Seven studies with a total of 1,191 participants met the inclusion criteria and were included in the meta-analysis. The meta-analysis showed that continuous meropenem infusion was superior to intermittent infusion in terms of mortality (combined risk ratio (RR) = 0.66, 95% confidence interval (95% CI) = 0.46–0.98,  $p = 0.03$ ), clinical cure rate (combined RR = 1.15, 95% CI = 1.02–1.30,  $p = 0.026$ ) and microbiological eradication (combined RR = 1.20, 95% CI = 1.01–1.42,  $p = 0.04$ ), although it may increase the incidence of some adverse events (AEs). Compared with intermittent dosing, administration of meropenem antibiotics through continuous infusion in patients with sepsis is associated with decreased hospital mortality, increased clinical cure rates and greater microbiological eradication. Further high-quality studies should be conducted to confirm our findings.

**Key words:** sepsis, meropenem, continuous infusion

## Cite as

Chen P, Chen F, Lei J, Zhou B. Clinical outcomes of continuous vs intermittent meropenem infusion for the treatment of sepsis: A systematic review and meta-analysis.

*Adv Clin Exp Med.* 2020;29(8):993–1000.

doi:10.17219/acem/121934

## DOI

10.17219/acem/121934

## Copyright

© 2020 by Wrocław Medical University

This is an article distributed under the terms of the Creative Commons Attribution 3.0 Unported (CC BY 3.0)

(<https://creativecommons.org/licenses/by/3.0/>)

## Introduction

Severe infections in critically ill patients are a major burden in the intensive care unit (ICU), with persistently high mortality rates.<sup>1</sup> Optimized antibiotic therapy has been suggested as an intervention likely to improve treatment outcomes for critically ill patients.<sup>2</sup> However, antibiotic resistance has become a major healthcare problem affecting morbidity and mortality in the clinical setting. Antibacterial drug discovery and development have slowed considerably in recent years.<sup>3</sup> With the increase of antibiotic resistance and the decrease of the development of new anti-biological drugs, more research on existing antibiotics is needed. In recent years, the effort to maximize antibiotic activity has led to an interest in optimizing antibiotic dosing using the pharmacokinetic (PK) and pharmacodynamic (PD) principles of antibiotics.<sup>4</sup>

Due to the wide-spectrum activity against variety of Gram-negative and Gram-positive microorganisms, and good penetration of body fluids and tissues, meropenem become a common choice for the treatment of critically ill patients.<sup>5</sup> Similar to other  $\beta$ -lactam antibiotics, it displays time-dependent bactericidal activity and PK/PD characteristics. The parameter that can best predict antibacterial efficacy is the percentage of the dosing interval that free drug concentrations remain above the minimum inhibitory concentration (MIC) during each dosing interval (referred to as %*f*T > MIC).<sup>6,7</sup> The optimal outcome of treatment of critically ill patients is most likely to occur when the PK/PD targets are achieved, which is closely related to the maximum antibiotic activity. A minimum standard for carbapenems is that T > MIC should be maintained at least 40%, and a T > MIC of 100% is associated with significantly better clinical and bacteriological outcomes in patients with serious bacterial infections.<sup>8,9</sup>

Pharmacokinetic studies in both non-critically ill and critically ill patients have demonstrated that administration of  $\beta$ -lactam antibiotics using continuous infusion results in consistent attainment of drug exposures associated with maximal antibacterial effects.<sup>10</sup> Thus, continuous infusion of meropenem has been suggested to maximize the therapeutic potential in critically ill patients. Recently, the use of continuous administration of meropenem among patients with sepsis has been studied in some trials and indicated greater PK efficacy, bacteriological eradication and clinical cure rates.<sup>11,12</sup> However, the efficacy and safety information of these clinical studies are not identical. Thus, the goal of our analysis was to evaluate the clinical efficacy and safety of continuous compared to intermittent meropenem infusion for the treatment of sepsis, to provide systematic clinical evidence for antibiotic therapy.

## Material and methods

### Data sources and literature search

We performed a systematic review and meta-analysis to compare continuous and intermittent infusion of meropenem in patients with sepsis. Two reviewers independently searched the medical literature for relevant clinical trials using the electronic databases of PubMed, Excerpta Medica (EMBASE), Cochrane Library, China National Knowledge Infrastructure (CNKI; www.cnki.net), Chinese Scientific Journals Full Text database (CSJFT), Wanfang Data Knowledge Service Platform (WKSP; www.wanfang-data.com.cn), and Chinese Biomedical Literature Service System (CBMdisc), through August 2018. This was supplemented by searching the reference lists of all retrieved studies, review articles, abstracts, and conference reports. The key words used in this search were: [Meropenem], [Antipseudomonal  $\beta$ -lactams], [Continuous infusion], [Prolonged infusion], [Intermittent infusion], [Short-term intravenous infusion], [Critically ill patients], and [Sepsis]. There were no language restrictions.

### Study selection

Clinical trials that met the following criteria were included: 1) randomized, controlled trials (RCTs) or cohort studies; 2) prospective clinical trials of continuous compared to intermittent infusion of meropenem treatment in patients with sepsis; 3) studies with all patients enrolled fulfilling the criteria of sepsis; 4) studies reporting data on mortality, clinical cure, microbiological eradication, as well as adverse events (AEs) etc. Exclusion criteria were the following: 1) repeat studies, abstracts, letters, reviews, editorials, or comments; 2) studies reporting on the comparative outcomes of extended or continuous compared to intermittent but for different meropenem products duration in the 2 arms; 3) case reports and case series including <10 patients; or 4) studies reporting only PK or PD outcomes.

### Data extraction and quality assessment

Two review authors independently screened the titles and abstracts of each study. The following information was extracted from each study: the first author, the year of publication, the number of patients enrolled in the study, and the therapeutic regimen and doses, in order to understand the baseline of all the included studies. A modified Jadad scale was used to assess the quality of the included randomized studies. The scores of high-quality studies ranged from 4 to 8, whereas low-quality studies ranged from 0 to 3. For non-randomized studies, the quality was assessed using Newcastle-Ottawa Quality Assessment Scale. Each study was graded as either low quality (0–5) or high quality (6–9). Any disagreements were resolved by the 3<sup>rd</sup> author.

## Statistical analysis

The differences between the continuous compared to intermittent administration of meropenem were assessed using the pooled risk ratio (RR) with 95% confidence intervals (95% CI). The summary RR assessments were conducted using a random- or fixed-effect model. Inter-study heterogeneity was tested using the Q-statistic and quantified using the  $I^2$  statistic. If  $I^2$  was  $< 50\%$  ( $P_{\text{heterogeneity}} > 0.1$ ), the Mantel–Haenszel fixed-effect model was used; if not, the random-effect model was used. The sensitivity analyses were performed according to the risk of bias. We assessed publication bias using visual inspection of the funnel plot and Egger's test. All calculations were performed using Stata v. 12.0 software (Stata Corporation LLC, College Station, USA). The level of significance was set at p-value less than 0.05 or 0.01.

## Results

### Search results

The systematic search of the literature for trials on continuous compared to intermittent meropenem infusion for sepsis therapy produced 108 potentially relevant records from the primary search of databases. Of the studies initially identified, we excluded reports that did not fulfill our inclusion criteria after first screening of the titles and abstracts. Finally, 7 studies<sup>13–19</sup> were considered eligible for the meta-analysis, including 1 RCT<sup>15</sup> and 6 prospective studies.<sup>13,14,16–19</sup> A flowchart describing the trial screening and selection procedure is shown in Fig. 1. The 7 selected studies, involving a total of 1,191 patients (continuous

group: 587 patients; intermittent group: 604 patients), were published between 2012 and 2018. The sample sizes of these studies ranged from 20 to 220. The total daily dose of meropenem varied both within and between the individual studies. When reported, the duration of treatment was also a variable (Table 1). The Jadad scores of the 7 studies included in the meta-analysis are also listed in Table 1; the mean Jadad score was 4.23 (range: 3–6), suggesting that the overall study quality was fair.

## Statistical analysis of efficacy outcomes

### Mortality

Four trials<sup>13,14,17,18</sup> presented information analyzing mortality. Overall, the meta-analysis showed that continuous infusion of meropenem was associated with a lower mortality rate than intermittent intravenous infusion (484 patients, RR = 0.66, 95% CI = 0.46–0.98, Z = 2.17, p = 0.03; Fig. 2), suggesting that the risk of death in patients with sepsis treated with continuous infusion of meropenem was 34% lower compared with patients treated with intermittent infusion, using the fixed-effects model (heterogeneity test,  $\chi^2 = 1.42$ , degrees of freedom (df) = 3 (p = 0.702),  $I^2 = 0\%$ ).

### Clinical cure rate

The RR of the clinical cure rate was reported in all studies.<sup>13–19</sup> Pooling the outcomes of the 7 studies showed that there was a significant statistical difference in the clinical cure rates between sepsis patients receiving continuous meropenem infusion and those receiving intermittent infusion (557 patients, RR = 1.15, 95% CI = 1.02–1.30,

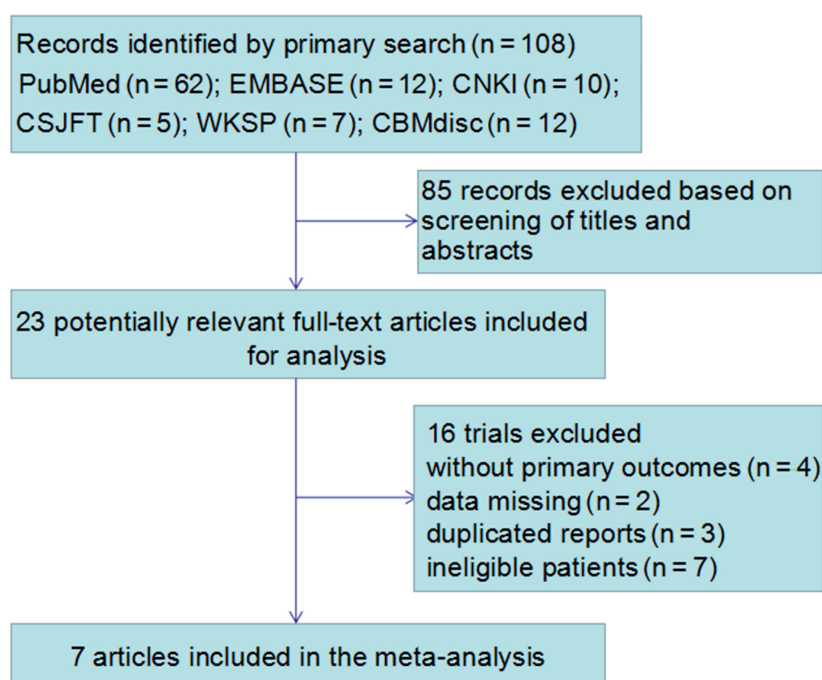


Fig. 1. Flowchart of included and excluded studies

Table 1. Baseline characteristics of the trials included in the meta-analysis

Author	Year	n		Age [years]		APACHE II, SOFA scores (mean $\pm$ SD)	Duration of treatment	Study design	Continuous group	Intermittent group	Jadad score
		CI	IT	CI	IT						
Shabaan et al. <sup>13</sup>	2017	n = 51 (30/21)	n = 51 (25/26)	NA	NA	NA; NA	up to 7 days	prospective	intravenous infusion of meropenem (20 mg/kg) over 30 min every 8 h	intravenous infusion of meropenem (20 mg/kg) over 30 min every 8 h	5
Zhao et al. <sup>14</sup>	2018	n = 25 (10/15)	n = 25 (11/14)	68.0 $\pm$ 15.4	67.0 $\pm$ 12.2	19.4 $\pm$ 5.0 vs 19.7 $\pm$ 5.9; 8.0 $\pm$ 2.8 vs 8.5 $\pm$ 2.4	median 7 days	prospective	loading dose of 0.5 g of meropenem followed by a continuous infusion of 3 g/day	initial dose of 1.5 g followed by 1 g for every 8 h	4
Dulhunty et al. <sup>15</sup>	2015	n = 212 (130/82)	n = 220 (135/85)	64 (54–72)	65 (53–72)	21 (17–26) vs 20 (16–25); NA	up to 28 days	RCT	loading dose of 3.0 g of meropenem over 30 min followed by intermittent infusion	loading dose of 3.0 g of meropenem over 30 min followed by intermittent infusion	6
Abdul-Aziz et al. <sup>16</sup>	2016	n = 21 (NA/NA)	n = 21 (NA/NA)	NA	NA	21 (17–26) vs 21 (15–26); 8 (6–10) vs 7 (5–9)	up to 14 days	prospective	loading dose of 1.0 g of meropenem over 30 min followed by intermittent infusion	loading dose of 1.0 g of meropenem over 30 min followed by intermittent infusion	4
Chytra et al. <sup>17</sup>	2012	n = 120 (78/42)	n = 120 (83/37)	44.9 $\pm$ 17.8	47.2 $\pm$ 16.3	21.4 $\pm$ 7.9 vs 22.1 $\pm$ 8.79; 10.4 $\pm$ 2.9 vs 10.6 $\pm$ 3.5	median 7 days	prospective	loading dose of 2 g of meropenem followed by a continuous infusion of 4 g of meropenem over 24 h	2 g of meropenem over 30 min every 8 h	5
Helmy et al. <sup>18</sup>	2015	n = 50 (33/17)	n = 50 (25/25)	53 (42–61)	55 (40–67)	NA; NA	up to 28 days	prospective	loading dose of 2 g of meropenem intravenously over 30 min followed by continuous infusion of 4 g of meropenem over 24 h	2 g of meropenem over 30 min every 8 h	3
Hassan et al. <sup>19</sup>	2016	n = 108 (NA/NA)	n = 117 (NA/NA)	NA	NA	NA; NA	up to 14 days	prospective	loading dose of 1.0 g of meropenem intravenously over 4 h every 24 h	2 g of meropenem over 30 min every 8 h	3

n – sample size; CI – continuous; IT – intermittent; APACHE II scores – Acute Physiology and Chronic Health Evaluation (Apache) II scores; SOFA scores – Sequential Organ Failure Assessment (SOFA) scores; SD – standard deviation; N/A – not applicable; RCT – randomized controlled trial.

Z = 2.22, p = 0.026; Fig. 3). Heterogeneity was not observed in the studies ( $\chi^2 = 4.62$ , df = 6 (p = 0.594), I<sup>2</sup> = 0%).

### Microbiological eradication

Data on comparisons of the microbiological eradication of continuous compared to intermittent intravenous administration of meropenem was reported in 4 trials.<sup>13,14,17,18</sup> The results of our fixed-effects ( $\chi^2 = 3.93$ , df = 3 (p = 0.378), I<sup>2</sup> = 2.9%) meta-analysis for microbiological eradication are summarized in Fig. 4. The results indicated that the microbiological eradication for the continuous group was significantly higher than in the intermittent group (484 patients, RR = 1.20, 95% CI = 1.01–1.42, Z = 1.78, p = 0.04; Fig. 4).

### Adverse events

Three studies<sup>13,15,17</sup> provided data regarding AEs that occurred during treatment. In 1 study, out of 212 patients in the continuous group, 39 (18.4%) experienced AEs, compared with 53 of 220 (24.1%) in the intermittent group.<sup>15</sup> Abnormalities in liver and kidney function tests were reported in 1 study, in which 3 out of 51 patients (6%) in the continuous group experienced acute kidney injury, whereas 18 of 12 patients (23.5%) in the intermittent group experienced them.<sup>13</sup> It has been suggested that gastrointestinal AEs (diarrhea and vomiting) are the most frequent side effects of meropenem in adults, with no significant difference between continuous infusion and intermittent administration (4.2% with diarrhea in the constant group compared to 5.8% in the intermittent group and 1.7% experiencing vomiting in the constant group compared to 2.5% in the intermittent group).<sup>17</sup>

### Other outcomes of the meta-analysis

Other clinical outcomes of continuous compared to intermittent meropenem infusion for the treatment of sepsis, such as the length of ICU stay, length of hospital stay, ICU survival, ICU-free days, etc., were reported in the included studies and are listed in Table 2.

### Publication bias

We assessed publication bias using a funnel plot and Egger's test in this study (Fig. 5). The funnel plot had a certain asymmetry, indicating that

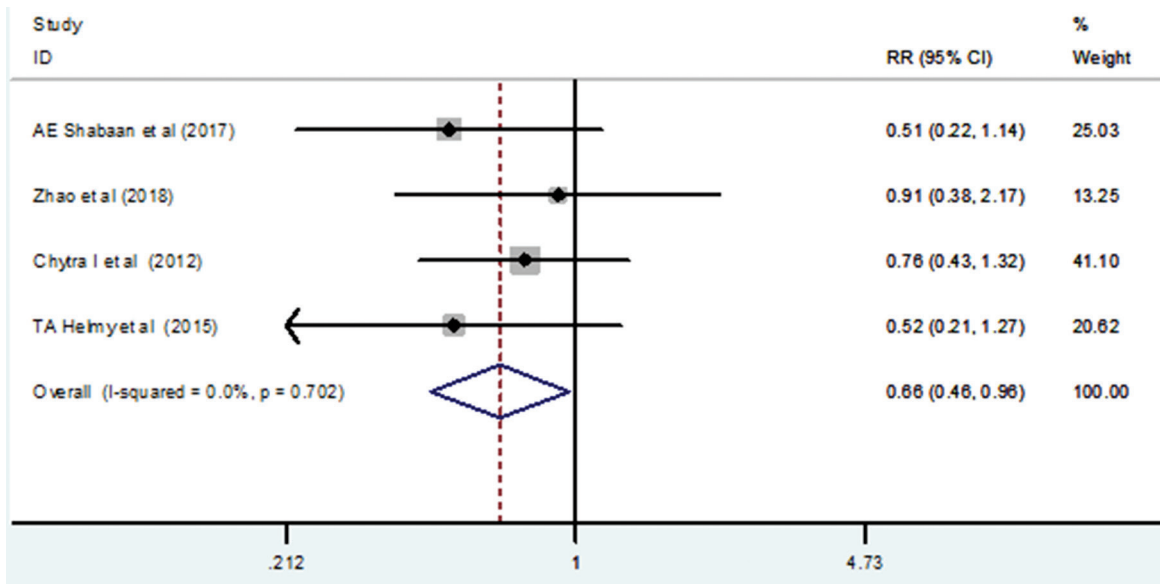


Fig. 2. Forest plot analysis of the mortality rates of continuous compared to intermittent meropenem

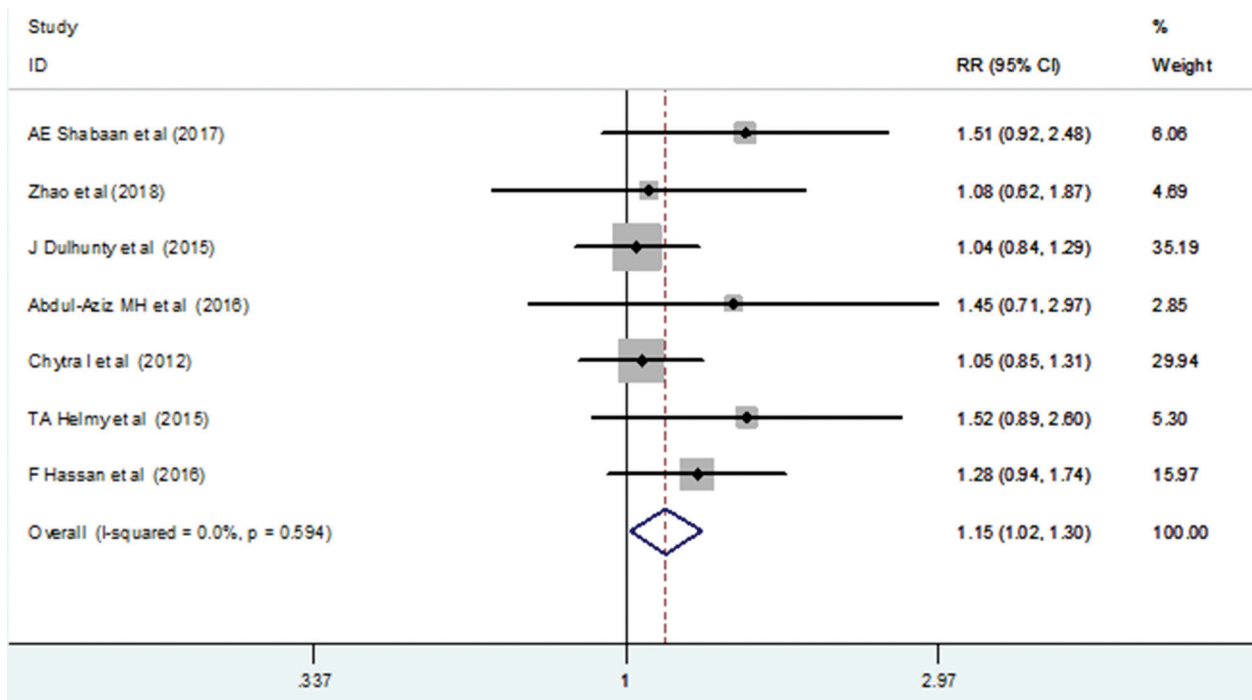


Fig. 3. Forest plots analysis of the clinical cure rates of continuous compared to intermittent meropenem

Table 2. Other outcomes of continuous compared to intermittent meropenem infusion for the treatment of sepsis

Outcomes	Studies	Patients		RR/WMD (95% CI)	Heterogeneity (I <sup>2</sup> , P)	p-value
		continuous group	intermittent group			
Length of ICU stay	3	166	166	-1.40 (-2.19, -0.61)	66%; 0.65	0.005
Hospital length of stay	3	288	296	-1.87 (-2.23, -1.50)	41%; 0.18	<0.01
ICU survival	4	378	386	-0.30 (-0.73, 0.13)	0%; 0.54	0.62
ICU-free days	4	378	386	-0.11 (-0.54, 0.32)	12%; 0.57	0.60
Emergence of resistance	2	332	340	-16.23 (-29.86, -2.59)	88%; 0.004	0.02

ICU – intensive care unit.



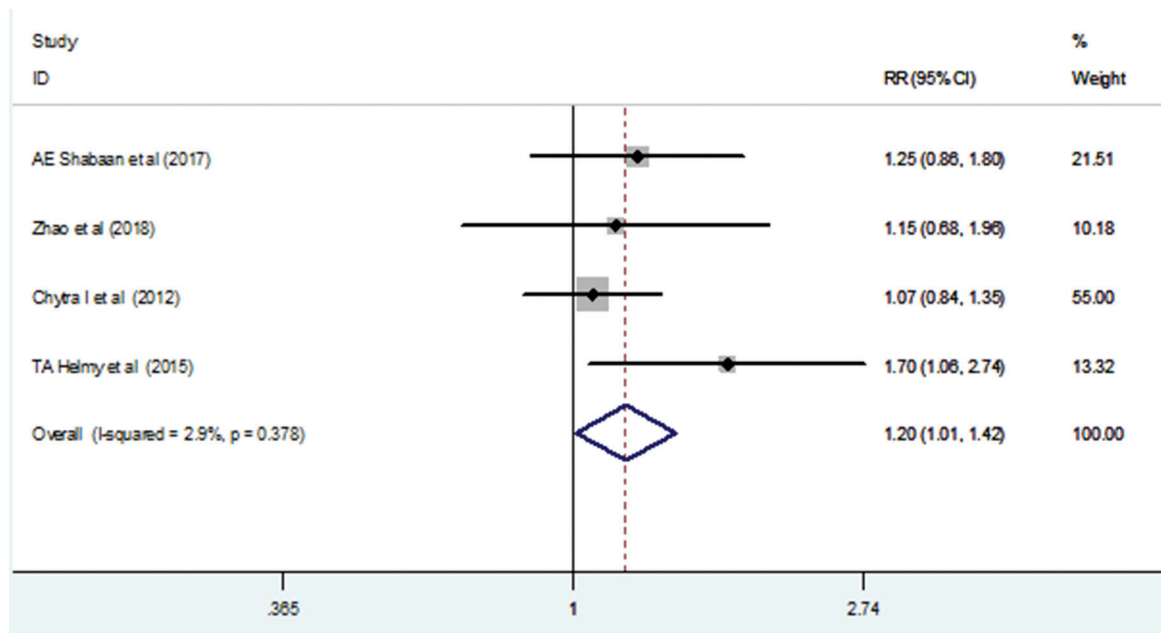


Fig. 4. Forest plot analysis of the microbiological eradication of continuous compared to intermittent meropenem

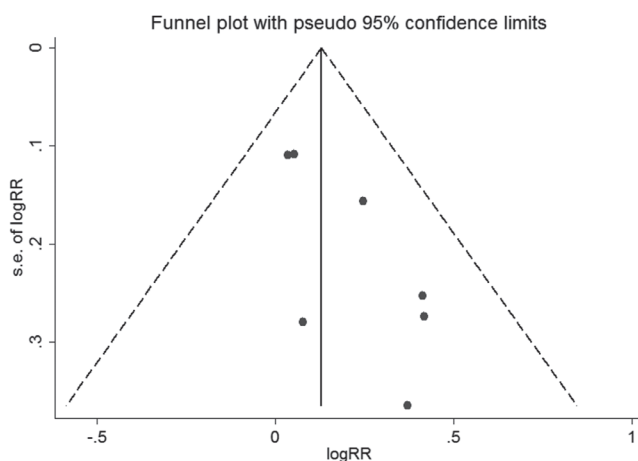


Fig. 5. Funnel plot of publication bias

there is some degree of publication bias in the literature. However, the number of studies included is small, so the funnel plot may not be convincing. Additionally, it was revealed that publication bias was not significant according to Egger's test for the incidence of AEs ( $Z = 1.54$ ;  $p = 0.41$ ).

## Discussion

### Key findings

To our knowledge, this study is the first meta-analysis to compare outcomes of sepsis patients receiving continuous compared to intermittent intravenous meropenem. In this meta-analysis, which includes data from 1,191 patients, we found that continuous infusion of meropenem resulted in lower mortality than intermittent infusion.

Compared with intermittent infusion, continuous infusion of meropenem was associated with superior clinical cure rates, which is a more subjective outcome.<sup>20</sup> Furthermore, a significantly higher rate of microbiological eradication was found in the continuous group compared with the intermittent group, although an insufficient number of patients or studies was included in most of these analyses.<sup>21</sup> The findings of this meta-analysis suggest that continuous infusion of meropenem could achieve significant clinical improvement in the treatment of sepsis patients.

### Relationship to previous studies

Studies of continuous infusion of  $\beta$ -lactam antibiotics, including meropenem, are numerous.<sup>22</sup> These studies suggest that continuous infusion achieves a greater likelihood of achieving PK/PD targets than standard intermittent infusion in critically ill patients.<sup>23</sup> However, the clinical value of continuous infusion with meropenem for patients with sepsis has not been systematically analyzed. It has been confirmed that sepsis patients are more likely to have pathophysiological changes leading to sub-therapeutic drug concentrations.<sup>24,25</sup> A number of PK studies of critically ill patients with sepsis have reported that administration through continuous infusion increases the achievement of target concentrations, both in plasma and in tissues, compared with intermittent dosing.<sup>26</sup> More important, previous meta-analyses were less selective than the present analysis in their inclusion criteria, included data from both critically ill and non-critically ill patients, and allowed different  $\beta$ -lactam antibiotics in the 2 treatment groups, which may have diluted any advantage of continuous infusion.<sup>27</sup> Our meta-analysis narrowed the subject to sepsis patients and the study drug to meropenem, which could overcome the deficiencies above.

## Implications of study findings

Besides the main outcome parameters (clinical cure, mortality and microbiological eradication), there are other factors that differentiate continuous administration from intermittent administration.<sup>28</sup> Our results showed that continuous infusion of meropenem could shorten ICU stays and total hospitalization times, which indicates that continuous administration may be a more economical therapy than intermittent administration for sepsis patients.<sup>29</sup> Regarding safety, the most commonly reported AEs associated with continuous meropenem infusion included diarrhea, rash, seizures, nausea, and vomiting, as well as hepatic injury.<sup>30</sup> Our study implied that administration of meropenem through continuous infusion in sepsis patients was safer compared with intermittent infusion, although the relationship with clinical cure was more complex.

## Other considerations

Increasing the %  $fT > MIC$  for  $\beta$ -lactams has been associated with increased therapeutic efficacy and delaying the emergence of resistance, and these benefits can be achieved with continuous infusion.<sup>31,32</sup> However, theoretically speaking, carbapenems such as meropenem may be unsuitable for administration through continuous infusion due to stability issues.<sup>33</sup> Patel et al. showed that 1 mg/mL of meropenem was stable for a longer time than 20 mg/mL and 50 mg/mL at 4–5°C after storage for 3–4 h.<sup>34</sup> Tomasello et al. found that there were no statistical differences in the percentage deviation values of the stability profile between concentrations of 4 mg/mL and 10 mg/mL of meropenem after 3–8 h when the temperature was controlled at 25°C.<sup>35</sup> Katip et al. demonstrated that 10 mg/mL meropenem solution was stable (maintained more than 90% of its initial concentration) for up to 10 h at 25°C, and that 20 mg/mL meropenem solution was stable for 6 h at 25°C.<sup>36</sup> More importantly, meropenem is only stable for 8–12 h at room temperature, thus casting doubts on any potential benefit of continuous delivery.<sup>37</sup> This is an important issue in tropical countries where meropenem concentrations decreased by 4% and 12% when stored at room temperature for 3 h and 8 h, respectively, although 24-hour stability can be maintained if meropenem temperature is kept below 4°C.<sup>38</sup>

## Strengths and limitations

There are several limitations in this meta-analysis that should be considered when interpreting the data. First, the number of studies and patients included in this study is small, which will make the conclusion less reliable. Second, differences in treatment regimens and doses of drugs add to the clinical heterogeneity in the data. Third, the criteria used in most trials for the definition and severity of sepsis are not in accordance to the current definitions.

Finally, publication bias might have occurred, and it might not be completely reflected by funnel plot. Therefore, additional large-scale, high-quality, placebo-controlled, double-blind trials are needed to confirm our findings.

## Conclusions

The evidence from mainly non-randomized studies suggests that continuous infusion of meropenem could lead to superior treatment outcomes, including mortality, clinical cure, microbiological eradication, and AEs. However, well-designed RCTs are warranted to validate these findings before they can be widely applied in clinical practice.

## ORCID iDs

Benhong Zhou  <https://orcid.org/0000-0002-6129-0182>  
Peng Chen  <https://orcid.org/0000-0003-4936-2064>

## References

- Hidalgo F, Mas D, Rubio M, Garcia-Hierro P. Infections in critically ill burn patients. *Med Intensiva*. 2016;40(3):179–185.
- McKinney CW, Pruden A. Ultraviolet disinfection of antibiotic resistant bacteria and their antibiotic resistance genes in water and wastewater. *Environ Sci Technol*. 2012;46(24):13393–13400.
- Liu YF, Yan JJ, Lei HY, et al. Loss of outer membrane protein C in *Escherichia coli* contributes to both antibiotic resistance and escaping antibody-dependent bactericidal activity. *Infect Immun*. 2012;80(5):1815–1822.
- Wiklund S, Fagerberg I, Örtqvist Å, et al. Knowledge and understanding of antibiotic resistance and the risk of becoming a carrier when travelling abroad: A qualitative study of Swedish travelers. *Scand J Public Health*. 2015;43(3):302–308.
- Tiberi S, Payen MC, Sotgiu G, et al. Effectiveness and safety of meropenem/clavulanate-containing regimens in the treatment of MDR- and XDR-TB. *Eur Respir J*. 2016;47(4):1235–1243.
- Afshartous D, Bauer SR, Connor MJ, et al. Pharmacokinetics and pharmacodynamics of imipenem and meropenem in critically ill patients treated with continuous venovenous hemodialysis. *Am J Kidney Dis*. 2014;63(1):170–171.
- Chalhoub H, Sáenz Y, Rodríguezvillalobos H, et al. High-level resistance to meropenem in clinical isolates of *Pseudomonas aeruginosa* in the absence of carbapenemases: Role of active efflux and porin alterations. *Int J Antimicrob Agents*. 2016;48(6):740–743.
- Laishram S, Anandan S, Devi BY, et al. Determination of synergy between sulbactam, meropenem and colistin in carbapenem-resistant *Klebsiella pneumoniae* and *Acinetobacter baumannii* isolates and correlation with the molecular mechanism of resistance. *J Chemother*. 2016;28(4):297–303.
- Payen MC, Muylle I, Vandenberg O, et al. Meropenem-clavulanate for drug-resistant tuberculosis: A follow-up of relapse-free cases. *Int J Tuberc Lung Dis*. 2018;22(1):34–39.
- Cheatham SC, Fleming MR, Healy DP, et al. Steady-state pharmacokinetics and pharmacodynamics of meropenem in morbidly obese patients hospitalized in an intensive care unit. *J Clin Pharmacol*. 2014;54(3):324–330.
- Lenhard JR, Bulitta JB, Connell TD, et al. High-intensity meropenem combinations with polymyxin B: New strategies to overcome carbapenem resistance in *Acinetobacter baumannii*. *J Antimicrob Chemother*. 2017;72(1):153–165.
- McCarthy MW, Walsh TJ. Meropenem/vaborbactam fixed combination for the treatment of patients with complicated urinary tract infections. *Drugs Today (Barc)*. 2017;53(10):521–530.
- Shabaan AE, Nour I, Eldeglia HE, Nasef H, Shouman B, Abdel-Hady H. Conventional versus prolonged infusion of meropenem in neonates with Gram-negative late onset sepsis: A randomized controlled trial. *Pediatr Infect Dis J*. 2017;36(4):358–363.

14. Zhao HY, Gu J, Jie L, et al. Pharmacokinetic and pharmacodynamic efficacies of continuous versus intermittent administration of meropenem in patients with severe sepsis and septic shock: A prospective randomized pilot study. *Chin Med J (Eng)*. 2017;130(10):1139–1145.
15. Dulhunty JM, Roberts JA, Davis JS, et al; BLING II Investigators for the ANZICS Clinical Trials Group. A multicenter randomized trial of continuous versus intermittent  $\beta$ -lactam infusion in severe sepsis. *Am J Respir Crit Care Med*. 2015;192(11):1298–1305.
16. Abdul-Aziz MH, Sulaiman H, Mat-Nor MB, et al. Beta-Lactam Infusion in Severe Sepsis (BLISS): A prospective, two-centre, open-labelled-randomised controlled trial of continuous versus intermittent beta-lactam infusion in critically ill patients with severe sepsis. *Intensive Care Med*. 2016;42(10):1535–1545.
17. Chytra I, Stepan M, Benes J, et al. Clinical and microbiological efficacy of continuous versus intermittent application of meropenem in critically ill patients: A randomized open-label controlled trial. *Crit Care*. 2012;16(3):R113–R116.
18. Helmy TA, Abdelghaffar AA, Fathy EM, et al. Continuous versus intermittent intravenous meropenem in severe sepsis. *IJPBS*. 2015;5:4457.
19. Fahmi H, Noorizan AA, Yahaya H, Hazlinda AH. Clinical outcomes of critically ill patients with sepsis receiving extended and standard-meropenem infusion in Malaysian hospitals. *Int J Pharm Pharm Sci*. 2016;10:S12512.
20. Yusuf E, Spapen H, Pierard D. Prolonged vs intermittent infusion of piperacillin/tazobactam in critically ill patients: A narrative and systematic review. *J Crit Care*. 2014;29(6):1089–1095.
21. Chu DC, Mehta AB, Walkey AJ. Practice patterns and outcomes associated with procalcitonin use in critically ill patients with sepsis. *Clin Infect Dis*. 2017;64(11):1509–1515.
22. Zielske J, Bohne S, Brunkhorst FM, Axer H, Guntinas-Lichius O. Acute and long-term dysphagia in critically ill patients with severe sepsis: Results of a prospective controlled observational study. *Eur Arch Otorhinolaryngol*. 2014;271(11):3085–3093.
23. Del BV, Giacobbe DR, Marchese A, et al. Meropenem for treating KPC-producing *Klebsiella pneumoniae* bloodstream infections: Should we get to the PK/PD root of the paradox? *Virulence*. 2016;8(1):66–73.
24. Kristoffersson AN, David-Pierson P, Parrott NJ. Simulation-based evaluation of PK/PD indices for meropenem across patient groups and experimental designs. *Pharm Res*. 2016;33(5):1115–1125.
25. Vardakas KZ, Voulgaris GL, Maliaros A, Samonis G, Falagas ME. Prolonged versus short-term intravenous infusion of antipseudomonal  $\beta$ -lactams for patients with sepsis: A systematic review and meta-analysis of randomised trials. *Lancet Infect Dis*. 2018;18(1):108–120.
26. Dong H, Zhong Y. Response to: Continuous versus intermittent infusion of vancomycin in adult patients: A systematic review and meta-analysis. *Int J Antimicrob Agents*. 2016;48(1):114–115.
27. Yang H, Zhang C, Zhou Q, Wang Y, Chen L. Clinical outcomes with alternative dosing strategies for piperacillin/tazobactam: A systematic review and meta-analysis. *PLoS One*. 2016;10(1):274–289.
28. Sato Y, Sandoh M, Hanaki H, et al. Evaluation of usefulness and PK-PD analysis of meropenem in children with various infections. *Gan To Kagaku Ryoho*. 2012;60(3):335–341.
29. Delfino E, Fucile C, Del VB, et al. Pharmacokinetics of high-dose extended-infusion meropenem during pulmonary exacerbation in adult cystic fibrosis patients: A case series. *New Microbiol*. 2018;41(1):47–51.
30. Sjövall F, Alobaid AS, Wallis SC, Perner A, Lipman J, Roberts JA. Maximally effective dosing regimens of meropenem in patients with septic shock. *J Antimicrob Chemother*. 2018;73(1):191–198.
31. Shotwell MS, Nesbitt R, Madonia PN, et al. Pharmacokinetics and pharmacodynamics of extended infusion versus short infusion piperacillin-tazobactam in critically ill patients undergoing CRRT. *Clin J Am Soc Nephrol*. 2016;11(8):1377–1383.
32. Cojutti PG, Barbarino C, De AM, Hope W, Pea F. Higher than standard meropenem and linezolid dosages needed for appropriate treatment of an intracerebral hemorrhage patient with augmented renal clearance. *Eur J Clin Pharmacol*. 2018;74(8):1091–1092.
33. Martínková J, Malbrain ML, Havel E, Šafránek P, Bezouška J, Kaška M. A pilot study on pharmacokinetic/pharmacodynamic target attainment in critically ill patients receiving piperacillin/tazobactam. *Anaesthesiol Intensive Ther*. 2015;48(1):23–30.
34. Patel PR, Cook SE. Stability of meropenem in intravenous solutions. *Am J Health Syst Pharm*. 1997;54(4):412–421.
35. Tomasello C, Leggieri A, Cavalli R, Di Perri G, D'Avolio A. In vitro stability evaluation of different pharmaceutical products containing meropenem. *Hosp Pharm*. 2015;50(4):296–303.
36. Katip W, Wientong P, Sornsuvit C. The stability of generic meropenem in tropical countries. *Int J Pharm Pharm Sci*. 2015;7(1):236–238.
37. Franceschi L, Cojutti P, Baraldo M, Pea F. Stability of generic meropenem solutions for administration by continuous infusion at normal and elevated temperatures. *Ther Drug Monit*. 2014;36(5):674–669.
38. Roberts DM, Roberts JA, Roberts MS, et al; RENAL Replacement Therapy Study Investigators. Variability of antibiotic concentrations in critically ill patients receiving continuous renal replacement therapy: A multicentre pharmacokinetic study. *Crit Care Med*. 2012;40(5):1523–1528.

# Association of gene polymorphisms of *KLK3* and prostate cancer: A meta-analysis

\*Huifeng Li<sup>1,C</sup>, \*Xiawei Fei<sup>1,A,C</sup>, Yanting Shen<sup>2,A</sup>, Zhenqi Wu<sup>1,F</sup>

<sup>1</sup> Department of Urology, Qingpu Branch of Zhongshan Hospital affiliated to Fudan University, Shanghai, China

<sup>2</sup> School of Biological Science and Medical Engineering, Southeast University, Nanjing, China

A – research concept and design; B – collection and/or assembly of data; C – data analysis and interpretation; D – writing the article; E – critical revision of the article; F – final approval of the article

Advances in Clinical and Experimental Medicine, ISSN 1899–5276 (print), ISSN 2451–2680 (online)

*Adv Clin Exp Med.* 2020;29(8):1001–1009

## Address for correspondence

Zhenqi Wu

E-mail: zhenqi\_wu1976@sina.com

## Funding sources

The meta-analysis was supported by the Science and Technology Development Foundation of Qingpu (project No. QKY2017-12) and by the Qingpu Branch of Zhongshan Hospital affiliated to Fudan University Research Project (project No. QY2017-05).

## Conflict of interest

None declared

\*Huifeng Li and Xiawei Fei contributed equally to this work.

Received on September 11, 2018

Reviewed on October 14, 2018

Accepted on April 30, 2020

Published online on September 1, 2020

## Abstract

Previous studies have suggested that prostate-specific antigen (PSA) plays a role in the etiology of prostate cancer (PCa), and that polymorphisms of *KLK3* may be associated with PCa. However, these results were conflicting. Therefore, we performed a meta-analysis to illuminate this problem. We searched the PubMed and Web of Science databases. Ten single nucleotide polymorphisms (SNPs) were involved in this meta-analysis. The pooled results showed that the minor alleles of rs1058205, rs2735839, rs174776, rs17632542, rs266849, rs266878, and rs2569735 were significantly associated with PCa. Compared to genotypes of the common homozygotes, the heterozygous genotypes of rs1058205, rs2735839, rs174776, rs17632542, rs266849, and rs266878 were significantly associated with PCa, as well as the homozygous genotypes of rs1058205, rs2735839, rs17632542, rs266878, rs266876, and rs2569735. Only rs2735839 was involved in the Gleason score (GS). The pooled results showed that when compared with GS  $\geq 8$  PCa, the A-allele was the protective factor for GS  $< 7$  PCa. It was also a protective factor for GS  $\geq 4+3$  when compared to GS  $\leq 3+4$  PCa. A strong association was observed between PCa and rs1058205, rs2735839, rs266882, rs174776, rs17632542, rs266849, rs266878, rs266876, rs1058274, and rs2569735. The G-allele of rs2735839 was a risk factor for GS  $< 7$  PCa when compared with the GS  $\geq 8$  PCa, as well as for the GS  $\geq 4+3$  when compared to the GS  $\leq 3+4$  PCa. Therefore, these SNPs may be valuable as biomarkers for PCa in the future.

**Key words:** *KLK3*, prostate-specific antigen, polymorphisms, prostate cancer, meta-analysis

## Cite as

Li H, Fei X, Shen Y, Wu Z. Association of gene polymorphisms of *KLK3* and prostate cancer: A meta-analysis. *Adv Clin Exp Med.* 2020;29(8):1001–1009. doi:10.17219/acem/121521

## DOI

10.17219/acem/121521

## Copyright

© 2020 by Wrocław Medical University

This is an article distributed under the terms of the Creative Commons Attribution 3.0 Unported (CC BY 3.0) (<https://creativecommons.org/licenses/by/3.0/>)

Prostate cancer (PCa) is the 2<sup>nd</sup> most frequently diagnosed cancer in men around the world, and one of the leading causes of cancer death among men of all races.<sup>1</sup> With the aging of the population and the improvement of living conditions in recent years, the incidence of PCa has been increasing every year.<sup>2</sup> Serum levels of prostate-specific antigen (PSA) are widely used for screening for PCa. The PSA levels are known to be influenced by genetic components: Around 40–45% of the variance in PSA is thought to be explained by genetic components.<sup>3,4</sup> Previous studies have revealed that kallikrein 3 (*KLK3*) is the strongest genetic factor to influence levels of PSA, and its single nucleotide polymorphism (SNP) loci have been shown to be associated with PCa.<sup>5–7</sup>

The *KLK3* is located on chromosome 19q13.33, which encodes PSA and is a member of the serine protease kallikrein family. We searched the PubMed and Web of Science databases without language restrictions up to January 8, 2018, for relevant studies about the association of the SNPs of *KLK3* and PCa. We found that nearly 59 SNP loci were mentioned in studies in these databases, and among them, 21 SNP loci were involved in more than 2 studies (Fig. 1). However, these results were conflicting and there was still a lack of any relevant comprehensive analysis to clarify the confusion.

Therefore, in this study, we performed a literature review and a meta-analysis to explore the association between the risk of PCa and the 21 SNP loci of *KLK3* that were mentioned in more than 2 studies.

## Material and methods

### Search strategy

We searched the PubMed and Web of Science databases through September, 2018, without language restrictions, for relevant studies about associations of the SNPs of *KLK3* and PCa. The search term was (((*KLK3*) AND ((single nucleotide polymorphism) OR SNP))) AND ((prostate cancer) OR PSA).

### Inclusion/exclusion criteria

The title, abstract and full text of the candidate studies were independently screened by 2 reviewers. A study was included when all of the following criteria were met: 1) Non-familial studies that examined the association between SNPs of *KLK3* and PCa were included; 2) studies that had complete data or data that could be used to calculate an odds ratio (OR) and a 95% confidence interval (95% CI) were included; 3) studies that had incomplete data were excluded.

### Data extraction

Information was carefully extracted from all the eligible publications by 2 independent reviewers (Li and Fei), based on the aforementioned inclusion criteria. Any

disagreements were arbitrated by discussion with a 3<sup>rd</sup> reviewer (Shen). The following data were collected from each study: the 1<sup>st</sup> author's surname, the year of publication, the country, the laboratory methods used to detect *KLK3* polymorphisms, and the number of cases and controls.

### Quality assessment

We used the Newcastle-Ottawa scale (NOS) to assess the quality of each eligible study. The NOS contains 8 items: 1) The cases were independently validated; 2) Cases were representative of a population; 3) There were community controls; 4) The controls had no history of PCa; 5A) The study was controlled for age; 5B) The study was controlled for additional factors; 6) Exposure was ascertained by blinded interview or record; 7) The same method of ascertainment was used for both the cases and the controls; 8) The non-response rate was the same for the cases and the controls. When a study fulfilled 1 criterion, it got 1 score. The NOS is arranged from 0 up to 9 scores, and a study is considered high quality if it gets more than 4 scores.

### Statistical analysis

The strength of the association between *KLK3* polymorphism and the risk of PCa was shown using an OR with a 95% CI. If a study just provided the frequency (assumption: the frequency of allele 1 or genotype 1 in the case group was A; the frequency of allele 2 or genotype 2 in the case group was B; the frequency of allele 1 or genotype 1 in the control group was C; the frequency of allele 2 or genotype 2 in the control group was D), we used the formulas “OR = (A/B)/(C/D)” and “95% CI of ln OR = ln (OR) ± 1.96(1/A + 1/B + 1/C + 1/D)<sup>0.5</sup>” to calculate the OR and its 95% CI.

The statistical significance of the pooled OR was assessed with a Z-test, and a p-value of 0.05 was considered significant. A  $\chi^2$ -based Q-test was conducted to measure the heterogeneity of the eligible studies, and the heterogeneity was considered significant if the p-value for the heterogeneity test was 0.05. A sensitivity analysis in which 1 study was excluded at a time was conducted to evaluate the influence of an individual study on the results. Begg's funnel plot and Egger's regression test were used to evaluate the publication bias (no publication bias was indicated by a two-sided p-value  $\geq 0.05$ ). All the analyses were conducted using Stata v. 11.0 software (StataCorp LLC, College Station, USA), and a two-sided p-value  $\geq 0.05$  indicated no significance.

## Results

### Literature search

The study selection process is shown in Fig. 2. The primary literature search identified 45 studies. After the titles and abstracts were screened, 13 studies were excluded:





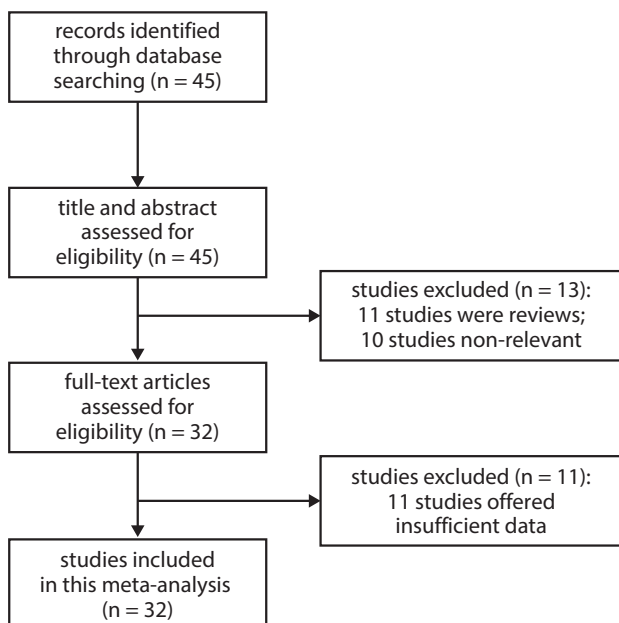


Fig. 2. The study selection process

3 were reviews and 10 were irrelevant studies. The full texts of the remaining 32 studies were then evaluated. As a result, 12 studies were excluded because of useless data and 21 studies were included in the meta-analysis.<sup>8–28</sup> The 21 eligible studies were assessed with the NOS (Table 1). Each had a score more than 4, which means that all the studies were of high quality.

## Meta-analysis of associations between SNPs and PCa risk

We found that 10 SNP loci were available to perform a meta-analysis to illuminate associations between the SNPs of *KLK3* and PCa risk. They were rs1058205, rs2735839, rs266882, rs174776, rs17632542, rs266849, rs266878, rs266876, rs1058274, and rs2569735.<sup>8–10,12,14,16–22,25–28</sup> Their genetic information is presented in Table 2. The pooled results are shown in Table 3.

For the alleles, we found that except rs266882, rs266876 and rs1058274, the remaining 7 SNP loci were significantly

Table 1. Characteristics and quality assessment of eligible studies in the meta-analysis

Fist author	Patients	Detection method	Year	Quality indicators from NOS										Score
				1	2	3	4	5A	5B	6	7	8		
Choe EK <sup>8</sup>	Korean	genotyping arrays	2017	yes	yes	no	yes	no	no	yes	yes	yes	6	
Chen C <sup>9</sup>	Chinese	PCR-HRM	2017	yes	yes	no	yes	yes	yes	yes	yes	yes	8	
Stegeman S <sup>10</sup>	European	Illumina Infinium Array	2015	yes	yes	no	yes	no	no	yes	yes	yes	6	
He Y <sup>11</sup>	Caucasian men	Illumina BeadXpress Reader	2014	yes	yes	no	yes	no	no	yes	yes	yes	6	
Hu J <sup>12</sup>	Chinese	TaqMan/MGB Assay	2014	yes	yes	yes	yes	no	no	yes	yes	yes	7	
Shui IM <sup>13</sup>	European	TaqMan Assay	2014	yes	yes	no	yes	no	no	yes	yes	yes	6	
Wang NN <sup>14</sup>	Chinese	PCR-HRM	2013	yes	yes	no	yes	no	no	yes	yes	yes	6	
Soni A <sup>15</sup>	India	PCR-RFLP	2012	yes	yes	no	yes	no	no	yes	yes	yes	6	
Kwon EM <sup>16</sup>	Caucasian and African American men	genotyping arrays	2012	yes	yes	yes	yes	yes	no	yes	yes	yes	8	
Kote-Jarai Z <sup>17</sup>	UK/Australian	genotyping arrays	2011	yes	yes	no	yes	no	no	yes	yes	yes	6	
Penney KL <sup>18</sup>	American	Sequenom technology	2011	yes	yes	no	yes	no	no	yes	yes	yes	6	
Lindstrom S <sup>19</sup>	European	TaqMan Assay	2011	yes	yes	no	yes	no	no	yes	yes	yes	6	
Ciampa J <sup>20</sup>	European	Illumina Chips	2011	yes	yes	no	yes	no	no	yes	yes	yes	6	
Parikh H <sup>21</sup>	European	TaqMan Assays	2011	yes	yes	no	yes	no	no	yes	yes	yes	6	
Gudmundsson J <sup>22</sup>	Icelandic	Illumina Chips	2010	yes	yes	no	yes	yes	no	yes	yes	yes	7	
Gallagher DJ <sup>23</sup>	Ashkenazi Jewish ancestry	Mass ARRAY QGE iPLEX System	2010	yes	yes	no	yes	no	no	yes	yes	yes	6	
Kader AK <sup>24</sup>	European	Mass ARRAY QGE iPLEX System	2009	yes	yes	no	yes	no	no	yes	yes	yes	6	
Xu J <sup>25</sup>	European	Mass ARRAY QGE iPLEX System	2008	yes	yes	no	yes	no	no	yes	yes	yes	6	
Eeles RA <sup>26</sup>	UK and Australia	sequencing	2008	yes	yes	no	yes	no	no	yes	yes	yes	6	
Lai J <sup>27</sup>	Caucasian men	PCR-RFLP	2007	yes	yes	no	yes	no	no	yes	yes	yes	6	
Cicek MS <sup>28</sup>	American	PCR-RFLP	2005	yes	yes	no	yes	no	no	yes	yes	yes	6	

PCR-HRM – high-resolution melting curve polymerase chain reaction method; PCR-RFLP – PCR-restriction fragment length polymorphism; NOS – Newcastle-Ottawa scale.

**Table 2.** Genetic information for 10 SNPs of *KLK3*

SNP	Chromosome <sup>a</sup>	Functional consequence <sup>a</sup>	Position (bp) <sup>a</sup>		Minor allele	Major allele
			GRCh38.p7	GRCh37.p13		
rs1058205	19:50860142	URT variant 3 prime	50860142	51363398	C allele	T allele
rs2735839	19:50861367	downstream	50861367	51364623	A allele	G allele
rs266882	19:50854757	upstream variant 2KB	50854757	51358013	A allele	G allele
rs174776	19:50856596	intron variant	50856596	51359852	T allele	C allele
rs17632542	19:50858501	missense	50858501	51361757	T allele	C allele
rs266849	19:50845834	intron variant	50845834	51349090	G allele	A allele
rs266878	19:50855858	intron variant	50855858	51359114	G allele	C allele
rs266876	19:50857562	intron variant	50857562	51360818	C allele	T allele
rs1058274	19:50860192	URT variant 3 prime	50860192	51363448	G allele	A allele
rs2569735	19:50861013	downstream variant 500B	50861013	51364269	A allele	G allele

<sup>a</sup>The information was provided by the dbSNP database (<http://www.ncbi.nlm.nih.gov/SNP/>); URT – untranslated regions; SNP – single nucleotide polymorphism; *KLK3* – kallikrein 3.

**Table 3.** Meta-analysis of associations between SNPs and PCa risk

SNP	Number of studies	Test for overall effect			Test for heterogeneity		Test for publish bias	
		OR (95% CI)	Z-score	p-value	I <sup>2</sup>	p-value	P <sub>egger's</sub>	P <sub>egg's</sub>
<i>rs1058205</i>								
C allele vs T allele	8 [9, 10, 16–18, 21] a7 [9, 10, 16–18, 21]	0.79 (0.73–0.87) 0.85 (0.82–0.88)	5.09 8.81	<0.001 <0.001	83.2% 10.8%	<0.001 0.347	– 0.085	– 0.133
TC vs TT	7 [9, 10, 17, 18, 21] a6 [9, 10, 17, 18, 21]	0.79 (0.72–0.86) 0.84 (0.80–0.88)	5.08 7.87	<0.001 <0.001	77.6% 15.8%	<0.001 0.312	– 0.303	– 0.707
CC vs TT	7 [9, 10, 17, 18, 21] a6 [9, 10, 17, 18, 21]	0.62 (0.49–0.77) 0.67 (0.61–0.73)	4.28 8.29	<0.001 <0.001	72.2% 0.0%	0.001 0.540	– 0.520	– 1.000
<i>rs2735839</i>								
A allele vs G allele	14 [8, 12, 14, 17, 19–22, 25, 26] b11 [8, 14, 17, 19–22, 25, 26]	0.78 (0.71–0.86) 0.86 (0.82–0.90)	4.96 6.35	<0.001 <0.001	87.5% 36.4%	<0.001 0.108	– 0.152	– 0.533
AG vs GG	10 [12, 14, 17, 19, 21, 26] b7 [14, 17, 19, 21, 26]	0.80 (0.71–0.91) 0.85 (0.80–0.90)	3.52 5.50	0.001 <0.001	87.3% 36.7%	<0.001 0.148	– 0.424	– 1.000
AA vs GG	10 [12, 14, 17, 19, 21, 26] b7 [14, 17, 19, 21, 26]	0.77 (0.54–1.10) 0.81 (0.67–0.97)	1.46 2.32	0.144 0.020	88.1% 39.0%	<0.001 0.131	– 0.158	– 0.230
<i>rs266882</i>								
A allele vs G allele	4 [15, 18, 27, 28] c2 [18, 28]	1.26 (0.97–1.64) 1.00 (0.91–1.10)	1.71 0.01	0.087 0.995	83.7% 0.0%	<0.001 0.978	– –	– –
AG vs GG	4 [15, 18, 27, 28] d3 [15, 18, 28]	1.40 (0.92–2.13) 1.20 (0.82–1.76)	1.56 0.95	0.119 0.340	68.2% 57.1%	0.024 0.097	– 0.622	– 0.296
AA vs GG	4 [15, 18, 27, 28] d3 [15, 18, 28]	1.45 (0.92–2.29) 1.18 (0.80–1.72)	1.59 0.84	0.112 0.402	74.4% 62.9%	0.008 0.068	– 0.277	– 0.296
<i>rs174776</i>								
T allele vs C allele	3 [16, 18, 21]	0.86 (0.80–0.93)	3.74	<0.001	0.0%	0.619	0.326	1.000
CT vs CC	2 [18, 21]	0.87 (0.79–0.97)	2.58	0.010	0.0%	0.844	–	–
TT vs CC	2 [18, 21]	0.77 (0.55–1.06)	1.62	0.106	0.0%	0.436	–	–
<i>rs17632542</i>								
T allele vs C allele	4 [17, 22] a3 [17, 22]	0.61 (0.43–0.86) 0.72 (0.64–0.82)	2.79 4.99	0.005 <0.001	95.0% 50.2%	<0.001 0.134	– 0.659	– 1.000
TC vs CC	3 [17] a2 [17]	0.57 (0.37–0.87) 0.72 (0.59–0.87)	2.61 3.43	0.009 0.001	95.4% 72.2%	<0.001 0.058	– –	– –
TT vs CC	3 [17] a2 [17]	0.32 (0.14–0.75) 0.50 (0.30–0.83)	2.62 2.68	0.009 0.007	73.1% 0.0%	0.024 0.819	– –	– –

**Table 3.** Meta-analysis of associations between SNPs and PCa risk – cont.

SNP	Number of studies	Test for overall effect			Test for heterogeneity		Test for publish bias	
		OR (95% CI)	Z-score	p-value	I <sup>2</sup>	p-value	P <sub>egger's</sub>	P <sub>begg's</sub>
<i>rs266849</i>								
G allele vs A allele	8 [17, 19, 26] e5 [17, 19, 26]	0.81 (0.71~0.92) 0.94 (0.89~0.98)	3.16 2.68	0.002 0.007	92.2% 17.0%	<0.001 0.306	– 0.289	– 0.462
GA vs AA	7 [17, 19, 26] e4 [17, 19, 26]	0.80 (0.70~0.91) 0.91 (0.85~0.98)	3.40 2.55	0.001 0.011	90.1% 43.8%	<0.001 0.149	– 0.927	– 0.734
GG vs AA	7 [17, 19, 26] e4 [17, 19, 26]	0.73 (0.55~0.97) 0.98 (0.86~1.10)	2.15 0.39	0.032 0.699	87.2% 4.4%	<0.001 0.371	– 0.812	– 1.000
<i>rs266878</i>								
G allele vs C allele	2 [18, 21]	0.86 (0.78~0.94)	3.23	0.001	0.0%	0.410	–	–
GC vs CC	2 [18, 21]	0.87 (0.78~0.97)	2.60	0.009	0.0%	1.000	–	–
GG vs CC	2 [18, 21]	0.72 (0.52~0.98)	2.10	0.036	0.0%	0.354	–	–
<i>rs266876</i>								
C allele vs T allele	2 [18, 21]	0.83 (0.63~1.08)	1.42	0.157	90.9%	0.001	–	–
CT vs TT	2 [18, 21]	0.99 (0.90~1.08)	0.22	0.825	0.0%	0.703	–	–
CC vs TT	2 [18, 21]	0.77 (0.65~0.91)	3.02	0.003	0.0%	0.784	–	–
<i>rs1058274</i>								
G allele vs A allele	2 [18, 21]	0.98 (0.92~1.05)	0.56	0.578	0.0%	0.669	–	–
GA vs AA	2 [18, 21]	1.01 (0.92~1.11)	0.15	0.878	0.0%	0.926	–	–
GG vs AA	2 [18, 21]	0.94 (0.82~1.09)	0.81	0.419	0.0%	0.658	–	–
<i>rs2569735</i>								
A allele vs G allele	2 [18, 21]	0.90 (0.82~0.99)	2.14	0.032	8.4%	0.296	–	–
AG vs GG	2 [18, 21]	0.92 (0.83~1.02)	1.61	0.108	0.0%	0.464	–	–
AA vs GG	2 [18, 21]	0.72 (0.52~0.99)	2.03	0.042	0.0%	0.583	–	–

<sup>a</sup>The heterogeneity test showed that the data of Kote-Jarai et al.<sup>17</sup> (stage 1) was heterogeneous. After excluding it, the heterogeneity was eliminated;

<sup>b</sup>The heterogeneity test showed that the data of Kote-Jarai et al.<sup>17</sup> (stage 1), Eeles et al.<sup>26</sup> (stage 1) and Hu et al.<sup>12</sup> was heterogeneous. After excluding it,

the heterogeneity was eliminated; <sup>c</sup>The heterogeneity test showed that the data of Soni et al.<sup>15</sup> and Lai et al.<sup>27</sup> was heterogeneous. After excluding it,

the heterogeneity was eliminated; <sup>d</sup>The heterogeneity test showed that the data of Lai et al.<sup>27</sup> was heterogeneous. After excluding it, the heterogeneity was

eliminated; <sup>e</sup>The heterogeneity test showed that the data of Kote-Jarai et al.<sup>17</sup> (stage 1), Kote-Jarai et al.<sup>17</sup> (stage 3) and Eeles et al.<sup>26</sup> (stage 1) was heterogeneous. After excluding it, the heterogeneity was eliminated.

SNP – single nucleotide polymorphism; PCa – prostate cancer; 95% CI – 95% confidence interval. Kote-Jarai et al.<sup>17</sup> was identified as 3 studies (stage 1, stage 2 and stage 3); Eeles et al.<sup>26</sup> was also identified as 3 studies (stage 1, stage 2 UK and stage 2 Australia).

associated with the risk of PCa (rs1058205 C vs T allele: OR = 0.79, 95% CI = 0.73~0.87, p-value <0.001; rs2735839 A vs G allele: OR = 0.78, 95% CI = 0.71~0.86, p-value <0.001; rs174776 T vs C allele: OR = 0.86, 95% CI = 0.80~0.93, p-value <0.001; rs17632542 T vs C allele: OR = 0.61, 95% CI = 0.43~0.86, p-value = 0.005; rs266849 G vs A allele: OR = 0.81, 95% CI = 0.71~0.92, p-value = 0.002; rs266878 G vs C allele: OR = 0.86, 95% CI = 0.78~0.94, p-value = 0.001; rs2569735 A vs G: OR = 0.90, 95% CI = 0.82~0.99, p-value = 0.032). For the genotypes, the pooled results showed that the genotype TC (TC vs TT: OR = 0.79, 95% CI = 0.72~0.86, p-value <0.001) and CC (CC vs TT: OR = 0.62, 95% CI = 0.49~0.77, p-value <0.001) of rs1058205, the genotype AG (AG vs GG: OR = 0.80, 95% CI = 0.71~0.91, p-value = 0.001) of rs2735839, the genotype CT (CT vs CC: OR = 0.87, 95% CI = 0.79~0.97, p-value = 0.010) of rs174776, the genotype TC (TC vs CC: OR = 0.57, 95% CI = 0.37~0.87, p-value = 0.009) and TT (TT vs CC: OR = 0.32, 95% CI = 0.14~0.75, p-value = 0.009) of rs17632542, the genotype GA (GA vs AA: OR = 0.80,

95% CI = 0.70~0.91, p-value = 0.001) and GG (GG vs AA: OR = 0.73, 95% CI = 0.55~0.97, p-value = 0.032) of rs266849, the genotype GC (GC vs CC: OR = 0.87, 95% CI = 0.78~0.97, p-value = 0.009) and GG (GG vs CC: OR = 0.72, 95% CI = 0.52~0.98, p-value = 0.036) of rs266878, the genotype CC (CC vs TT: OR = 0.77, 95% CI = 0.65~0.91, p-value = 0.003) of rs266876, and the genotype AA (AA vs GG: OR = 0.72, 95% CI = 0.52~0.99, p-value = 0.042) of rs2569735 were statistically associated with PCa risk, while there was no significance for the genotype AA of rs2735839, the genotype AG and AA of rs266882, the genotype TT of rs174776, the genotype CT of rs266876, the genotype GA and GG of rs1058274, or the genotype AG of rs2569735.

### Meta-analysis of associations between SNPs of *KLK3* and the Gleason score of PCa

Only rs2735839 was involved in the meta-analysis of associations between SNPs of *KLK3* and the Gleason score

Table 4. Meta-analysis for associations between SNPs and the GS of PCa

SNP	Number of studies	Test for overall effect			Test for heterogeneity		Test for publish bias	
		OR (95% CI)	Z-score	p-value	I <sup>2</sup>	p-value	P <sub>egger's</sub>	P <sub>begg's</sub>
<i>rs2735839</i> GS < 7 vs GS ≥ 8								
A allele vs G allele	3 [12, 24]	0.598 (0.465~0.770)	3.99	<0.001	0.0%	0.806	–	–
AG/GG vs AA	2 [11,12]	2.731 (0.622~12.00)	1.33	0.183	75.5%	0.043	–	–
<i>rs2735839</i> GS < 8 vs control								
G allele vs A allele	2 [19, 21]	0.841 (0.796~0.889)	6.14	<0.001	0.0%	0.883	–	–
<i>rs2735839</i> GS ≥ 8 vs control								
G allele vs A allele	2 [19, 21]	1.09 (0.991~1.201)	1.77	0.077	0.0%	0.517	–	–
<i>rs2735839</i> GS ≥ 4+3 vs GS ≤ 3+4								
G allele vs A allele	2 [11, 24]	1.413 (1.257~1.588)	5.80	<0.001	0.0%	0.360	–	–

SNP – single nucleotide polymorphism; GS – Gleason score; PCa – prostate cancer; 95% CI – 95% confidence interval.

(GS) of PCa.<sup>11,12,19,21,24</sup> As shown in Table 4, when compared with the group of GS ≥ 8 carrier, the A allele was a protective factor for the group of GS < 7 (A vs G allele: OR = 0.598, 95% CI = 0.465~0.770, p-value <0.001); when compared with the group of GS ≤ 3+4 carrier, the G allele was a risk factor for the group of GS ≥ 4+3 (G vs A allele: OR = 1.413, 95% CI = 1.257~1.588, p-value <0.001). When compared with the controls, the G allele was a protective factor for the group of GS < 8 (G vs A allele: OR = 0.841, 95% CI = 0.796~0.889, p-value <0.001), while not significantly associated with the group of GS ≥ 8 (G vs A allele: OR = 1.09, 95% CI = 0.991~1.201, p-value <0.077).

### Meta-analysis for associations between SNPs of *KLK3* and fatal PCa risk

SNP rs2735839 was also involved in the meta-analysis of associations between SNPs and the risk of fatal PCa.<sup>13,23</sup> The pooled result showed that there was no significance between rs2735839 and fatal PCa (G vs A allele: OR = 1.230, 95% CI = 0.725~2.088, p-value = 0.442).

### Heterogeneity test and sensitivity analysis

A heterogeneity test was performed and the results showed that heterogeneity existed in the meta-analysis of associations between the risk of PCa and rs1058205, rs2735839, rs266882, rs17632542, and rs266849. Therefore, a sensitivity analysis was conducted employing the sequential omission of individual studies to find the source of the heterogeneity. As shown in Table 3, after excluding some studies, the heterogeneity was eliminated. Most pooled results were not materially altered, indicating the robustness of the results of this meta-analysis, except the meta-analysis of the genotype (AA vs GG) of rs2735839 and the genotype (GG vs AA) of rs266849. After eliminating the heterogeneity, the genotype AA of rs2735839 was significantly associated with PCa risk (AA vs GG:

OR = 0.81, 95% CI = 0.67~0.97, p-value = 0.020), while there was no significant association between the genotype GG of rs266849 and PCa risk (GG vs AA: OR = 0.98, 95% CI = 0.86~1.10, p-value = 0.699).

### Publication bias assessment

Begg's funnel plot and Egger's test were performed to assess publication bias in the literature if the number of included studies was more than 3. The results of this meta-analysis showed that no evidence of publication bias was found for any of the analyses.

### Discussion

The etiology and pathogenesis of PCa is still elusive. However, recently, increasing evidence suggests that genetic factors are associated with PCa susceptibility. For many years, PSA, which plays an important role in sperm motility, has been used as a biomarker for PCa screening. The PSA is also involved in the proteolytic breakdown of the extracellular matrix in PCa tumorigenesis, which contributes to tumor invasion and metastasis<sup>29</sup>; high serum PSA correlates with mutations in p53 and overexpression of the B-cell lymphoma 2 protein, which inhibits apoptosis in tumor cells.<sup>30</sup> These findings strongly suggest that PSA plays a role in the etiology of PCa. The PSA protein is encoded by *KLK3*, and increasing numbers of studies have recently reported that the polymorphisms of *KLK3* associated with PSA levels may be associated with PCa. However, these results were conflicting and there was still no comprehensive analysis to clear up the confusion. Therefore, in this study, we performed a literature review and conducted a meta-analysis to explore the association between the SNPs of *KLK3* that were analyzed in more than 2 studies and the risk of PCa.

In total, 59 SNPs were mentioned in the literature, and among them, 21 SNPs were involved in more than



2 studies. Finally, 10 SNPs – rs1058205, rs2735839, rs266882, rs174776, rs17632542, rs266849, rs266878, rs266876, rs1058274, and rs2569735 – were eligible to be included in this meta-analysis. The pooled results indicated that the minor alleles of rs1058205 (C allele), rs2735839 (A allele), rs174776 (T allele), rs17632542 (T allele), rs266849 (G allele), rs266878 (G allele), and rs2569735 (A allele) were significantly associated with PCa risk. For the genotype analysis, when compared to genotypes of the common homozygotes (rs1058205: TT, rs2735839: GG, rs174776: CC, rs17632542: CC, rs266849: AA, rs266878: CC, rs266876: TT, and rs2569735: GG), the heterozygote genotype carriers of rs1058205 (CT), rs2735839 (AG), rs174776 (CT), rs17632542 (TC), rs266849 (GA), and rs266878 (GC) had a lower risk of PCa, as did the homozygotes genotype carrier of rs1058205 (CC), rs2735839 (AA), rs17632542 (TT), rs266878 (GG), rs266876 (CC), and rs2569735 (AA).

The Gleason grading system remains the most powerful prognostic predictor for PCa because it delineates the architectural patterns of tumors.<sup>31</sup> It is the core value in risk-scoring systems, including the D'Amico classification system,<sup>32</sup> which incorporates the GS, clinical stage and PSA level to stratify the risk of recurrence of localized PCa before treatment and is used to guide treatment selection. Thus, we subsequently performed the GS stratified analyses; only rs2735839 was involved in this part. The GS results range from 1 to 10, and can be divided into 3 grades: GS 1–6 is the low grade in the Gleason grading system; GS 8–10 is the high grade; and GS 7 is the intermediate grade. Our pooled results showed that when compared with GS  $\geq$  8 PCa (high grade), the A allele was a protective factor for GS < 7 PCa. Patients with GS 7 PCa are a heterogeneous group, consisting of 2 subtypes: GS 3+4 and GS 4+3.<sup>33</sup> The GS 4+3 subtype has had less favorable clinical outcomes than the GS 3+4 subtype.<sup>33–35</sup> Therefore, the GS 3+4 subtype can be treated as low grade, while GS 4+3 subtype is high grade. Currently there are no reliable biomarkers to further stratify this group. Some studies have therefore stratified GS 7 PCa to explore effective biomarkers. We pooled their relevant data, and the results indicated that when compared to the GS  $\leq$  3+4 PCa carrier, the G allele was a risk factor for the GS  $\geq$  4+3 carrier.

Finally, we also performed a meta-analysis of associations of the SNPs of *KLK3* and fatal PCa, and again only rs2735839 was involved in this analysis. Our pooled results suggested that there was no significant association between them.

To our knowledge, this is the first study to review all of the SNPs of *KLK3* mentioned in the relevant literature and to perform meta-analyses to illuminate the association between the risk of PCa and SNPs of *KLK3* that have been involved in more than 2 studies. Although our study showed some positive results, this meta-analysis had 2 limitations that should be taken into consideration when assessing the results. First, the overall outcomes were based on unadjusted effect estimates. Among the included studies, only a few were matched for age or other factors.

Therefore, some other confounding factors could slightly modify the estimates, and a more precise evaluation would have to be adjusted for the potentially suspicious factors. Second, in some pooled analyses such as the GS analysis, the number of included studies was too small, so further relevant studies should be carried out in the future so that a stronger conclusion can be drawn.

## Conclusions

A strong association was observed between rs1058205, rs2735839, rs266882, rs174776, rs17632542, rs266849, rs266878, rs266876, rs1058274 and rs2569735, and PCa. Therefore, these SNPs may be valuable as biomarkers for PCa risk. Besides, G allele of rs2735839 was noted as a risk factor for the GS < 7 PCa carrier when compared with GS  $\geq$  8 PCa, as well as for the GS  $\geq$  4+3 carrier when compared to the GS  $\leq$  3+4 PCa carrier. Considering that the quality and quantity of the reviewed articles were limited, larger well-designed studies should be conducted in the future to further confirm the association between *KLK3* genetic polymorphisms and PCa.

## References

1. Askari F, Parizi MK, Jessri M, Rashidkhani B. Fruit and vegetable intake in relation to prostate cancer in Iranian men: A case-control study. *Asian Pac J Cancer Prev*. 2014;15(13):5223–5227.
2. Altekruse SF, Huang L, Cucinelli JE, McNeel TS, Wells KM, Oliver MN. Spatial patterns of localized-stage prostate cancer incidence among white and black men in the southeastern United States. *Cancer Epidemiol Biomarkers Prev*. 2010;19(6):1460–1467.
3. Pilia G, Chen WM, Scuteri A, et al. Heritability of cardiovascular and personality traits in 6,148 Sardinians. *PLoS Genet*. 2006;2(8):e132.
4. Bansal A, Murray DK, Wu JT, Stephenson RA, Middleton RG, Meikle AW. Heritability of prostate-specific antigen and relationship with zonal prostate volumes in aging twins. *J Clin Endocrinol Metab*. 2000;85(3):1272–1276.
5. Ahn J, Berndt SI, Wacholder S, et al. Variation in *KLK* genes, prostate-specific antigen and risk of prostate cancer. *Nat Genet*. 2008;40(9):1032–1034.
6. Wiklund F, Zheng SL, Sun J, et al. Association of reported prostate cancer risk alleles with PSA levels among men without a diagnosis of prostate cancer. *Prostate*. 2009;69(4):419–427.
7. Eeles RA, Kote-Jarai Z, Giles GG, et al. Multiple newly identified loci associated with prostate cancer susceptibility. *Nat Genet*. 2008;40(3):316–321.
8. Choe EK, Lee Y, Cho JY, et al. Search for genetic factor association with cancer-free prostate-specific antigen level elevation on the basis of a genome-wide association study in the Korean population. *Eur J Cancer Prev*. 2017;27(5):453–460. doi:10.1097/CEJ.0000000000000359
9. Chen C, Xin Z. Single-nucleotide polymorphism rs1058205 of *KLK3* is associated with the risk of prostate cancer: A case-control study of Han Chinese men in Northeast China. *Medicine (Baltimore)*. 2017;96(10):e6280.
10. Stegeman S, Amankwah E, Klein K, et al. A large-scale analysis of genetic variants within putative miRNA binding sites in prostate cancer. *Cancer Discov*. 2015;5(4):368–379.
11. He Y, Gu J, Strom S, Logothetis CJ, Kim J, Wu X. The prostate cancer susceptibility variant rs2735839 near *KLK3* gene is associated with aggressive prostate cancer and can stratify Gleason score 7 patients. *Clin Cancer Res*. 2014;20(19):5133–5139.
12. Hu J, Qiu Z, Zhang L, Cui F. Kallikrein 3 and vitamin D receptor polymorphisms: Potentials environmental risk factors for prostate cancer. *Diagn Pathol*. 2014; 9:84.

13. Shui IM, Lindström S, Kibel AS, et al. Prostate cancer (PCa) risk variants and risk of fatal PCa in the National Cancer Institute Breast and Prostate Cancer Cohort Consortium. *Eur Urol*. 2014;6(6):1069–1075.
14. Wang NN, Xu Y, Yang K, et al. Susceptibility loci associations with prostate cancer risk in Northern Chinese men. *Asian Pac J Cancer Prev*. 2013;14(5):3075–3078.
15. Soni A, Bansal A, Mishra AK, et al. Association of androgen receptor, prostate-specific antigen, and *CYP19* gene polymorphisms with prostate carcinoma and benign prostatic hyperplasia in a North Indian population. *Genet Test Mol Biomarkers*. 2012;16(8):835–840.
16. Kwon EM, Holt SK, Fu R, et al. Androgen metabolism and JAK/STAT pathway genes and prostate cancer risk. *Cancer Epidemiol*. 2012;36(4):347–353.
17. Kote-Jarai Z, Amin AI, Olama A, et al. Identification of a novel prostate cancer susceptibility variant in the *KLK3* gene transcript. *Hum Genet*. 2011;129(6):687–694.
18. Penney KL, Schumacher FR, Kraft P, et al. Association of *KLK3* (PSA) genetic variants with prostate cancer risk and PSA levels. *Carcinogenesis*. 2011;32(6):853–859.
19. Lindstrom S, Schumacher F, Siddiq A, et al. Characterizing associations and SNP-environment interactions for GWAS-identified prostate cancer risk markers—results from BPC3. *PLoS One*. 2011;6(2):e17142.
20. Ciampa J, Yeager M, Amundadottir L, et al. Large-scale exploration of gene–gene interactions in prostate cancer using a multistage genome-wide association study. *Cancer Res*. 2011;71(9):3287–3295.
21. Parikh H, Wang Z, Pettigrew KA, et al. Fine mapping the *KLK3* locus on chromosome 19q13.33 associated with prostate cancer susceptibility and PSA levels. *Hum Genet*. 2011;129(6):675–685.
22. Gudmundsson J, Besenbacher S, Sulem P, et al. Genetic correction of PSA values using sequence variants associated with PSA levels. *Sci Transl Med*. 2010;2(62):62ra92.
23. Gallagher DJ, Vijai J, Cronin AM, et al. Susceptibility loci associated with prostate cancer progression and mortality. *Clin Cancer Res*. 2010;16(10):2819–2832.
24. Kader AK, Sun J, Isaacs SD, et al. Individual and cumulative effect of prostate cancer risk-associated variants on clinicopathologic variables in 5,895 prostate cancer patients. *Prostate*. 2009;69(11):1195–1205.
25. Xu J, Isaacs SD, Sun J, et al. Association of prostate cancer risk variants with clinicopathologic characteristics of the disease. *Clin Cancer Res*. 2008;14(18):5819–5824.
26. Eeles RA, Kote-Jarai Z, Giles GG, et al. Multiple newly identified loci associated with prostate cancer susceptibility. *Nat Genet*. 2008;40(3):316–321.
27. Lai J, Kedda MA, Hinze K, et al. *PSA/KLK3 ARE1* promoter polymorphism alters androgen receptor binding and is associated with prostate cancer susceptibility. *Carcinogenesis*. 2007;28(5):1032–1039.
28. Cicek MS, Liu X, Casey G, Witte JS. Role of androgen metabolism genes *CYP1B1*, *PSA/KLK3*, and *CYP11alpha* in prostate cancer risk and aggressiveness. *Cancer Epidemiol Biomarkers Prev*. 2005;14(9):2173–2177.
29. Webber MM, Waghray A, Bello D. Prostate-specific antigen, a serine protease, facilitates human prostate cancer cell invasion. *Clin Cancer Res*. 1995;1(10):1089–1094.
30. Lin JT, Wang JS, Jiann BP, et al. Correlation of p53 protein accumulation and Bcl-2 overexpression with histopathological features in prostatic cancer. *J Formos Med Assoc*. 2005;104(11):864–867.
31. Epstein JI, Allsbrook WC Jr, Amin MB, Egevad LL. The 2005 International Society of Urological Pathology (ISUP) Consensus Conference on Gleason Grading of Prostatic Carcinoma. *Am J Surg Pathol*. 2005;29(9):1228–1242.
32. D’Amico AV, Whittington R, Malkowicz SB, et al. Biochemical outcome after radical prostatectomy, external beam radiation therapy, or interstitial radiation therapy for clinically localized prostate cancer. *JAMA*. 1998;280(11):969–974.
33. Orozco R, O’Dowd G, Kunnel B, Miller MC, Veltri RW. Observations on pathology trends in 62,537 prostate biopsies obtained from urology private practices in the United States. *Urology*. 1998;51(2):186–195.
34. Sakr WA, Tefilli MV, Grignon DJ, et al. Gleason score 7 prostate cancer: A heterogeneous entity? Correlation with pathologic parameters and disease-free survival. *Urology*. 2000;56(5):730–734.
35. Chan TY, Partin AW, Walsh PC, Epstein JI. Prognostic significance of Gleason score 3+4 versus Gleason score 4+3 tumor at radical prostatectomy. *Urology*. 2000;56(5):823–827.



# Methods for assessing the severity of perinatal asphyxia and early prognostic tools in neonates with hypoxic–ischemic encephalopathy treated with therapeutic hypothermia

Wojciech Walas<sup>1,A–F</sup>, Maria Wilińska<sup>2,A,B,F</sup>, Monika Bekiesińska-Figatowska<sup>3,A,B,F</sup>, Zenon Halaba<sup>4,A,B,F</sup>, Robert Śmigiel<sup>5,A,B,E,F</sup>

<sup>1</sup> Pediatric and Neonatal Intensive Care Unit, University Hospital in Opole, Poland

<sup>2</sup> Department of Neonatology, Centre of Postgraduate Medical Education, Warszawa, Poland

<sup>3</sup> Department of Diagnostic Imaging, Institute of Mother and Child, Warszawa, Poland

<sup>4</sup> Department of Pediatrics, Institute of Medical Sciences, University of Opole, Poland

<sup>5</sup> Department of Pediatrics, Division of Propaedeutic Pediatrics and Rare Disorders, Wrocław Medical University, Poland

A – research concept and design; B – collection and/or assembly of data; C – data analysis and interpretation;

D – writing the article; E – critical revision of the article; F – final approval of the article

Advances in Clinical and Experimental Medicine, ISSN 1899–5276 (print), ISSN 2451–2680 (online)

*Adv Clin Exp Med.* 2020;29(8):1011–1016

## Address for correspondence

Wojciech Walas

E-mail: wojciechwalas@wp.pl

## Funding sources

This research was partially carried out within framework of the National Science Centre (NCN), Poland, project No. UMO-2018/29/B/ST8/01490.

## Conflict of interest

None declared

Received on April 28, 2020

Reviewed on May 7, 2020

Accepted on June 22, 2020

Published online on August 21, 2020

## Abstract

Despite the progress in perinatal care, perinatal asphyxia (PA) remains a significant problem in neonatology. The development of therapeutic hypothermia (TH) has improved the prognosis, but it still remains uncertain in hypoxic neonates. The evaluation of the severity of ischemia/hypoxia after birth is crucial to the choice of treatment, and with accurate long-term prognosis, appropriate further patient care can be planned. This article presents various methods for the preliminary assessment of brain damage and prognosis in newborns with PA treated with TH. The importance of assessing the neurological condition and the usefulness of laboratory and electrophysiological testing and imaging are discussed. New methods are also noted, which are at the stage of clinical trials. A combination of the prognostic tests presented in this article can provide greater prognostic accuracy for predicting long-term neurological outcomes in infants with hypoxic–ischemic encephalopathy (HIE) undergoing TH than either of these tests independently. Acknowledging the limitations of individual tools in certain clinical situations and the integration of the information available from multiple biomarkers may help improve the accuracy of prognostication.

**Key words:** perinatal asphyxia, neonate, prediction factors, therapeutic hypothermia, hypoxic–ischemic encephalopathy

## Cite as

Walas W, Wilińska M, Bekiesińska-Figatowska M, Halaba Z, Śmigiel R. Methods for assessing the severity of perinatal asphyxia and early prognostic tools in neonates with hypoxic–ischemic encephalopathy treated with therapeutic hypothermia. *Adv Clin Exp Med.* 2020;29(8):1011–1016. doi:10.17219/acem/124437

## DOI

10.17219/acem/124437

## Copyright

© 2020 by Wrocław Medical University

This is an article distributed under the terms of the Creative Commons Attribution 3.0 Unported (CC BY 3.0) (<https://creativecommons.org/licenses/by/3.0/>)

## Introduction

Despite recent advances in perinatal care, neonatal hypoxic–ischemic encephalopathy (HIE) is one of the most common causes of severe neurological deficit in children, present in approx. 15 out of 10,000 live births.<sup>1</sup> According to the World Health Organization (WHO), perinatal asphyxia (PA) represents the 3<sup>rd</sup> most common cause of neonatal death (23%). This means that all over the world, almost 600,000 newborns die every year, and at least as many develop severe complications such as epilepsy, cerebral palsy and developmental delay due to acute perinatal sentinel events.<sup>2</sup> Therapeutic hypothermia (TH) is a method of treatment that has proven effective in protecting the brain against the effects of ischemia/hypoxia in neonates after PA; it is recommended in both term and near-term newborns.<sup>3,4</sup> The qualification criteria and contraindications for TH are adjusted as knowledge progresses and they are included in recommendations and standards for the treatment of newborns. In this age group, 2 methods of cooling are available: selective head hypothermia and whole body hypothermia. Although the incidence rate of HIE is known and TH is increasingly available, no accurate data on the frequency of this treatment are available.

The mechanism for such neurological protection is thought to be multifactorial, including limitation of post-arrest endothelial dysfunction, decreased free radical release and blunting of the post-reperfusion inflammatory cascade. Early evaluation of the degree of brain damage in newborns after PA is of great importance in determining the appropriate management and prognosis. This assessment is based on a complex analysis of different factors.

The aim of this article is to present the methods used to estimate the severity of PA and the prognostic tools for neonates with HIE treated with TH.

## Clinical assessment of neurological status

The neurological status at birth and during treatment is routinely assessed in neonatal wards. Assessing a newborn's neurological status after PA is usually difficult due to the serious overall condition and the need to use drugs which affect the brain. The use of scales makes it possible to objectify the evaluation and compare results between different patients.

The Apgar scale is primarily used to assess the condition of a newborn at birth and is one of the basic criteria for pre-qualification for TH treatment. It is also useful as a prognostic tool, though the results of studies are ambiguous. Lupton et al. showed that the Apgar score at 10 min provides useful prognostic data for infants with HIE. They noticed that death or moderate/severe disability is common, but not uniform, with Apgar scores <3.<sup>5</sup> Shah et al. found that 1/3 of infants with a 10-min Apgar score

of 0 who survived to reach the neonatal intensive care unit had normal scores on formal developmental assessments.<sup>6</sup>

The Sarnat scale estimates the severity of neurological disorders in newborns after PA. It distinguishes 3 stages of HIE: stage 1 – mild encephalopathy associated with hyperalertness, sympathetic overdrive and a normal electroencephalogram (EEG); stage 2 – moderate encephalopathy marked by obtundation, hypotonia, multifocal seizures, and an EEG showing periodic or continuous delta activity; and stage 3 – severe encephalopathy in which infants are stuporous and flaccid with an isoelectric or periodic EEG. This scale is one of the factors which is widely used in qualifying a newborn for TH treatment, but it is also a prognostic tool. The creators of the scale noted that infants who did not enter stage 3 and who had signs of stage 2 for fewer than 5 days had developed normally on follow-up, but persistence of stage 2 for a week or failure of the EEG to normalize predicted later neurological impairment or death.<sup>7</sup> Short-term neurological improvement expressed by the Sarnat scale predicts a neurodevelopmental outcome at 18–24 months.<sup>8</sup>

The Thompson scale is also suitable for assessing the neurological status of neonates after PA. It takes into account 9 parameters; the score ranges from 0–22 points and is directly proportional to the severity of the neurological condition. This scale is also helpful in determining the prognosis for neurological development. Thompson et al. noted that children with a maximum of 10 points developed properly in the 1<sup>st</sup> year of life, while 65% of those with more than 10 points and 92% with more than 15 points developed incorrectly.<sup>9</sup> Mendler et al. demonstrated the usefulness of this scale as a prognostic tool.<sup>10</sup>

## Laboratory tests

Among the laboratory tests, acid-base balance holds a special place because metabolic acidosis is the 2<sup>nd</sup> pre-qualification criterion for TH treatment, next to the Apgar assessment. The consensus is that the severity of lactacidemia reflects the degree of fetal hypoxia–ischemia, but a single lactate measurement gives no definitive information regarding the duration of asphyxia. Metabolic acidosis also has a prognostic value. Worsening metabolic acidosis at birth correlated with severe brain injury in neonates who were treated with TH.<sup>11</sup> Moreover, higher serum level of lactate following TH and abnormal results of brain magnetic resonance imaging (MRI) are associated with a poor neurodevelopmental outcome.<sup>12</sup> Results obtained by other authors are similar. Also, the meta-analysis carried out by Malin et al. showed that low arterial cord pH was significantly associated with neonatal mortality, HIE, intraventricular hemorrhage, or periventricular leukomalacia.<sup>13</sup>

Because PA affects the whole body, it is understandable that it causes an increase in the activity of enzymes which are markers of damage to various organs. Liver enzymes,



myocardial injury biomarkers and other enzymes are often measured in newborns with HIE, being widely available and relatively cheap. Muniraman et al. demonstrated a relationship between the degree of hypoxia and transaminases (aspartate transaminase (AST) and alanine transaminase (ALT)), alkaline phosphatase and ammonia levels.<sup>14</sup> Research conducted by Montaldo et al. showed that early cardiac troponin I (CT-1) concentration correlates with the severity of HIE and with development at 18 months.<sup>15</sup> It is suggested to use CT-1, myoglobin and creatine kinase-Mb as new biomarkers for diagnosis of neonatal HIE.<sup>16</sup> Changes in lactate dehydrogenase are associated with central gray matter lesions and may be a useful biomarker for predicting future neurodevelopmental prognosis in infants with HIE.<sup>17</sup> Although the hypoxia markers mentioned above have been studied many times and are quite widely used in clinical practice, there are currently no consistent data to establish thresholds corresponding to HIE severity.

A consistent finding across a number of studies is the up-regulation of the innate immune system, as evidenced by the increased levels of cytokines in newborns with HIE. Levels of inflammatory interleukins (ILs; IL-1 $\beta$ , IL-2, IL-4, IL-6, IL-8, IL-10, IL-13, and IL-10), monocyte chemoattractant protein-1 (MCP-1) and tumor necrosis factor  $\alpha$  (TNF- $\alpha$ ) increase significantly in newborns with HIE and correlate with both the severity of HIE and outcomes.<sup>18</sup> Attention was also paid to the usefulness of determining the levels of specific biomarkers targeting the so-called “neurovascular unit”, which may be helpful in assessing the severity of HIE and prognosis, but which are currently at the stage of clinical trials, are usually expensive and are difficult to obtain. Calcium-binding proteins and other brain biomarkers have been taken into account. Roka et al. and Giuseppe et al. noted that serum S100B protein and neuron-specific enolase (NSE) levels are elevated in newborns with HIE.<sup>19,20</sup> Moreover, it was also shown that serum S100B and NSE levels in babies with HIE are associated with neurodevelopmental disorders at 15 months.<sup>21</sup> Ennen et al. noted that serum glial fibrillary acidic protein levels during the 1<sup>st</sup> week of life were elevated in neonates with HIE and were predictive of brain injury on MRI.<sup>22</sup> Florio et al. have shown that newborns with HIE have elevated serum levels of activin A and concluded that this parameter is also taken into account as a prognostic tool.<sup>23</sup> Douglas-Escobar et al. showed that ubiquitin C-terminal hydrolase L1 levels have the potential to predict long-term neurological disorder in these patients.<sup>24</sup> Lv et al. noted the predictive value of serum tau protein level for neurodevelopmental outcome in neonates with HIE.<sup>25</sup>

There have been a few publications on the basis of which it can be assumed that other markers may prove useful in assessing HIE severity and predicting prognosis. The following markers have been considered: plasma neurofilament light protein, interferon, sercetoneurin, osteopontin, monocyte chemoattractant protein-1, macrophage inflammatory protein 1a, vascular endothelial growth factor (VEGF),

leptin, adiponectin, and erythropoietin.<sup>26–31</sup> The metabolic products of HIE reveal early biomarkers of injury which deprive the neonatal brain of oxygen and glucose, and which trigger a biochemical cascade of many adverse reactions. The details and range of metabolic change occurring in response to HIE remains unclear, but research on the relationship between the severity of HIE and metabolomic profile analysis in umbilical cord blood, serum and urine (mainly amino acid, acylcarnitine and organic acid profiles) is promising and suggest they might be used as a new prognostic tool and treatment targets, but these studies are at the experimental stage. Moreover, the laboratory equipment for metabolome assays is not very accessible.<sup>32,33</sup>

## Electrophysiological tests

Among electrophysiological tests, amplitude-integrated EEG (aEEG) plays a special role, because it is one of the qualification factors for TH treatment and it is routinely monitored during such treatment. It requires 3 electrodes to be placed on the head of the newborn; it is quite easy to perform and the recording is interpreted in comparison to several patterns. Continuous monitoring of aEEG allows the bioelectrical function of the brain and its trend to be estimated. It is also very useful in detecting subclinical seizures. Its usefulness in the prognosis of newborns after PA has also been demonstrated. Liu et al. noted that aEEG reflects the degree of the lesion as well as the long-term prognosis of newborns with HIE.<sup>34</sup> The usefulness of aEEG in the prognosis of newborns after PA has been confirmed in research conducted by other authors.<sup>35–37</sup> Also, from the systematic literature review carried out by Del Río, it follows that aEEG background activity, recorded during the first 72 h of life, has a strong predictive value in infants with HIE treated with TH or not. In another meta-analysis, the authors concluded that a persistently abnormal aEEG at 48 h or later is associated with an adverse neurodevelopmental outcome.<sup>38,39</sup> The implementation and especially the interpretation of the classic, multi-channel EEG is more difficult, but provides additional information on the degree of brain damage and prognosis. It has been noted that electrographic seizure burden is associated with severity of brain injury on MRI in newborns with HIE undergoing TH.<sup>40</sup> Other authors have demonstrated that burst suppression, low voltage and flat traces in the EEG of term neonates with HIE most accurately predict the long-term neurodevelopmental outcome and that excessive EEG discontinuity is associated with increased cerebral tissue injury on MRI and is predictive of abnormal neurodevelopmental outcome in infants treated with TH.<sup>41,42</sup> Weeke et al. noted that severely abnormal EEG background activity at 36 h and 48 h of life was associated with severe injury on MRI and abnormal neurodevelopmental outcomes.<sup>43</sup> A meta-analysis performed by Han et al. found that EEG

background activity is predictive of long-term neurological outcome in TH-treated neonates with HIE, and that burst suppression, low voltage and flat trace are potential predictors of death or neurodevelopmental impairment.<sup>44</sup> Another systematic review and meta-analysis confirms the immense usefulness of EEG as a prognostic tool.<sup>45</sup>

The brain injury after PA affects various areas of the brain and may also include the brainstem. Brainstem evoked potentials (BEPs) are used to diagnose various types of brain damage. Some authors note the usefulness of the BEPs in predicting prognosis in newborns with HIE, while others have reported that a bilateral absence of cortical somatosensory evoked potentials (SSEPs) predicts moderate/severe MRI pattern of injury in newborns treated with TH.<sup>46</sup> Cainelli et al. considered that among BEPs, visual evoked potentials (VEP) constitute the single best neurophysiological prognostic marker, but the combination of neurophysiological tests is more valuable.<sup>47</sup>

## Neuroimaging

Neuroimaging plays a special role in determining the prognosis of newborns with HIE. Cranial ultrasound (CUS) is a readily available, inexpensive bedside examination that is routinely performed on children with HIE, but its prognostic value is limited. It has several limitations, such as low sensitivity for detecting cortical, cerebellar and brainstem lesions, marked inter-observer variability, and operator dependency. Edema dominates in early brain ultrasound imaging in newborns after PA, and assessment of its echostructure is difficult and subjective. Cranial Doppler ultrasonography is a method that objectively assesses cerebral arterial blood flow and resistance. Measurements using the Doppler technique are usually taken in the middle cerebral artery. It was noted that TH reduced the importance of measuring resistance in cerebral vessels; nevertheless, Gerner et al. found that pre- and post-cooling transfontanellar duplex brain sonography resistive index (RI) values may be a useful prognostic tool, in conjunction with other clinical information for neonates with HIE.<sup>48</sup> Likewise, Annink et al. developed and validated a CUS scoring system that takes into account the RI and the sum of deep grey matter and white matter involvement, and noted that it is associated with neurodevelopmental outcome in these patients.<sup>49</sup>

The importance of computed tomography (CT) in diagnosing HIE and predicting prognosis has diminished considerably with the popularization of MRI. The CT is less sensitive and less specific than MRI in diagnosing neonatal HIE with much lower tissue resolution; another major disadvantage is radiation exposure. For these reasons, CT is usually omitted in the diagnostic chain. However, CT is more sensitive in detecting intracranial hemorrhage than ultrasonography and requires much less time than MRI; therefore, it may be useful in some situations.<sup>50</sup>

The MRI is nowadays a standard tool for determining the pattern and severity of brain injury as well as the prognosis in infants with HIE. This method yields equal insight into all brain structures. Conventional MRI techniques have proven useful in assessing the severity of brain damage and predicting the development of newborns with HIE.<sup>51</sup> Newer MRI techniques have also been developed that are useful in assessing the brains of newborns with HIE. Gradient-echo T2\*-weighted images and susceptibility-weighted imaging (SWI) allow for the detection of both hemorrhage and calcifications, which is important because as many as 38% of TH-treated patients have intracranial hemorrhage (ICH). Although preliminary results suggest that HIE remains an independent risk factor for delayed neurodevelopment in these neonates – while ICH seems to have no significant effect – further studies are needed to elucidate this.<sup>52</sup> Diffusion-weighted imaging (DWI) has also been studied.<sup>53</sup> Rana et al. noted that apparent diffusion coefficient value can be used as a marker to detect chronic hypoxic–ischemic brain injury.<sup>54</sup>

Magnetic resonance spectroscopy (MRS) is increasingly being performed. Mitra et al. showed that lactate/N-acetylaspartate levels in proton MRS within 2 weeks of birth accurately predict two-year motor, cognitive and language outcomes in neonatal encephalopathy after TH.<sup>55</sup> Lemmon et al. noted that diffusion tensor imaging (DTI) may be useful in predicting the development of newborns with HIE.<sup>56</sup> Some authors have proposed study models and MRI estimation scales to objectify the results. Trivedi et al. proposed a validated clinical MRI injury scoring system in neonates with HIE, wherein signal abnormality was scored on T1-weighted, T2-weighted and DWI sequences, and was assessed in 5 regions; MRI injury was graded as none, mild, moderate, or severe. They showed that this scoring system is a significant predictor of neurodevelopmental outcome at 18–24 months in neonates with HIE.<sup>57</sup> Also, Weeke et al. suggested a novel MRI score, which includes DWI and proton MRS (HMRS), assesses all important brain areas and has predictive value for outcomes at 2 years of age and at school age in infants with HIE.<sup>58</sup>

## Other methods

There are several articles whose authors point out the importance of near infra-red spectroscopy in prognosis in newborns with HIE. Jain et al. found that increasing regional oxygen saturation is associated with moderate/severe brain injury as assessed using MRI and correlates with poor neurodevelopmental outcomes in infants with HIE undergoing TH.<sup>59</sup> Heart rate variability analysis is also drawing attention. Kayton et al. found a correlation between heart rate characteristic index score and severity of brain injury in neonates with HIE.<sup>60</sup> Because brain damage causes a dysfunction of the thermoregulation center, the method of assessing the degree of brain damage and

prognosis based on non-invasive estimation of endogenous heat production has also garnered interest recently.<sup>61</sup> Preliminary results are encouraging. Mietzsch et al. examined the correlation between servo-controlled mattress temperature and the degree of brain damage in newborns treated with TH, and concluded that the output temperature of cooling devices is a potential and easily obtainable early physiological biomarker of outcome.<sup>62</sup>

## Summary

A reliable, evidence-based prognosis is essential for parental counseling regarding possible long-term sequelae. Despite the significant development of various diagnostic methods, assessing the degree of brain damage and prognosis in newborns with HIE treated with TH still remains a challenge, because all diagnostic tools have limitations: none are fully sensitive and specific, some cannot be performed in the intensive care unit, others are expensive, and some are only at the stage of assessing clinical suitability. The predictive value of an individual test for subsequent outcomes leaves a great deal to be desired. It seems that a combination of the prognostic tests presented in this article would provide greater prognostic accuracy for predicting long-term neurological outcomes in infants with HIE undergoing HT than any of these tests independently.<sup>38,45</sup>

Acknowledging the limitations of individual tools in certain clinical situations and integrating the information available from multiple biomarkers may help improve the accuracy of prognostication.

## ORCID iDs

Wojciech Walas  <https://orcid.org/0000-0001-7941-2718>  
 Maria Wilińska  <https://orcid.org/0000-0002-7557-3714>  
 Monika Bekiesińska-Figatowska  <https://orcid.org/0000-0003-1787-3425>  
 Zenon Halaba  <https://orcid.org/0000-0002-2905-0437>  
 Robert Śmigiel  <https://orcid.org/0000-0003-2930-9549>

## References

- Graham EM, Ruis KA, Hartman AL, Northington FJ, Fox HE. A systematic review of the role of intrapartum hypoxia-ischemia in the causation of neonatal encephalopathy. *Am J Obstet Gynecol*. 2008;199(6):587–595.
- World Health Organization. <http://www.childmortality.org/>. Global Health Observatory (GHO); WHO 2016. Accessed April 10, 2020.
- Jacobs SE, Berg M, Hunt R, Tarnow-Mordi WO, Inder TE, Davis PG. Cooling for newborns with hypoxic-ischaemic encephalopathy. *Cochrane Syst Rev*. 2013;2013(1):CD003311. <https://doi.org/10.1002/14651858.CD003311.pub3>
- Wyllie J, Bruinenberg J, Roehr CC, Rüdiger M, Trevisanuto D, Urlesberger B. European Resuscitation Council Guidelines for Resuscitation 2015. Section 7. Resuscitation and support of transition of babies at birth. *Resuscitation*. 2015;95:249–263.
- Laptook AR, Shankaran S, Ambalavanan N, et al; Hypothermia Subcommittee of the NICHD Neonatal Research Network. Outcome of term infants using Apgar scores at 10 minutes following hypoxic-ischemic encephalopathy. *Pediatrics*. 2009;124(6):1619–1626.
- Shah P, Anvekar A, McMichael J, Rao S. Outcomes of infants with Apgar score of zero at 10 min: The West Australian experience. *Arch Dis Child Fetal Neonatal Ed*. 2015;100(6):492–494.
- Sarnat HB, Sarnat MS. Neonatal encephalopathy following fetal distress: A clinical and encephalographic study. *Arch Neurol*. 1976;33(10):696–705.
- Grass B, Scheidegger S, Latal B, Hagmann C, Held U, Brotschi B; National Asphyxia and Cooling Register Group; Follow-up Group. Short-term neurological improvement in neonates with hypoxic-ischemic encephalopathy predicts neurodevelopmental outcome at 18–24 months. *J Perinat Med*. 2020;48(3):296–303.
- Thompson CM, Puterman AS, Linley LL, et al. The value of a scoring system for hypoxic-ischaemic encephalopathy in predicting neurodevelopmental outcome. *Acta Paediatr*. 1997;86(7):757–761.
- Mendler MR, Mendler I, Hassan MA, Mayer B, Bode H, Hummler HD. Predictive value of Thompson score for long-term neurological and cognitive outcome in term newborns with perinatal asphyxia and hypoxic-ischemic encephalopathy undergoing controlled hypothermia treatment. *Neonatology*. 2018;114(4):341–347.
- Wayock CP, Meserole RL, Saria S, et al. Perinatal risk factors for severe injury in neonates treated with whole-body hypothermia for encephalopathy. *Am J Obstet Gynecol*. 2014;211(1):41.e1–41.e8.
- Chiang MC, Lien R, Chu SM, et al. Serum lactate, brain magnetic resonance imaging and outcome of neonatal hypoxic-ischemic encephalopathy after therapeutic hypothermia. *Pediatr Neonatol*. 2016;57(1):35–40.
- Malin GL, Morris RK, Khan KS. Strength of association between umbilical cord pH and perinatal and long term outcomes: Systematic review and meta-analysis. *BMJ*. 2010;340:c1471.
- Muniraman H, Gardner D, Skinner J, et al. Biomarkers of hepatic injury and function in neonatal hypoxic-ischemic encephalopathy and with therapeutic hypothermia. *Eur J Pediatr*. 2017;176(10):1295–1303.
- Montaldo P, Rosso R, Chello G, Giliberti P. Cardiac troponin I concentrations as a marker of neurodevelopmental outcome at 18 months in newborns with perinatal asphyxia. *J Perinatol*. 2014;34(4):292–295.
- Hong F, Song L, Zhu YY, Ji JH, Zhu MJ, Xu M. Cardiac troponin I, myoglobin, and creatine kinase-Mb as new biomarkers for diagnosis of neonatal hypoxic-ischemic encephalopathy. *J Biol Regul Homeost Agents*. 2019;33(4):1201–1207.
- Yum SK, Moon CJ, Youn YA, Sung IK. Changes in lactate dehydrogenase are associated with central gray matter lesions in newborns with hypoxic-ischemic encephalopathy. *J Matern Fetal Neonatal Med*. 2017;30(10):1177–1181.
- Chaparro-Huerta V, Flores-Soto ME, Merin Sigala ME, et al. Proinflammatory cytokines, enolase and S-100 as early biochemical indicators of hypoxic-ischemic encephalopathy following perinatal asphyxia in newborns. *Pediatr Neonatol*. 2017;58(1):70–76.
- Roka A, Kelen D, Halasz J, Beko G, Azzopardi D, Szabo M. Serum S100B and neuron-specific enolase levels in normothermic and hypothermic infants after perinatal asphyxia. *Acta Paediatr*. 2012;101(3):319–323.
- Giuseppe D, Sergio C, Pasqua B, et al. Perinatal asphyxia in preterm neonates leads to serum changes in protein S-100 and neuron specific enolase. *Curr Neurovasc Res*. 2009;6(2):110–116.
- Massaro AN, Chang T, Baumgart S, McCarter R, Nelson KB, Glass P. Biomarkers S100B and neuron-specific enolase predict outcome in hypothermia-treated encephalopathic newborns. *Pediatr Crit Care Med*. 2014;15(7):615–622.
- Ennen CS, Huisman TA, Savage WJ, et al. Glial fibrillary acidic protein as a biomarker for neonatal hypoxic-ischemic encephalopathy treated with whole-body cooling. *Am J Obstet Gynecol*. 2011;205(3):251.e1–e7.
- Florio P, Frigiola A, Battista R, et al. Activin A in asphyxiated full-term newborns with hypoxic-ischemic encephalopathy. *Front Biosci (Elite Ed)*. 2010;2:36–42.
- Douglas-Escobar MV, Heaton SC, Bennett J, et al. UCH-L1 and GFAP serum levels in neonates with hypoxic-ischemic encephalopathy: A single center pilot study. *Front Neurol*. 2014;5:273.
- Lv HY, Wu SJ, Gu XL, et al. Predictive value of neurodevelopmental outcome and serum tau protein level in neonates with hypoxic-ischemic encephalopathy. *Clin Lab*. 2017;63(7):1153–1162.
- Shah DK, Ponnusamy V, Evanson J, et al. Raised plasma neurofilament light protein levels are associated with abnormal MRI outcomes in newborns undergoing therapeutic hypothermia. *Front Neurol*. 2018;9:86.
- Chalack LF, Sánchez PJ, Adams-Huet B, Laptook AR, Heyne RJ, Rosenfeld CR. Biomarkers for severity of neonatal hypoxic-ischemic encephalopathy and outcomes in newborns receiving hypothermia therapy. *J Pediatr*. 2014;164(3):468–474.



28. Graham EM, Everett AD, Delpech JC, Northington FJ. Blood biomarkers for evaluation of perinatal encephalopathy: State of the art. *Curr Opin Pediatr.* 2018;30(2):199–203.
29. Li Y, Dammer EB, Zhang-Brotzge X, et al. Osteopontin is a blood biomarker for microglial activation and brain injury in experimental hypoxic–ischemic encephalopathy. *eNeuro.* 2017;4(1):ENEURO.0253–16.2016. doi:10.1523/ENEURO.0253–16.2016
30. Aly H, Hassanein S, Nada A, Mohamed MH, Atef SH, Atia W. Vascular endothelial growth factor in neonates with perinatal asphyxia. *Brain Dev.* 2009;31(8):600–604.
31. Hagag AA, El Frargy MS, Abd El-Latif AE. Study of cord blood erythropoietin, leptin and adiponectin levels in neonates with hypoxic–ischemic encephalopathy. *Endocr Metab Immune Disord Drug Targets.* 2020;20(2):213–220.
32. Ahearne CE, Denihan NM, Walsh BH, et al. Early cord metabolite index and outcome in perinatal asphyxia and hypoxic–ischaemic encephalopathy. *Neonatology.* 2016;110(4):296–302.
33. Denihan NM, Kirwan JA, Walsh BH, et al. Untargeted metabolomic analysis and pathway discovery in perinatal asphyxia and hypoxic–ischaemic encephalopathy. *J Cereb Blood Flow Metab.* 2019;39(1):147–162.
34. Liu JF, Wu HW, Li ZG, Lu GZ, Yang X. aEEG monitoring analysis of lesion degree and long-term prognosis in newborns with HIE. *Eur Rev Med Pharmacol Sci.* 2016;20(13):2863–2867.
35. Sewell EK, Vezina G, Chang T, et al. Evolution of amplitude-integrated electroencephalogram as a predictor of outcome in term encephalopathic neonates receiving therapeutic hypothermia. *Am J Perinatol.* 2018;35(3):277–285.
36. Goeral K, Urlesberger B, Giordano V, et al. Prediction of outcome in neonates with hypoxic–ischemic encephalopathy II: Role of amplitude-integrated electroencephalography and cerebral oxygen saturation measured by near-infrared spectroscopy. *Neonatology.* 2017;112(3):193–202.
37. Skranes JH, Løhaugen G, Schumacher EM, et al. Amplitude-integrated electroencephalography improves the identification of infants with encephalopathy for therapeutic hypothermia and predicts neurodevelopmental outcomes at 2 years of age. *J Pediatr.* 2017;187:34–42.
38. Del Río R, Ochoa C, Alarcon A, Arnáez J, Blanco D, García-Alix A. Amplitude integrated electroencephalogram as a prognostic tool in neonates with hypoxic–ischemic encephalopathy: A systematic review. *PLoS One.* 2016;11(11):e0165744.
39. Chandrasekaran M, Chaban B, Montaldo P, Thayyil S. Predictive value of amplitude-integrated EEG (aEEG) after rescue hypothermic neuroprotection for hypoxic–ischemic encephalopathy: A meta-analysis. *J Perinatol.* 2017;37(6):684–689.
40. Shah DK, Wusthoff CJ, Clarke P, et al. Electrographic seizures are associated with brain injury in newborns undergoing therapeutic hypothermia. *Arch Dis Child Fetal Neonatal Ed.* 2014;99(3):219–224.
41. Awal MA, Lai MM, Azemi G, Boashash B, Colditz PB. EEG background features that predict outcome in term neonates with hypoxic–ischaemic encephalopathy: A structured review. *Clin Neurophysiol.* 2016;127(1):285–296.
42. Dunne JM, Wertheim D, Clarke P, et al. Automated electroencephalographic discontinuity in cooled newborns predicts cerebral MRI and neurodevelopmental outcome. *Arch Dis Child Fetal Neonatal Ed.* 2017;102(1):58–64.
43. Weeke LC, Boylan GB, Pressler RM, et al. Neonatal seizure treatment with Medication Off-patent (NEMO) consortium. Role of EEG background activity, seizure burden and MRI in predicting neurodevelopmental outcome in full-term infants with hypoxic–ischaemic encephalopathy in the era of therapeutic hypothermia. *Eur J Paediatr Neurol.* 2016;20(6):855–864.
44. Han Y, Fu N, Chen W, et al. Prognostic value of electroencephalography in hypothermia-treated neonates with hypoxic–ischemic encephalopathy: A meta-analysis. *Pediatr Neurol.* 2019;93:3–10.
45. Liu W, Yang Q, Wei H, Dong W, Fan Y, Hua Z. Prognostic value of clinical tests in neonates with hypoxic–ischemic encephalopathy treated with therapeutic hypothermia: A systematic review and meta-analysis. *Front Neurol.* 2020;11:133.
46. Suppiej A, Cappellari A, Talenti G, et al. Bilateral loss of cortical SEPs predicts severe MRI lesions in neonatal hypoxic–ischemic encephalopathy treated with hypothermia. *Clin Neurophysiol.* 2018;129(1):95–100.
47. Cainelli E, Trevisanuto D, Cavallin F, Manara R, Suppiej A. Evoked potentials predict psychomotor development in neonates with normal MRI after hypothermia for hypoxic–ischemic encephalopathy. *Clin Neurophysiol.* 2018;129(6):1300–1306.
48. Gerner GJ, Burton VJ, Poretti A, et al. Transfontanellar duplex brain ultrasonography resistive indices as a prognostic tool in neonatal hypoxic–ischemic encephalopathy before and after treatment with therapeutic hypothermia. *J Perinatol.* 2016;36(3):202–206.
49. Annink KV, de Vries LS, Groenendaal F, et al. The development and validation of a cerebral ultrasound scoring system for infants with hypoxic–ischaemic encephalopathy. *Pediatr Res.* 2020;87(Suppl 1):59–66.
50. Zhang Y, Zhang JL, Li Y. Computed tomography diagnosis of neonatal hypoxic–ischemic encephalopathy combined with intracranial hemorrhage and clinical nursing treatment. *J Biol Regul Homeost Agents.* 2016;30(2):511–515.
51. Thayyil S, Chandrasekaran M, Taylor A, et al. Cerebral magnetic resonance biomarkers in neonatal encephalopathy: A meta-analysis. *Pediatrics.* 2010;125(2):382–395.
52. Lakatos A, Kolossváry M, Szabó M, et al. Neurodevelopmental effect of intracranial hemorrhage observed in hypoxic–ischemic brain injury in hypothermia-treated asphyxiated neonates: An MRI study. *NCBINCB Logo BMC Pediatr.* 2019;19(1):430.
53. Bekiesinska-Figatowska M, Duczkowska A, Szkudlinska-Pawlak S, et al. Diffusion restriction in the corticospinal tracts and the corpus callosum in neonates after cerebral insult. *Brain Dev.* 2017;39(3):203–210.
54. Rana L, Sood D, Chauhan R, et al. MR imaging of hypoxic–ischemic encephalopathy: Distribution patterns and ADC value correlations. *Eur J Radiol Open.* 2018;5:215–220.
55. Mitra S, Kendall GS, Bainbridge A, et al. Proton magnetic resonance spectroscopy lactate/N-acetylaspartate within 2 weeks of birth accurately predicts 2-year motor, cognitive and language outcomes in neonatal encephalopathy after therapeutic hypothermia. *Arch Dis Child Fetal Neonatal Ed.* 2019;104(4):424–432.
56. Lemmon ME, Wagner MW, Bosemani T, et al. Diffusion tensor imaging detects occult cerebellar injury in severe neonatal hypoxic–ischemic encephalopathy. *Dev Neurosci.* 2017;39(1–4):207–214.
57. Trivedi SB, Vesoulis ZA, Rao R, et al. A validated clinical MRI injury scoring system in neonatal hypoxic–ischemic encephalopathy. *Pediatr Radiol.* 2017;47(11):1491–1499.
58. Weeke LC, Groenendaal F, Mudigonda K, et al. A novel magnetic resonance imaging score predicts neurodevelopmental outcome after perinatal asphyxia and therapeutic hypothermia. *J Pediatr.* 2018;192:33–40.e2.
59. Jain SV, Pagano L, Gillam-Krakauer M, Slaughter JC, Pruthi S, Engelhardt B. Cerebral regional oxygen saturation trends in infants with hypoxic–ischemic encephalopathy. *Early Hum Dev.* 2017;113:55–61.
60. Kayton A, DeGrazia M, Sharpe E, Smith D, Perez JA, Weiss MD. Correlation between heart rate characteristic index score and severity of brain injury in neonates with hypoxic–ischemic encephalopathy. *Adv Neonatal Care.* 2020;20(4):E70–E82. doi:10.1097/ANC.0000000000000686
61. Gonzaga e Silva ABC, Laszczyk J, Wrobel LC, Ribeiro FLC, Nowak AJ. A thermoregulation model for hypothermic treatment of neonates. *Med Eng Phys.* 2016;38(9):988–998.
62. Mietzsch U, Radhakrishnan R, Boyle FA, Juul S, Wood TR. Active cooling temperature required to achieve therapeutic hypothermia correlates with short-term outcome in neonatal hypoxic–ischaemic encephalopathy. *J Physiol.* 2020;598(2):415–424.